

TRANSFORMING TAILS INTO TOOLS:
FROM EVOLUTIONARY MORPHOLOGY OF PREHENSILE TAILS IN SYNGNATHID
FISHES TO EXPLORING BIO-INSPIRATION POTENTIALS

CÉLINE NEUTENS

Thesis submitted to obtain the degree of
Doctor in Sciences (Biology)

Proefschrift voorgedragen tot het
bekomen van de graad van
Doctor in de Wetenschappen (Biologie)

Academic year 2015-2016

Rector: Prof. Dr. Anne De Paepe
Dean: Prof. Dr. Herwig Dejonghe
Promotor: Prof. Dr. Dominique Adriaens
Co-promotor: Prof. Dr. Ir. Matthieu De Beule

© All rights reserved. This thesis contains confidential information and confidential research results that are property to the UGent (Research group Evolutionary Morphology of Vertebrates, Department of Biology). The contents of this thesis may under no circumstances be made public, nor complete or partial, without the explicit and preceding permission of the UGent representative, i.e. the supervisor. The thesis may under no circumstances be copied or duplicated in any form, unless permission granted in written form. Any violation of the confidential nature of this thesis may impose irreparable damage to the UGent. In case of a dispute that may arise within the context of this declaration, the Judicial Court of Gent only is competent to be notified.

© Cover photograph: Art Wolfe

Examination Committee

Prof. Dr. Dominique Adriaens (Promotor)	(Ghent University, Belgium)
Prof. Dr. Ir. Matthieu De Beule (Co-promotor)	(Ghent University, Belgium)
Prof. Dr. Ann Huyseune (Chair)	(Ghent University, Belgium)
Dr. Sam Van Wassenbergh (Secretary)	(CNRS, France)
Prof. Dr. Anthony Herrel	(Ghent University, Belgium; CNRS, France)
Prof. Dr. Peter Aerts	(Antwerp University, Belgium)
Prof. Dr. Ir. Michael Porter	(Clemson University, U.S.A.)
Prof. Dr. Ir. Benedict Verhegghe	(Ghent University, Belgium)
Dr. Ir. Tomas Praet	(Xeikon International B.V.)
Prof. Dr. Pieter Cornillie	(Ghent University, Belgium)

Rummaging through a box labeled “spare parts”, a mischievous god finds a horse’s head and, feeling the desire for experimentation, places it on top of the pouched torso of a kangaroo. This playful god adds a pair of swiveling chameleon eyes and the prehensile tail of a tree-dwelling monkey for embellishment – then she stands back to admire her work. Not bad, but how about a suit of magical color-changing armor, a perfect fit, and a crown borrowed from a fairy princess, shaped as intricately and uniquely as a human fingerprint? Shrink it all down to the size of a chess piece and the new creature is complete.

- H. Scales -

Dankwoord

Traditioneel hoort bij een schrijven van een doctoraat een woordje van dank. Dankzij de hulp van velen is dit doctoraat het boekje geworden dat nu voor jullie ligt! Het liefst zou ik hier gewoon “Merci iedereen” willen neerschrijven om er zeker van te zijn dat ik niemand vergeet, maar sommigen verdienen toch een extra woordje van dank.

In de eerste plaats een dikke merci aan Dominique, een promotor uit de duizend! Jij stond letterlijk dag en nacht klaar om te helpen en mijn teksten na te lezen. Je was altijd enthousiast als ik weer eens afkwam met de vraag om iets te 3D-tekenen of -printen. We hebben de afgelopen jaren veel interessante discussies gevoerd en je feedback heeft deze thesis ongetwijfeld tot een hoger niveau getilt!

Ook had ik graag mijn co-promotor, Matthieu, en alle andere mensen met een ingenieursachtergrond die mij geholpen hebben bij het experimenteren en modelleren bedankt: Benedict, Tom, Tomas, Michael, Nic en Jurgen. Matthieu, Benedict en Tom had ik graag bedankt voor de verschillende brainstorm-sessies die we gehouden hebben en Benedict in het bijzonder voor de hulp met pyFormex. Tomas, zonder jouw hulp was het zesde hoofdstuk van dit doctoraat zeker niet geworden wat het nu is! Bedankt om mij te willen helpen mijn ideeën te vertalen in een werkend script, altijd klaar te staan om mijn vragen te beantwoorden en dit alles te willen doen in je schaarse vrije tijd. Mensen zoals jij, die willen helpen met als drijfveer passie en nieuwsgierigheid, kom je slechts zelden tegen! Also a special thank you for Michael. Although we never actually met, you helped me a lot with your knowledge (and explaining the difficult engineering stuff in such a way that a simple biologist could understand it), your feedback and answers to my many questions! Nic en Jurgen had ik graag bedankt voor de hulp met de Inston-machine.

Verder had ik ook graag Peter en Bart bedankt voor de hulp bij (het aanpassen van de software voor) het uitvoeren van de 3D-morfometrische analyses en de heel aangename samenwerking! Ook een dankjewel aan Renauld en Anthony voor het maken van de synchrotron scans en aan het UGCT voor het maken van de μ CT-scans. Graag had ik ook Anthony bedankt voor de hulp bij het maken van de ancestral state reconstructie.

Binnen onze eigen onderzoeksgroep had ik graag Barbara en Joachim bedankt voor de hulp met allerlei praktisch werk: kleuringen, snijden van coupes, lijmen, verzorgen van dieren en aquaria, etc. Also, I wish to thank Paulina for assisting me during the bending experiments. Gedurende de afgelopen vier jaar werd inspanning gelukkig regelmatig afgewisseld door ontspanning. Een hele reeks collega's passeerden de revue en draagden allen hun steentje

bij tot de leuke sfeer op het werk: Niels, Tim, Emilie, Tom, Anabela, Sandra, David, Sam, Charlotte, Mathias, Jens, Barbara, Joachim, Miranda, Hilde, Inge en (andere) Barbara. Al moet ik wel toegeven dat we de laatste jaren met drie een bureau deelden die er qua sfeer en gezelligheid bovenuit springt!

Gezien dit onderzoek niet mogelijk was geweest zonder dieren of financiering, bedankt aan alle musea en instellingen voor het ontlenen en doneren van de specimens: het Vlaams Instituut voor de Zee (VLIZ, België), het Koninklijk Belgisch Instituut voor Natuurwetenschappen (KBIN, België), het South Australian Museum (SAM, Australië), de Commonwealth Scientific and Industrial Research Organisation (CSIRO, Australië), het Field Museum (V.S) en het Museum National d'Histoire Naturelle (MNHN, Frankrijk) en aan het Instituut voor Innovatie door Wetenschap en Technologie (IWT) voor het toekennen van een doctoraatsbeurs.

Als laatste had ik graag nog een woordje van dank gericht aan mijn familie. Geen doctoraat zonder voorafgaande studies, die ik dankzij de hulp van mijn ouders mocht aanvragen en tot een goed einde kon brengen. Een bijzondere dankjewel voor mijn mama, die de afgelopen jaren steeds voor me klaarstond! De hopen liefde die ik binnen mijn eigen, kleine gezinnetje krijg, hebben er ook zeker mee voor gezorgd dat dit doctoraat hier nu voor jullie ligt. Matti, jij bent er altijd in blijven geloven dat dit moment er zeker zou komen! Tijdens het schrijven van dit doctoraat kon ik voor gelijk wat op je rekenen, een gevoel dat enorm veel deugd doet! Eleonora, mijn kleine spruitje, misschien lees je op een dag dit tekstje in mama haar boek en kom je nu te weten dat jouw schaterlach en eeuwig enthousiasme me altijd deden opfleuren na een dagje schrijven aan dit boek. Ik zie jullie graag!

Table of Contents

CHAPTER 1: INTRODUCTION	3
1.1 General context	3
1.1.1 General morphology of the fish tail	3
1.1.2 Syngnathid fishes.....	7
1.1.3. Mimicry, biomimetics and designs from nature	13
1.2. Aims and thesis outline.....	15
1.2.1. General aims.....	15
1.2.2. Thesis outline and specific aims	16
CHAPTER 2: MATERIAL & METHODS	19
2.1 Material	21
2.2 Methods.....	22
2.2.1. Scanning procedures	22
2.2.2 <i>In toto</i> clearing and staining.....	23
2.2.3 Histological sectioning.....	24
2.2.4 Nitric acid treatment	24
2.2.5 3D-reconstructing.....	24
2.2.6 Morphometry	25
2.2.7 Tail stiffness.....	25
2.2.8 Syngnathid tail modelling.....	25
CHAPTER 3: MORPHOLOGY.....	29
3.1 Abstract.....	31
3.2 Introduction.....	31
3.3 Material and methods	35
3.3.1 Specimens studied.....	35
3.3.2 Musculoskeletal morphology	35
3.3.3 Muscle fiber length.....	36
3.3.4 Bending performance.....	37
3.4 Results.....	37
3.4.1 Musculoskeletal morphology	37
3.4.2 Bending capacity	44

3.5 Discussion	46
CHAPTER 4: MORPHOMETRICS	53
4.1 Abstract.....	55
4.2 Introduction.....	55
4.3 Material and methods	59
4.3.1 Specimens studied.....	59
4.3.2 Skeletal morphology.....	60
4.3.3 3D morphometric analysis.....	61
4.3.4 Measurements	63
4.4 Results.....	64
4.4.1 Proximo-distal intra-individual shape variation	64
4.4.2 Dorso-ventral intra-individual shape variation	65
4.4.3 Inter-individual shape variation	69
4.5 Discussion	73
CHAPTER 5: BENDING EXPERIMENTS.....	81
5.1 Abstract.....	83
5.2 Graphical abstract.....	83
5.3 Introduction.....	84
5.4 Material and Methods	87
5.4.1 Test samples	87
5.4.2 Stiffness tests	87
5.5 Results.....	90
5.5.1 Directional differences	90
5.5.2 Regional differences	92
5.5.3 Tissue-related differences	94
5.5.4 Morphotype-related differences.....	97
5.6 Discussion	97
CHAPTER 6: DYNAMIC TAIL MODELLING.....	105
6.1 Introduction.....	107
6.2 Material and Methods	109
6.2.1 Initial seahorse model	109

6.2.2 Adapted seahorse model	116
6.2.3 Simulations	118
6.3 Results.....	120
6.3.1 Simulations of the individual shape differences	120
6.3.2 Simulations of the combined shape differences	125
6.4 Discussion	125
CHAPTER 7: GENERAL DISCUSSION	135
7.1 Combining morphology, morphometrics and virtual modelling to understand the evolution of tail grasping	137
7.2 Future perspectives	141
7.3 Bio-mimetics and bio-inspiration.....	146
7.3.1 Robotics.....	146
7.3.2 Potentials for protective clothing.....	150
7.3.3 Modular racing circuit for kids	152
CHAPTER 8: SUMMARY	157
8.1 Summary.....	159
8.2 Samenvatting.....	162
REFERENCES.....	167
CURRICULUM	
APPENDICES	

CHAPTER 1: INTRODUCTION

This thesis deals with the fascinating tail morphology of seahorses (belonging to the genus *Hippocampus*) and their close relatives. Within the family of the Syngnathidae (meaning ‘jaw-fused’), a flexible tail evolved from a rigid one more than once during evolution. Although studies have focused on tail grasping, the detailed musculoskeletal morphology behind this, as well as the pattern of evolutionary transformations that made this possible are poorly understood.

In the first part of this chapter, a short introduction on the general morphology of the tail of fishes will be given, as well as the phylogenetic position of the Syngnathidae (seahorses and their allies) and an overview of the different types of syngnathid fishes. Also the concepts of mimicry, biomimetics and designs from nature will be shortly discussed. The second part of this first chapter deals with the specific aims of this PhD research and will provide the reader with a short overview of the different chapters.

1.1 General context

1.1.1 General morphology of the fish tail

1.1.1.1 Orientation terminology (FIGURE 1.1)

Anterior	relating to the front portion of the fish
Posterior	relating to the rear end of the fish
Dorsal	pertaining to the back of the fish
Ventral	pertaining to the abdomen of the fish
Proximal	at the base (of an appendix) or closest to the body/center of an organism
Distal	at the tip (of an appendix) or farthest away from the body/center of an organism

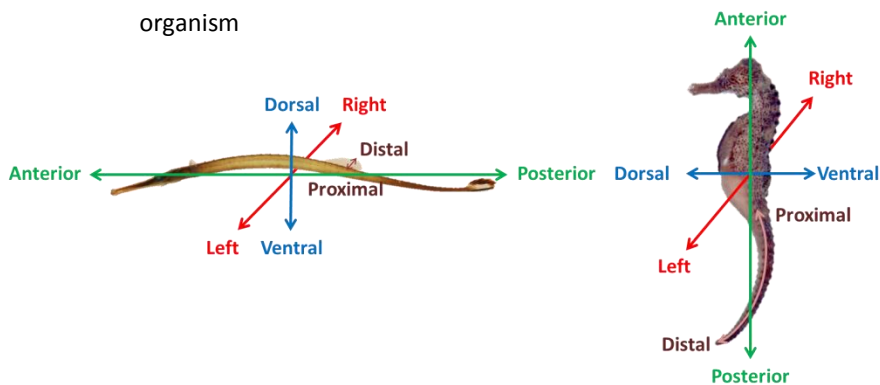


FIGURE 1.1 – The three main body axes, with the antero-posterior axis in green, the dorso-ventral axis in blue and the left-right axis in red, and an indication of a proximo-distal axis (in bordeaux) illustrated on a pipefish (*Doryrhamphys janssi* - left) and a seahorse (*Hippocampus reidi* - right).

1.1.1.2 Body coverage

The skin of most fishes comprises of scales, embedded in soft tissue. These scales exhibit a high diversity in shapes, sizes and structures when comparing them between different fish species. Scales typically consist of bone, covered by dentine and enamel (or enamel-like tissue). Dentine is produced by cells of neural crest origin and strongly resembles bone, but differs in the arrangement of cells and matrix, while enamel is of epidermal origin and is the hardest tissue in the body. The general classification of scales includes placoid, cosmoid, ganoid and elasmoid scales. **Placoid scales** can be found in cartilaginous fishes (Chondrichthyes). These scales consist of dentine, surrounding a vascular pulp cavity, and are capped by a layer of hard material. This material contains the same amelogenin proteins as found in enamel, but also some fibrous material of dermal origin and is therefore called enameloid (FIGURE 1.2A). The other three types of scales can be found in bony fishes (Osteichthyes). In contrast to the scales in cartilaginous fishes, scales do not actually pierce the epidermis in bony fishes. **Cosmoid scales** can be found in the primary

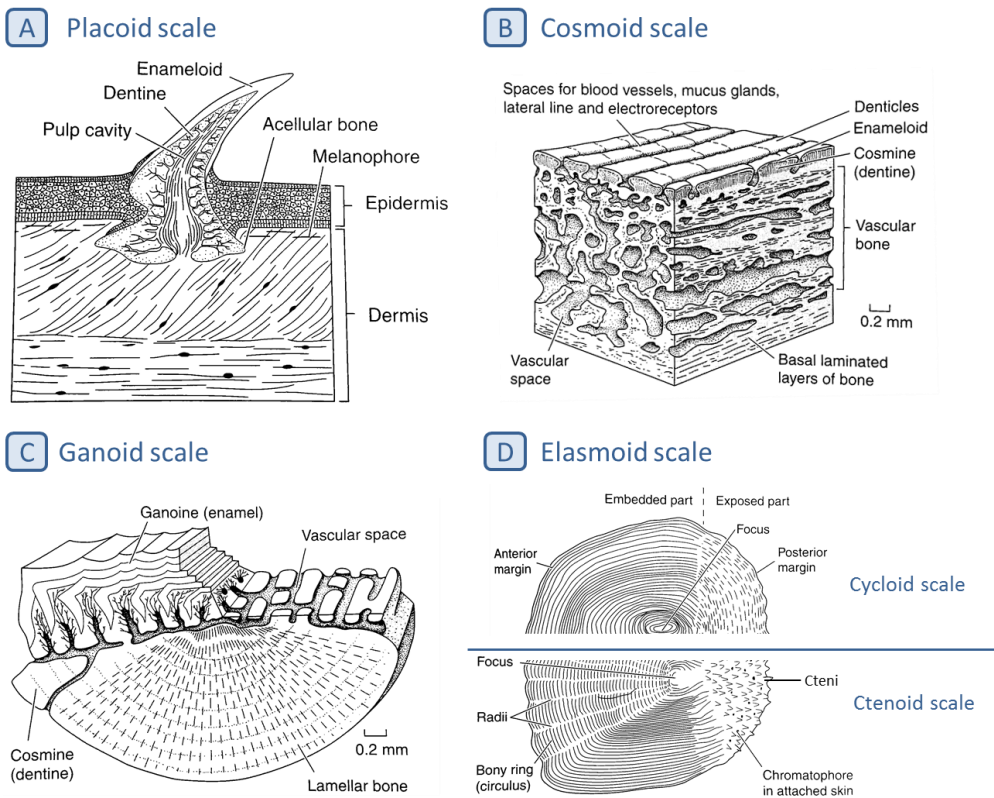


FIGURE 1.2 – Different scale types in fishes, section through (A) a placoid scale of a shark, (B) a cosmoid scale, (C) a ganoid scale and (D) a surface view of the two different types of elasmoid scales (modified from Liem et al (2001)).

dermal armor of ancestral, jawless vertebrates and is composed of a layer of compact and a layer of spongy bone, covered by a thick layer of dentin and a thin layer of enamel-like tissue (possibly hard cosmine that develops in the dermis) (FIGURE 1.2B). **Ganoid scales** are composed of lamellar bone, overlain by many layers of enamel (FIGURE 1.2C). Some ganoid scales contain small amounts of bone and dentine, others don't. **Elasmoid scales** are characteristic for teleost fishes and are composed of a bony surface covering a fibrous layer that is composed largely of collagen. These scales develop in overlapping skinfold, so that the scales themselves overlap (a condition called imbricating). Elasmoid scales can be subdivided into two different types: cycloid scales, that are sculptured by a pattern of concentric growth rings, and ctenoid scales, possessing a series of comb like projections (ctenii) on the posterior part of the scale (nearest the skin surface) (FIGURE 1.2D) (Kardong, 1998, Liem et al., 2001, Helfman et al., 2009, Burdak, 1986).

Among various teleosts, the elasmoid-type scales are replaced by **plates of cell-rich bone** (FIGURE 1.3). In armored catfish, these bony plates are capped by a layer of hyaloine. In other taxa, including the Syngnathiformes, no capping tissue is formed and the resulting dermal plates are composed exclusively of bone (Sire et al., 2009).

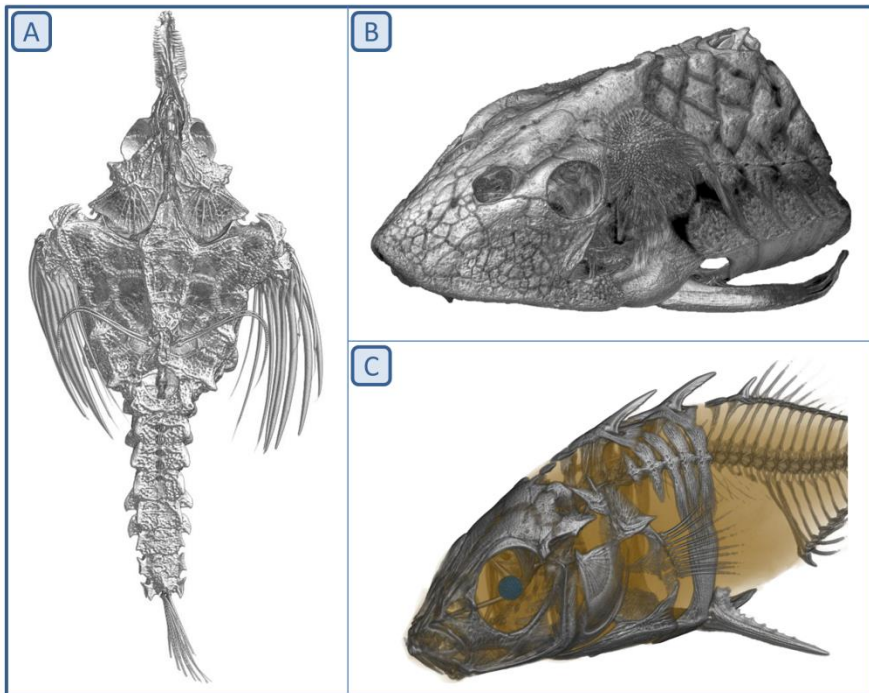


FIGURE 1.3 – Examples of the occurrence of bony plates in teleost fishes: (A) the little dragonfish (*Eurypegasus draconis* - Pegasidae), (B) the vermiculated sailfin catfish (*Pterygoplichthys disjunctivus* - Loricariidae) and (C) the three-spined stickleback (*Gasterosteus aculeatus* - Gasterosteidae).

Individual scales are known to resist penetration and provide a physical barrier against the attack from predators (Chen et al., 2011, Zhu et al., 2011, Burdak, 1986). At a higher level, the arrangement of the scales provides a flexible skin that allows for changes in fish shape during swimming (Sudo et al., 2002). The dermal scales in teleosts are typically arranged as overlapping structures, which minimizes drag under water (Yang et al., 2013a). The scaled skin has proven to play a critical, structural role in fish locomotion by regulating wave propagation (Long et al., 1996, Long et al., 2002) and by acting as an external tendon, storing mechanical energy in order to make swimming more efficient. The dermal plates in seahorses are frequently ornamented, just as the plates in Ostracodermi, Loricariidae and other members of the Syngnathidae (Lees et al., 2011, Burdak, 1986). The role of fish skin, including scales, in function of swimming behavior has been thoroughly studied in the past (*i.e.* Browning et al., 2013; Yang et al., 2013a). The tail in seahorses and some of their close relatives however, is no longer used during swimming, but has evolved into a prehensile structure (Hale, 1996, Neutens et al., 2014, also see CHAPTER 3). Previous research already suggested that the dermal plates in seahorses do not only provide body support and protection, but also give them the ability to bend their tails and grasp and hold onto seagrasses and other objects and thus play an essential role in axial bending and the prehensibility of the seahorse tail (Hale, 1996, Praet et al., 2012).

1.1.1.3 Muscular organization

The trunk and tail muscles of fish consist of short muscle fibers, organized in myomeres that are separated from each other by collagenous sheets, called myosepta (Van Leeuwen, 1999). Within the vertebrates, three main groups comprising fishes can be distinguished, each characterized by a remarkably different muscular organization. Petromyzontids are characterized by the absence of either a conical myoseptal organization or distinct myoseptal tendons. Myxinids possess asymmetric myosepta with long cones, but lack distinct myoseptal tendons, as well as myoseptal-skin connections. In the last group, the gnathostomes (to which seahorses belong), the ancestral condition is represented by fishes that have both a conical organization of their myosepta and distinct tendinous structures that are firmly anchored in the skin (Gemballa and Vogel, 2002).

Teleost fishes, belonging to the group of the gnathostomes, exhibit a typical W-shaped organization of the myosepta (when projected in 2D – FIGURE 1.4). The myosepta are separated by the horizontal septum (HS) into an epaxial part at the dorsal side and a hypaxial part at the ventral side. In the epaxial half, each myosepta is folded into two cones, a (main) dorsal anterior cone (mDAC) and a dorsal posterior cone (DPC). Sometimes a third cone is present (then called the secondary dorsal anterior cone - sDAC). Cones of successive

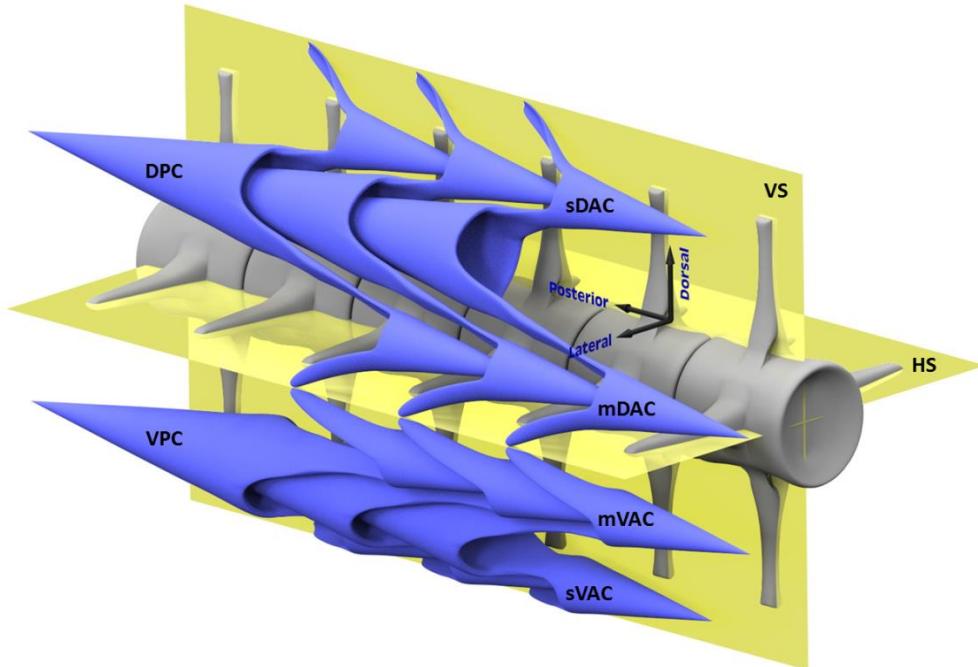


FIGURE 1.4 – Schematic overview of the general configuration of the tail muscles in a teleost. Myosepta in blue, vertebrae in grey, VS: vertical septum, HS: horizontal septum, sDAC: secondary dorsal anterior cone, DPC: dorsal posterior cone, mDAC: main dorsal anterior cone, mVAC: main ventral anterior cone, VPC: ventral posterior cone, sVAC: secondary ventral anterior cone.

myosepta are nested within each other. The same, but mirrored pattern is present in the hypaxial part (Gemballa et al., 2003) (FIGURE 1.4).

1.1.2 Syngnathid fishes

The Syngnathidae belong to the Teleostei, a group including 96% of all living fishes and the most diversified group within the vertebrates, having radiated into more niches and adaptive zones than all other vertebrate groups combined. This group comprises fishes that live in different habitats (rivers, lakes, oceans and some can even survive on land), exhibit a large variety of locomotion behaviors (swimming, gliding, walking or staying immobile), have diverse brooding strategies (substrate to mouth brooders) and have extremely diverse diets (*e.g.* algae, zooplankton, snails, insect larvae, other fish, amphibians, blood, faeces, fish eyes and scales) (Helfman et al., 2009).

The Eutelostei (or “true teleosts”) are ranked as one of the four subgroups within the group of teleost fishes and are the most diversified subgroup, comprising 22262 species, placed in 28 orders, 391 families, and 3795 genera. The euteleosts are not characterized by unique, shared characteristics common to all members (Helfman et al., 2009).

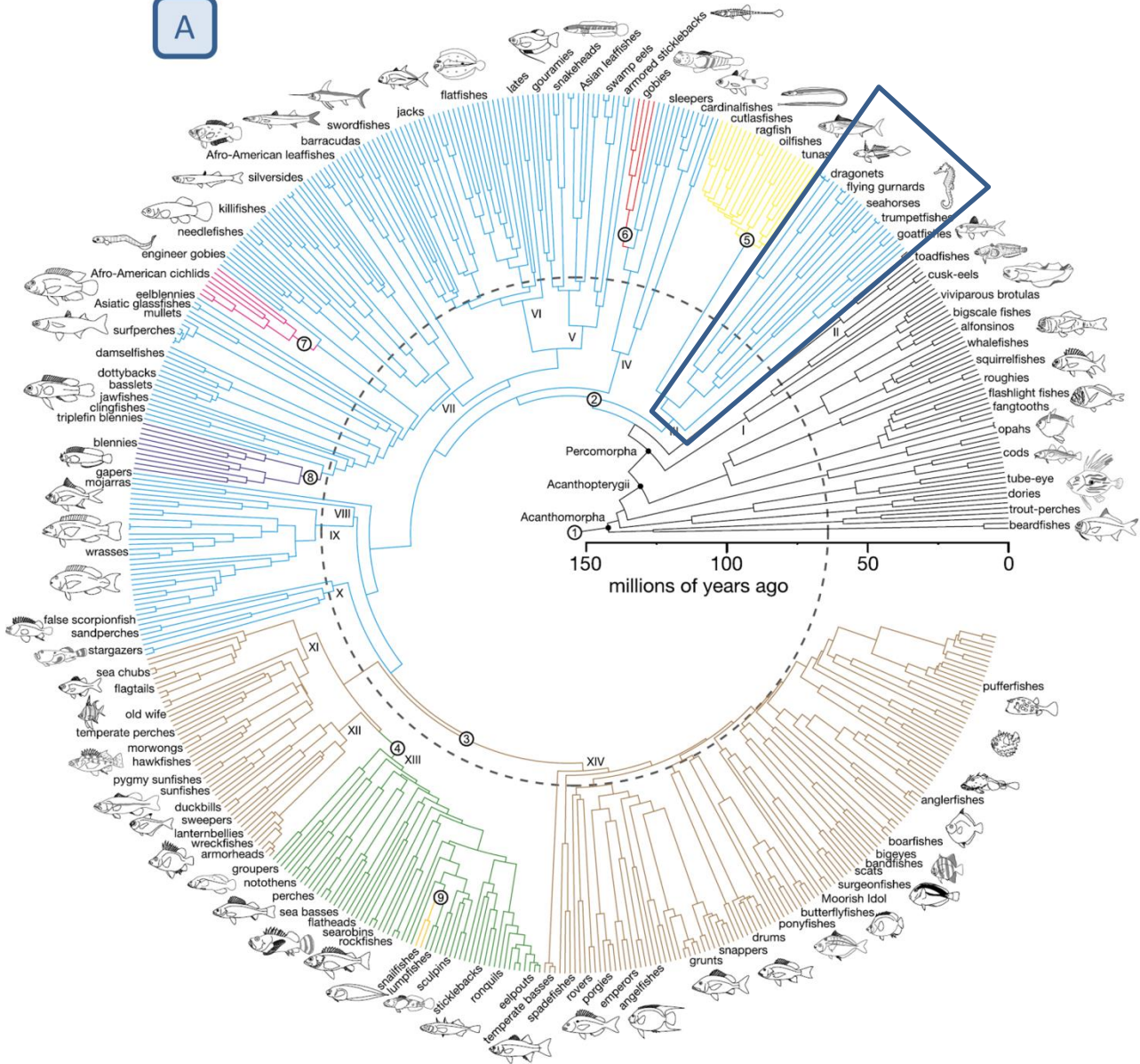
The appearance of true fin spines (instead of hardened segmented rays) marks a major evolutionary step in the evolution of bony fishes. These true spines occur in the dorsal, anal and pelvic fins of the spiny teleosts (the Acanthomorpha). Locomotion in these fishes was improved by the strengthening of the zygapophyses, providing body stiffening and better attachment for muscles. These changes allowed a shift from slow, sinusoidal motion of the entire body to rapid oscillations of the tail region, driven by tendons attached to the tail base (Helfman et al., 2009). The acantomorphs include, next to the seahorses and their close relatives, some of the most economically and scientifically important fish species, such as cods, tunas, sticklebacks and cichlids (FIGURE 1.5A) (Near et al., 2013).

The Percomorpha, within the Acanthomorpha, is the most advanced euteleosteian clade, containing more than 17000, mainly marine, species (Near et al., 2013). They are characterized by an anteriorly placed pelvic girdle that is connected to the pectoral girdle directly or by a ligament (Helfman et al., 2009). Until recently, seahorses and their allies were encompassed by the order of the Gasterosteiformes, a group of fishes characterized by a dermal armor covering the body. However, recent phylogenetic studies (Near et al., 2013, Chen et al., 2003, Dettai and Lecointre, 2005, Kawahara et al., 2008) indicate that the monophyletic position of the Gasterosteiformes is no longer supported. According to the most recent phylogenetic study of Near et al. (2013), seahorses and their allies belong to the Syngnathiformes (ray-finned fishes) and are closely related to the Mullidae (goatfishes) and the Scombriformes (including mackerel and tuna) (FIGURE 1.5A).

Most Syngnathiformes have slender, elongated bodies with a small mouth at the end of a relatively long tubular snout. Their armored bodies are partially or completely covered by dermal plates and they share various specializations in skeletal morphology, including the absence of an anterior processes directly connecting the pelvic fins to the cleithra, the absence of supramaxillary, orbitosphenoid and basisphenoid bones and the absence of a strong ligament connecting the shoulder girdle to either the posterior cranial base or an anterior vertebra (Bray, 2011). Within the Syngathiformes, five families can be discerned: the Centriscidae (comprising the razorfishes, shrimpfishes and snipefishes), the Solenostomidae (comprising the false pipefishes, ghost pipefishes and tubemouth fishes), the Syngnathidae (comprising the seahorses and their close relatives), the Aulostomidae (or trumpetfishes) and the Fistulariidae (or cornetfishes) (FIGURE 1.5B).

The family of the syngnathid fishes is well known for its highly specialized morphology and the diversity of morphological forms found within this family has made it difficult to understand their evolutionary origin and pattern of diversification (Wilson and Orr, 2011). Syngnathid fishes mainly use their dorsal (and to a lesser extent their pectoral) fins for

A



B

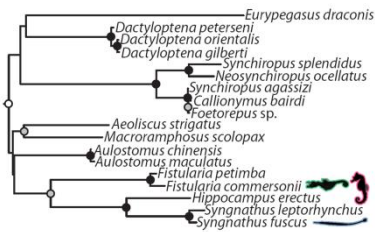


FIGURE 1.5 – Phylogenetic position of the seahorses and their close relatives within the Acanthomorpha. (A) Time calibrated phylogenetic tree of the Acanthomorpha, including 520 species calibrated with 37 fossil-based age constraints, with indication of the phylogenetic position of the Syngnathiformes and (B) Phylogenetic relationships within the Syngnathiformes in more detail (modified from Near et al., 2013).

locomotion (called amiiform locomotion) (Jungersen, 1910, Ashley-Ross, 2002). These fishes undulate their dorsal fins at very high frequencies (Breder and Edgerton, 1942, Blake, 1976), but with low amplitude, leading to a reduced efficiency and very slow swimming speeds (Blake, 1980). Despite the fact that all syngnathid fishes are slow swimmers, they evolved different strategies to escape predation. One strategy is the ability to adopt colors and camouflage specific to their environment, also known as crypsis. Also the fast oscillations of their dorsal and pectoral fins (up to 35 times per second) exceed the flicker fusion threshold of their predators and the fins are thus rendered effectively invisible for the predator as they propel the animal (Ashley-Ross, 2002, Breder and Edgerton, 1942, Consi et al., 2001). Apart from their peculiar look and slow swimming speed, all syngnathid fishes share another interesting characteristic, being their reproductive strategy in which the male gets pregnant. After a relatively long period (in fish terms) of incubating the eggs, the male gives birth to an already well developed offspring (Stölting and Wilson, 2007).

The family of the syngnathid fishes can be subdivided into five different morphotypes: pipefishes, seahorses, type I pipehorses, type II pipehorses and seadragons. Keeping their body horizontal, pipefishes (representing the ancestral condition within the family) forage in the open water (especially the flagtail pipefishes - Doryrhampinae, (Kuitert, 2009)) or close to the sea floor (FIGURE 1.6B). They are characterized by a relatively stiff tail, explaining the limited use of it during swimming (Ashley-Ross, 2002).

Seahorses have a vertical body posture, with their head in a right angle to their body axis and possess a prehensile tail. During ontogeny, the caudal fin becomes lost (Franz-Odendaal and Adriaens, 2014). It was already suggested that their vertical position in the water column originated in association with an Indo-Pacific expansion of sea grass habitats (Teske and Beheregaray, 2009) and that the bent orientation of their head (perpendicular to their vertical positioned body) could be adaptive for their specific way of feeding, *i.e.* pivot feeding (Van Wassenbergh et al., 2011). When considering all these features, it is not a surprise that many people find it difficult to believe that they are actually a kind of fish (FIGURES 1.6A & 1.6E) (Kuitert, 2003).

Pipehorses in general show a seemingly intermediate morphology between seahorses and pipefishes, with a horizontal body posture and the presence of a prehensile tail. Type I pipehorses comprise a group of small sized, seahorse-like fishes (but with a horizontal body posture) and are also called the pygmy pipehorses (genera *Idiotropiscis*, *Acentronura*, *Kyonemichthys* and *Ampheikturus*) (FIGURES 1.6D) (Gomon, 2007, Kuitert, 2009, Teske and Beheregaray, 2009). Type II pipehorses show a similar morphology to that of pipefishes,

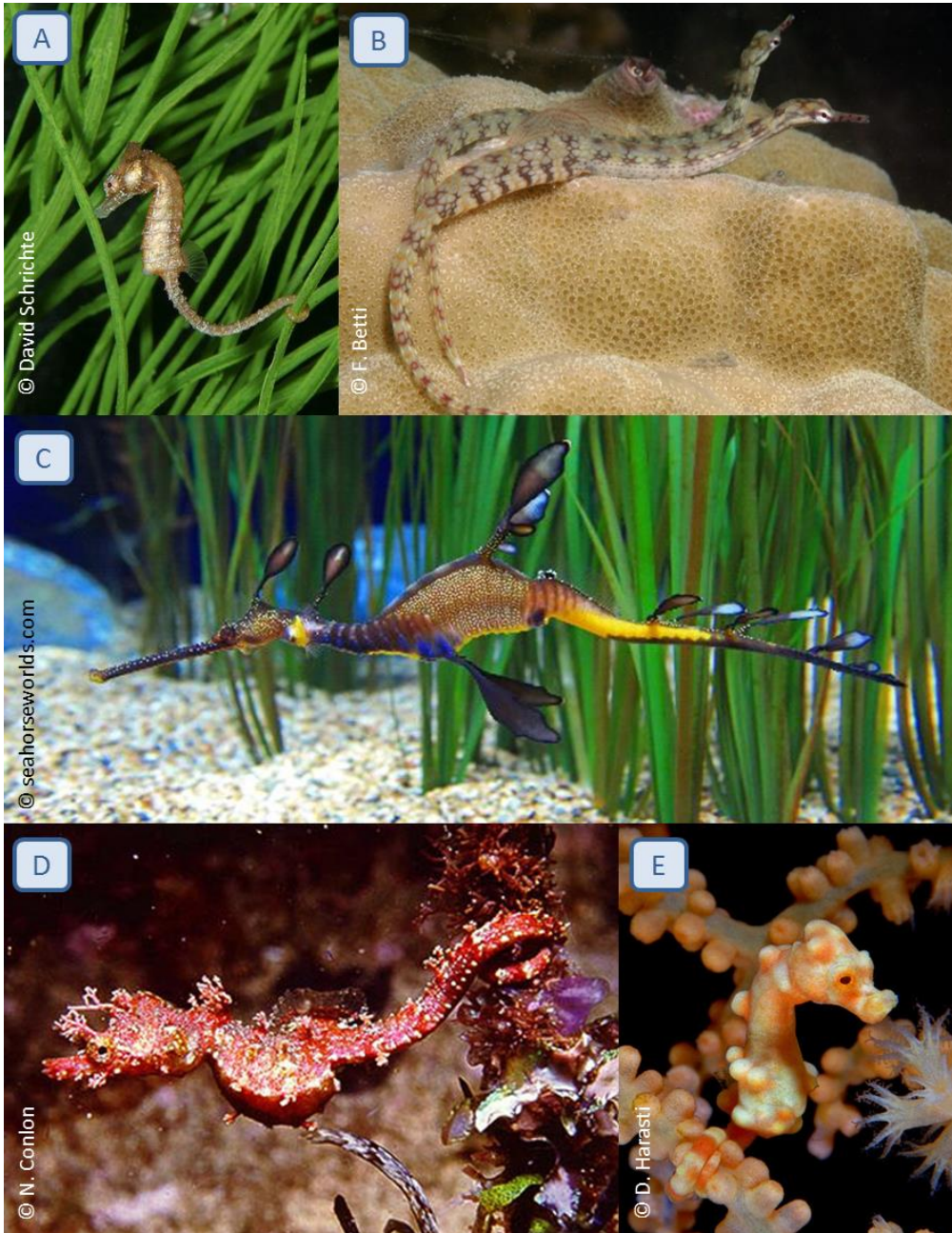


FIGURE 1.6 – Illustration of the morphological diversity within the Syngnathidae. A *Hippocampus zosterae* (seahorse) B *Corythoichthys intestinalis* (pipefish), C *Phyllopteryx taeniolatus* (seadragon), D *Idiotropiscis lumnitzeri* (type I pipehorse) and E *Hippocampus denise* (seahorse).

but lack a caudal fin and possess a prehensile tail. These pipehorses do not form a monophyletic group and are phylogenetically nested within the pipefishes (FIGURE 1.7 – green branches).

Seadragons are relatively large fishes and highly ornamented by leafy appendages. Only three seadragon species, subdivided into two genera, exist: *Phyllopteryx taeniolatus* (the weedy seadragon, FIGURE 1.6C), *Phyllopteryx dewysea* and *Phycodurus eques* (the leafy seadragon) (Kuitert, 2009, Stiller et al., 2015).

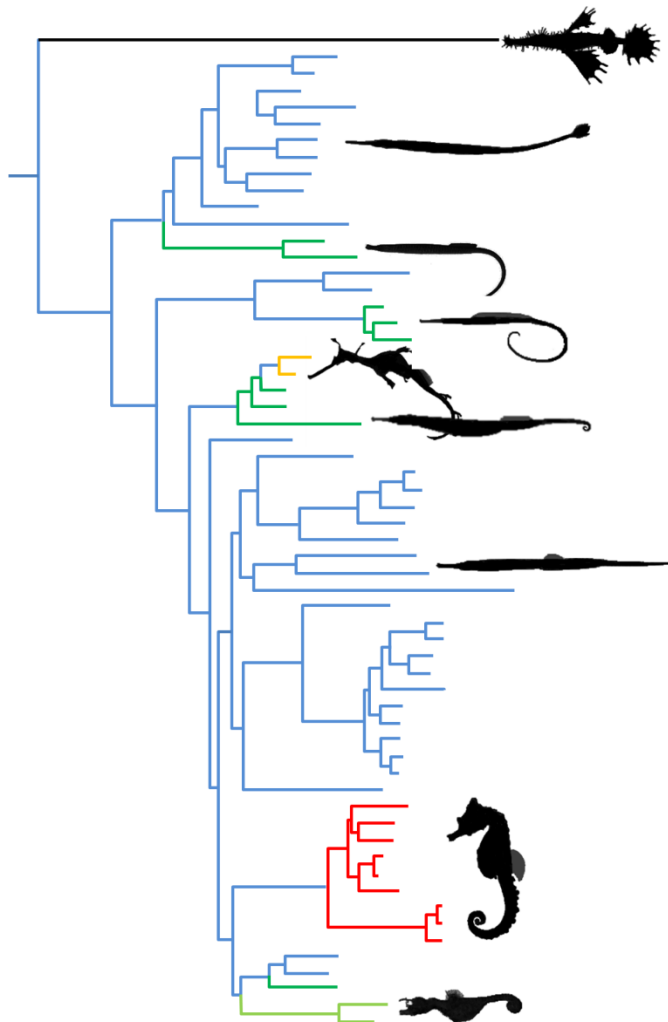


FIGURE 1.7 – Polyphyletic origin of grasping tails in syngnathids. Phylogenetic pattern towards the independent evolution from an ancestral tail possessing a tail fin (blue), towards a tail lacking a tail fin without grasping capacities (yellow) and with grasping capacities in pipehorses (type I – light green and type II – dark green) and seahorses (pink). Solenostomus (black) belongs to a separate family of Solenostomidae, sister to Syngnathidae and is used as an outgroup. Cladogram based on Hamilton et al. (2009). Modified from Neutens et al. (2014).

1.1.3. Mimicry, biomimetics and designs from nature

1.1.3.1 Definitions

Mimicry is a condition found in nature in which features of one species have evolved to resemble those of another species and leading to convergent evolution of a specific trait. Several types of mimicry can be encountered in nature, of which the two main types are discussed here. The first occurs when a palatable or harmless animal evolves a morphological resemblance to an unpalatable or dangerous animal. An example of this is when flies adopt the colors of wasps. Predators that learn to avoid wasps because of their stinging behavior, will also avoid the flies that mimicked the colors of the wasps. A second type occurs when two or more distasteful species that share one or more common predators evolve similar characteristics. A predator that previously encountered one of the species in the past, will also avoid the other one because of the associated unpleasant experience (Futuyma, 2005).

Biomimetics (derived from the Greek βίος (bios), meaning life and μίμησις (mīmēsis), meaning imitation) or **biomimicry** is the imitation of models, systems or elements found in nature for the purpose of solving complex human problems (Vincent et al., 2006). The term was used for the first time by Otto Schmitt in the 1950s for the transfer of ideas and analogues from nature to technology, during his research to produce a device that mimicked the electrical action of a nerve. Only in 1974 the word biomimetics made it to a dictionary for the first time (Harkness, 2002), accompanied by the following definition:

“The study of the formation, structure, or function of biologically produced substances and materials (as enzymes or silk) and biological mechanisms and processes (as protein synthesis or photosynthesis) especially for the purpose of synthesizing similar products by artificial mechanisms which mimic natural ones.”

Following terms will occur frequently in this thesis and are therefore also defined in this introduction:

Flexible	capable of being bent or flexed, pliable	Stiff/rigid	difficult to bend or fold
Firm	Resistant to externally applied pressure	Fragile	easily broken, damaged or destroyed; lacking physical strength

1.1.3.2 Designs from nature

In nature, mimicry is almost always coupled to an evolutionary advantage during predator-prey interactions. Although the principle of copying characteristics of a certain organism is also the starting point in biomimetics, the main aim, however, is not confusion or deception, but solely to use these characteristics as a source of inspiration for solving human problems. Biomimicry can thus be seen as a way of learning from nature. When these ideas are used for developing and designing actual tools or materials, designs from nature originate. Humans have been looking to nature as a solution for their problems for centuries. Already 3000 years ago, the Chinese have been studying the silkworm (*Bombyx mori*) and tried to produce artificial silk. Also, many people were intrigued by the flying behavior of birds and other animals. A German engineer, Otto Lilienthal, even jumped off a hill in 1896 with wings strapped to his arms in an attempt to fly. Although he killed himself during this experiment, he inspired the Wright brothers for the development their airplanes in the beginning of the 20th century (FIGURE 1.8).

The development and innovation of products can be compared to thousands of years of natural selection, where morphologies that have a selective advantage are often favored over others. One of the most famous inspirations from nature is probably Velcro, which was invented by the Swiss engineer George De Mestral. The idea for this new material occurred by looking at burrs that often got stuck into his dog's hair and discovering that those burrs have tiny hooks at the end of each spine. By mimicking these hooks on a fabric, Velcro arose (De Mestral, 1973).

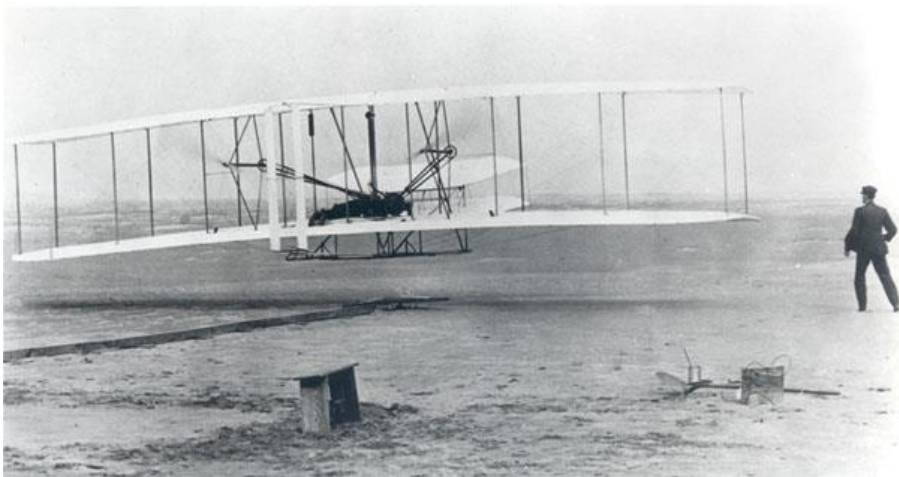


FIGURE 1.8 – The Wright brothers' first heavier-than-air flight on December 17, 1903 (Adapted from GRIN – Great Images in NASA).

In recent years, designs from nature gain popularity, which manifests in an increasing amount of publications and conference contributions within the field of biomimetics during the last 15 years (Lepora et al., 2013). A lot of research has been performed in the field of soft robotic designs, inspired by specialized structures encountered in animals, such as the elephant trunk (Hannan and Walker, 2002), the tentacles of octopus (Calisti et al., 2011, Laschi et al., 2009), the body of snakes (Hopkins et al., 2009, Kai and Simaan, 2006, Simaan, 2005, Simaan et al., 2004, Xu and Simaan, 2006) or the tail of lizards (Zhao et al., 2013, Sanders, 2012).

When studying the tail morphology of syngnathid fishes, the idea originated to use it as bio-inspiration for the development of serially articulated systems that are characterized by a combination of firmness, flexibility and have the potential for miniaturization. The natural variation among the tails of these different morphotypes goes from very firm and rigid systems (as seen in pipefishes and seadragons) to very flexible, but less firm systems (as seen in some pipehorses) but also systems that combine flexibility and firmness (as seen in seahorses). As the smallest adult seahorse known (*Hippocampus denise*) has a length of only 16 mm (Lourie and Randall, 2003), this biological system is also suitable for miniaturization.

1.2. Aims and thesis outline

1.2.1. General aims

This thesis is a continuation of an interdisciplinary project funded by the Research Foundation – Flanders (FWO, grand number 3G013709) that focused on biological engineering. The main aim of this interdisciplinary project was to study the biomechanics of the seahorse tail (more specific, the tail of the longsnout seahorse – *Hippocampus reidi*) and transform this into a virtual, dynamic, parametric model that could mimic the grasping behavior of this animal and could help to understand the relation between form and function of different parameters (Praet, 2013). By using this model, the influence of different parameters (from which it could be expected that they play a role in the grasping behavior of the tail) could be tested, as well as the impact of changing these parameters on tail bending (both at the mechanical and kinematical level).

In this thesis, not only additional prehensile species (seahorses as well as pipehorses) are studied, but also the ancestral condition (as found in pipefishes). By doing so, the evolutionary pattern from a non-prehensile tail to a prehensile one could be studied within the family of the syngnathid fishes and the structural and functional differences between prehensile and non-prehensile tails could be characterized by comparing the different

morphotypes. It can be assumed that natural selection for an increased grasping performance in prehensile tailed species will be translated into a typical morphology, that is different from the one observed in non-prehensile species. By trying to determine the characteristics that go along with this shift from a non-prehensile to a prehensile tail within an evolutionary framework, it should be possible to translate these characteristics into a database which links form and function of relevant operators and variables.

1.2.2. Thesis outline and specific aims

This thesis is composed of nine chapters.

The **1ST (AND CURRENT) CHAPTER** provides the reader with a short introduction covering the morphology of fish tails in general and the species diversity within syngnathid fishes. Also the concepts mimicry, biomimetics and design from nature are shortly explained and illustrated. This chapter concludes with the general aims and an overview of the outline of this thesis.

In the **2ND CHAPTER**, an overview of the examined specimens, their origin and the methods they're used for is given. Also, a brief overview of the used techniques is provided in this chapter. The next chapters dealing with the more specific topics of this thesis will comprise a detailed description of the used methods.

The results part of this thesis starts with the **3RD CHAPTER**. This chapter explores the pattern that characterizes the convergent evolution towards tail grasping within the family of syngnathid fishes by comparing the caudal musculoskeletal organization, as well as the passive bending capacities in pipefish (the ancestral condition), seahorse and pipehorse (possessing a convergently evolved prehensile tail). The overall hypothesis of this chapter is that prehensile functioning of the tail only became possible after substantial modifications of the musculoskeletal system (as observed in seahorses; Hale, 1996) and that the configuration in the pipehorse representatives would be similar to those in seahorses and thus differing from that in pipefish representatives. Differences in passive bending capacities between species, but also between the different bending directions are expected.

In the **4TH CHAPTER**, the morphological variation within and between the tails of different syngnathid fishes is explored by using 3D morphometric analyses based on surface meshes. Both proximo-distal and dorso-ventral shape variation within tails are studied, as well as inter-individual differences between prehensile and non-prehensile species. This chapter

focuses only on the variation of the skeletal elements and not on the different muscles organizations encountered in CHAPTER 3.

The 5TH CHAPTER covers bending experiments performed on fresh tail tissue of both seahorse and pipefish to determine if there is a difference in tail stiffness between those two morphotypes, as well as to look for regional differences within one tail. Also, it was investigated how the outer skin, dermal plates, muscles and vertebrae each contribute to the tail stiffness.

In the 6TH CHAPTER, the observed shape differences within and between the tails of the different syngnathid morphotypes obtained through the morphometrics study (CHAPTER 4) were implemented into a virtual, dynamic model to study if these differences can be related to tail flexibility. For each shape difference, an addition to an existing model developed by Tomas Praet (Praet, 2013) was written, so that the influence of each characteristic separately could be studied as well as the effect of combining them.

All results are discussed in CHAPTER 7. The obtained results from the four results chapters are combined and integrated with each other to explain how tail grasping could evolve within the family of the syngnathid fishes. Also future perspectives will be discussed. To finish, three potential applications that can benefit from the knowledge obtained within the framework of this thesis will be presented.

A brief summary of this doctoral thesis (in both Dutch and English) can be found in CHAPTER 8.

CHAPTER 2: MATERIAL & METHODS

2.1 Material

Several specimens of different seahorse, pipehorse, pipefish and seadragon species were used during the course of this PhD research. An overview of the used specimens and their origin can be found in TABLE 2.1. Specimens are either commercially obtained (C), obtained from museum collections (MNHN - Museum National d'Histoire Naturelle, SAMA - South Australian Museum) or obtained from research institutes (CSIRO - Commonwealth Scientific and Industrial Research Organization). Collection numbers can be found in TABLE 2.2. Commercially obtained specimens were all euthanized by using an overdose of MS222 (Sigma Aldrich) or benzocaine, prior to fixation or freezing. Species were selected based on their phylogenetic position within syngnathids, so that the major clade-related morphotypes, from primitive to derived, were included. All specimens studied were adult specimens.

species name	Origin	Method
Seahorse		
<i>Hippocampus abdominalis</i>	C	μCT-scanning with staining for soft tissue, 3D reconstructing
<i>Hippocampus abdominalis</i>	C	dissection + nitric acid treatment
<i>Hippocampus abdominalis</i>	C	bending experiment
<i>Hippocampus breviceps</i>	MNHN	μCT-scanning, 3D reconstructing, morphometry
<i>Hippocampus reidi</i>	C	phase contrast synchrotron x-ray radiation, 3D reconstructing
<i>Hippocampus reidi</i>	C	μCT-scanning, 3D reconstructing, morphometry
<i>Hippocampus reidi</i>	C	histological sectioning
<i>Hippocampus reidi</i>	C	clearing and staining
<i>Hippocampus subelongatus</i>	C	bending experiment
<i>Hippocampus zosterae</i>	C	phase contrast synchrotron x-ray radiation, 3D reconstructing, morphometry
Pipefish		
<i>Corythoichthys intestinalis</i>	C	μCT-scanning, 3D reconstructing, morphometry
<i>Corythoichthys intestinalis</i>	C	μCT-scanning with staining for soft tissue, 3D reconstructing
<i>Corythoichthys intestinalis</i>	C	clearing and staining
<i>Corythoichthys intestinalis</i>	C	bending experiment
<i>Dunckerocampus pessuliferus</i>	C	μCT-scanning, 3D reconstructing
<i>Doryrhamphus melanopleura</i>	C	μCT-scanning, 3D reconstructing
<i>Syngnathus acus</i>	C	μCT-scanning with staining for soft tissue, 3D reconstructing
<i>Syngnathus acus</i>	C	dissection + nitric acid treatment
Pipehorse		
<i>Acentronura gracilissima</i>	MNHN	μCT-scanning, 3D reconstructing, morphometry
<i>Haliichthys taeniophorus</i>	CSIRO	phase contrast synchrotron x-ray radiation, 3D reconstructing, morphometry
<i>Haliichthys taeniophorus</i>	CSIRO	clearing and staining
<i>Idiotropiscis australe</i>	SAMA	μCT-scanning, 3D reconstructing
<i>Solengnathus hardwickii</i>	MNHN	μCT-scanning, 3D reconstructing, morphometry
<i>Syngnathoides biaculeatus</i>	C	phase contrast synchrotron x-ray radiation, 3D reconstructing, morphometry
<i>Syngnathoides biaculeatus</i>	C	histological sectioning
<i>Syngnathoides biaculeatus</i>	C	clearing and staining
Seadragon		
<i>Phyllopteryx taeniolatus</i>	MNHN	μCT-scanning, 3D reconstructing, morphometry

TABLE 2.1 – Overview of used species, their origin and the methods they're used for. C: commercially obtained, MNHN: Museum National d'Histoire Naturelle (France), SAMA: South Australian Museum (Australia), CSIRO: Commonwealth Scientific and Industrial Research Organization (Australia).

species name	Origin	Collection number
<i>Hippocampus breviceps</i>	MNHN	1890-0371
<i>Acentronura gracilissima</i>	MNHN	1904-0298
<i>Haliichthys taeniophorus</i>	CSIRO	unregistered specimens
<i>Haliichthys taeniophorus</i>	CSIRO	unregistered specimens
<i>Idiotropiscis australe</i>	SAMA	F720
<i>Solengnathus hardwickii</i>	MNHN	0000-6042
<i>Phyllopteryx taeniolatus</i>	MNHN	0000-9213

TABLE 2.2 – Collection number of loaned specimens

2.2 Methods

What follows below is a summarized overview of all the analytical methods that were applied. Details about each of the methods are provided in the corresponding chapters.

2.2.1. Scanning procedures

Three different scanning methods were used and are described below. More details about the resulting voxel sizes can be found in CHAPTER 3 (SECTION 3.3.2).

2.2.1.1 μ CT-scanning

All μ CT-scans (except those of *Idiotropiscis australe*) were performed at the Centre for X-ray Tomography of Ghent University (UGCT), using the transmission tube head, at 100 kV tube voltage and with 1000 projections over 360°. The pixel pitch of the detector varied between 127 μ m and 400 μ m. One specimen of *I. australe* was scanned at the Australian museum (with the pixel pitch of the detector being 8.6 μ m), and the raw data was further processed at the UGCT.

2.2.1.2. μ CT-scanning with staining for soft tissue visualization

To visualize soft tissue, certain animals (see Table 2.1) were stained before scanning. Phosphomolybdic acid (PMA) was chosen as coloring agent, as previous research showed that this is the best coloring agent for the visualization of muscle tissue, as well as it avoids shrinkage effects as frequently induced by Lugol's iodine solution (Descamps et al., 2014). The PMA staining was performed for 36 hours, with a concentration of 2.5% solution in demineralized water. Different attempts were made to MRI scan specimens at the preclinical imaging research facility of Ghent University (Infinity Lab) in order to visualize soft tissue. However, the resulting resolution was not sufficient enough to discriminate between different tissue types and/or to make soft tissue reconstructions in Amira.

2.2.1.3 Phase contrast synchrotron x-ray radiation

The phase contrast synchrotron x-ray radiations, a high-performant way of μ CT-scanning, were performed at the European Synchrotron Radiation Facility in Grenoble by Renaud Boistel (Université de Poitiers). This allowed a detailed visualization of muscle and connective tissue organization without threatening the specimens with any coloring agent. The amount of radiographic images taken per specimen varied between 800 and 1844, with a resolution of 2048 x 2048 pixels (except for *Hippocampus zosterae*, with a resolution of 2007 x 2007) and a resulting voxel size of 7.46 μ m (except for *H. zosterae*, with a voxel size of 8 μ m). The radiographic images were acquired using a FReLoN CCD camera.

2.2.2 *In toto* clearing and staining

To study the gross plate morphology (see chapter three), specimens were *in toto* cleared and stained following a modified protocol of Taylor and Van Dyke (1985). Modifications consist of not performing the degreasing, bleaching, final cleaning and guanine removal steps and adjusting the time steps for neutralization and clearing (TABLE 2.3).

step	solution	duration
fixation	buffered formaldehyde solution (10%)	24h
dehydration	50 % ethyl alcohol	12h
	70 % ethyl alcohol	12h
	96 % ethyl alcohol	12h
	absolute alcohol	12h
	absolute alcohol	12h
cartilage staining	9-30 mg alcian blue 8GX in 100 ml of 40 % glacial acetic acid and 60% absolute ethyl alcohol	21h
neutralisation	saturated borax ($\text{Na}_2\text{B}_4\text{O}_7 \cdot 10\text{H}_2\text{O}$)	51h
clearing	enzyme buffer of 0.45 g purified trypsin in 400 ml of 30% saturated borax	100h
bone staining	0.1% alzarine red S solution in 0.5% KOH	
cleaning	rinse in distilled water	
Glycerin storage	40% glycerine + 60% 0.5% KOH	12h
	70% glycerine + 30% 0.5% KOH	12h
	100% glycerine	storage

TABLE 2.3 – Clearing and staining protocol modified from Taylor and Van Dyke (1985)

2.2.3 Histological sectioning

Serial histological sections were used for a more detailed study of the anatomical differences, and more specific the study of tendon attachment sites (see CHAPTER 3). To generate these sections, the tail was embedded in Technovit 7100 and 5- μm sections were cut with a Polycut Leica SM2500 microtome with a tungsten-carbide knife and stained with toluidine. Images of the sections were obtained using an Olympus BX41 microscope and Colorview camera.

2.2.4 Nitric acid treatment

To determine the average fiber length, the hypaxial muscles of the distal part of the tail of a *Syngnathus acus* and a *H. abdominalis* specimen were dissected and immersed in 30% nitric acid (HNO_3 , Sigma - Fluka, product number 79560, CAS 51429-74-4). After about 20h, individual fibers were teased apart and the nitric acid reaction was stopped with an excess of saturated Borax solution (disodium tetraborate) (Herrel et al., 1998). The individual fibers were photographed using a Colorview 8CCD camera mounted on an Olympus SZX9 stereoscope and measured using ANALYSIS 5.0. The corresponding measurements are discussed in CHAPTER 3.

2.2.5 3D-reconstructing

All scanned data was processed to generate graphical 3D-reconstructions of both skeletal and muscular tissue using Amira 5.2.2 (Visage Imaging, San Diego, CA, USA). All musculoskeletal elements were separately segmented, using the Segmentation Editor, a tool for interactively segmenting 3D image data. Segmentation was done by first selecting voxels belonging to the same element (*e.g.* the most proximal vertebra) by using the Magic Wand (in case of good quality image data) or by using the Brush (in case of lower quality image data) and then assigning these voxels to a particular material (*e.g.* vertebra_1). Labels were stored in a LabelField and used to render polygonal surfaces, by using the SurfaceGen Module. This module computes a triangular approximation of the interfaces between the different materials in the LabelField Module. The smoothing option was set to “none” to avoid uncontrolled loss of details because of too extensive smoothing. By using an additional SmoothSurface Module, surfaces were smoothed by shifting its vertices towards the average position of its neighbours. In case of boundary vertices, only the neighbours that are also located on a boundary are considered. In this way, sharp boundaries are preserved, which is not the case if one of the smoothing options in the SurfaceGen Module is used. Finally, the 3D-surface can be visualized by using a SurfaceView

Module. A detailed analysis of these reconstructions can be found in chapter three. Based on these detailed reconstructions, schematic overviews of muscles and tendons were made using Rhinoceros 5 (R. McNeel & associates) (also see CHAPTER 3).

2.2.6 Morphometry

To determine the specific differences in skeletal structure within and between the studied specimens, morphometric analyses were performed using a MevisLab application designed by Peter Claes and Bart de Dobbelaer at the Medical Imaging Research Centre at the University Hospital Gasthuisberg (Leuven, Belgium). This software was adapted specifically for this research and more details on the workflow can be found in CHAPTER 4.

A 3D surface-mesh based approach was preferred over a 2D landmark based one. This method provides a more comprehensive quantification of shape variation, which is particularly relevant for this study for the following reasons. First, the skeletal elements to be studied have a rather complex shape, what makes it difficult to visualize each element in the same standardized 2D orientation. Second, when using a traditional 2D landmark based approach, essential spatial information on segment length, depth and width is lacking in the analyses. Third, because of the complexity of the structures, it appeared to be difficult to find enough landmarks that could provide a comprehensive description of the overall shape of plates and vertebrae.

2.2.7 Tail stiffness

Tail stiffness was determined by using an experimental setup that was designed and drawn in 3D using Rhinoceros (version 5, R. McNeel & associates) and 3D printed on a Stratasys UPrint SE plus 3D printer, using ABSplus P430. This setup could be mounted onto an Instron 5944 electromechanical testing system (Instron, Norwood, MA, USA), which was equipped with a 10N load cell. Tissue samples of 5 segments were fixated into the experimental setup. A bending movement could be induced and the force needed to obtain a certain translation could be measured. More details on the experimental setup can be found in CHAPTER 5.

2.2.8 Syngnathid tail modelling

Virtual, dynamic models were used to determine what the implications are of the different skeletal characteristics (based on the morphometric study) on the kinematics and bending performance of the tail and which specific morphological adaptations could lead to the observed differences in tail flexibility (see CHAPTER 6). During a former study, a pyFormex

script was created to mimic the tail bending of *Hippocampus reidi* (Praet, 2013). Four additions on this script were written in which the geometry of vertebrae and/or dermal plates could be altered. The result of running these different script in pyFormex (version 0.9.1) are Abaqus input files. These files were solved using Abaqus (version 6.11-1, Dassault Systems, Vlizy-Villacoublay, France) and the results could be processed in the visualization module of Abaqus.

CHAPTER 3: MORPHOLOGY

GRASPING CONVERGENT EVOLUTION IN SYNGNATHIDS:
A UNIQUE TALE OF TAILS

MODIFIED FROM NEUTENS C, ADRIAENS D, CHRISTIAENS J, DE KEGEL B, DIERICK M,
BOISTEL R & VAN HOOREBEKE L, JOURNAL OF ANATOMY (2014)

3.1 Abstract

Seahorses and pipehorses both possess a prehensile tail, a unique characteristic among teleost fishes, allowing them to grasp and hold onto substrates such as sea grasses. Although studies have focused on tail grasping, the pattern of evolutionary transformations that made this possible is poorly understood. Recent phylogenetic studies show that the prehensile tail evolved independently in different syngnathid lineages, including seahorses and several types of so-called pipehorses. This study explores the pattern that characterizes this convergent evolution towards a prehensile tail, by comparing the caudal musculoskeletal organization, as well as passive bending capacities in pipefish (representing the ancestral state), pipehorse and seahorse. To study the complex musculoskeletal morphology, histological sectioning, μ CT-scanning and phase contrast synchrotron scanning were combined with virtual 3D-reconstructions. Results suggest that the independent evolution towards tail grasping in syngnathids reflects at least two quite different strategies in which the ancestral condition of a heavy plated and rigid system became modified into a highly flexible one. Intermediate skeletal morphologies (between the ancestral condition and seahorses) could be found in the pygmy pipehorses and *H. taeniophorus*, which are phylogenetically closely affiliated with seahorses. This study suggests that the characteristic parallel myoseptal organization as already described in seahorse (compared with a conical organization in pipefish and pipehorse) may not be a necessity for grasping, but represents an apomorphy for seahorses, as this pattern is not found in other syngnathid species possessing a prehensile tail. One could suggest that the functionality of grasping evolved before the specialized, parallel myoseptal organization seen in seahorses. However, as the grasping system in pipehorses is a totally different one, this cannot be concluded from this study.

3.2 Introduction

Unlike in pipefishes and other teleost fishes, the tail of seahorses and pipehorses has become modified into a prehensile apparatus, a function unique among fishes. Seahorses and pipehorses no longer possess a caudal fin (which is also characteristic of seadragons) and are able to grasp and hold on substrates during feeding and hiding, by using their tail (Blake, 1976, Hale, 1996, Teske and Beheregaray, 2009, Weber, 1926). It was already suggested that their vertical position in the water column originated in association with an Indo-Pacific expansion of sea grass habitats (Teske and Beheregaray, 2009) and that the bent orientation of their head (perpendicular to their vertical positioned body) could be adaptive for their specific way of feeding, *i.e.* pivot feeding (Van Wassenbergh et al., 2011).

Despite the fact that they are slowly moving organisms, they can escape predation by crypsis, adopting colors and camouflage specific to their environment, by their fast dorsal fin movement, which exceeds the flicker fusion threshold of their predators (Breder and Edgerton, 1942), or by being nocturnal (Kuitert, 2009, Teske and Beheregaray, 2009).

The syngnathid tail comprises a series of articulating, and frequently ornamented (Kuitert, 2009, Lees et al., 2011), bony plates (four plates per body segment) surrounding the caudal muscle bundles, which are anchored on the central vertebral column (Hale, 1996). A recent study (Porter et al., 2013) showed that this array of bony plates in seahorses functions as a flexible, dermal armor and protects the tail segments and vertebrae from fracture. The ancestral syngnathid condition, as seen in ghost pipefishes (genus *Solenostomus*, sister taxon to Syngnathidae) and true pipefishes (Jungersen, 1910), is characterized by a relatively stiff tail. This explains its limited use in swimming, which is mainly done with dorsal and pectoral fins (Ashley-Ross, 2002). Keeping their body horizontal, pipefishes forage in the open water (especially the flagtail pipefishes – Doryrhamphinae; Kuitert, 2009) or close to the sea floor. Pipehorses, seemingly intermediate between seahorses and pipefishes, also exist and are characterized by a horizontal body posture, the absence of a tail fin and the presence of a prehensile tail and can be subdivided into two morphotypes. The first type (further referred to as ‘type I pipehorse’) comprises the very rare pygmy pipehorses (genera *Idiotropiscis*, *Acentronura*, *Kyonemichthys* and *Amphelikurus*), which superficially look like seahorses (to which they are a sister group), but with a horizontal body posture (Gomon, 2007, Kuitert, 2009, Teske and Beheregaray, 2009). The second type (further referred to as ‘type II pipehorse’) shows a similar morphology to that of pipefishes but possesses a prehensile tail. These pipehorses do not form a monophyletic group and are phylogenetically nested within the pipefishes (FIGURE 1.7). The name pipehorse thus refers rather to a morphological characteristic (the presence of a prehensile tail) than to a phylogenetically accepted name. There is still some debate about the common name of *H. taeniophorus*. Like seahorse and pipehorse, it possesses a prehensile tail and is referred to as the ribboned seadragon (Kuitert, 2009), the ribboned pipehorse (Munro, 1958) or the ribboned pipefish (Dawson, 1985). There is also no consensus on the phylogenetic position of *H. taeniophorus*. According to some studies, this species is nested within the pipefishes (Wilson and Orr, 2011, Wilson and Rouse, 2010), whereas others (Hamilton et al., 2009) suggest a close relation to the pygmy pipehorses and a sister-relation to the seahorses. We chose to assign *H. taeniophorus* to the type 2 pipehorses because of the similarities in external morphology (thus possessing a pipefish-like body with a prehensile tail). Seadragons – comprising only three species, *Phyllopteryx taeniolatus*, *Phyllopteryx dewysea*

and *Phycodurus eques* – are characterized by a horizontal body posture and the absence of both a caudal fin and a prehensile tail.

Tail prehension is not unique for vertebrates, having arisen in sauropsids (Zippel et al., 1999, Bergmann et al., 2003) and mammals (German, 1982, Organ, 2010) as well. Although it might seem quite unlikely that during evolution, a complex system such as the musculoskeletal caudal system in fishes would have independently evolved into a prehensile tail more than once within a single clade at the family level, recent phylogenetic studies (Hamilton et al., 2009, Teske and Beheregaray, 2009, Wilson and Orr, 2011) suggest this to be a likely scenario (FIGURE 3.1). Prehensile tails seem to have originated several times independently in syngnathid fishes, although it is not yet clear how many times exactly (Teske and Beheregaray, 2009, Wilson and Orr, 2011, Wilson and Rouse, 2010).

Little is known about the modifications of the caudal musculoskeletal system associated with such a drastic functional shift (from a non-prehensile to a prehensile tail). Previous studies (Anthony and Chevroton, 1913, Hale, 1996) showed that seahorses have plates interconnected by sliding joints that are created by elongated spines. In addition, hypaxial muscle fibers lie in between parallel sheets of connective tissue (myosepta), rather than within a conical organization more typically found in teleost fishes (Gemballa and Roder, 2004). Unlike in these teleosts, the myosepta in seahorses span several vertebral segments between their medial and lateral insertion (Hale, 1996). Median ventral muscles, interconnecting hemal spines on the vertebrae in seahorses, are considered to be modified ventral fin muscles (infracarinalis posterior muscles) (Hale, 1996). It is hypothesized that these median ventral muscles are responsible for sustained holding, whereas hypaxials may power fast grasping (Anthony and Chevroton, 1913, Hale, 1996). However, the structural basis for the apparent complex motor control of which seahorses seem to be capable, is so far not properly understood. As no comparison with the ancestral condition, as found in pipefishes, or the convergent condition in pipehorses has been performed, it is not possible to draw any conclusions about how this unique trajectory towards tail grasping within syngnathid fishes (and fishes in general) could have evolved.

In this study, we test several hypotheses that may help to elucidate this, by comparing the musculoskeletal anatomy and bending capacity in pipefish, seahorse, pipehorse (both morphotypes) and *H. taeniophorus*. As such, this study may provide a solid base for a more comprehensive survey of the structural modifications of the tail in the different lineages within the Syngnathidae, and their implications for function with respect to grasping. The overall hypothesis of this study is that prehensile function only became possible after substantial modifications of the musculoskeletal system (as observed in seahorses; Hale,

1996) and that the configuration in the studied pipehorse representatives would be similar to that in seahorses, thus differing from that in the pipefish representatives. The maximal bending angle of the tail (in lateral, ventral and dorsal direction) is quantified to determine the passive prehensile capacities of the tail of pipefish (reflecting the ancestral syngnathid condition with limited ventral and dorsal bending), seahorse and type II pipehorse. For the latter two, we expect ventral bending capacities to be more extensive (as in seahorses; Peters, 1951, Weber, 1926). We expect that the passive bending capacity is mainly influenced by the bony plate morphology and that the vertebral column shows the same flexibility in all species studied. Concerning the skeletal morphology, we expect that species with a prehensile tail share the condition where plates are interconnected by elongated, sliding joints (rather than fully abutting edges, as seen in non-prehensile species). As gradual reduction in plate size is present towards the distal tip in seahorses (Hale, 1996), with a consequent increasing flexibility, we expected to find a similar reduction in plate size in those species possessing a prehensile tail. The vertebral morphology of *Hippocampus kuda* and *H. hippocampus*, both seahorses, has already been described (Bruner and Bartolino, 2008, Hale, 1996). To our knowledge, no detailed information on that in other seahorses, pipehorses, pipefishes and seadragons is available. As it is generally assumed that the number of vertebrae is related to body flexibility (Brainerd and Patek, 1998, Breder, 1926), we expect species with a prehensile tail to have a higher vertebral count than pipefishes. Concerning the muscular organization, we expect to find parallel myoseptal sheet spanning multiple vertebrae in species with a prehensile tail (compared with a conical organization in pipefishes). We also expect the presence of median ventral muscles (MVM), interconnecting subsequent hemal spines, hypothesized to be responsible for sustained grasping (Hale, 1996). Also, as extensive ventral bending is presumed to be facilitated by a substantial shortening of muscles involved (based on the assumption that a maximal shortening of 50% of the muscle fibers is achieved; Gordon et al., 1966, Hall, 1999), we expect to find longer muscle fibers in the hypaxial muscles of species possessing a prehensile tail. To further test the hypothesis on the convergent evolution of the prehensile tail in syngnathid fishes, a character state reconstruction was performed based on two different phylogenies (Hamilton et al., 2009, Wilson and Orr, 2011).

As shown below, the predictability of the morphology based on functional performance is not as straightforward as might be suggested. Even more striking than the fact that grasping tails evolved more than once within syngnathids, is that at least two evolutionary strategies have resulted in different solutions to the same problem. Although no generalizing predictions can yet be made about evolutionary modifications that characterize the multiple lineages of pipehorses, these different evolutionary strategies do seem to

corroborate the hypothesis that seahorses and both morphotypes of pipehorses became adapted within a different ecological context where grasping proved to be beneficial: hanging vertically while grasping on sea grasses vs. horizontally while attached to macroalgae (Teske and Beheregaray, 2009). Taking into account estimated time divergences of the different lineages (Teske et al., 2004), these apparently extreme functional shifts towards tail grasping in syngnathids did occur multiple times during evolution, within a short time frame (*i.e.* somewhere between 50 and 25 mya).

3.3 Material and methods

3.3.1 Specimens studied

Several specimens (see TABLE 2.1) of four seahorse species (*Hippocampus reidi*, *H. capensis*, *H. abdominalis* and *H. breviceps*), five pipehorse species (*Syngnathoides biaculeatus*, *Solegnathus hardwickii*, *Idiotropiscis australe*, *Acentronura gracilissima* and *Haliichthys taeniophorus*) and four pipefish species (*Corythoichthys intestinalis*, *Dunckerocampus pessuliferus*, *Doryrhamphus melanopleura* and *Syngnathus acus*) were studied. Species were selected based on their phylogenetic position within syngnathids, so that the major clade-related morphotypes, from primitive to derived, were included. All pipefishes, *H. reidi*, *H. capensis*, *H. abdominalis* and *S. biaculeatus* were commercially obtained through the aquarium trade. These specimens were euthanized with an overdose of MS222 (Sigma Aldrich), prior to fixation in 4% formaldehyde. Specimens of *H. breviceps*, *S. hardwickii* and *A. gracilissima* were obtained from the Muséum National d'Histoire Naturelle (MNHN – France, resp. MNHN 1890-0371, MNHN 0000-6042 and MNHN 1904-0298) and two *H. taeniophorus* specimens from the Commonwealth Scientific and Industrial Research Organization (CSIRO – Australia, unregistered specimens). The *I. australe* specimen belongs to the collections of the South Australian Museum (SAMA F720).

3.3.2 Musculoskeletal morphology

One specimen of *D. pessuliferus*, *D. melanopleura*, *H. breviceps*, *S. hardwickii* and *A. gracilissima* were μ CT-scanned to study the skeletal organization. To visualize 3D soft tissue anatomy, one specimen each of *S. acus*, *C. intestinalis* and *H. abdominalis* was treated with phosphomolybdic acid (submerged in 2.5% solutions for 36 h) (Metscher, 2009) and submitted to μ CT-scanning. All the above specimens were scanned at the Centre for X-ray Tomography at Ghent University (UGCT), using the following setup: 7 kV tube voltage and 1000 projections over 360°. The pixel pitch of the detector varied between 127 μ m and 400 μ m and the resulting voxel sizes were respectively 3.52, 35.17, 33.12, 32.99 and 8.91 μ m for

the non-stained specimens and 23.56, 26.54 and 32.14 μm for the specimens treated with phosphomolybdic acid. Two adult specimens of *H. reidi* and one specimen each of *S. biaculeatus* and *H. taeniophorus* were scanned at the European Synchrotron Radiation Facility in Grenoble, using phase contrast synchrotron x-ray radiation. A total of respectively 1677, 1844 and 1844 radiographic images with a resolution of 2048 x 2048 pixels and a voxel size of 7.46 μm were acquired using a FReLoN CCD camera. This allowed a detailed visualization of muscle and connective tissue organization. One specimen of *I. australe* was scanned at the Australian Museum (with a pixel pitch of the detector of 8.60 μm and a resulting voxel size of 6.46 μm) and the raw data was reconstructed at the UGCT. All μCT -data were processed to generate graphical 3D-reconstructions of bony plates and myosepta using AMIRA 5.2.2 (Visage Imaging, San Diego, CA, USA). Based on these detailed reconstructions, schematic overviews of muscles and tendons were made using RHINOCEROS (Version 5, R. McNeel & associates).

Gross plate morphology was studied on in toto cleared and stained specimens of *S. biaculeatus*, *C. intestinalis*, *H. reidi*, *H. capensis* and *H. taeniophorus* (protocol following Taylor and Van Dyke, 1985). The organization of myosepta and the attachment of tendons on the bony plates and vertebrae were also examined based on histological sections of *S. rostellatus*, *H. reidi* and *S. biaculeatus*. To generate these sections, the tail was embedded in Technovit 7100 and 5- μm sections were cut off with a Prosan Leica SM2500 microtome and stained with toluidine. Images of the sections were obtained using an Olympus BX41 microscope and Colorview camera. A parsimony ancestral state reconstruction was performed on cladograms resulting from different phylogenetic studies (Hamilton et al., 2009, Teske and Beheregaray, 2009, Wilson and Orr, 2011) using MESQUITE 2.75 (<http://mesquiteproject.org>).

3.3.3 Muscle fiber length

The hypaxial muscles of the distal part of the tail of an *S. acus* and *H. abdominalis* specimen were dissected and treated with nitric acid to separate the individual muscle fibers. Fibers were photographed using a Colorview 8CCD camera mounted on an Olympus SZX9 stereoscope. The length of 30 muscle fibers was measured using ANALYSIS 5.0. The hypaxial muscle fiber length of *S. biaculeatus* and *H. reidi* was determined using serial histological sections of the tail (embedded in Technovit 7100, 5- μm sections cut with a Leica SM2500 microtome and stained with toluidine). Images were obtained using an Olympus BX41 microscope and Colorview camera, and aligned in AMIRA 5.2.2 after which x, y and z coordinates of the origin and insertion of 30 muscle fibers were determined to calculate the average muscle fiber length. As specimens differed in total body size and hence segment

length, differences in muscle fiber length between species were tested using the ratio of the muscle fiber length vs. vertebral length in four species, referred to as relative muscle fiber length, with a Bonferroni-corrected Kruskal–Wallis test using PAST (Hammer et al., 2001).

3.3.4 Bending performance

Passive joint flexibility was determined by measuring the maximum angle of bending in both a pure ventral, dorsal and lateral direction. Cleared and stained specimens were secured with pins in a maximally bent position and photographs were taken with a canon EOS550 camera and a Sigma 150-mm macro lens. The line at the level of the vertebral column was traced three times for each species and each view using tpsDIG (Rohlf, 2008), which was subsequently subdivided into 100 equally sized segments. The angle between all segments was calculated, and the average angles (of the three replicated digitizations) were plotted.

3.4 Results

3.4.1 Musculoskeletal morphology

Plotting the characteristic ‘prehensile tail’ on the existing phylogenies, one can conclude that the prehensile tail evolved multiple times independently. If the phylogenetic study of Hamilton et al. (2009) is considered, the prehensile tail evolved four times independently within the family of syngnathid fishes (FIGURE 3.1). However, based on the second ancestral state reconstruction (phylogenetic study of Wilson and Orr, 2011, combined with the one of Teske and Beheregaray, 2009 for the position of the pygmy pipehorses), the prehensile tail evolved five times, but the independent evolution of it is not confirmed.

In pipefish, each vertebra is surrounded by four bony plates (further referred to as one segment), being a bilateral set of a dorsal and a ventral plate. Plates within a single segment interconnect through scarf joints [joints with overlapping flat surfaces (Hildebrand, 1995)], whereas subsequent segments interlock through a distinct caudal spine, which slides into a corresponding furrow on the plate posterior to it (further called the anterior furrow). Plates in pipefish form a tight set of articulating, skeletal segments, where any space in between segments is covered by intercalating plates (FIGURE 3.2A). Plates are connected through connective tissue to the vertebrae at the level of the neural arch (dorsal) and the transverse (lateral) and hemal (ventral) spines. In *Hippocampus*, plates are substantially reduced to a tetrahedral-like structure, still bearing a caudal spine that glides into a distinctive anterior furrow in the corresponding plate of the consecutive segment. The caudal spine is relatively

longer than in pipefish, due to the observed plate reduction. The intrasegmental connection is a reduced scarf joint, with only three ridges and corresponding furrows (FIGURE 3.3A). In the four pipehorse species studied, three different skeletal conditions were observed. In *S. biaculeatus* (a type II pipehorse), a similar condition as in the pipefish is found in the

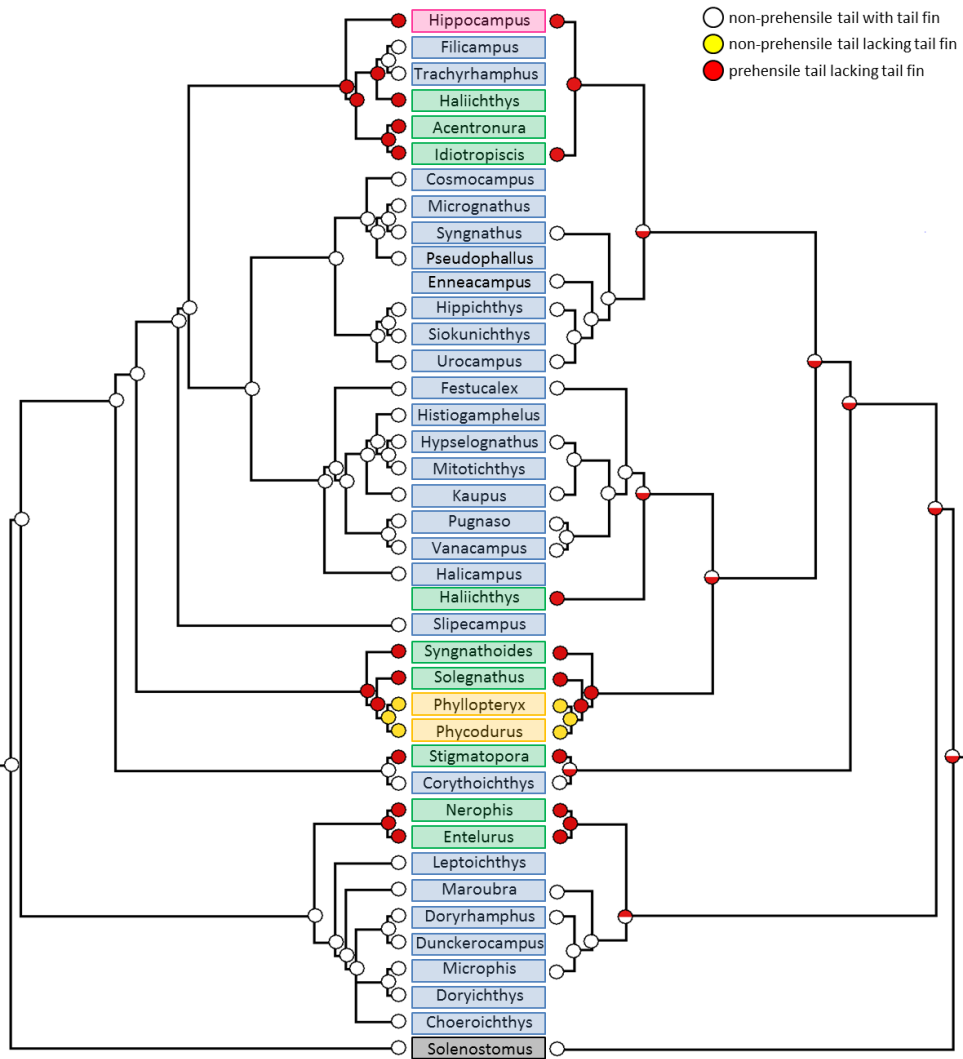


FIGURE 3.1 - Ancestral state reconstruction of grasping tails in syngnathids. Phylogenetic pattern towards the independent evolution of the prehensile tail in syngnathid fishes. Three different conditions can be discerned: (white circle) species with a non-prehensile tail possessing a tail fin, as seen in pipefish; (yellow circle) species with a non-prehensile tail lacking a tail fin, as seen in the seadragon species *Phyllopteryx taeniolatus* and *Phycodurus eques*; (red circle) species with a prehensile tail lacking a tail fin, as seen in pipe- and seahorses. The left cladogram is based on the phylogenetic study of Hamilton et al. (2009), the right on the study of Wilson & Orr (2011), with inclusion of the pygmy pipehorse (genus *Idiotropiscis*) based on Teske & Beheregaray (2009). *Solenostomus* belongs to a separate family of Solenostomidae, sister to Syngnathidae, and is used as an outgroup. The background color behind each genus name represents the common group to which the genus belongs (pipefish in blue, seadragon in yellow, pipehorse in green, seahorse in pink, Solenostomus in black).

proximal part of the tail (first 70% of the tail), but without the presence of intercalating plates. However, towards the distal tip (last 30%), plates become smaller until completely absent, ending in a series of approximately 20 vertebrae that are no longer surrounded by any plates (FIGURE 3.4A). This reduction of the plates starts more anteriorly at the ventral side, at a point where the dorsal plates still interlock through a caudal spine. In seahorse, the plates also become reduced in size, but each vertebra is covered by four bony plates up to the distal-most vertebrae. The organization of the proximal part of the tail (first 70%) in *S. hardwickii* (also a type II pipehorse and closely related to *S. biaculeatus*) is also similar to the one in pipefish (but with the presence of intercalating plates). In the prehensile part of the tail (last 30%), however, the ventral and dorsal plates of one segment are no longer directly opposite to each other, but show an alternating pattern of ventral and dorsal plates in the lateral view (FIGURE 3.4B1). There is also a reduction of the medial side of the ventral plates, which leaves out a gap in between the contralateral ventral plates (FIGURE 3.4B2). Thus, in this last 30% of the tail of *S. hardwickii*, there is, within one segment, no longer a connection through scarf joints between the contralateral ventral plates and between the dorsal and ventral plates. In addition, the last four vertebrae are no longer covered by any plates at the ventral side (FIGURE 3.4B). *Acentronura gracilissima* and *I. australe* (pygmy pipehorses, type I), both belonging to the sister group of *Hippocampus*, are characterized by an intermediate plate morphology. The dorsal bony plates are very similar to the plates of pipefish (forming a tight set of articulating, skeletal elements), but without the presence of intercalating plates, whereas the ventral plates are more similar to those observed in seahorses, with a strong reduction in plate size (FIGURE 3.4C). The plate morphology of *H. taeniophorus* strongly resembles the intermediate plate morphology seen in *A. gracilissima* and *I. australe* (FIGURE 3.5A).

The vertebral morphology in pipefish and pipehorse is similar to that of seahorse, *i.e.* amphicoelous vertebrae with a well-developed neural arch and anteroposteriorly thickened lateral processes (Hale, 1996). In a lateral view, the ventral side of the body of the vertebrae in the prehensile part of the tail of seahorse and pipehorse is shorter than its dorsal side, whereas the vertebrae in the non-prehensile part and those of pipefish are rectangular, as seen in most teleost fishes. As for the vertebral count, there is no significant difference in the total number of vertebrae between seahorse, pipehorse, seadragon and pipefish ($P > 0.05$) but the ratio of the number of vertebrae in the tail relative to the total number of vertebrae was significantly higher in species with a prehensile tail ($F = 11.216$; $P = 0.0092$).

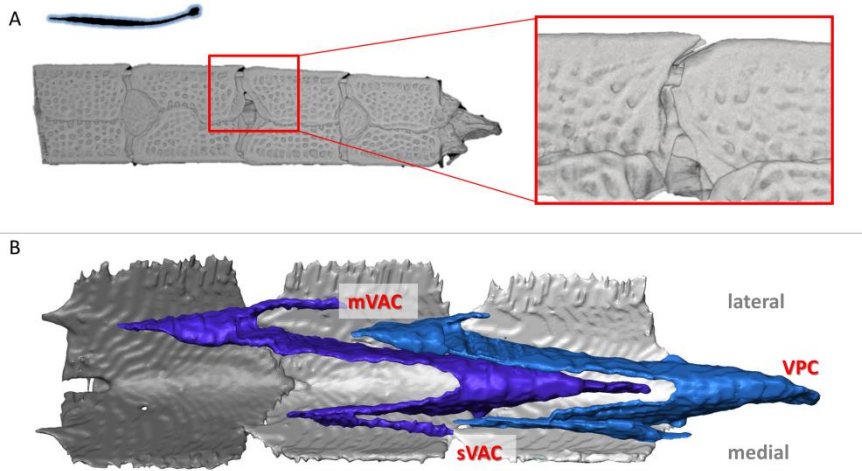


FIGURE 3.2 - Musculoskeletal organization in pipefish. High resolution 3D reconstructions of CT-data on the caudal part of the tail in pipefish (horizontal body posture, non-prehensile tail with tail fin), represented by *Corytoichthys intestinalis*. (A) Reconstruction of the caudal skeletal part of the tail (dermal and intercalating plates in grey), detail shows a lateral view of the caudal spine on the dorsal plates fitting into an anterior groove on the subsequent plate. (B) Reconstruction of the conical myoseptal organization (dermal plates in grey, myosepta in blue), with a main ventral anterior cone (mVAC), ventral posterior cone (VPC) and a secondary ventral anterior cone (sVAC).

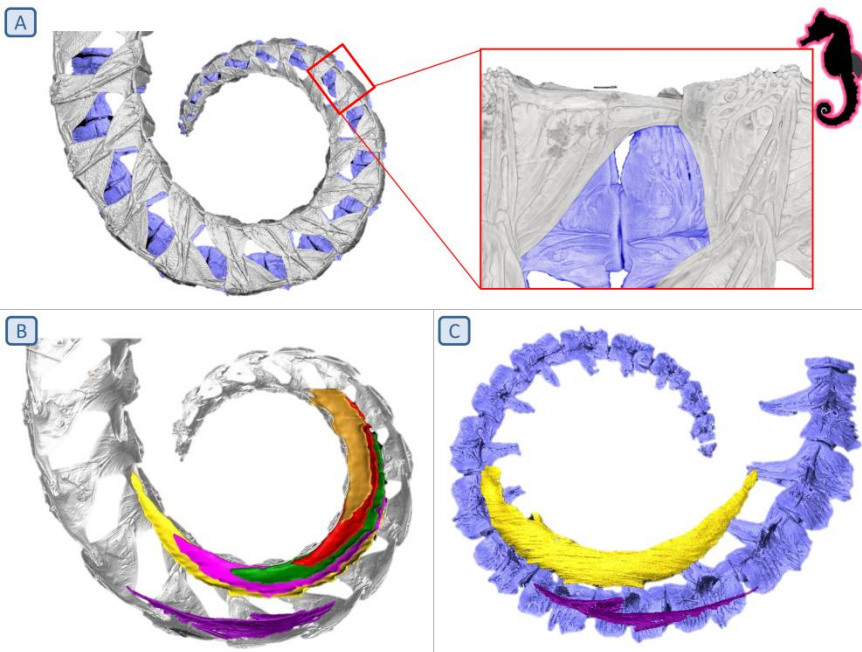


FIGURE 3.3 - Musculoskeletal organization in seahorse. High resolution 3D reconstructions of CT-data on the caudal part of the tail in seahorses (vertical body posture, prehensile tail lacking a tail fin), represented by *Hippocampus reidi*. (A) Reconstruction of the caudal skeletal part of the tail (dermal plates in grey, vertebrae in blue); detail shows a lateral view of the caudal spine on the dorsal plates fitting into an anterior groove on the subsequent plate, (B-C) Reconstruction of the parallel myoseptal organization (dermal plates in grey, vertebrae in blue, myosepta in different bright colors), from (B) a medial viewpoint with vertebrae removed and (C) a lateral viewpoint with dermal plates removed.

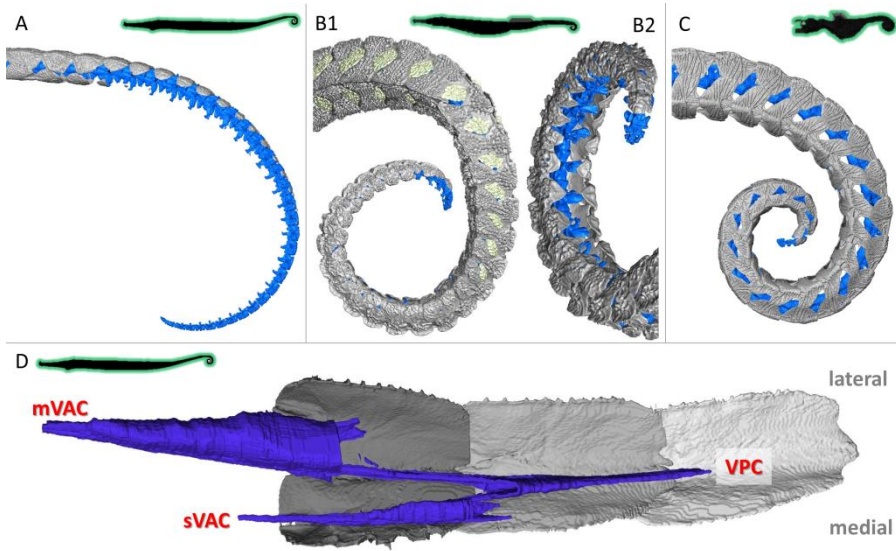


FIGURE.3. 4 - Musculoskeletal organization in pipehorse (part1). High resolution 3D reconstructions of CT-data on the caudal part of the tail in pipehorses (horizontal body posture, prehensile tail lacking a tail fin), represented by (A,D) *Syngnathoides biaculeatus* (type II pipehorse), (B) *Solegnathus hardwickii* (type II pipehorse) and (C) *Acentronura gracilissima* (type I/pygmy pipehorse). (A-C) Reconstruction of the caudal skeletal part of the tail (dermal plates in grey, vertebrae in blue). (D) Reconstruction of the conical myoseptal organization (dermal plates in grey, myosepta in blue), with a main ventral anterior cone (mVAC), ventral posterior cone (VPC) and a secondary ventral anterior cone (sVAC).

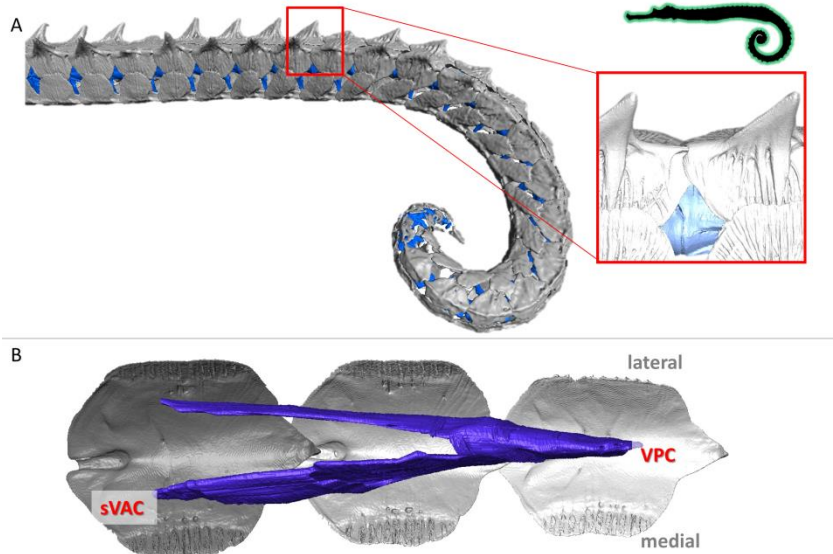


FIGURE.3.5 - Musculoskeletal organization in pipehorse (part 2). High resolution 3D reconstructions of CT-data on the caudal part of the tail in *H. taeniophorys* (horizontal body posture, prehensile tail lacking a tail fin). (A) Reconstruction of the caudal skeletal part of the tail (dermal plates in grey, vertebrae in blue); detail shows a lateral view of the caudal spine on the dorsal plates fitting into an anterior groove on the subsequent plate. (B) Reconstruction of the conical myoseptal organization (dermal plates in grey, myosepta in blue), with ventral posterior cone (VPC) and a secondary ventral anterior cone (sVAC).

In *Corythoichthys* and *Syngnathus* pipefish, myosepta in the hypaxial muscles are organized as conical structures, where three cones per segment lie between the transverse process and the hemal spine. This three-cone organization consists of two anterior pointing cones – one main (mVAC) and one secondary (sVAC) ventral anterior cone – and one ventral posterior pointing cone (VPC). In pipefish, this VPC is the largest cone, the mVAC and sVAC being of equal size, but smaller than the VPC (Gemballa et al., 2006). All three cones are connected to the ventral plates through a distinctive tendon (FIGURE 3.6). The mVAC connects through a lateral tendon (LT) on the plate anterior to the one bearing the connection with the sVAC through a secondary myorhabdoid tendon (SMT). These two tendons attach to two small spines at the anterior side of the plate, respectively at the lateral and ventral side of the anterior furrow. The VPC attaches through a myorhabdoid tendon (MT), which anteriorly splits into two slips that attach on both sides of the distinctive furrow at the rostral side of each plate. The tip of the caudal spine is embedded in this tendon (FIGURE 3.6). The epineural tendon (ENT) in these pipefish species is fused with the horizontal septum and thus is no longer visible as a thick, distinct tendon (terminology based on Gemballa et al., 2003, Gemballa et al., 2006). In seahorse, a completely different hypaxial myoseptal pattern is present, as was suggested in the literature (Hale, 1996), where parallel sheets of connective tissue interconnect the vertebrae with the plates. However, it is still not clear whether this connection is continuous along the length of the whole myoseptum or occurs by means of one attachment point (e.g. through a tendon) at both the anterior and the posterior side. In this study we found that these myosepta span up to eight segments, resulting in an increased number of septa enclosed in a single segment (FIGURES 3.4B & 3.4C). At their ventral face, the myosepta bear a distinct MT, inserting on a small elevation on the anterior side of the plate, at the ventral side of the anterior furrow (FIGURE 3.7B). In seahorse, the tip of the caudal spine is not embedded in the MT, which is the only tendon that can be distinguished in the hypaxial muscles of seahorses. The epaxial muscles show a modified conical pattern,

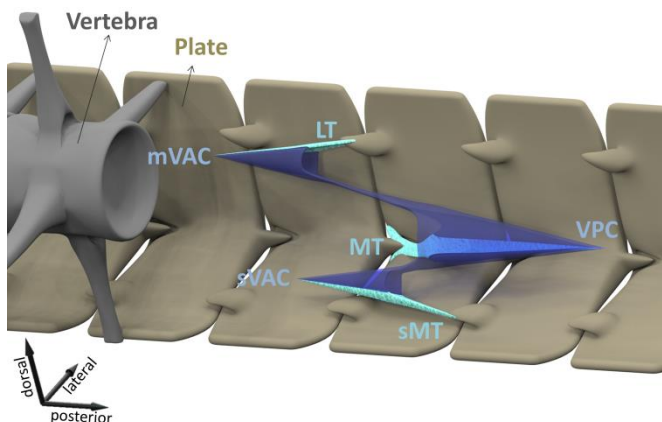


FIGURE 3.6 - Schematic overview of the conical organization of myosepta and tendons as found in the ancestral condition. Plates in brown, vertebra in grey, myosepta in blue (mVAC: main ventral anterior cone; VPC: ventral posterior cone; sVAC: secondary ventral anterior cone) and tendons in light green (LT: lateral tendon; MT: myorhabdoid tendon; SMT: secondary myorhabdoid tendon).

in which the main dorsal anterior cone (mDAC) is reduced. At the dorsal side, only the secondary dorsal anterior cone (sDAC) interconnects to the small anterior spine on the plate through a tendon, whereas the epaxial sloping part (ESP – the part between the dorsal posterior cone (DPC) and the mDAC) is connected to the parapophysis of the vertebrae (FIGURES 3.4B,C & 3.7B). In all seahorse species studied, the hemal spines are interconnected with median ventral muscles (MVM) (FIGURE 3.8B), which are absent in pipefish (FIGURE 3.8A). In *H. abdominalis* (one of the largest seahorse species), a similar muscular organization is also present on the dorsal side (median dorsal muscles – MDM), interconnecting two consecutive neural arches. In the *Syngnathoides* pipehorse, a pipefish-like three-cone organization of the hypaxial myosepta is present, but is distinct at two levels. First, the cones are extended, hence spanning about three segments instead of two. Secondly, the VPC is equal in size to the sVAC and the mVAC is the largest in size (FIGURE 3.5D). The myosepta are attached to the bony elements through three distinct tendons, similar to the pipefish. In the tip of the tail, where the bony plates are lacking, the myosepta fuse with the connective tissue of the skin. This pipehorse shares the presence of MVM with seahorses, interconnecting two consecutive hemal spines (FIGURE 3.8C). In *H. taeniophorus*, a conical organization of the myosepta was observed, with a reduced mVAC, similar to the epaxials in seahorses (FIGURE 3.6B). However, as no attachment site of the myosepta to the bony plates could be unambiguously visualized, it cannot be excluded that

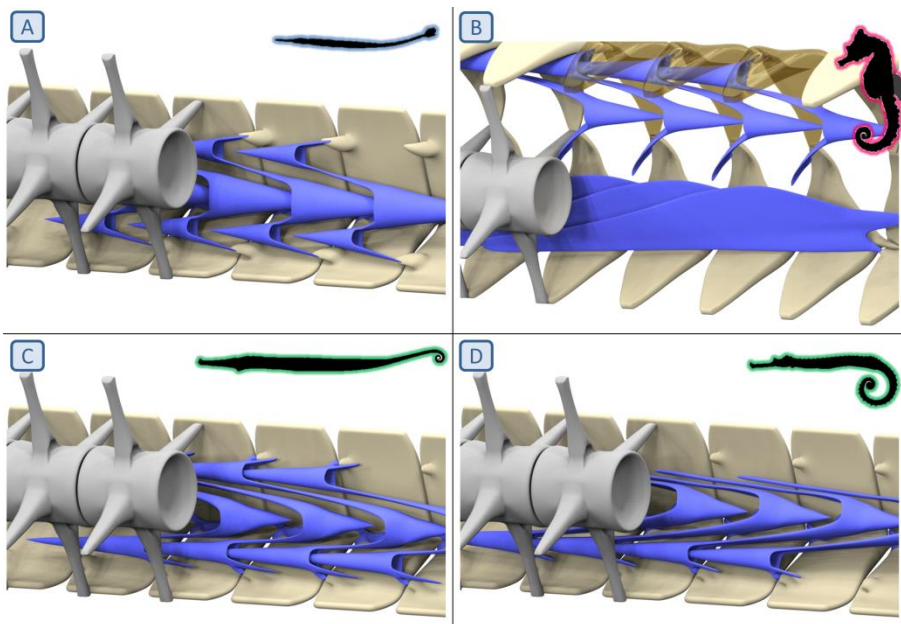


FIGURE 3.7 - Schematic overview of the myoseptal organization in (A) pipefish, (B) seahorse, (C) pipehorse and (D) seadragon.

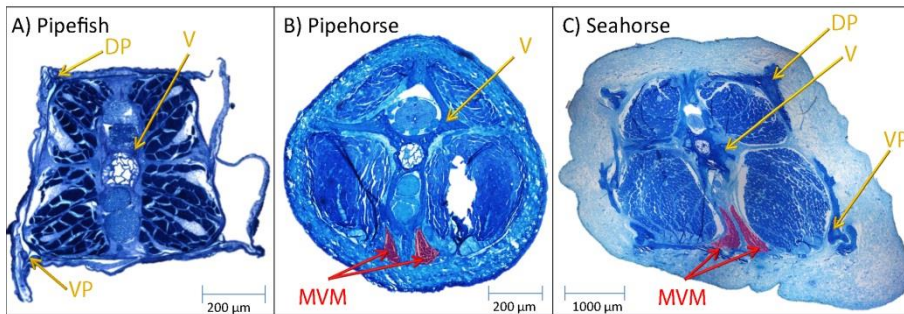


FIGURE 3.8 - Median ventral muscle illustrated on histological sections. The median ventral muscle (MVM) is absent in (A) pipefish and present in both (B) pipehorse and (C) seahorse. DP, dorsal plate; VP, ventral plate; V, vertebra.

the reduction of the mVAC may be an artefact due to limited quality of the synchrotron scans. For the same reason, it was also not possible to visualize the MVM. Due to the rarity of the *S. hardwickii*, *A. gracilissima* and *I. australe* specimens, they could not be stained with contrast agents for soft tissue visualization or histology, and thus only information on the skeletal elements could be obtained.

3.4.2 Bending capacity

The hypothesis on relative muscle fiber length of the hypaxials (with respect to the vertebral length) seems to be supported, as in both seahorse species studied (*H. abdominalis* and *H. reidi*, 0.24 ± 0.02 SD and 0.23 ± 0.06 SD, respectively) the relative muscle fiber length was significantly longer than in a pipefish (*Syngnathus acus*, 0.15 ± 0.02 SD; $P < 0.05$). However, this was not the case for *S. biaculeatus* (a pipehorse, 0.15 ± 0.03 SD), where the relative muscle fiber length was not significantly different from that in pipefish ($P = 0.33$; and hence significantly shorter than in seahorses). Among the two seahorse species studied, the fibers had similar relative length values, although with a larger range in the largest specimen (*H. abdominalis*). However, this could be a methodological artifact (as fiber length was measured on histological sections with a thickness of $5 \mu\text{m}$ in *H. reidi* and those of *H. abdominalis* on dissected fibers).

As expected, plate interconnectivity proved to constrain bending capacities substantially in pipefish (*Corythoichthys*): maximal passive bending in all three directions (dorsal, ventral and lateral) was similar along the tail, gradually increasing to a total angle of about 300° . In a seahorse (*H. capensis*), the bending angle also increases gradually, but at a steeper slope, giving an increased flexibility in the caudal 30% of the tail length. A maximal cumulative bending of around 800° was achieved in a ventral direction, but also in a lateral one, in

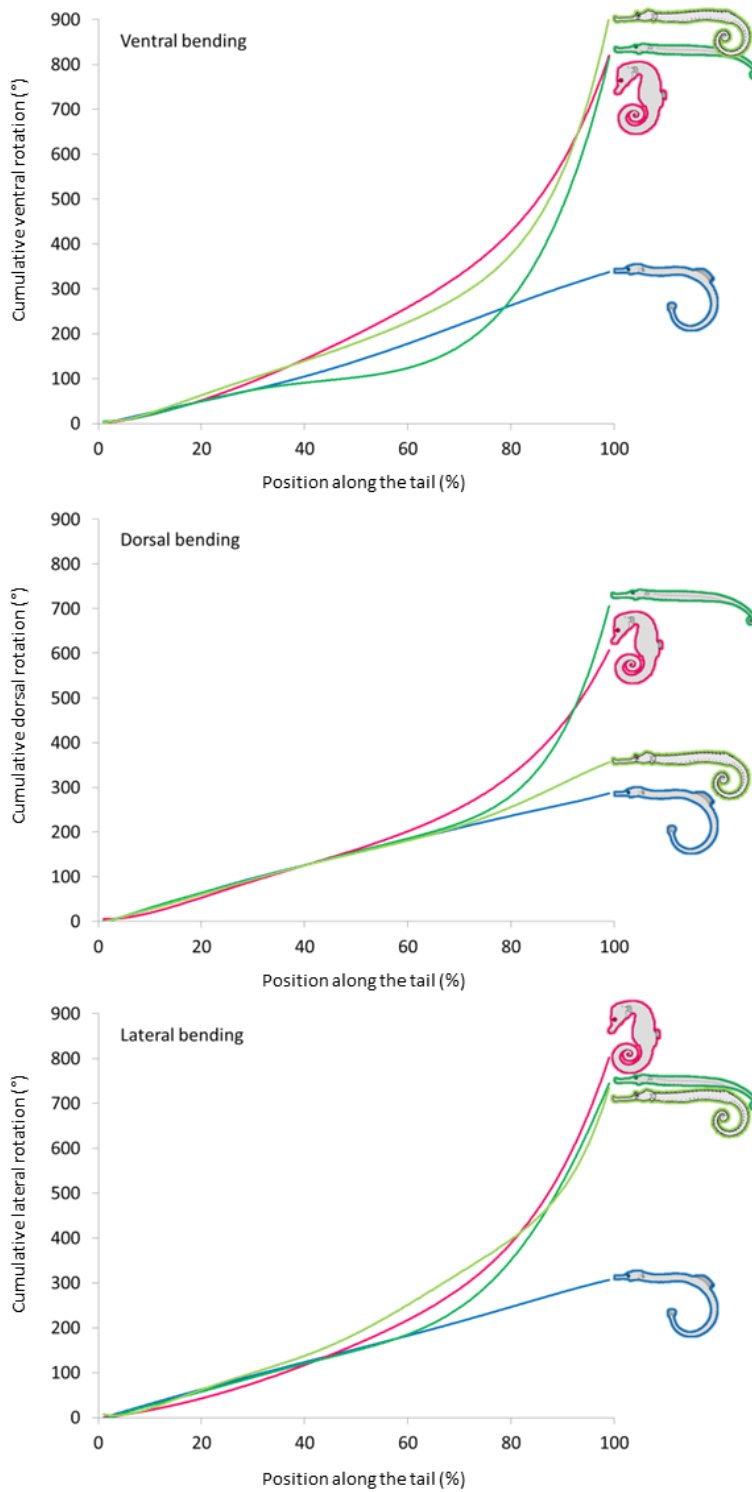


FIGURE 3.9: Passive bending capacities. Bending pattern of pipefish (blue), seahorse (pink) and pipehorse (green). The upper graph shows the passive bending pattern in the ventral plane, the middle one in the dorsal plane and the lower one in the lateral plane.

reached a total of around 600°. We expected a similar pattern for *S. biaculeatus* (a pipehorse); however, contrast to what we expected. As expected, dorsal bending was most constrained, but still aquarium observations already showed that they grasp with the distal part of the tail only, keeping the proximal part rather rigid. The data obtained confirm this, the anterior 70% of the tail following a pattern very similar to that in pipefish, whereas the caudal 30% is highly flexible, even more than in seahorses. As such, they also reach a cumulative total curvature of around 800° for ventral bending and only slightly lower values for lateral and dorsal bending. In *H. taeniophorus*, extensive ventral and lateral bending was observed (respectively ca. 900° and 750°). The bending range in the dorsal direction, however, is restricted (ca. 350°) and only slightly higher than the dorsal bending capacity of pipefishes, which is ca. 300° (FIGURE 3.9). To our knowledge, there are no morphological indications that there should be marked differences in the way the vertebrae influence the passive bending capacities of the above syngnathid fishes.

3.5 Discussion

As expected, seahorse, pipehorse and *H. taeniophorus* are capable of bending the caudal part of their tail more ventrally, compared with pipefish. However, our hypothesis that bending capacities would be highest in a ventral direction is refuted, as the tail in seahorse and pipehorse bends almost equally well in a lateral direction. Our observations from manipulating the tail confirm life observations of tail grasping on vertical objects, such as sea grass leaves (Peters, 1951, Weber, 1926), where extensive lateral bending is functionally important for a proper hold while keeping the body both vertical (seahorse) or horizontal (pipehorse). Still, extensive bending in a vertical plane is structurally and functionally not inherently linked to extensive lateral bending, as seen in chameleons, where tail mobility is extensive in the vertical plane, but only a limited amount of lateral undulation occurs during locomotion (Bergmann et al., 2003); nor is the presence of a dorsoventral symmetry in the tail musculature a prerequisite for multidirectional bending (as suggested for prehensile skinks; Zippel et al., 1999). As it was not possible to clear and stain a specimen of *S. hardwickii* and *A. gracilissima* (due to their rarity and value), the same bending experiment could not be performed on these species. However, based on the skeletal morphology, we would expect a similar bending pattern in *S. hardwickii* as seen in the *Syngnathoides* pipehorse (with the anterior 70% following a pattern similar to that in pipefish and a flexible caudal 30% of the tail). The dermal plates in the first 70% of the tail of *S. hardwickii* form a tight set of articulating segments, where any space in between plates is covered by intercalating plates. Based on the similarities in plate morphology between *S. hardwickii* and pipefish, we expect that this part of the tail is rather stiff, just like

the tail of pipefish. However, the last 30% of the tail is characterized by a loss of connection between dermal plates (either by reduction or by a shift) at the ventral and lateral side. Although there is a difference in plate morphology between *S. hardwickii* and *S. biaculeatus* in the last 30% of the tail (only a loss of connection and respectively a complete reduction until absent in the tip), we still would expect this last part of the tail of *Solegnathus* to be highly flexible compared with the first 70%. *Acentronura*, on the other hand, is characterized by a plate morphology similar to pipefish at the dorsal side and one similar to seahorse at the ventral side, just as in *Haliichthys*. Based on this plate morphology, we would expect a similar bending pattern for *A. gracilissima* as observed in *H. taeniophorus*, with extensive bending in a ventral and lateral direction but a limited bending range in the dorsal direction. Plates in pipefish form a tight set of articulating, skeletal segments, where any space in between segments is covered by intercalating plates (FIGURE 3.2A).

The ancestral state reconstruction based on the phylogenetic hypothesis of Hamilton et al. (2009) (FIGURE 3.1) suggests that two different evolutionary strategies enabling the capacity for tail bending (both at the structural level and at subsequent functional one) evolved independently. In all syngnathid fishes possessing a prehensile tail, plates become reduced distally, being present but small in seahorse and *H. taeniophorus*, only present at the dorsal side in *S. hardwickii* and completely absent in *S. biaculeatus* (both at the ventral and dorsal side). In *S. hardwickii*, plates are no longer contralaterally and medially interconnected. Also, an intermediate skeletal morphology between pipefish and seahorse was found, as both *H. taeniophorus* (sister relationship to *Hippocampus* according to Hamilton et al., 2009) and the two studied pygmy pipehorses (type I) share similar body plating with seahorse at their ventral side and the rigid plate structure of pipefish at their dorsal side. These differences at the level of plate modifications could explain the passive bending capacities, where the tail in seahorse, *H. taeniophorus* and, based on the morphology, probably also in pygmy pipehorse (type I), bends in a more gradual manner, whereas in *S. biaculeatus* (and based on the external habitus, possibly also in *S. hardwickii*) the tail combines an extremely flexible distal tip with a rigid proximal part. This rigidity in type II pipehorse is explained by the large plates that lack sliding joints around a large posterior process (as found in seahorse), and this, in contrast to our expectations, reflects the ancestral condition as seen in pipefish.

Although there is still some debate about the effect of dermal ossification on bending capacities (Gemballa and Bartsch, 2002, Long et al., 1996), we believe that they are, in this case, related to each other. In the studied type II pipehorse species, the change in dermal plate morphology [from reduced to distally absent (*S. biaculeatus*) or absence of a

connection between the contralateral ventral plates and between the dorsal and ventral plates within one segment (*S. hardwickii*) starts at the same position along the tail as the sudden increase in bending angle. Another example that supports this conclusion is the restricted passive bending capacity in dorsal direction (ca. 350°) in *H. taeniophorus* (and, given the similarities in body plating, pygmy pipehorses probably share this restricted dorsal bending), combined with an extensive passive bending capacity in both a ventral and lateral direction, as the skeletal morphology of the dorsal plates strongly resembles that of pipefish and the ventral plates show the similar characteristics as in seahorse. This also shows, as would be expected, that compression is more constrained by the plates than is extension. The prehensile tail of all of the above described species is also characterized by a substantial reduction in size of the distal vertebrae, a feature already observed in *H. hippocampus* (Bruner and Bartolino, 2008), as well as in other vertebrates with a prehensile tail (Boistel et al., 2010).

The modifications on the myoseptal level in seahorse suggest a structural link with the ventral bending capacities. However, these parallel myosepta were not observed in pipehorse. Based on the muscular organization, it seems that it is the presence of the modified median ventral muscles that is important for extensive coiling (ventral muscle differentiations are also present in tail grasping chameleons; Boistel et al., 2010), whereas the apparent drastic myoseptal reorganization found in seahorse (longitudinal sheets instead of conical septa) seems to be an autapomorphy for the genus *Hippocampus* and not a necessity for extensive tail bending. However, the different skeletal configuration in *S. biaculeatus* and *H. taeniophorus* may dictate a different musculoskeletal mechanism for tail bending. The fact that we only observe longer muscle fibers (relative to vertebral length) in hypaxial muscles in seahorse and not in pipehorse may also indicate that this is not crucial for prehensibility.

Although there is no consensus about the extensiveness of the convergent lineages leading to a prehensile tail in syngnathid fishes based on the two phylogenetic hypotheses, it seems well supported, considering the morphological data from this study, that prehensile tails in syngnathids are the result of convergent evolution. The modifications at the skeletal level allowing bending in *S. biaculeatus* and *S. hardwickii* are far from similar compared with the ones in seahorse, pygmy pipehorse and *H. taeniophorus*. Looking at the bending patterns, there is a clear distinction between the studied type II pipehorses (having a rigid first 70% of the tail and a highly flexible last 30%) and all other studied species possessing a prehensile tail (showing a gradual bending pattern). The skeletal morphology of *H. taeniophorus* is very similar to the one of *I. australe* and *A. gracilissima* and supports their sister relationship as

indicated in the phylogenetic study of Hamilton et al. (2009). It has been proposed that, based on recent phylogenetic research, this sister relationship to *Hippocampus* is no longer supported and that *Idiotropiscis*, *Acentronura* and *Haliichthys* are nested within the clade of the pacific pipefishes (G. Short, personal communication). Based on this phylogeny, the intermediate body plating as seen in both *Idiotropiscis*, *Acentronura* and *Haliichthys* may be due to convergent evolution and similar requirements, and does not represent an intermediate stage between pipefish and seahorse. The phylogeny still supports the independent evolution of tail grasping within the family of syngnathid fishes.

With the current information, the differences in ecological affinities of seahorses, seadragons and pipehorses cannot be related to the observed structural and functional strategies for tail bending. Although we now have an idea about the musculoskeletal organization of the tail of syngnathid fishes possessing a prehensile tail, we still don't know how the kinematics across species work (although some data are available on seahorse kinematics during grasping; Maia and Adriaens, in prep.). Having a plated (body and) tail is considered to be a multifunctional device that provides structural support and protection (Porter et al., 2013) and that can guide bending in a certain plane, but also impede it in another one (Gemballa and Bartsch, 2002). The reduced plate morphology in seahorses (and in type I pipehorses and *H. taeniophorus*) thus may improve sustained grasping performance, whereas this may not be an issue for the less stationary pipehorses. Syngnathiform fishes (comprising Syngnathidae, Aulostomidae, Centriscidae, Fistulariidae and Solenostomidae) all possess a body covered with bony plates, including its closely related group of Pegasidae (seamoths). This is unlike fishes belonging to the sister groups Mullidae and Scombriformes, all of which lack any form of dermal plating (Near et al., 2013). Other families characterized by dermal bony plates, such as the Gasterosteidae or Loricariidae, are only distantly related to these Syngnathiformes. As it has been suggested that only a small number of genes control major alterations in body armor, a parallel evolution towards non-plated but highly flexible tail tips in the independent pipehorse lineages might not be so unlikely and may be an explanation for the multiple origin of tail prehensility. However, with feeding performances also being linked to body posture, it has already been suggested that differences in feeding kinematics (especially related to the distance to the prey at a feeding strike) may also explain the evolutionary transitions from pipefish morphotypes to seahorse morphotypes, through intermediate pigmy pipehorse (type I) morphotypes (Van Wassenbergh et al., 2011). A comparative developmental study of the caudal musculoskeletal system in syngnathids may also unravel the mechanism behind the extensive reorganization of myosepta, which seems to have originated in *Hippocampus* (or in the clade leading to seahorses and pigmy pipehorses, as there are

indications of a reduction of the hMAC in *H. taeniophorus* and in the epaxial muscles of *Hippocampus*), a hypothesis that remains to be tested.

The more complex evolutionary problems are, the less frequent one would expect solutions to have occurred. Still, in this study we showed that in syngnathids it seems that at least two solutions arose towards improved prehensile capacities, a unique key innovation in fishes. However, further work on additional pipehorse species from different lineages (certainly on the muscular morphology) is required to unravel the detailed pattern and mechanisms that gave rise to these highly modified caudal systems.

CHAPTER 4: MORPHOMETRICS

PREHENSILE AND NON-PREHENSILE TAILS AMONG SYNGNATHID FISHES:
WHAT'S THE DIFFERENCE?

MODIFIED FROM NEUTENS C, DE DOBBELAER B, CLAES P & ADRIAENS D,
ZOOLOGY (UNDER REVIEW)

4.1 Abstract

All syngnathid fishes are characterized by a tail with a vertebral column that is surrounded by dermal plates – four per vertebra. Seahorses and pipehorses have prehensile tails, a unique characteristic among teleosts that allows them to grasp and hold onto substrates. Pipefishes on the contrary, possess a more rigid tail. Previous research (Neutens et al., 2014) showed a wide range of variation within the skeletal morphology of different members in the syngnathid family. The goal of this study is to explore whether the diversity in the three dimensional shape of different tail types reflects grasping performance, and to what degree grasping tails occupy a different and more constrained diversity. For this, a 3D-morphometrical analysis based on surfaces was performed. Four different analyses were performed on the tail skeleton of nine species exhibiting different levels of tail grasping capacities (four pipehorse, three seahorse, one pipefish and one seadragon species) to examine the intra-individual variation across the proximo-distal and dorso-ventral axis. In the two interspecific analyses, all vertebrae and all dermal plates were mutually compared. Overall, intra-individual variation was larger in species with a prehensile tail. The analysis on the vertebrae showed differences in the length and orientation of the hemal spine, as well as the inclination angle between the anterior and posterior surface of the vertebral body. This was observed at an intra-individual level across the proximo-distal axis in prehensile species and at an inter-individual level between prehensile and non-prehensile species. Across the proximo-distal axis in prehensile tails, the overall shape of the plates changes from rectangular at the proximal end to square at the distal end. Across the dorso-ventral axis, the ventral dermal plates carry a significantly longer caudal spine than the dorsal ones in all prehensile-tailed species. It can therefore be concluded that prehensile tails exhibit a larger proximo-distal and dorso-ventral shape variation within the tail than non-prehensile ones. However, the hypothesis that there is a more constrained shape variation among prehensile species compared to non-prehensile ones had to be rejected.

4.2 Introduction

Syngnathid fishes, comprising pipefishes, pipehorses, seahorses and seadragons, use an amiiform mode of swimming, relying on fast oscillations of their dorsal and pectoral fins for propulsion – up to 35 times per second (Breder and Edgerton, 1942, Ashley-Ross, 2002, Consi et al., 2001). This type of locomotion, called hovering, is widespread among fishes that swim with a slow speed, but need high maneuverability, optimal for living in a complex, obstacle-strewn environment such as sea grasses and coral reefs (Lindsey, 1978). This fast oscillating dorsal fin has another advantage, as the speed exceeds the flicker fusion

threshold of their predators and the dorsal fin is rendered effectively invisible as it propels the animal (Breder and Edgerton, 1942, Ashley-Ross, 2002). Swimming in pipefishes occurs through pectoral and dorsal fin movement and the use of the tail is rather limited during swimming (*e.g.* for escape reactions). Seahorses and pipehorses lack a caudal fin and are the only fishes able to bend their tails ventrally over more than 800° and use it as a prehensile appendage.

The ancestral syngnathid condition is represented by the pipefishes (Jungersen, 1910). These fishes are characterized by a horizontal body posture, a relatively stiff tail and the presence of a caudal fin. In a pipefish tail, each vertebra is surrounded by four bony plates (within a vertebral segment), that overlap through extended scarf joints (Hildebrand, 1995) within one segment and through four sliding joints between two consecutive segments, formed by a distinct caudal spine which slides into the posterior furrow on the corresponding plate of the subsequent segment (Neutens et al., 2014, Jungersen, 1910, Azzarello, 1990) (FIGURE 4.1).

Within the pipehorses, two different morphotypes can be distinguished. The first type comprises the clade of the rare pygmy pipehorses (genera *Idiotropiscis*, *Acentronura*, *Kyonemichthys* and *Amphelikurus*), which superficially look like seahorses, but have a horizontally body posture (Gomon, 2007, Kuitert, 2009, Teske and Beheregaray, 2009). The second type comprises a polyphyletic group nested within the pipefishes, with a similar morphology to them but with a prehensile tail. It is assumed that ventral tail bending in seahorse is partially related to the skeletal structure of the tail (Bruner and Bartolino, 2008, Neutens et al., 2014). In seahorses, plates are substantially reduced to tetrahedral-like structures, with a relatively longer caudal spine (due to the plate reduction). The overlapping area of the extended scarf joints, as seen in pipefishes, is also reduced in seahorses (Hale, 1996, Neutens et al., 2014). At the interspecific level, different skeletal conditions are observed in the studied pipehorses species, including plate reduction, the absence of bony plates or the absence of scarf joints (within one segment) and/or sliding joints (between two segments) (Neutens et al., 2014). Research also showed that the vertebral morphology in pipefish and pipehorse (Neutens et al., 2014) is similar to that of seahorse (Hale, 1996): amphicoelous vertebrae with a well-developed neural arch and anteroposteriorly thickened lateral processes.

As described above, the caudal musculoskeletal morphology of different members of the syngnathid family is already thoroughly studied (Hale, 1996, Neutens et al., 2014), but until now, only one study covering the shape variation within the seahorse vertebral system (Bruner and Bartolino, 2008) was performed in *Hippocampus hippocampus*, using a single

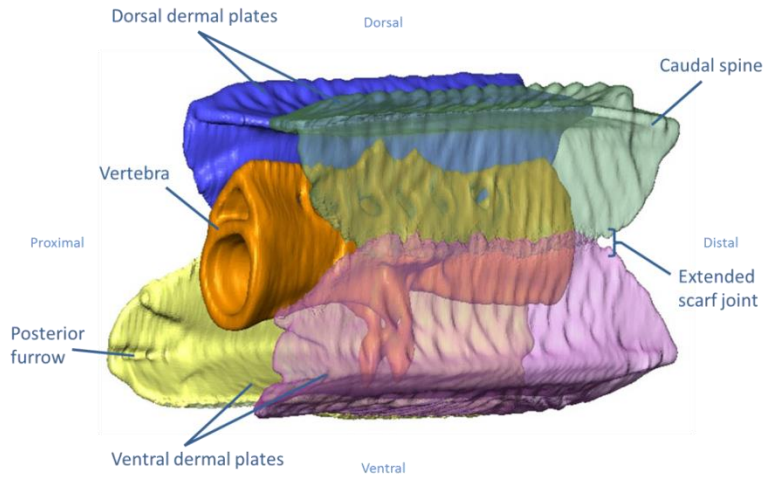


FIGURE 4.1 – Overview of the anatomical structures present in one segment of a pipefish (from a proximo-lateral view).

specimen. A principal component analysis, using a (limited) set of seven 2D landmarks, performed on the caudal vertebrae showed that there is a marked size decrease combined with allometric shape changes involving the increased tilting of the posterior vertebral border, causing a natural ventral bending of the tail (Bruner and Bartolino, 2008). However, to what degree vertebral variation is consistent among seahorses and differs from (non-prehensile) pipefish, as well as to what degree the plates also reflect functional differences related to tail prehension remains unexplored.

The main goal of this research is to quantify the observed morphological differences within and between the tails of syngnathid fishes (as observed in CHAPTER 3) and to determine if certain shape differences can be linked to differences in tail use (prehensile vs. non-prehensile tails). To study this, three main hypotheses are postulated, two at the intra-individual level and one at the inter-individual level. First, it is expected that prehensile tailed species will show a wider range of proximo-distal variation in the shape of their vertebrae and dermal plates within one tail, compared to non-prehensile species. The tail of pipefishes shows a linear increase in bending curvature from proximal to distal (Neutens et al., 2014). The curvature of the tail in seahorses and type I pipehorses however, approximates the shape of a golden spiral (a logarithmic spiral whose growth factor is the golden ratio) when in a maximally bended position (Praet, 2013, Neutens et al., 2014). The amount of curvature of the tail thus increases towards the distal end of the tail. In type II pipehorses, the tail can be divided into a rigid proximal part and a flexible distal part (Neutens et al., 2014). It can be expected that segments in the more distal region in both seahorses and pipehorses will show adaptations related to increased bending capacities

(compared to the proximal region). A previous study already showed that there is an increasing proximal-distal trend in the inclination angle between the anterior and posterior surface of the vertebral body (Bruner and Bartolino, 2008). This probably induces an already ventrally curled resting position of the tail (instead of a straight resting position). It can be expected that this increase in inclination angle will be found in other prehensile tailed species and will be absent in the non-prehensile ones. Neutens et al. (2014) already described that the dermal plates become reduced distally in different syngnathid fishes possessing a prehensile tails. However, it can be expected that, next to differences in size, there will be differences in shape from proximal to distal. A proximal-distal increase in the length of the caudal spine and corresponding proximal furrow are expected. An elongation of these features causes a more elaborate sliding joint, allowing a wider range of motion between two consecutive segments and thus enhances tail prehensility.

As the passive tail flexibility in seahorses (and to a lesser extent in pipehorses) is greater in the ventral direction than in the dorsal one, a second hypothesis is that shape differences between the ventral and dorsal dermal plates within one tail, allowing more flexibility in the ventral direction, will occur within the tail of prehensile species and that this difference will be absent in non-prehensile tails. As plates at the ventral side have to slide into each other during ventral bending, a longer sliding joint (and thus a longer caudal spine and posterior furrow) is expected in prehensile tailed species. Also, a reduced scarf joint is expected to occur at the ventral side in prehensile tailed species, as this will allow the dermal plates to move over a greater angle towards each other and thus a higher amount of total tail curvature.

As a third and final hypothesis, it is expected that extensive and efficient prehensile capacities require specific mechanical properties of the skeletal phenotype. As such, we expect to find a constrained variation among prehensile species. As plates at the ventral side have to slide into each other during bending, it is probable that there is a higher constraint in plate morphology at the ventral side in species with a prehensile tail, compared to their dorsal side and to the bony plates of non-prehensile tails. We especially expect this to be distinct in the orientation and length of the caudal spine. It can be expected that such variation comprises an inter- and intraspecific component. However, in this study, skeletal data of only one specimen per species was used, as the focus is on macro evolutionary patterns that may reflect adaptive evolution towards tail prehension. As such, intraspecific variation is limited to the intra-individual level (proximo-distal and dorso-ventral).

4.3 Material and methods

4.3.1 Specimens studied

One specimen of three seahorse species (*Hippocampus reidi*, *H. breviceps* and *H. zosterae*), four pipehorse species (*Acentronura gracilissima*, *Solegnathus hardwickii*, *Haliichthys taeniophorus* and *Syngnathoides biaculeatus*), one seadragon species (*Phyllopteryx taeniolatus*) and one pipefish species (*Corythoichthys intestinalis*) were studied. Two seahorse specimens (*H. reidi* and *H. zosterae*), the pipehorse (*C. intestinalis*) and one pipehorse (*S. biaculeatus*) were obtained through the aquarium trade. These specimens were euthanized with an overdose of MS222 (Sigma Aldrich), prior to fixation in 4% formaldehyde. The *H. breviceps*, *A. gracilissima*, *S. hardwickii* and *P. taeniolatus* specimens were obtained from the Muséum National d'Histoire Naturelle (MNHN – France, resp. voucher numbers MNHN 1890-0371, MNHN 1904-0298, MNHN 0000-6042 and MNHN 0000-9213) and the *H. taeniophorus* specimen from the Commonwealth Scientific and Industrial Research organization (CSIRO – Australia, unregistered specimens). All specimens studied were adult specimens (measurements of their total length (TL) can be found in TABLE 4.1).

	TL (mm)
<i>Hippocampus reidi</i>	112
<i>Hippocampus breviceps</i>	51
<i>Hippocampus zosterae</i>	22
<i>Acentronura gracilissima</i>	45
<i>Solegnathus hardwickii</i>	382
<i>Haliichthys taeniophorus</i>	204
<i>Syngnathoides biaculeatus</i>	144
<i>Phyllopteryx taeniolatus</i>	240
<i>Corythoichthys intestinalis</i>	124

TABLE 4.1 – Overview of the total length (TL, in mm) of the used specimens.

Due to the rarity of some of the specimens and the fact that 3D reconstructing the different tails is a very time intensive job, only one specimen of each species is included in this study. As the main goal is to look for differences in general patterns, we believe the use of a single specimen per species is justified. The included non-prehensile species are used as an outgroup and form a reference to compare the different prehensile patterns observed with, rather than as a generalization of the pipefish morphotype or to study differences among non-prehensile tailed species.

4.3.2 Skeletal morphology

All specimens, except *Hippocampus zosterae*, were μ CT-scanned at the Centre for X-ray tomography at Ghent University (UGCT) to study the skeletal organization, using the following setup: 7kV tube voltage, 1000 projections over 360° and a voxel size between 127 μ m and 400 μ m. One specimen of *H. zosterae* was scanned at the European Synchrotron Radiation facility in Grenoble, using phase contrast synchrotron x-ray radiation. All μ CT-data were processed to generate graphical 3D reconstructions of both bony plates and vertebrae using Amira 5.2.2 (Visage Imaging, San Diego, CA, USA). Based on these 3D reconstructions, the surface of each vertebra and bony plate was saved as a separate .obj-file. Due to slight deformations of the vertebrae in the seadragon (at the level of the lateral and hemal spines), only the dermal plates we included in the shape analysis.

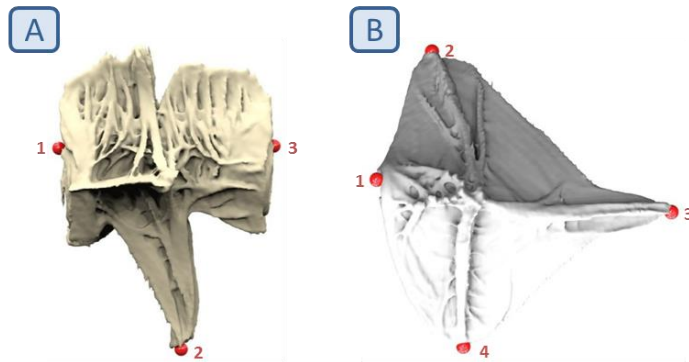


FIGURE 4.2 - Position of the initialization points on *Hippocampus reidi* on (A) a vertebra, with (1) the most dorsal point on the anterior side of the vertebral body, (2) the central tip of the vertebral haemal arch and (3) most ventral point on the posterior side of the vertebral body and (B) dorsal dermal plate, with (1) the most rostral and lateral point on the anterior rim that borders the anterior furrow, (2) the most medial point of the dorsal plate wing, (3) the most posterior tip of the caudal spine and (4) the most ventral point of the lateral plate wing (top = dorsal, bottom = ventral).

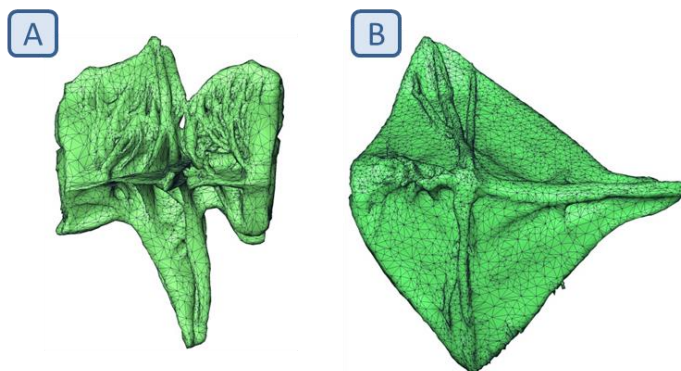


FIGURE 4.3 - Surface mesh of (A) a vertebra and (B) a dorsal dermal plate of *Hippocampus reidi* (top = dorsal, bottom = ventral)

4.3.3 3D morphometric analysis

The extracted surface data were uploaded into a MevisLab application designed at the Medical Imaging Research Centre at the University Hospital Gasthuisberg (Leuven, Belgium). To make sure that the different bony elements roughly have the same orientation prior to further surface matching, initialization points were put on each element. During this initialization procedure, points had to be assigned in the same order and may not lie in one straight line. Three initialization points were sampled on each vertebra: 1) the most dorsal point on the anterior side of the vertebral body, 2) the central tip of the vertebral haemal arch, 3) most ventral point on the posterior side of the vertebral body (FIGURE 4.2A) and four landmarks on each bony plate. On the dorsal dermal plates, landmarks were placed on 1) the most rostral and lateral point on the anterior rim that borders the anterior furrow, 2) the most medial point of the dorsal plate wing, 3) the most posterior tip of the caudal spine and 4) the most ventral point of the lateral plate wing (FIGURE 4.2B). For the ventral plates, initializations points one and three are identical to those on the ventral plates, but initializations point two was placed on the most medial point of the ventral plate wing and initializations point four on the most dorsal point of the lateral plate wing. These initialization points are not used during the general Procrustes and morphometric analyses (which are solely based on meshes) and thus only serve to roughly align elements prior to the actual analyses.

As one of the purposes of this study is to see if size is related to tail flexibility, there was no correction for differences in size between and within animals at the start of the morphometric analyses. After the initialization procedure, the 3D morphometric analyses were performed based on the 3D surface meshes (FIGURE 4.3). The performed 3D morphometric analyses consist of two phases.

- (1) The first phase of the analysis consists of matching homologous and spatially-dense point correspondences between different surface meshes using surface registration techniques. During matching, both floating and reference down-sampled surface meshes (=pyramids) were used to reduce computing time. As described in Snyders et al. (2014) and Giachetti et al. (2014), and applied to human skull and facial surfaces in Claes et al. (2015), a surface registration framework was used during the matching procedure, consisting of three main modules (in which multiple algorithms are implemented) that are performed iteratively in sequence (FIGURE 4.4). The first module is responsible for finding one-to-one correspondences between the floating surfaces and the reference surface. The amount of nodes in all meshes was recomputed in every analysis to the same amount of nodes present in the reference element during

matching. During the first analysis, all elements are compared to a randomly chosen reference element. From this first analysis, a consensus shape is saved and used as the reference in the next analysis of the same dataset, until the consensus of the previous analysis is no longer different from the one of the current analysis. In the transformation module, the difference \vec{d}_i between the position of each floating surface node \vec{f}_i and the position of its corresponding node on the reference surface \vec{c}_i is used as an estimate of a non-parametric deformation that maps the floating surface onto the target surface:

$$\vec{d}_i = \vec{c}_i - \vec{f}_i$$

The transformation block regularizes the deformation before applying it. In our analyses, a visco-elastic transformation model was used (Yuille and Grzywacz, 1989). During registration, the goal is to minimize the distance between the floating surface and the reference surface. In- and outliers will influence the end-result, which is unwanted behavior. To correct for this, an inlier distribution of distances between nodes and their corresponding points is modelled. A node is then considered an outlier if the distance to its corresponding point is highly unlikely to be generated from that distribution.

- (2) The second phase consists of a traditional Generalized Procrustes Analysis (scaling, rotating and translating of objects to minimize the Procrustes (or surface) distance) . After this, a principal component analysis was performed based on the 3D coordinates of the nodes in the surface meshes. To determine which PC axes represent the significant shape variations, a scree plot with broken stick analysis was performed using PAST (Hammer et al., 2001). All following results are only those related to significant PC-axes.

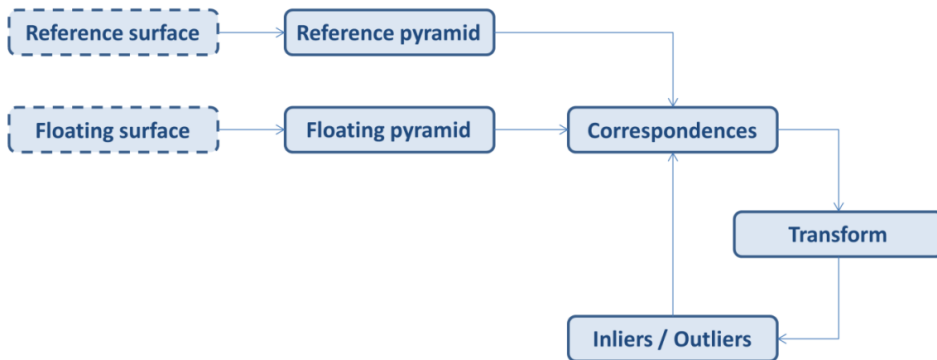


FIGURE 4.4: Surface registration framework (adapted from (Snyders et al., 2014)).

The above described methodology was applied on different (sub)sets of data. To test the first hypothesis that prehensile species show a wider range of shape variation within their tail than non-prehensile ones, three subsets for each species were created and used in individual matching analyses: only ventral plates, only dorsal plates and only vertebrae. To test our second hypothesis on differences in plate morphology related to facilitated ventral bending (compared to dorsal bending) at the intra-individual level, a subset of the pooled ventral and dorsal dermal plates was used to search for shape differences between the two sides. To test the third and last hypothesis on more constrained shape variation among prehensile species compared to non-prehensile pipefish, the dermal plates, resp. vertebrae of all species were compared.

4.3.4 Measurements

All lengths were measured on the 3D surfaces using the “3D Length” measure tool in Amira 5.2.2 (Visage Imaging, San Diego, CA, USA – FIGURE 4.5 A, B & C). Angles were measured by using ImageJ (Abramoff et al., 2004), based on images exported from Amira 5.2.2 (FIGURE 4.5 B). Measurements are defined in TABLE 4.2. Statistical analyses were performed using PAST (Hammer et al., 2001).

Measurement	Definition	Figure
<i>Vertebral measurements</i>		<i>Figure 4.5A, B</i>
Position vertebral body	Center of the vertebral body to tip of the hemal spine	yellow arrow
Height vertebra	Tip of the neural spine to tip of the hemal spine	red arrow
Length vertebra	The most antero-lateral point of vertebral body to the most postero-lateral point of vertebral body	blue arrow
Anterior surface	Line interconnecting the most antero-dorsal and the most antero-ventral point on the vertebral body	red line
Posterior surface	Line interconnecting the most postero-dorsal and the most postero-ventral point on the vertebral body	yellow line
<i>Plate measurements</i>		<i>Figure 4.5C</i>
Caudal spine length	The most anterior point of the sliding joint to the posterior tip of the caudal spine	yellow arrow
Medial plate edge length	The most antero-medial point of the plate to the most postero-medial point of the plate	blue arrow
Total plate length	The most anterior point of the furrow to the most posterior tip of the caudal spine	red arrow

TABLE 4.2 – Definitions of length and angle measurements taken on the vertebrae and dermal plates as illustrated in FIGURE 4.5.

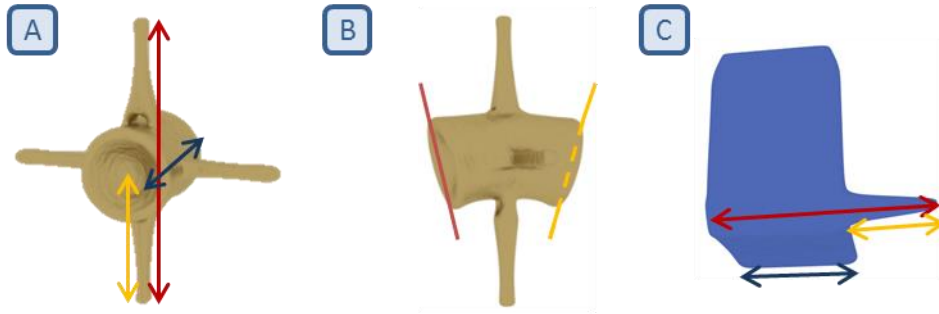


FIGURE 4.5 – Illustration of the performed length and angle measurements on (A) and (B) the vertebrae and (C) the dermal plates. The color-coded arrows and lines are defined in TABLE 4.2.

4.4 Results

A lot of shape variation in the dorsal and ventral dermal plates within and between individuals was observed, especially in the length and thickness of the caudal spine, the length, depth and shape (triangular vs. rectangular) of the plate wings, as well as the presence, shape and amount of ornamentation (bony ridges on the surface). The same applies to the vertebrae, where major variation is situated at the level of inclination angle between the anterior and posterior surface of the vertebral body, the length, thickness and orientation of the neural or haemal spines, the radius of the vertebral body, the length of the transverse processes and the implantation site of these lateral spines on the vertebral body. As the goal of this study is to find changes in morphology at different levels (proximal vs. distal, dorsal vs. ventral and prehensile vs. non-prehensile), only characteristics that appear in such a pattern and are supported by a significant PC axis will be described in the results section below. An overview of species specific shape changes can be found in APPENDIX A. Measurements corresponding to the variation of these prehensibility-related characteristics can be found in APPENDIX B.

4.4.1 Proximo-distal intra-individual shape variation

Within all studied specimens, even non-prehensile ones, PC1 (explaining min. 78% of the variation) represents size variation, showing a decline in segment size from proximal to distal. However, this decline is steeper in species with a prehensile tail than in pipefish (the length of the most distal element varies between 19 and 37% of the length of the most proximal segment in prehensile species vs. 58% of the length of the most proximal segment in pipefish). Beside this difference in size, two major shape differences can be related to a proximo-distal pattern within the tail of all studied syngnathid fishes, being the relation

between height and length of the vertebrae and the inclination angle between the anterior and posterior surface of the vertebral body.

In all species, except *Solegnathus hardwickii*, *Syngnathoides biaculeatus* and *Haliichthys taeniophorus*, the ratio of segment height to length declines from proximal to distal. In seahorse and the pigmy pipehorse (*Acentronura gracilissima*) proximal segments are rectangular, with height being larger than length. From proximal to distal, segment height decreases more than the length, resulting in practically cubic segments at the distal end.

The pipefish (*Corytoichthys intestinalis*) is the only species with beamlike segments at the distal tail end (instead of cubic ones), with length as the largest dimension. In *H. taeniophorus*, segments are practically cubical along the whole length of the tail. *Solegnathus hardwickii* and *S. biaculeatus* both show a typical pattern with beamlike segments (with length as the largest dimension) at the proximal end of the tail (the non-prehensile tail part), becoming rectangular in the middle part of the tail (with height being larger than length) and eventually cubic towards the end of the tail (FIGURE 4.6).

The second observed proximo-distal shape difference in species with a prehensile tail is the inclination angle between the anterior and posterior surface of the vertebral body. This angle ranges from 0 to 5 degrees at the proximal end of the tail and up to 25 degrees at the distal end in sea- and pipehorses and even up to 33 degrees in the pigmy pipehorse (*A. gracilissima*). The studied pipefish, however, does not show such a marked increase (ranges only from 0° to 7°) (FIGURE 4.7).

4.4.2 Dorso-ventral intra-individual shape variation

Concerning the differences between the ventral and dorsal plates within one specimen, two shape differences could be observed, being the length of the caudal spine and the length of the medial plate edge (both relative to total length).

In all species, except *Phyllopteryx taeniolatus* ($p > 0.05$) and *S. hardwickii*, the relative length of the dorsal caudal spines is significantly smaller than the relative length of the ventral ones (TABLE 4.3, ROW 1). In *S. hardwickii*, starting from tail segment 12 on, a caudal spine is lacking at the ventral side. The relative length of the ventral caudal spine is longer than the relative length of the dorsal one in *C. intestinalis*, *H. breviceps* and *A. gracilissima*, but both the ventral as well as the dorsal spine decline at a similar slope from proximal to distal. In *H. zosterae* and *H. reidi*, the relative length of the dorsal caudal spine decreases from proximal to distal, while the length of the ventral one stays approximately the same. *Haliichthys taeniophorus* is the only species in which the ventral caudal spine length follows

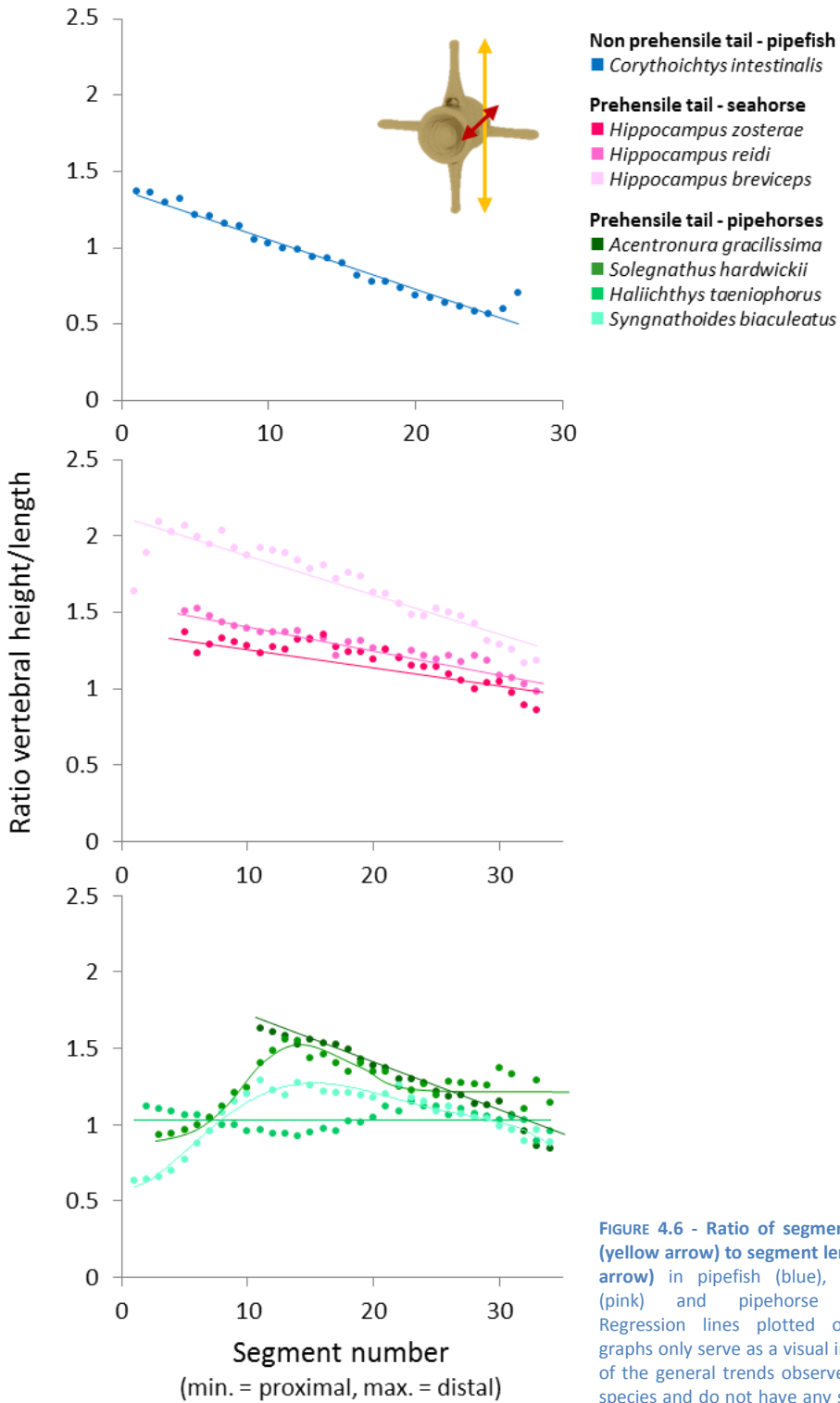


FIGURE 4.6 - Ratio of segment height (yellow arrow) to segment length (red arrow) in pipefish (blue), seahorse (pink) and pipehorse (green). Regression lines plotted onto the graphs only serve as a visual indication of the general trends observed within species and do not have any statistical value.

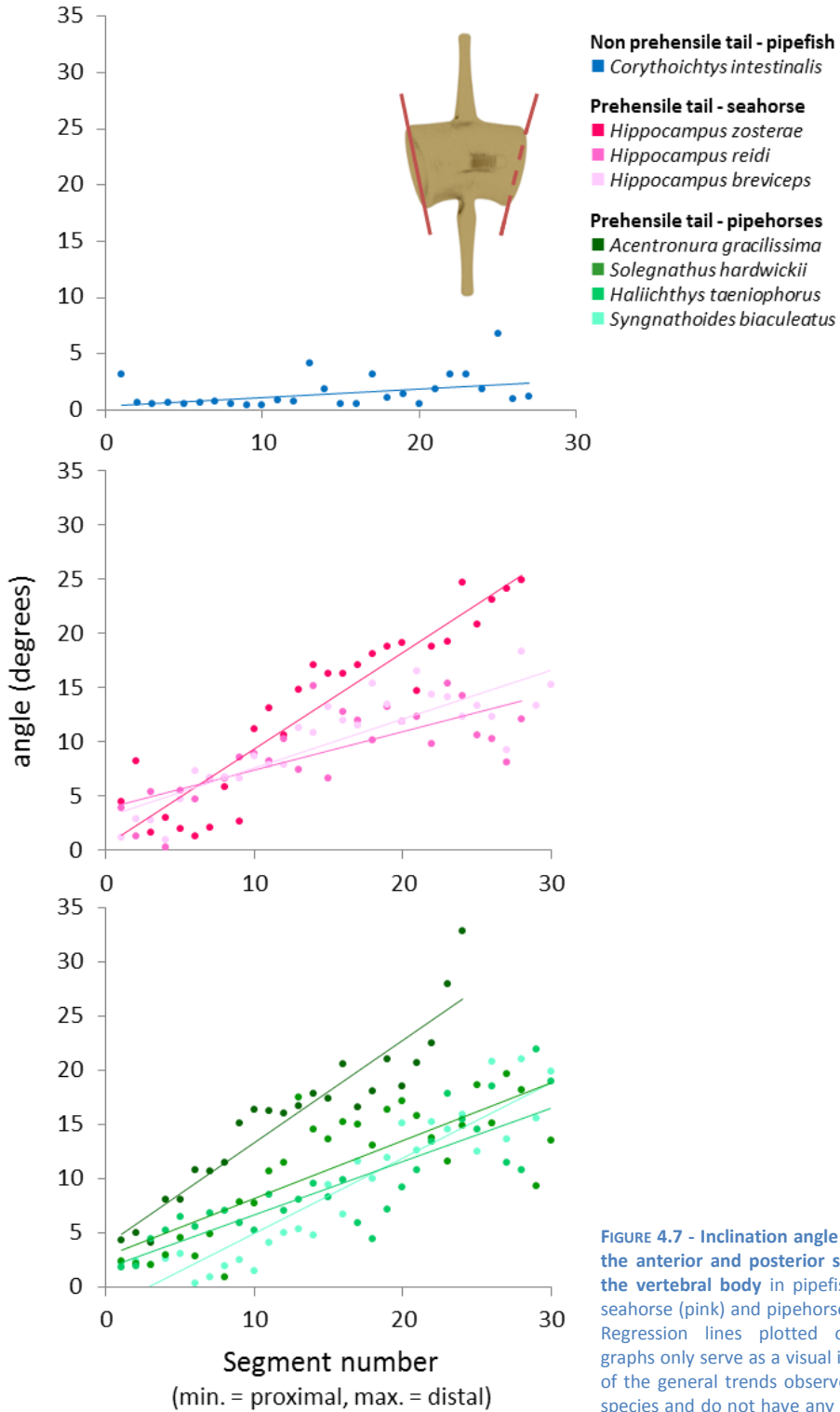


FIGURE 4.7 - Inclination angle between the anterior and posterior surface of the vertebral body in pipefish (blue), seahorse (pink) and pipehorse (green). Regression lines plotted onto the graphs only serve as a visual indication of the general trends observed within species and do not have any statistical value.

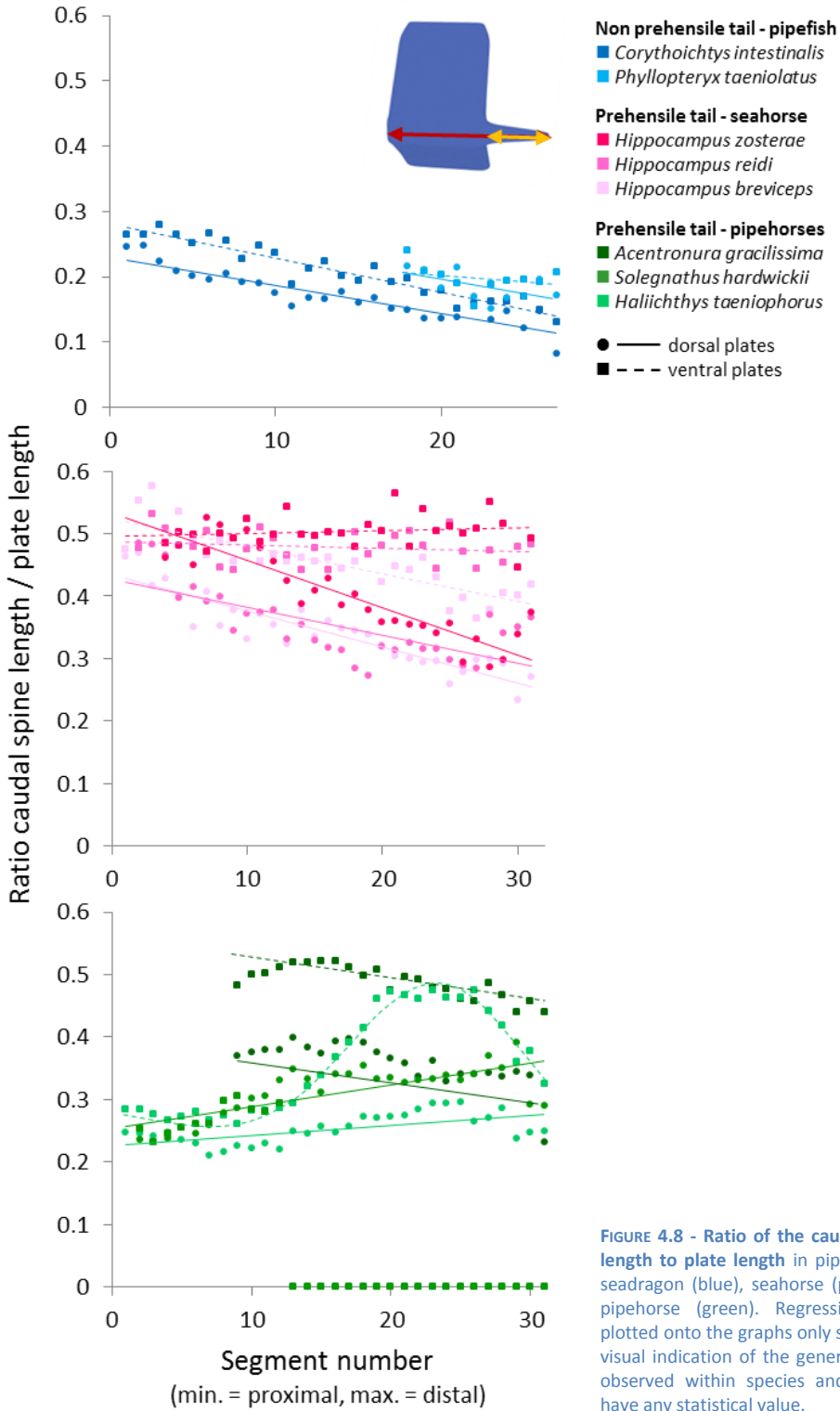


FIGURE 4.8 - Ratio of the caudal spine length to plate length in pipefish and seadragon (blue), seahorse (pink) and pipehorse (green). Regression lines plotted onto the graphs only serve as a visual indication of the general trends observed within species and do not have any statistical value.

a distinctly different pattern from proximal to distal compared to the dorsal one. The segments of the proximal part of the tail are characterized by a ventral caudal spine that has approximately the same length as the dorsal one. In the distal part of the tail however, the ventral caudal spine length increases to almost double the length of the dorsal caudal spine, decreasing again towards the distal tip (FIGURE 4.8).

In all studied pipehorse species and two seahorse species (*H. breviceps* and *H. zosterae*), the length of the medial plate edge is significantly different between the dorsal and the ventral plates, with the former being longer than in the ventral one ($p < 0.05$). In *C. intestinalis*, *P. taeniolatus* and *H. reidi*, no significant difference could be observed (FIGURE 4.9, TABLE 4.3, ROW 2). In all studied pipehorses, a declining proximo-distal trend could be observed in the length of the medial plate edge of the ventral plates, while this is not present in the dorsal plates or in other species (except *Phyllopteryx taeniolatus*) (FIGURE 4.9).

4.4.3 Inter-individual shape variation

In the inter-individual analyses, PC1 no longer reflects differences in size (as in the intra-individual analyses), but differences in shape. Plots of PC1 against PC2 of the inter-individual variation in dermal plates and in vertebrae both show that the syngnathid morphospace is markedly constrained to a U-shaped pattern, with hardly any deviations (FIGURE 4.10, ZONE B). The morphospace outside this U-shaped range (FIGURE 4.10, ZONE A) comprises both plate and vertebral morphologies that look peculiar and are mainly a combination of characteristics of both seahorse and pipefish occurring in the same plate or vertebra, or unrealistic shapes, such as vertebrae with a neural and hemal spine attached directly onto each other, lacking a vertebral body. However, exploration of the morphospace enclosed by the U-shaped pattern (FIGURE 10, ZONE C) shows that the shape variation within this area is very similar to shapes occurring in nature and represented in the syngnathid morphospace (FIGURE 4.10, ZONE B).

Across prehensile species, the variation among the dermal plates is larger than for non-prehensile species and together with this the morphospace is less constrained between species with a prehensile tail (FIGURE 4.10, TOP). The length of the caudal spine and the

	<i>Corythoichthys intestinalis</i>	<i>Phyllopteryx taeniolatus</i>	<i>Hippocampus breviceps</i>	<i>Hippocampus reidi</i>	<i>Hippocampus zosterae</i>	<i>Solegnathus hardwickii</i>	<i>Acentronura gracilissima</i>	<i>Hallichthys taeniophorus</i>
Caudal spine	< 0.05 [♠]	0.09 [♠]	< 0.05 [♠]	< 0.05 [♿]	< 0.05 [♠]	< 0.05 [♿]	< 0.05 [♿]	< 0.05 [♿]
Plate edge	0.08 [♿]	0.76 [♠]	0.03 [♿]	0.24 [♿]	< 0.05 [♿]	< 0.05 [♠]	< 0.05 [♿]	0.01 [♿]

TABLE 4.3 - Differences in plate morphology between the dorsal and ventral plates within specimens, showing p-values of a paired t-test (for the normal distributed data, indicated with [♿]) or a Wilcoxon with Monte Carlo permutation test (for the not normal distributed data, indicated with [♠]) on caudal spine length relative to plate length (first row) and plate edge length relative to plate length (second row).

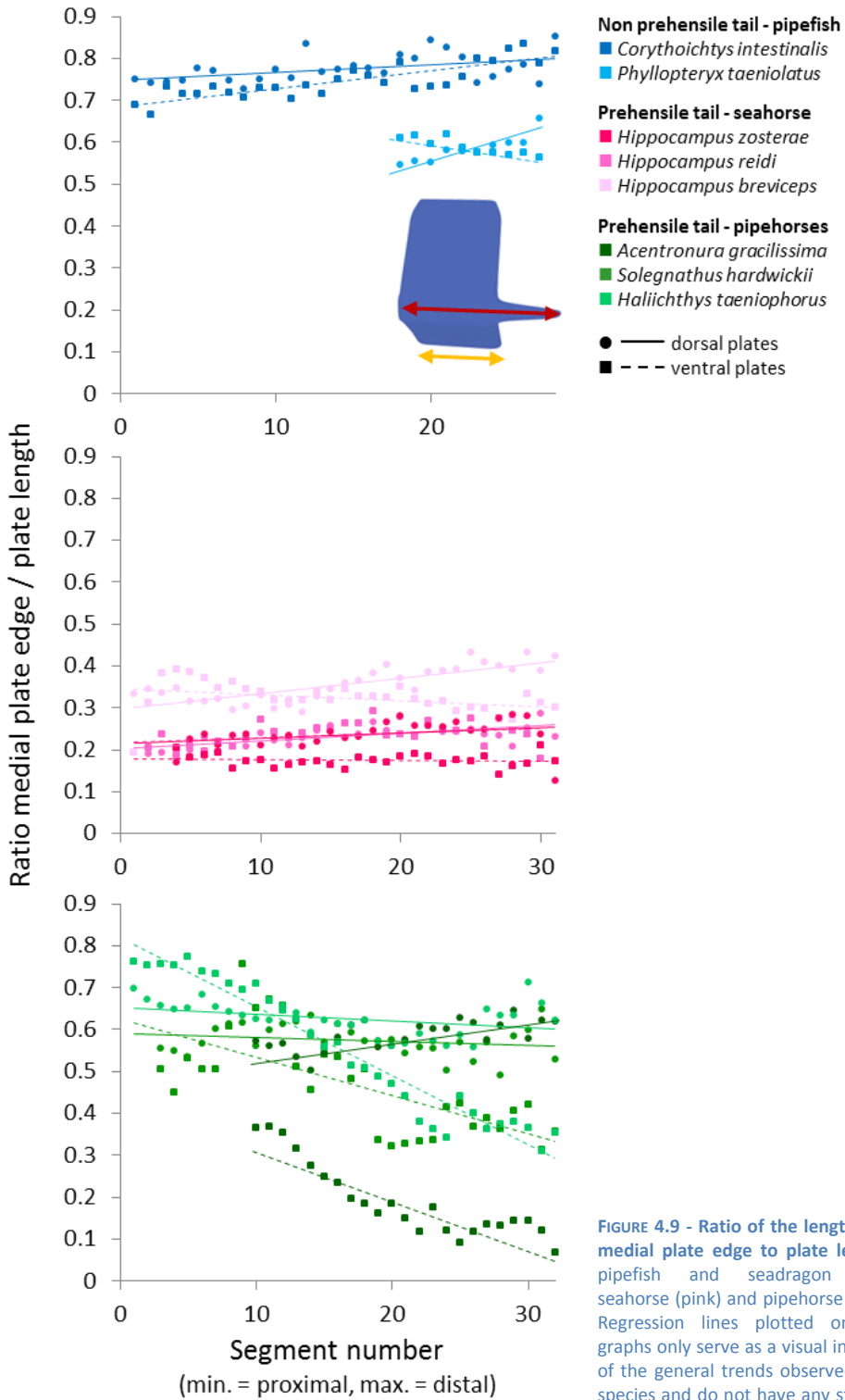


FIGURE 4.9 - Ratio of the length of the medial plate edge to plate length in pipefish and seadragon (blue), seahorse (pink) and pipehorse (green). Regression lines plotted onto the graphs only serve as a visual indication of the general trends observed within species and do not have any statistical value.

length of medial plate edges are not only the main dorso-ventral, intra-individual shape variations (see RESULTS SECTION 4.4.2), but also the main inter-individual variation (PC1: 63.75% and PC2: 16.40 %). A proximal-distal enlargement of the caudal spine is observed along PC1 (from negative to positive, FIGURE 4.10, TOP). In prehensile species, the relative length of both the dorsal and ventral caudal spine is larger than in the non-prehensile ones (*C. intestinalis* and *P. taeniolatus*). The relative dorsal caudal spine length falls in approximately the same range in the different seahorse and pipehorse specimens. However, the proximo-distal trend in both the *S. hardwickii* and *H. taeniophorus* specimens, shows the opposite pattern as in the three seahorses and the *A. gracilissima* specimen (an increase in relative caudal spine length from proximal to distal instead of a decrease). Concerning the relative ventral caudal spine length, no difference could be observed between the three seahorses and the *A. gracilissima* specimen. The relative ventral caudal spine length of *H. taeniophorus* shows a specific pattern from proximal to distal (see RESULTS SECTION 4.4.1) and therefore differs from all other studied species. In *S. hardwickii*, from tail segment 12 on, a ventral caudal spine is lacking (FIGURE 4.8).

Dermal plate edge enlargement could be observed along both PC1 (63.75 %) and PC2 (16.40 %). PC1 covers variation in the overall shape of the plate wings, varying from a triangular shape (negative PC scores) to a rectangular one (positive PC scores). Along PC2, the overall depth of the plate wing increases from negative to positive. The mediodorsal and -ventral plate edges of *C. intestinalis* are relatively the longest, with an average length of 78 %, resp. 75 % of the total plate length. The relative mediodorsal and -ventral plate edge of the other studied species lacking a prehensile tail (*P. taeniolatus*), however, showed to be shorter (mean = 58 % of total plate length) than in *C. intestinalis*. The relative length of the plate edges is similar among the different seahorse specimens studied. The same applies among the pipehorse specimens, with exception of the medioventral plate edge in the *A. gracilissima* specimen, which falls within approximately the same range as the seahorse specimens. When looking at the overall inter-individual patterns, the largest plate edges could be found in the pipefish specimen, followed by the seadragon and pipehorse specimens and the seahorse specimens (FIGURE 4.9).

At the level of the vertebrae, two main shape changes could be observed when combining PC1 (69.20 %) and PC2 (12.31 %). First, an increase in the inclination angle between the posterior and anterior surface of the vertebral body (angle of zero when both PC1 and PC2 are negative to maximum angle at positive PC1 and PC2), second the vertical position of the vertebral body within a body segment (as derived from the relative length from the hemal spine versus the total height of the vertebra) (FIGURE 4.10, BOTTOM).

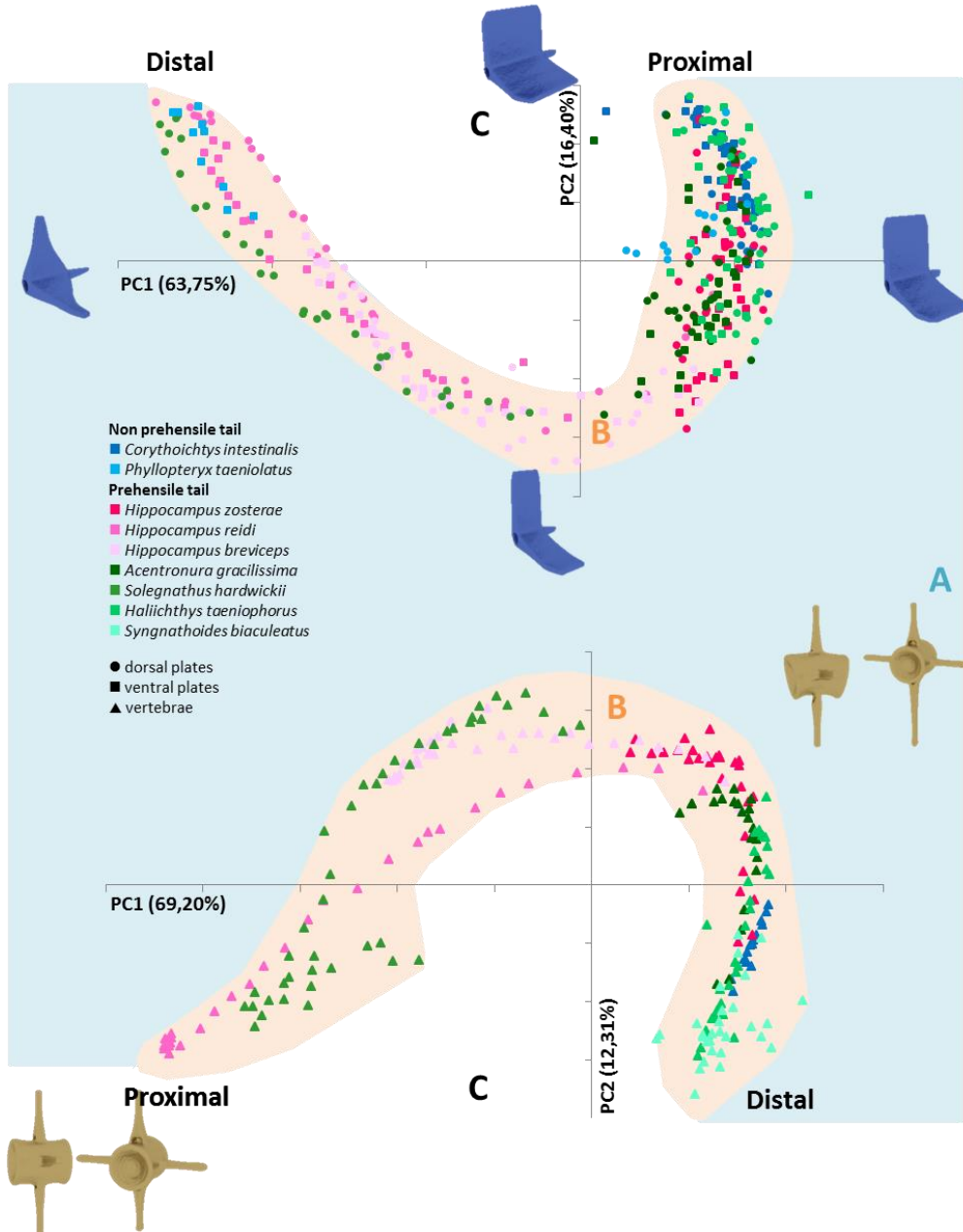


FIGURE 4.10 - PC1 vs. PC2 of the interspecific variation in dermal plates (top) and vertebrae (bottom). The observed shape variation is illustrated at the extremes of the PC1 and PC2 axis for the dermal plate (top) and as a diagonal trend (combining PC1 and PC2) for the vertebrae (bottom). The graphs can be divided into three zones, with B being the syngnathid morphospace, A being the zone outside this U-shaped morphospace and C being the zone enclosed by this morphospace.

Concerning the inclination angle, not only a proximal-distal pattern within the tail of prehensile species (see RESULTS SECTION 4.4.1), but also a difference between species could be observed. *Acentronura gracilissima* and *H. zosteræ* have a similar pattern with the strongest angular increase from proximal to distal, on average almost 1 degree per vertebra. The weakest increase is observed in the pipefish *C. intestinalis*, with only 0.08 degrees per vertebra. All other species show an intermediate pattern, varying from 0.29 degrees per vertebra in *H. reidi* to 0.69 degrees in *H. taeniophorus* (FIGURE 4.7).

The vertebral body, corrected for segment height, is positioned along the horizontal midline in species lacking a prehensile tail, but lie dorsal to the midline in all other species, except for *S. hardwickii*. All prehensile species, except *H. breviceps*, show a specific pattern with the vertebral body at a more dorsal position in the middle section of the (prehensile part of the) tail compared to the proximal and distal part of the tail. The vertebral body in *H. breviceps* is positioned more dorsal along the complete length of the tail (instead of only in the middle part of the tail (FIGURE 4.11).

4.5 Discussion

A previous, comparative study (Neutens et al., 2014) showed that there is a distinct difference in plate morphology between pipefish, pipehorse and seahorse. Based on the same morphological study, the overall vertebral morphology is assumed to be similar in pipefish, pipehorse and seahorse. Until now, shape variation within a seahorse tail has been quantitatively analyzed in a single explorative study on the caudal vertebral series of one adult individual of *Hippocampus hippocampus*, using 2D landmark based data (Bruner and Bartolino, 2008). However, a 3D surface mesh based approach provides a more comprehensive quantification of shape variation, which is particularly relevant for this study for the following reasons. First, the skeletal elements to be studied have a rather complex shape, what makes it difficult to visualize each element in the same standardized 2D orientation. Second, when using a traditional 2D landmark based approach, essential spatial information on segment length, depth and width is lacking in the analyses. Third, because of the complexity of the structures, it appeared to be difficult to find enough landmarks that could provide a comprehensive description of the overall shape of plates and vertebrae. Also, when using a methodology based on landmarks instead of meshes, finding homologous type 1 landmarks over the whole length of the tail, as well as in different species, proved to be impossible.

In contrast to most other teleost fish, syngnathids possess bony plates instead of scales. These plates are arranged in squared, articulating segments, which, next to providing body

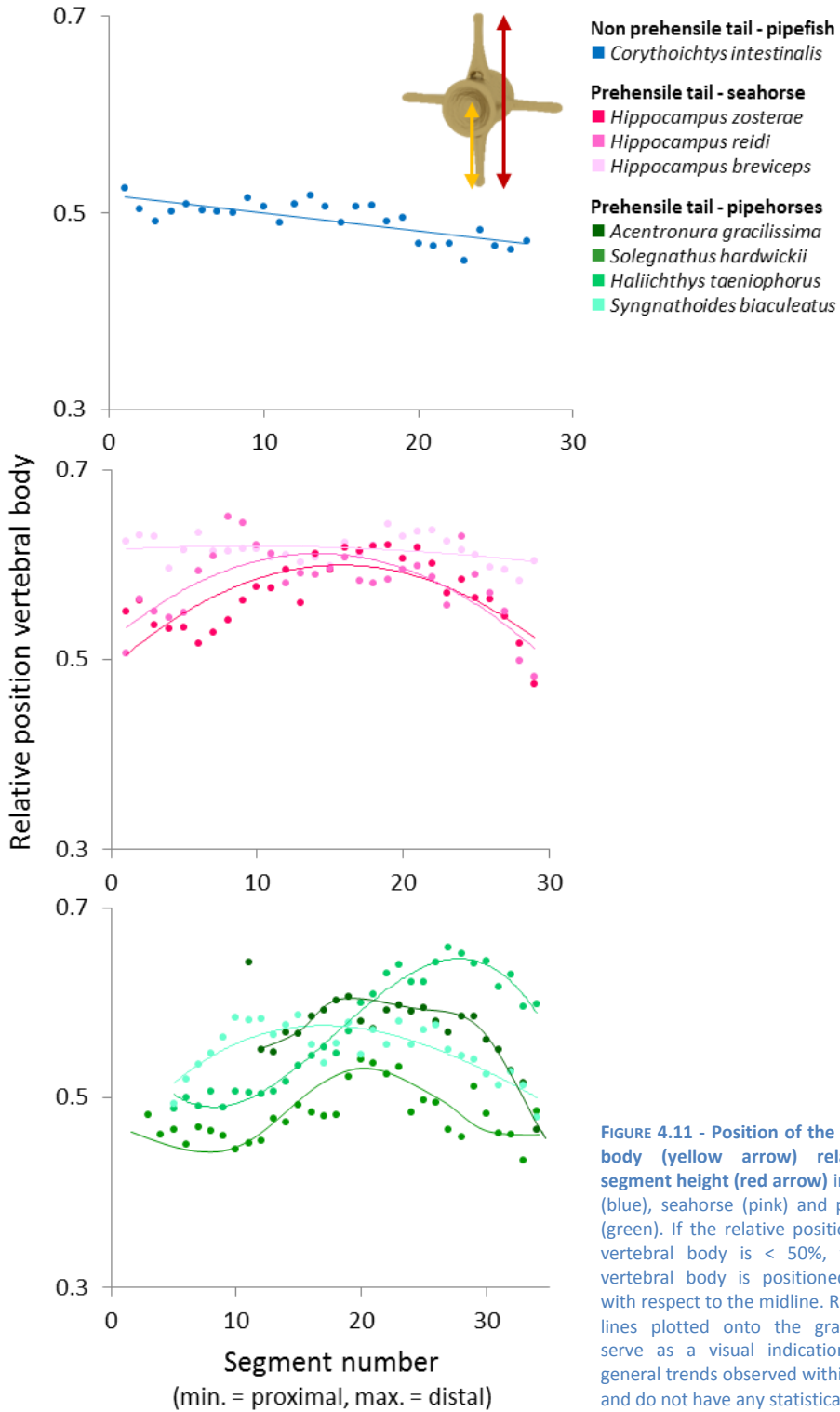


FIGURE 4.11 - Position of the vertebral body (yellow arrow) relative to segment height (red arrow) in pipefish (blue), seahorse (pink) and pipehorse (green). If the relative position of the vertebral body is < 50%, then the vertebral body is positioned ventral with respect to the midline. Regression lines plotted onto the graphs only serve as a visual indication of the general trends observed within species and do not have any statistical value.

support and protection, play an essential role in axial tail bending and the ability to grasp and hold on to objects (Hale, 1996, Neutens et al., 2014, Praet et al., 2012, Porter et al., 2013). Based on this morphometric study, it can be confirmed that there is a relation between the shape and size of both the plates and vertebrae and prehensile capacities.

Bruner and Bartolino (2008) found that there is a strong correlation between size, shape, posterior angle and serial position of the vertebrae in *H. hippocampus*. The main morphological variation along the caudal vertebral series in *H. hippocampus* is the increase in the angle between the anterior and posterior surface of the vertebral body from proximal to distal, causing a trapezoidal shape in the sagittal plane, rather than a rectangular one. It was also suggested that the resulting tail position after normal ventral bending in seahorse (*H. hippocampus*) is the result of the reduction in vertebral size, making the tail a spiral that becomes more tightened towards the end of the tail (Bruner and Bartolino, 2008). Previous research also showed that the curvature of the tail in *H. reidi* approximates the golden spiral (a specific case of a logarithmic spiral whose growth factor is the golden ratio) and that this curvature becomes progressively larger towards the distal tip of the tail (Praet, 2013). This is the result of a combination of increased muscle shortening and smaller segment lengths towards the tail tip. Other studies on chameleons (Herrel et al., 2013), lizards (Zippel et al., 1999) and monkeys (German, 1982, Deane et al., 2014) state that prehensile tailed species are characterized by longer tails with smaller distal vertebrae, to generate tighter coils around the substrate and thus better gripping. This study suggests that the active, natural ventral curling of the tail in syngnathid fishes is not only a result of a reduction in size, but also of the change in inclination angle between the anterior and posterior surface of the vertebral body (as this was one of the main proximo-distal shape changes within the tail of prehensile species). In pipefish, there was also a small increase in the inclination angle, but even the most distal vertebral elements had a lower angle between the anterior and posterior surface of the vertebral body than the most proximal ones in prehensile species. Praet (2013) already suggested that the higher inclination angle in the more distal segments in *H. reidi* could be related to a more optimized design for higher ventral bending, since these segments will be more often in a bended position and with a higher curvature. The same study also showed that the increased inclination angle is coupled to a lower bending energy usage, both in ventral and combined ventro-lateral tail bending. Another reason why this increase in inclination angle could be advantageous for tail prehensility is that, as the angle increases and the relative size and shape of the intervertebral disk stays equal, there will be less deformation of the intervertebral joints during ventral tail bending. Bruner and Bartolino (2008) also observed that as vertebral size decreases, the neural arch becomes relatively larger in *H. hippocampus*. However, our study

suggests that this is a species-specific shape variation and not correlated to tail prehensility, as this increase in neural area was only found in two of the prehensile tailed species (*H. breviceps* and *Haliichthys taeniophorus*) as well as it was found in the non-prehensile *Corythoichthys intestinalis*.

In all studied pipehorse and two of the seahorse species (*H. breviceps* and *H. zosterae*), a significant difference between the mediodorsal and -ventral plate edge was observed, with the dorsal plate edge being more extensive. This reduction of the medioventral plate edge could be advantageous for ventral curling, as it creates more space in between the ventral plates of two consecutive segments. This could also explain the observed difference in passive bending performance in the different directions, where bending capacities in prehensile tails are extensive in both the ventral as the lateral direction, but more limited in the dorsal one (Neutens et al., 2014, Porter et al., 2015). Next to a dorso-ventral difference in length of the medial plate edge, a difference in the caudal spine lengths could be observed in prehensile species, showing a more extensive caudal spine on ventral plates than on the dorsal ones. The asymmetry in caudal spine length, with a longer caudal spine at the ventral side, can be related to the more dorsal position of the vertebral body in prehensile tails (see below). As this shifts the bending axis away from the mid-horizontal plane, there will be more displacement of the bony elements at the ventral side, thus requiring a longer sliding joint.

Based on our study, the hypothesis that there is a more constrained shape variation among prehensile species has to be rejected. Especially at the level of the dermal plate morphology, as different solutions (change in plate shape at the level of both the plate edge as well as the caudal spines, absence/presence of sliding joints between two consecutive segments, absence/presence of dermal plates) to obtain tail prehensility could be detected. Although there are discrete differences between both the vertebrae and the plates across prehensile and non-prehensile species and that different solutions to obtain tail flexibility are encountered during this study, all skeletal elements share one constrained morphospace. As stated in the results, the morphospace outside the U-shaped pattern (FIGURE 4.10, ZONE A) comprises morphologies that look peculiar and are not encountered in nature. However, exploration of the morphospace enclosed by the U-shaped pattern (FIGURE 4.10, ZONE C) shows that the shape variation within this area is very similar to shapes represented within the syngnathid morphospace (FIGURE 4.10, ZONE B). For the plates, a possible explanation can be that as plates become more triangular, extra robustness (represented by again an increase in plate depth) is needed to ensure the solidity of the plates. Concerning the vertebrae, the U-shaped pattern possibly can be coupled to the

position of the vertebral body, which is located more dorsally in the middle part of the tail and then again at a more ventral position at the most distal tip in all species, except for pipefish (FIGURE 4.11). A possible explanation for this is that, as the cross-section of the tail becomes smaller towards the distal tip, there is not enough space for the epaxial muscles to be functional when the vertebral body is in a more dorsal position and thus a shift to again a more ventral position is required.

Distal tail segments in the non-prehensile pipefish are beamlike instead of cubic (as seen in prehensile species) and possess a short caudal spine compared to their total length. Former studies showed that all spaces in between the dermal plates are covered with additional intercalary plates, making the pipefish tail rigid and heavily plated (Jungersen, 1910, Neutens et al., 2014). Dermal plates in seahorses and two of the studied pipefishes (*Acentronura gracilissima* and *H. taeniophorus*) are highly reduced to tetrahedral like structures with a long caudal spine. Neighboring segments are connected by four gliding joints where the caudal spines insert into the proximal grooves of the posterior plate (Hale, 1996, Neutens et al., 2014, Praet et al., 2012). When comparing caudal spine lengths, it could be observed that this spine is significantly larger in prehensile tailed species (except in *Solegnathus hardwickii* and *Syngnathoides biaculeatus* where the caudal spines are lacking and where dermal plates are absent in the prehensile part of the tail, respectively) than in those with a rigid tail. Following the same hypothesis for a functional explanation of dorso-ventral differences in caudal spine length, it can be suspected that when dermal plates are present, elongated caudal spines in prehensile species are required to allow dermal plates to slide over a longer distance (in the proximo-distal direction), increasing tail flexibility.

This study also showed that the vertebral body is positioned dorsally to the horizontal midline in species with a prehensile tail (except in *S. hardwickii*), which is not the case in non-prehensile species. This hypothesis is confirmed by the observations on ateline and cebine monkeys, where prehensile tailed species differ from non-prehensile ones in the position of the vertebral body, especially in the distal region where the vertebral hemal spines are significantly longer in prehensile tails (Deane et al., 2014). This shift in the position of the vertebral body makes that the hypaxial muscles can be larger than the epaxial ones, the elongated hemal spine creates more expanded muscle attachment site and that the lever arm for ventral bending motion becomes more force efficient in prehensile tailed species. The vertebral body in *S. hardwickii* is positioned more ventrally than in seahorses (similar to this in pipefishes), which would suggest that tail flexibility in *S. hardwickii* is more restricted than in the other studied prehensile species. However, the last approximately 20 segments in *S. hardwickii* are characterized by dorsal and ventral plates

that are no longer interconnected at the lateral and ventral side by any type of joint, suggesting an increase in flexibility towards the distal tip of the tail. As, no data is available on the actual flexibility of the different parts of the tail in this species, we could not confirm this hypothesis.

Neutens et al. (2014) already described that there is a morphological difference in plate shape between seahorses and pipefishes, being tetrahedral or rectangular, respectively. When comparing across species, it can be concluded that non-prehensile tails are characterized by a more extensive medial plate edge, both at the ventral and dorsal side, again limiting tail flexibility. In *S. biaculeatus*, dermal plates are becoming smaller from proximal to distal and are eventually lacking in the prehensile part of the tail. Bending capacities in this species are thus determined by the vertebrae and soft tissue only.

The inter-individual analysis also showed that there is a significant difference between the increase in angle between the anterior and posterior surface of the vertebral body from proximal to distal between *C. intestinalis* and all other studied prehensile species. Possible advantages related to this are already described in the beginning of the DISCUSSION.

CHAPTER 5: BENDING EXPERIMENTS

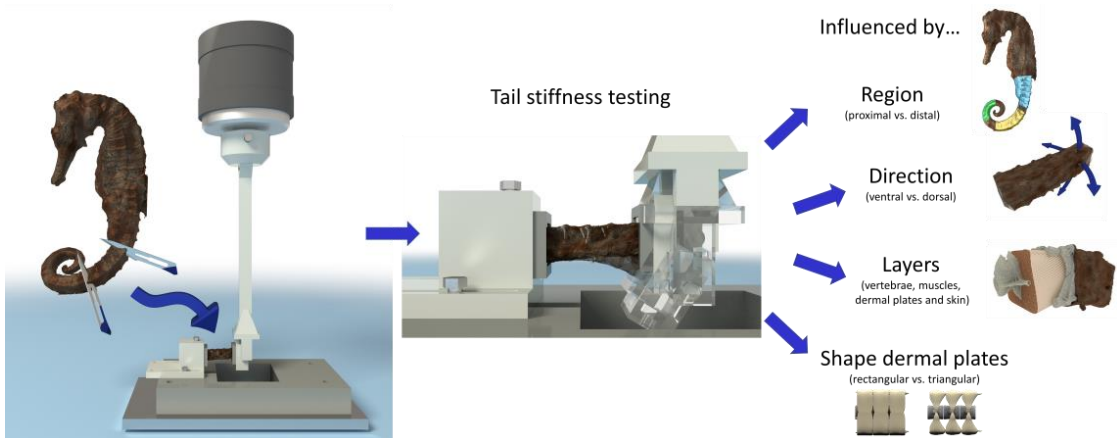
TO BEND OR NOT TO BEND:
EXPERIMENTAL TESTING OF TAIL STIFFNESS
IN SEAHORSE VS. PIPEFISH

MODIFIED FROM NEUTENS C, URBAN P, DE BEULE M, PORTER M & ADRIAENS D,
ACTA BIOMATERIALIA (IN PREP.)

5.1 Abstract

Seahorses are, together with pipehorses, the only teleost fishes known able to bend their tail ventrally over 800° and use it as a grasping appendage. Their close relatives, pipefishes, however have a rigid tail with rather limited bending capacities up to only 300° . However, the nature of bending performance, as well as the structural underpinning of this difference remains poorly understood. The goal of this study is to determine whether regional (proximal vs. distal end of the tail) differences in tail stiffness are present that could explain the different patterns of tail bending. Furthermore, it was investigated how the outer skin (mainly epidermis), dermal plates, muscles and vertebrae each contribute to their natural stiffness in bending. For comparison, we designed an experimental setup in which force-displacement measurements on the passive bending response could be recorded for the different tail sections of each fish (parts of the tail composed of five segments, representative of the different tail regions). The setup was designed in a way that the tail sections could be rotated 90° around the longitudinal axis to allow ventral, dorsal and lateral bending to be compared. Results showed that the skin and dermal plates have the largest influence on the bending stiffness of the tails, while the presence of the muscles and vertebrae contributes to tail stiffness to a lesser degree. Also the pipefish tail is considerably stiffer than the seahorse tail, which can be partly related to a difference in dermal plate morphology.

5.2 Graphical abstract



5.3 Introduction

Fish scales exhibit a wide range of size and shape variability - the general classification includes cosmoid, ganoid, placoid and elasmoid scales (Kardong, 1998) - and the individual scales are known to resist penetration and provide a physical barrier against the attack from predators (Chen et al., 2011, Zhu et al., 2011). At a higher level, the arrangement of the scales provides a flexible skin that allows for changes in fish shape during swimming, but also stress dissipation during puncturing (Vernerey and Barthelat, 2010). In fish locomotion, a scaled skin has proven to play a critical, structural role by regulating wave propagation (Long et al., 1996, Long et al., 2002) and by acting as an external tendon, storing mechanical energy in order to make swimming more efficient (Hebrank, 1982, Hebrank and Hebrank, 1986). Proving to be a highly efficient structure, fish skin has already inspired the development of modern armor systems (Rudykh et al., 2015). The role of fish skin, including scales, in function of swimming behavior has been thoroughly studied in the past (i.e. Yang et al., 2013b, Browning et al., 2013). In seahorses however, the tail is not covered with overlapping, flat scales or used as a swimming appendage, but has evolved into a complex plated armor forming a prehensile structure (Hale, 1996, Neutens et al., 2014). In seahorses, the bony plates that comprise the armor have been suggested to not only provide body support and protection, but also play an essential role in tail bending to grasp and hold onto seagrasses or other objects (Hale, 1996, Praet et al., 2012).

Seahorses (genus *Hippocampus*) belong to the syngnathid family, which comprises approximately 55 genera that can be categorized into four different morphotypes: pipefishes, pipehorses, seahorses and seadragons (Kuitert, 2009). All Syngnathidae are characterized by the presence of these bony plates covering the whole body (Hale, 1996, Jungersen, 1910, Neutens et al., 2014) and functioning as a fairly rigid dermal armor (Porter et al., 2013, Praet et al., 2012). However, only pipehorses and seahorses are characterized by a prehensile tail (Blake, 1976, Hale, 1996, Neutens et al., 2014, Weber, 1926). The bony plates in seahorses are substantially reduced to tetrahedral like structures, compared to the rectangular plates in pipefishes (Neutens et al., 2014, Hale, 1996, Jungersen, 1910, Neutens et al., under review). In pipehorses, different ways to obtain a prehensile tail are observed, including through plate size reduction, the absence of bony plates or the absence of scarf joints within one segment and/or sliding joints between two consecutive segments (Neutens et al., 2014).

The tail of syngnathid fishes can be divided into four main layers: the outer skin, the dermal plates, the muscle tissue and the vertebral column. These layers are all characterized by

different material properties and thus can influence the local and global stiffness of the tail in different ways.

Considering the influence of the outer skin and dermal plates on body flexibility, a previous study showed that cutting the dermis in longnose gar (*Lepososteus osseus*) significantly reduced the flexural stiffness of the body, but that bending properties were not significantly altered by the removal of a caudal scale row (Long et al., 1996). Others however, suggest that the shape and amount of overlap of the scales can change the amount of flexibility and protection (Browning et al., 2013). Also, it has been shown that the ratio of scale size to animal size can govern how flexible armor is with respect to size (generally the lower the ratio, the greater the flexibility) (Yang et al., 2013a). Praet (2013, 2012) and Neutens et al. (under review) already showed that the bony plates along the tail in seahorse decrease in size from proximal to distal. The resulting finer articulations at the distal end enable the seahorse to smoothly bend its tail, approximating a golden spiral (a specific case of a logarithmic spiral of which the growth factor is the golden ratio). As such, regional differences in bending performance can be expected, dictated by these differences in plate size.

Fish also use their muscles to modulate body stiffness, and therefore the natural oscillatory frequency of the body. It is likely that by tuning the natural frequency of the body to the tailbeat frequency, the mechanical cost of bending the body during undulatory swimming can be minimized (Long and Nipper, 1996). In most teleosts, these tail muscles are organized in a conical way. This is also the case for the dorsal body muscles (epaxials) in seahorses. However, their hypaxial muscles (ventral of the vertebral column) differ substantially from this pattern, as they are arranged in longitudinal sheets, spanning up to 8 vertebrae (Neutens et al., 2014). Also, seahorses are characterized by the presence of medial ventral muscles, interconnecting the hemal spines of two consecutive vertebrae (Hale, 1996, Neutens et al., 2014). Uniaxial tensile testing of seahorse tail muscles showed that, when comparing the passive response of the muscles, the hypaxials are approximately ten times stiffer in extension than the epaxials (even when correcting for the difference in cross sectional area), presumably because of this specific muscle architecture (Praet, 2013).

The backbone in fishes acts as a compression resisting element within the body to allow contractions of the lateral musculature to result in bending and to allow a more specialized style of swimming to occur. In some subcarangiform and thunniform swimmers, it has been shown that the mechanical properties of the backbone (during lateral bending) and the regional differences in backbone stiffness can be related to the swimming style of those fishes (Hebrank, 1982). Also suggested is that there is a strong correlation between the

maximal curvature that can be obtained by bending a fish in the lateral direction and the number of intervertebral joints present in that fish (Brainerd and Patek, 1998). The same study also suggests that the influence of this difference in number contributes more to the flexibility of the body than the intervertebral joint angle. The vertebral column in fishes thus provides both the stiffness and flexibility required for locomotion. The amount of flexibility can be altered by changing the shape and size of the individual vertebrae, but also by modifying the intervertebral joints that act as a hydrostatic hinge, resisting compressive loads, but still allowing for lateral bending (Nowroozi and Brainerd, 2012, Schmitz, 1995).

Based on all this information, it seems likely that differences in bending capacity in prehensile and non-prehensile syngnathid fishes may be explained by structural differences at different levels: regional variations across the tail length and variations among the major components of a tail (outer skin, dermal plates, muscles and vertebrae). As such, we tested four main hypotheses in two of the four morphotypes: seahorse (possessing a prehensile tail) and pipefish (possessing a rigid tail). First, it can be expected that the tail of seahorse will be characterized by a higher stiffness during dorsal bending, compared to ventral or lateral bending, while the stiffness in pipefish will be equal in the three bending directions. Second, the tail in seahorse will be characterized by a lower flexural stiffness at the distal tip of the tail, compared to the proximal part of the tail, as passive bending experiments showed an exponential increase in bending angle from proximal to distal in seahorse (Neutens et al., 2014, Porter et al., 2015). In pipefish however, it is expected that the stiffness will be constant over the complete length of the tail, as pipefish shows a linear increase in bending angle from proximal to distal (Neutens et al., 2014). While the goal of previously performed passive bending experiments (Neutens et al., 2014, Porter et al., 2015) was to determine the maximum passive bending angle of complete tails, this study focusses on the force needed to bend the regional parts of the tail over a certain distance. Third, it can be expected that the different layers (outer skin, dermal plates, muscles and vertebrae) each influence tail stiffness in a different way. Fourth, and based on the differences in plate morphology between pipefish and seahorse (Hale, 1996, Jungersen, 1910, Neutens et al., 2014, Neutens et al., under review), it can be expected that the flexural stiffness in seahorse and pipefish is different from each other when comparing the stiffness of the intact tail, but shows the same pattern after removal of the dermal plates.

5.4 Material and Methods

5.4.1 Test samples

Due to the experimental nature of the testing procedure and limited specimen access, only two seahorse specimens (one *Hippocampus subelongatus* and one *H. abdominalis*) and one pipefish specimen (*Corythoichthys intestinalis*) were studied. All specimens used were commercially obtained through the aquarium trade and euthanized with an overdose of benzocaine according to Belgian law legislation on animal welfare. The *H. abdominalis* specimen became ill and had to be euthanized before the experimental setup could be tested. This specimen was stored immediately at -80°C to avoid crystallization.

Each tail was divided into three regions (proximal – middle – distal) and a piece of five tail segments was isolated from each region. From this piece, one segment at each side was fixated with Technovit 3040 (Heraeus Kulzer) into an open box of 15x15x8 mm that could be mounted onto the experimental setup that was designed for this study (see STIFFNESS TESTS). The samples were kept hydrated by storing them in a saline solution (0.9% NaCl dissolved in demineralized H_2O) for 5 minutes after each time the bending and rotating protocol (see STIFFNESS TESTS) was applied and before removal of the subsequent tissue layer.

5.4.2 Stiffness tests

The experimental setup was designed and drawn in 3D using RHINOCEROS (Version 5, R. McNeel & associates), 3D printed on a Stratasys UPrint SE plus 3D printer, using ABSplus P430 (layer thickness of 0.245 mm, flexural modulus of 1.65 GPa). The setup consists of a platform (FIGURE 5.1A) that can be screwed onto the base of an Instron 5944 electromechanical test system (Instron, Norwood, MA, USA), located at IBiTech-bioMMeda, Ghent University. The Instron system was equipped with a 10 N load cell, on which a rod (FIGURE 5.1B) is mounted. The box holder (FIGURE 5.1C) is pinned onto the end of this rod and is able to rotate around its horizontal axis. The small boxes in which the tissue is embedded are fastened into this box holder. During the experiments, a translation of 6 mm was applied to the rod, thus inducing a bending movement on the sample fixed in the box holder. Small rotations of the top joint of the rod (around the horizontal axis) are allowed to avoid tensile stresses during translation. The starting position of the sample in the experiment corresponds to the resting tail position of the animal. This was done with a translation speed of 0.5 mm/s and for three consecutive cycles. A second box holder (FIGURE 5.1D) was mounted onto the platform (FIGURE 5.1A) and could be moved closer to or further away from the other box holder, depending on the sample size. The boxes were designed in

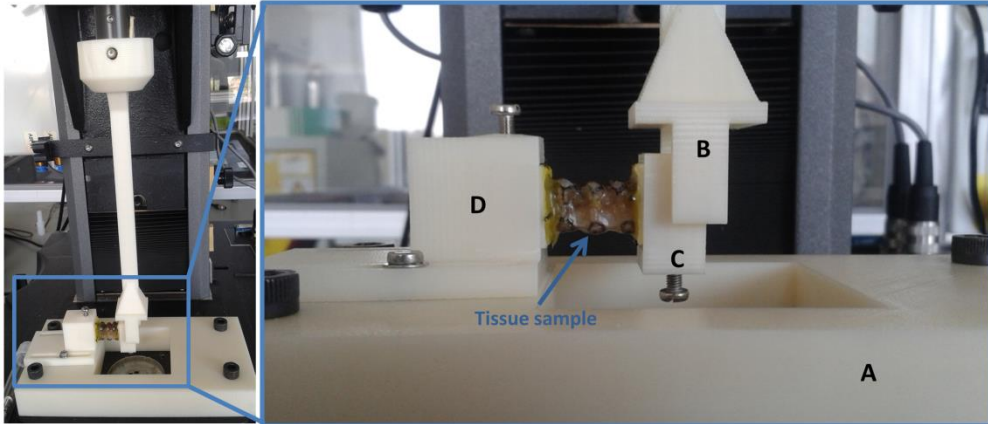


FIGURE 5.1 - Design of the experimental setup, with A = the mounting platform, B = rod mounted on the instron load cell, C = rotating block holder and D = fixed block holder.

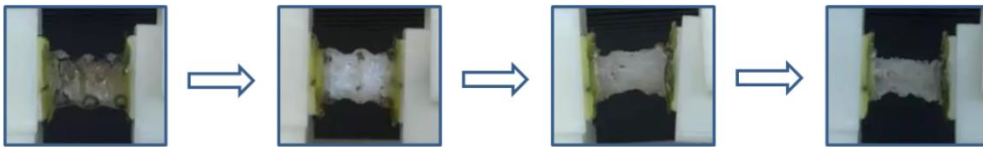


FIGURE 5.2 - Removal of the different layers of which a syngnathid tail consists illustrated on the proximal *Hippocampus subelongatus* tail piece. From left to right: intact tail, removal of the outer skin, removal of the dermal plates and removal of the muscle tissue (sample length (3 segments) = 14.63 mm).

such a way that the tail piece could be rotated over 90° around the longitudinal axis of the tissue sample and as such ventral, dorsal and lateral bending could be compared. Control testing was performed by applying the bending and rotating protocol twice on some of the tail pieces (randomly chosen) and measurements were compared. This was done to be sure that bending the tail does not damage the tail tissue and thereby influence the stiffness of the tail. As one of the goals of this study is to investigate the effect of outer skin, dermal plates, muscles and vertebral column on the flexibility of the tail, the outer skin was removed after rotating the complete tail piece four times over 90° around the longitudinal axis and the same protocol was applied. After this, the dermal plates were removed and the test was performed again. Eventually the muscles were removed so that in the end only a series of vertebrae could be tested (FIGURE 5.2). All experiments were captured using a JVC HD Everio camera.

These experiments were first performed on the (frozen) *H. abdominalis* tail pieces. When cutting the tail of the *H. subelongatus* specimen, it was ascertained that, due to its large size, the most proximal part (segment one to five) of the tail could not fit the printed boxes.

Taking into account that printing bigger boxes and holders could alter the results (and thus making them less comparable), it was opted to use the region consisting of segment six to ten.

The (absolute) flexural stiffness (EI , in $N \cdot mm^2$) was calculated using beam theory (Timoshenko, 1955):

$$EI = \frac{Fl^3}{3u}$$

where F is the (average) force measured (N), l the length of the tail piece (mm) and u the deflection (mm). The deflection in our study was always 6 mm (= the translation distance). To be able to compare different species and different tail regions with each other, we need to remove the effect of cross-sectional size. The flexural stiffness of a rectangular cross-section of width (w) and height (h), and made of homogeneous isotropic material with Young's modulus E , is given by (Timoshenko, 1955)

$$EI = \frac{Ewh^3}{12}$$

where E is the material parameter and wh^3 the size effect. The flexural stiffness was thus normalized in the following manner:

$$EI' = \frac{EI}{h^3w}$$

where h is the average height of the sample (mm) and w the average width (mm). This average height and width were determined by taking a section just anterior and posterior of each dissected tail piece and calculating the average of, respectively the width and height of both sections, assuming that tail size decreases gradually over the three consecutive segments. The height and width of the sample change depending on the direction of bending (as the height always corresponds to the axis of the applied loading).

The absolute flexural stiffness can be seen as a representation of the structural properties of the sample, whereas the normalized flexural stiffness represents the overall elasticity modulus and represents the material properties of the sample.

5.5 Results

5.5.1 Directional differences

The intact seahorse tail is more constrained during dorsal bending than during ventral or lateral bending in the proximal, middle and distal parts. The observed skew in dermal plates of a seahorse tail allows the tail to bend more in the ventral direction than in the dorsal direction (Porter et al., 2015). FIGURE 5.3 shows a comparison of the bending stiffness of the tails of the *Hippocampus subelongatus*, *H. abdominalis* and *C. intestinalis* specimens.

In the **proximal part** of the intact tail of the *H. subelongatus* specimen, the absolute flexural stiffness during dorsal bending is more than double than that during both lateral and ventral bending. After removal of the outer skin and dermal plates, the difference between the three bending directions is less pronounced. After removal of the muscles, only the absolute flexural stiffness in the lateral bending direction shows a small decline, while the one in the other two directions stays approximately the same as before muscle removal (FIGURE 5.3, FIRST ROW). In the **middle part** of the intact tail the absolute flexural stiffness during dorsal bending is again more than double than during to ventral bending. Lateral bending is again more constrained than ventral bending, but the difference in absolute flexural stiffness between the dorsal and lateral bending direction is less pronounced. Surprisingly, this difference between lateral and ventral flexural stiffness disappears after removal of the outer skin. The difference between the three bending directions is again less pronounced after plate removal. After removal of the muscles, only the absolute flexural stiffness of bending in the dorsal direction decreases, while the one in the other two directions increases (which probably is an artefact due to the setup, see DISCUSSION) (FIGURE 5.3, FIRST ROW). In the **distal part**, the absolute flexural stiffness during dorsal bending is higher than during lateral or ventral bending (although the difference is less pronounced than in the proximal or middle part of the tail). A decline in absolute flexural stiffness is observed after removal of the outer skin in all three bending directions. Dorsal bending is still the most constrained bending direction after skin removal, but lateral bending is more constrained than ventral bending. After removal of the dermal plates, the absolute flexural stiffness during dorsal bending further decreases, while an increase in absolute flexural stiffness is observed during ventral bending and no effect of layer removal was observed during lateral bending. After dermal plate removal, ventral bending is the most constrained, followed by lateral and dorsal bending. After removal of the muscles, the absolute flexural stiffness in all three bending directions increases and ventral bending is still the most constrained, followed by lateral and dorsal bending (FIGURE 5.3, FIRST ROW).

In the *H. abdominalis* specimen, the **proximal part** of the tail is unexpectedly less constrained during dorsal bending than during lateral or ventral bending, both for the complete tail, as after one by one removal of the different layers. Before removal of the outer skin and the dermal plates, tail bending is most constrained during ventral bending. However, after removal of the dermal plates and the muscles, lateral bending is most constrained (FIGURE 5.3, SECOND ROW). The **middle part** of the intact tail is characterized by a more constrained dorsal bending, followed by lateral and ventral bending. After removal of the outer skin however, the dorsal bending direction is the most flexible one and ventral bending becomes the most constrained one. The pattern with a more constrained dorsal bending, followed by lateral and ventral bending reappears after removal of the dermal plates. After removal of the muscles, only the absolute flexural stiffness of bending in the dorsal direction decreases, while the one in the other two directions increases. Ventral bending is again more constrained than lateral or dorsal bending when the muscles are removed (FIGURE 5.3, SECOND ROW). The **distal part** of the intact tail shows the same pattern as in *H. subelongatus*, although the difference between the more constrained dorsal bending and the less constrained ventral and lateral bending is smaller. The absolute flexural stiffness during ventral bending is the lowest after subsequent removal of the outer

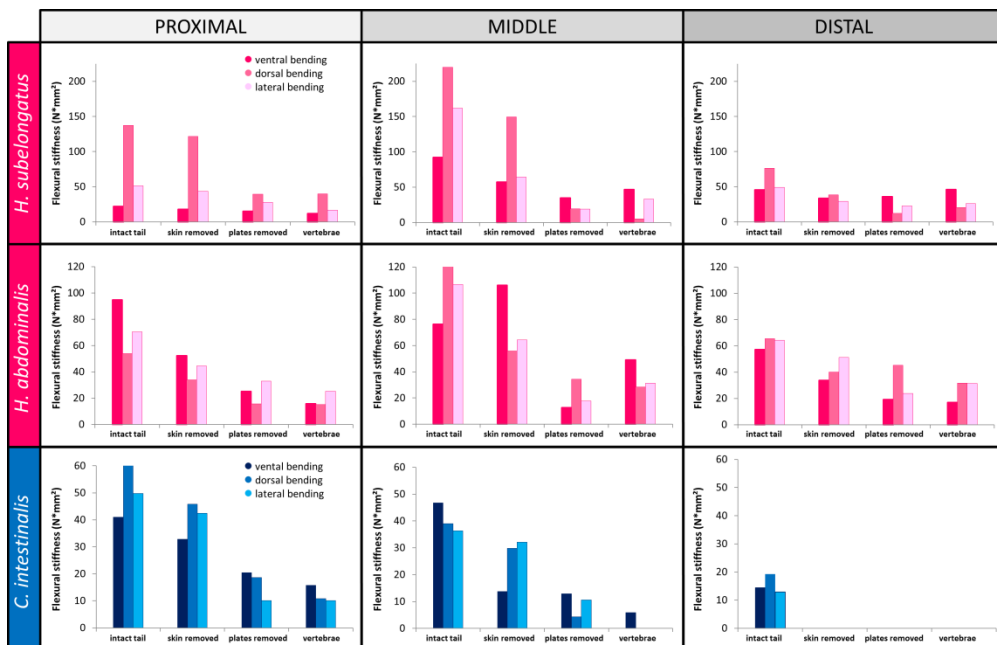


FIGURE 5.3 - Overview of the average absolute flexural stiffness ($N \cdot mm^2$) in two seahorse species (*Hippocampus subelongatus* and *H. abdominalis* - pink) and one pipefish species (*Corythoichthys intestinalis* - blue) during ventral, dorsal and lateral tail bending of the intact tail and after subsequent removal of the outer skin, dermal plates and muscles in three different part of the tail (proximal, middle and distal).

skin, dermal plates and muscles. After removal of the outer skin, the absolute flexural stiffness becomes higher during lateral bending than during dorsal bending. This effect disappears after removal of the dermal plates (FIGURE 5.3, SECOND ROW).

In the **proximal part** of the intact tail of the pipefish *C. intestinalis*, the absolute flexural stiffness is higher during dorsal bending than during lateral and ventral bending, but the opposite pattern could be observed after removal of the dermal plates and muscles (FIGURE 5.3, THIRD ROW). The **middle part** of the complete tail is characterized by a higher absolute flexural stiffness during ventral than during either dorsal or lateral bending. After removal of the epidermis, a decrease of the absolute flexural stiffness could be observed, especially in the ventral bending direction, which is now the most flexible bending direction. After removal of the dermal plates, ventral bending is again the most constrained one, followed by lateral and dorsal bending. Due to tissue rupture after ventral bending, there is no data available on lateral and dorsal bending after muscle removal (FIGURE 5.3, THIRD ROW). Only data on the absolute flexural stiffness of the intact tail of the **distal part** is available for the pipefish specimen, because the sample broke during the experiments due to its small size. This distal part of the intact tail is characterized by a more constrained dorsal bending, followed by ventral and lateral bending (FIGURE 5.3, THIRD ROW).

5.5.2 Regional differences

The *C. intestinalis* specimen is characterized by a markedly increasing normalized flexural stiffness distally during both dorsal and lateral bending of the intact tail (FIGURE 5.4). During ventral bending however, the distal part of the tail showed a lower normalized flexural stiffness, resulting in a more gradual increase along the tail. In both seahorse specimens, a small increase in normalized flexural stiffness could be observed between the proximal and middle part of the tail, but again slightly decreasing towards the most distal tip of the tail, indicating a higher flexibility at the proximal and distal tail ends than in the middle part of the tail. Although both seahorse species show the same pattern, the *H. abdominalis* specimen is characterized by a lower normalized flexural stiffness than the *H. subelongatus* specimen, in all bending directions as well as in the three different regions of the tail (although this difference is very small in the proximal region of the tail).

Even though the bending angle in the **proximal part** of the tail is approximately the same in pipefish and seahorse, the normalized flexural stiffness in this part of the tail of the pipefish specimen is higher in all three bending directions than in the seahorse specimens (FIGURE 5.4). The same applies during dorsal and lateral bending of the **middle part** of the tail. In the ventral bending direction however, the bending profiles are already diverging. This

increase in bending angle in the ventral direction goes along with a lower normalized flexural stiffness in the seahorse specimens and a higher one in the pipefish specimen during ventral bending (compared to dorsal or lateral bending) (FIGURE 5.4). In the **distal part** of the tail, a higher normalized flexural stiffness is observed during dorsal and lateral bending (compared to ventral bending) in the pipefish specimen, but this is not reflected in the bending capacity curves. Also the increased bending capacities in ventral and lateral direction in the seahorse specimens are not reflected in the normalized flexural stiffness values (the stiffness values only slightly decreases from the middle part to the distal part,

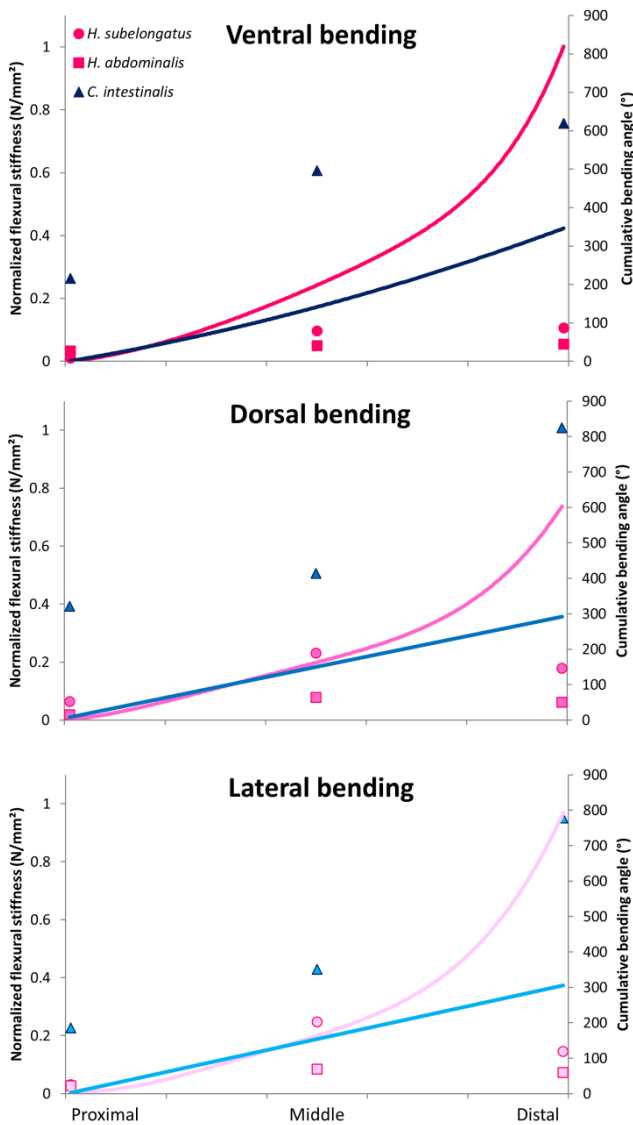


FIGURE 5.4 - Relation between the average normalized flexural stiffness and the passive bending pattern versus body region in the studied pipefish and seahorse specimens. The primary vertical axis shows the normalized flexural stiffness in one pipefish (*Corythoichthys intestinalis* – blue dots) and two seahorse specimens (*Hippocampus subelongatus* (pink dots) and *H. abdominalis* (pink squares)) in the three studied tail regions (proximal, middle and distal). The secondary vertical axis shows the passive bending pattern along the tail of *C. intestinalis* (blue line) and *H. reidi* (pink line) (adapted from Neutens et al. (2014)). The upper graph shows values related to bending in the vertical direction, the middle one in the lateral direction and the lower one in the dorsal direction.

but the bending capacity increases substantially). The bending capacities in the dorsal direction are lower (compared to the ventral and lateral bending direction), but still substantially higher than in the middle part of the tail. This is however not reflected in the normalized flexural stiffness values, which are, again, slightly lower in the distal part of the tail, compared to the middle part (FIGURE 5.4).

5.5.3 Tissue-related differences

In the *H. subelongatus* specimen, the absolute flexural stiffness in the **proximal part** of the tail drops with approximately 15 to 20% after removal of the outer skin in both the ventral, dorsal and lateral bending direction (compared to the intact tail stiffness). The influence of removal of the dermal plates however, is different when comparing the three bending directions. The effect of dermal plate removal is the biggest in the dorsal bending direction, followed by the lateral and ventral bending direction (drop in absolute flexural stiffness of resp. 60%, 30% and 13% - compared to the bending stiffness after removal of the outer skin). Removal of the muscles did not have an effect on the absolute tail stiffness during dorsal bending. During lateral and ventral bending, a drop in absolute flexural stiffness of

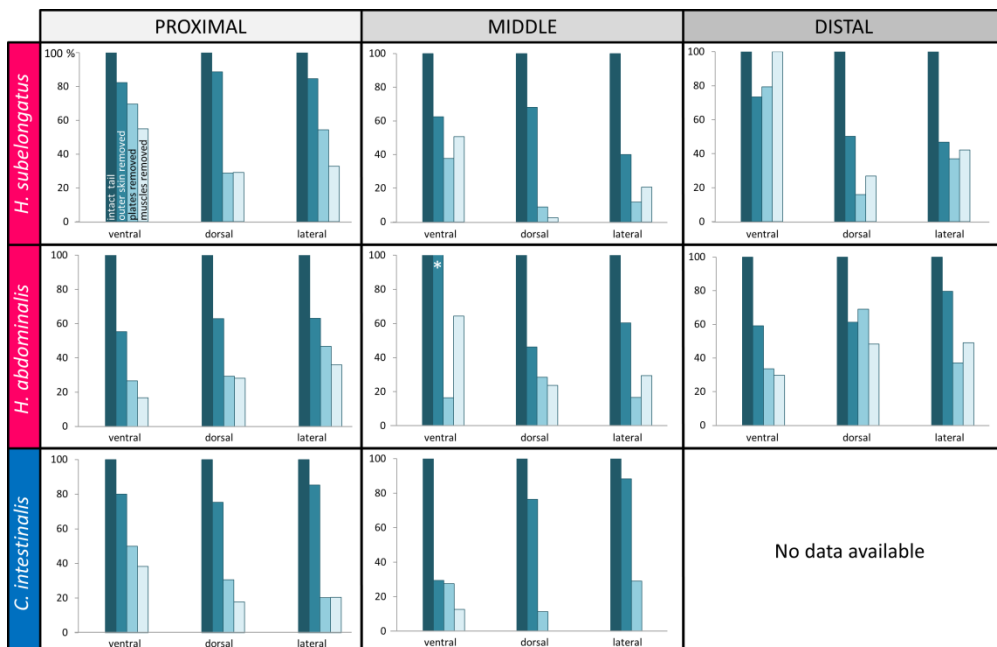


FIGURE 5.5 - Overview of the relative change of the average absolute flexural stiffness after one by one removal of outer skin, dermal plates and muscles (compared to the average absolute flexural stiffness of the intact tail) in two seahorse specimens (*H. subelongatus* and *H. abdominalis* - pink) and one pipefish specimen (*C. intestinalis* - blue) during dorsal, ventral and lateral tail bending in three different parts of the tail (proximal, middle and distal). The * indicates a stiffness higher than 100% of the initial stiffness value (134%).

resp. 22% and 15% after removal of the muscles could be observed (compared to the bending stiffness after dermal plate removal) (FIGURE 5.5, ROW 1). In the **middle part**, the influence of the outer skin on tail flexibility is bigger than in the proximal part and removal of this layer causes a decrease in absolute flexural stiffness of approximately 35% during dorsal and ventral bending and even 60% during lateral bending. Similar as in the proximal part of the tail, the effect of dermal plate removal is the biggest in the dorsal bending direction, followed by resp. the lateral and ventral bending direction (drop in absolute flexural stiffness of resp. 60%, 28% and 25% - compared to the bending stiffness after removal of the outer skin). Removal of the muscles decreases the absolute flexural stiffness with another 6% during dorsal bending. Surprisingly, removal of the muscles results in an increase in absolute stiffness during ventral and lateral bending (FIGURE 5.5, ROW 1). In the **distal part** of the tail, the removal of the outer skin has a pronounced effect on the bending stiffness during dorsal and lateral bending (decrease in absolute flexural stiffness of approximately 50%), but this effect was less pronounced in the ventral bending direction (decrease in absolute flexural stiffness of 27%). After removal of the dermal plates, a further decrease in absolute flexural stiffness could be observed during dorsal and lateral bending (35% and 10% resp.). An increase in absolute flexural stiffness could be observed during ventral bending and after removal of the muscles (in all bending directions) (FIGURE 5.5, ROW 1).

In the *H. abdominalis* specimen, the absolute flexural stiffness in the **proximal part** of the tail drops with approximately 40% after removal of the outer skin in both the ventral, dorsal and lateral bending direction (compared to the intact tail stiffness). Removal of the dermal plates results in a similar drop in absolute flexural stiffness during ventral and dorsal bending (resp. 28 and 33% compared to the bending stiffness after removal of the outer skin). Removal of the dermal plates has a less pronounced effect on the absolute flexural stiffness during lateral bending, which decreases with only 16%. Similar as observed in the *H. subelongatus* specimen, removal of the muscles does not have an effect on the tail stiffness during dorsal bending, while a decrease in absolute flexural stiffness during lateral and ventral bending could be observed (compared to the bending stiffness after dermal plate removal) (FIGURE 5.5, ROW 2). Removal of the outer skin has a pronounced effect on the absolute flexural stiffness during dorsal and lateral bending of the **middle part** of the tail (resp. 55% and 40%, compared to the intact tail stiffness). During ventral bending however, an increase in absolute flexural stiffness of 34% was observed after removal of the outer skin. Removal of the dermal plates has the same effect during ventral and lateral bending, when compared to the initial tail stiffness (decrease in absolute flexural stiffness to approximately 16%). Tail stiffness again increases after removal of the muscles during

ventral and lateral bending, while this removal doesn't have a pronounced effect on the absolute flexural stiffness during dorsal bending (FIGURE 5.5, ROW 2). In the **distal part** of the tail, removal of the outer skin again decreases tail stiffness by approximately 40% during ventral and dorsal bending and 20% during lateral bending. A further decrease in tail stiffness could be observed after removal of the dermal plates during ventral and lateral bending, but an increase could be observed during dorsal bending. After removal of the muscles however, a decrease of the absolute flexural stiffness was observed during ventral and dorsal bending, but an increase during lateral bending (FIGURE 5.5, ROW 2).

In the **proximal part** of the tail of the *C. intestinalis* specimen, the absolute flexural stiffness decreases with approximately 15 to 25% after removal of the outer skin during ventral, dorsal and lateral bending (compared to the stiffness of the intact tail). Removal of the dermal plates has the most pronounced effect during lateral bending (causes an increase of 65% compared to the stiffness before removal of the dermal plates), followed by dorsal and lateral bending (increase of resp. 45 and 30%). Removal of the muscles did not have an effect on the tail stiffness during lateral bending. During both dorsal and ventral bending, a drop in absolute flexural stiffness of approximately 12% removal of the muscles could be observed (compared to the bending stiffness after dermal plate removal) (FIGURE 5.5, ROW

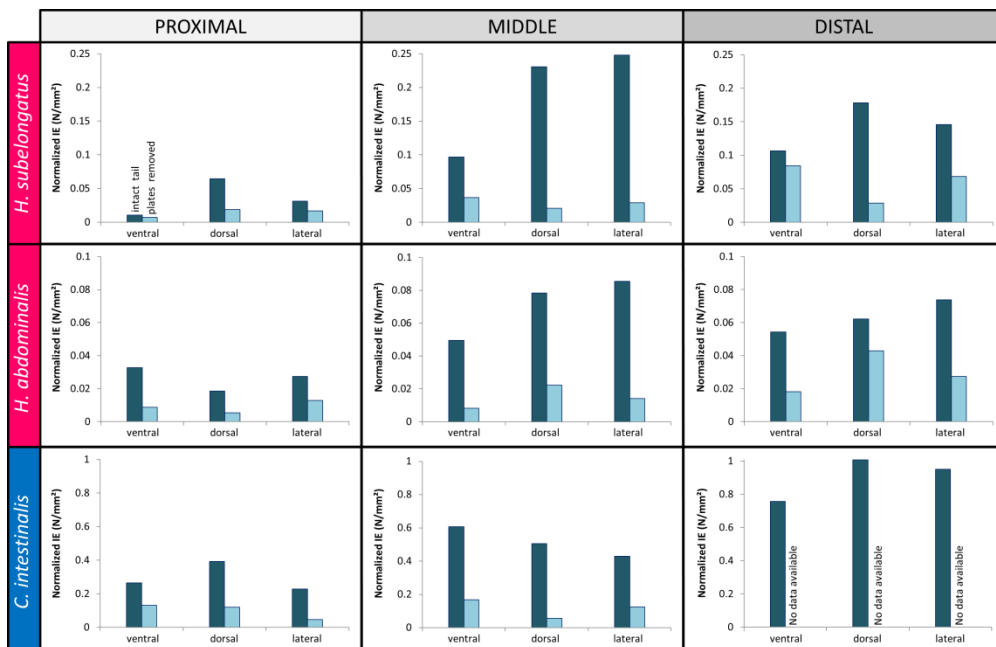


FIGURE 5.6 - Comparison of the average normalized flexural stiffness (N/mm²) of the intact tail with the average normalized flexural stiffness after removal of the dermal plates in two seahorse specimens (*Hippocampus subelongatus* and *H. abdominalis*) and one pipefish specimen (*Corythoichthys intestinalis*) in the three studied tail regions (proximal, middle and distal).

3). In the **middle part** of the tail, removal of the outer skin caused an increase in absolute flexural stiffness of more than 70%, while only a decrease in absolute flexural stiffness of 25% could be observed during dorsal bending and 12% during lateral bending. While removal of the plates did not have any influence on the absolute flexural stiffness in during ventral bending, this did have a pronounced effect during dorsal (increase of 65%) and lateral bending (increase of 59%). Removal of the muscles caused a further increase in tail stiffness during ventral bending, but the effect of muscle removal could not be studied during dorsal and lateral bending in the middle part of the tail due to tissue fracture (FIGURE 5.5, row 3). For the same reason, no data is available on the **distal part** of tail.

5.5.4 Morphotype-related differences

In both pipefish and seahorse, the normalized flexural stiffness is higher before plate removal than after (FIGURE 5.6). This difference is most pronounced in the proximal and middle part of the pipefish specimen (due to tissue rupture during the experiment, data after outer skin removal in the distal part of the tail is lacking). There is also a difference in normalized flexural stiffness between the two studied seahorse species before plate removal (with the *H. subelongatus* tail pieces being stiffer than those of the *H. abdominalis* specimen). However, this difference is less pronounced after removal of the dermal plates. In the proximal and middle part of the tail, the normalized flexural stiffness after removal of the plates is still higher in pipefish than in both seahorse species.

5.6 Discussion

It has to be mentioned it are preliminary results that are presented in this chapter and that these results can be influenced by the experimental setup. First, as the boxes containing the samples are not able to slide out of the box holders, it is possible that this will induce additional tensile stresses in the tail sections and will add an additional (unwanted) stiffness to the measurements. These tensile stresses are dependent on sample geometry and the degree of bending and can be problematic if the sample lengths are significantly different. However, if we would reconfigure the setup and allow the tails to freely slide out of the vertical plane at larger displacements, frictional effects due to the sliding should be taken into account, which might overcomplicate things. Small rotations of the top joint of the rod (around the horizontal axis) are allowed to minimize these tensile stresses during translation.

Second, the mechanical influence of the 3D printed parts is neglected, but currently we cannot validate this assumption. It is necessary to calibrate the setup properly before the test are performed to be sure that there is no stress distribution due to mechanical loading

of the 3D-printed elements and that the force measured is only related to the bending stiffness of the tissue. To do so, it would be necessary to test three or four solid beams of different material properties (and preferably of a constant cross sectional area equal to the tails that are tested) to cover the range of stiffness's observed in the animal tissues. By comparing the results of tensile testing these three or four samples, a calibration curve can be obtained, either to prove that the 3D-printed parts can be neglected or to use to adjust the final results. It would also be interesting to put markers on the tested materials, to determine if stretching of the material occurs during bending.

It is well known that fish skin has remarkable mechanical properties, largely dependent on the composition of the dermal layer (lightweight, ultra-thin, compliant and resistant to penetration) (Vernerey and Barthelat, 2010) and that it is very suitable to use as a source of biological inspiration for the development, design and fabrication of armored surfaces (Duro-Royo et al., 2015, Wen et al., 2014). Previous research already showed that the strength and flexibility of a dermal armor can be influenced by different factors, *i.e.* the size and arrangement of the scales (Wen et al., 2014), the scales being round or squared (Porter et al., 2015), the interaction between and the proportion of soft and hard tissue (Fratzl et al., 2016, Wen et al., 2014) and the amount of overlap (or the type of joints) between different segments (Porter et al., 2013, Wen et al., 2014).

First, it was expected that the tail of the seahorse specimens will be characterized by a higher flexural stiffness during dorsal bending, compared to lateral and ventral bending, while the stiffness in the pipefish specimen will be equal in the three bending directions. Overall, a more constrained flexibility during dorsal bending (compared to ventral and lateral bending) could be observed when studying the intact tail pieces. Only two exceptions could be observed. The first exception is that during bending of the proximal tail piece of *Hippocampus abdominalis*, tail flexibility is more constrained during ventral bending and least constrained during dorsal bending. The tail in seahorses doesn't only function as a grasping appendage, but is also used to keep their balance (Weber, 1926). When the proximal part of the tail (just under the abdomen) is slightly bended in the dorsal direction during tail curling or grasping, the complete tail will be positioned directly underneath the center of mass of the animal (FIGURES 5.7A & 5.7B) and not in front of it (which would be the case if only ventral curling occurs), leading to a more stable position (Weber, 1926). If this dorsal curling of the proximal part doesn't occur, the seahorse always has to bend head and abdomen more ventrally to remain in balance (FIGURE 5.7C), which would complicate their specific way of feeding (Roos et al., 2009). However, this lower flexural stiffness during dorsal bending of the proximal part of the tail was not observed in

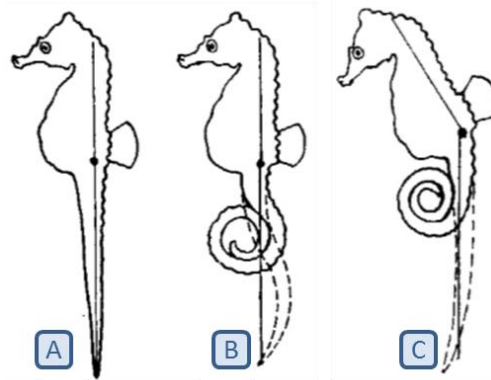


FIGURE 5.7 - Stable swimming positions in seahorses. A swimming with a straight tail, B and C swimming with a curled tail (modified from Weber, 1926)

H. subelongatus. Because of the large size of the animal, the most proximal part (segment 1-5) of the tail was too big to fit into the 3D printed boxes, so the part just underneath that could fit the boxes was used during the experiments (segment 6-10). When attached, this part of the tail containing segment six to ten does not show the dorsally bended position, but a ventrally bended one, as observed in the rest of the tail. The second exception is during bending of the middle part of *Corythoichthys intestinalis*. The lower flexural stiffness during dorsal bending is probably due to the fragility of the tail piece and due to tissue rupture after ventral bending, leading to lower values during dorsal and lateral bending (ventral bending was always performed first, followed by dorsal and lateral bending).

Second, it was expected that the tail in the seahorse specimens would be characterized by a lower flexural stiffness at the distal tip of the tail (compared to the proximal part of the tail), while the tail stiffness of the pipefish specimen will be constant over the complete length. This hypothesis could not be confirmed. The results indicate that the passive bending curves are rather size-dependent than stiffness-dependent. In seahorse, the proximal and distal ends of the tail are characterized by both a lower absolute and normalized flexural stiffness than the middle part of the tail. This observed higher flexural stiffness in the middle part of the tail is thus not due to a difference in diameter, but reflects the intrinsic stiffness of this tail region (as the absolute stiffness values are also higher in this middle region). It has been shown that the plate and vertebral morphology in the distal and proximal part of the tail are more similar to each other than to the skeletal elements of the middle part of the tail (Neutens et al., under review). The more limited flexibility in the middle part of the tail thus probably reflects this difference in plate and vertebral morphology and not to a difference in size of the tail samples (and thus also not to a difference in size of the dermal plates). In pipefish, it could be observed that there is an

increase in normalized flexural stiffness along the tail. Although, the more similar proximal and distal tail segments morphology was also observed in pipefish (Neutens et al., under review), previous studies also showed that there is a decline in segment size from proximal to distal in both seahorse and pipefish (Neutens et al., under review, Praet, 2013). The increase in normalized flexural stiffness from proximal to distal in pipefish is probably to counteract the decline in segment size (as the absolute flexural stiffness decreases from proximal to distal). The hypothesis that dermal plate size has an influence on tail flexibility (Yang et al., 2013a) is thus only valid for pipefish and not for (the distal part of) seahorse. It can be that this shape difference plays a more important role in determining tail stiffness in seahorse than the size difference and that the opposite is true for pipefish.

Third, it was expected that the different layers (outer skin, dermal plates, muscles and vertebrae) each influence tail stiffness in a different way. Removal of the outer skin and dermal plates almost always decreases tail stiffness with more than 50% (compared to the stiffness of the intact tail), indicating that these two layers together play a major role in tail stiffness in both the studied pipefish and seahorse specimens. However, the individual contribution of the outer skin and the dermal plates to tail stiffness is variable in the different samples. In four tail cases, the outer skin and dermal plates did not decrease tail stiffness with more than 50%, being during ventral and lateral bending of the proximal region of the *H. subelongatus* specimen, during ventral bending of the distal region of the *H. subelongatus* specimen and during dorsal bending of the distal region of the *H. abdominalis* specimen. No logical explanation can be thought of why the outer skin and dermal plates have a more limited influence on tail stiffness in these four cases. Removal of the muscle tissue often caused a further, however more limited, decrease in tail stiffness. Surprisingly, in eight tissue samples it caused an increase in stiffness (see further).

Fourth, it was expected that the flexural stiffness in seahorse and pipefish will be different from each other when comparing the stiffness of the intact tail, but will show the same pattern after removal of the dermal plates. When considering the intact tail, it could be observed that the tail of the studied pipefish specimen is indeed stiffer than the one of the two seahorse specimens studied (FIGURE 5.6). If these differences in tail stiffness are caused by the differences in dermal plate shape (as described in Hale, 1996, Jungersen, 1910, Neutens et al., 2014, Neutens et al., under review), it can be expected that after plate removal, the normalized flexural stiffness would be equal in seahorse and pipefish. After removal of the plates, the overall normalized flexural stiffness in pipefish is still higher than the one in seahorse, although it should be noted that the differences between the two morphotypes became rather small. This could indicate that the mechanical properties of

the muscles or the backbone itself also influence the stiffness of the tail, but that the differences in tail stiffness between the studied pipefish and seahorses are mainly determined by the differences in dermal plate morphology. Praet (2013) already showed that (when corrected for cross-sectional difference) during passive stretching the sheet-like myosepta in the hypaxials of seahorse are approximately ten times stiffer in extension than the conically shaped ones in the epaxials. Assuming that the mechanical properties of pipefish muscles (that are also characterized by a conical arrangement) are comparable to those of the epaxial muscles in seahorse, this difference in hypaxial muscle configuration can be an explanation for the difference in the observed normalized flexural stiffness. Considering the influence of the backbone on tail stiffness, Neutens et al. (under review) found that there is a difference between pipefish and seahorse when looking at both the inclination angle between the anterior and posterior surface of the vertebral body (with the angle being larger in seahorse) and the position of the vertebral body (with the vertebral body positioned more dorsally in seahorse). However, a previous study on four different species of fishes (*Monacanthus hispidus*, *Acanthurus chirurgus*, *Abudefduf saxatilis* and *Scarus coeruleus* - Brainerd and Patek (1998)) suggested that the difference in tail flexibility is mainly due to differences in the amount of segments present in each tail and not due to difference in intersegmental angle. As we always studied the same amount of segments, the differences in flexural stiffness we observed cannot originate from a difference in segment number. Also, the average intersegmental angle in the four species they studied was 8.4°, while the intersegmental angle in seahorse can be up to 25° (Neutens et al., under review). Two possible explanations for the difference in bending stiffness can be hypothesized. First, the intersegmental angle indeed doesn't influence bending stiffness, indicating that the dorso-ventral position of the vertebral centrum (relative to the position of the complete vertebra) is the only factor influencing tail stiffness. Second, the intersegmental angle does have an influence on the bending stiffness, but only when reaching a certain angle. As no intraspecific variation was included in this explorative study, it can be expected that there will be overlap between the measured stiffness values after plate removal in both morphotypes and that the contribution of the muscles and the backbone to the differences in tail stiffness between the two morphotypes is rather limited. Also, as there is only limited data available on the flexural stiffness of the backbone itself in pipefish, it is hard to determine if these small differences in normalized flexural stiffness after plate removal are caused by the stiffness of the muscles or the stiffness of the backbone.

Two striking things could be observed during the bending experiments. First, sometimes there is a switch in highest flexural stiffness values between dorsal and ventral bending (the

one being stiffer before, but less stiff than the other after removal of a certain layer). Previously performed passive bending experiments (Neutens et al., 2014, Porter et al., 2015) show higher flexibility during ventral and lateral bending, compared to dorsal bending. A possible explanation for this switch in flexural stiffness values is variation in the flexural stress being induced by putting the tails into their starting position for measuring stiffness. In case tails would be over or under stretched at the onset of bending, release of stored strain energy as well as differences in how caudal spines interlock (Rommens, 2010) may play a role. However, every test was performed three times in a row, so it can be expected that if spines are interlocked during the first cycle, they won't be interlocked anymore during the second and third cycle. Also, during the experiments, we tried to determine the initial starting position to correspond as correct as possible to the natural position of the tail piece. However, it cannot be excluded that slight deviations from this natural position have occurred in certain cases. Although it is unlikely that the slight deviations of the starting position compared to the natural curvature of the tail piece could cause a switch of this quantity between ventral and dorsal tail stiffness, its true cause currently remains unexplained. Second, it could be observed that sometimes there is a small increase in stiffness after the removal of a certain layer, which cannot be linked to a switch between ventral and dorsal bending as described above (FIGURE 5.3). This only occurs on the smaller tissue samples. Two possible explanations for this can be thought of. First, it is possible that smaller tissue samples dry out faster than larger samples and that this causes an increase in stiffness. Also, next to a smaller sample size, removal of the different layers can lead to faster tissue dehydration. Second, it is possible that the error on the measured values is relatively bigger when measuring very low forces and that the increase in stiffness is an artefact due to the testing device.

During all experiments, it could be observed that *H. abdominalis* is characterized by both a lower absolute and normalized flexural stiffness before dermal plate removal than *H. subelongatus*. Whether or not this reflects a specimen or species specific difference, or rather was a methodological artefact from deep freezing the *H. abdominalis* samples, could not be discerned.

CHAPTER 6: DYNAMIC TAIL MODELLING

6.1 Abstract

Morphometric analyses already showed that there are shape differences within and between the tails of the different syngnathid morphotypes (CHAPTER 4). The main goal of this study is to determine if these observed shape differences can be related to tail flexibility. To do so, these shape differences were implemented in a virtual, dynamic model. For each shape difference, an addition to the original model developed by Tomas Praet (Praet, 2013) was written, so that the influence of each characteristic could be studied separately, as well as the effect of combining them. Based on the virtual modelling of the major axes of variation of the vertebrae (as observed in CHAPTER 4), it can be derived that these axes indeed reflect traits that seem to improve bending capacities and are thus likely to be adaptive. The used modelling approach did, however, not allow determining if the morphological differences between the plates of the different morphotypes can be related to tail flexibility.

6.2 Introduction

One of the challenges engineers encounter during the design and development of new structures is how to create a structure that is stiff, strong and tough in a certain direction, but at the same time very flexible in another direction, a characteristic required for many applications. One could think of the steel cables of an elevator, which need to be strong enough to cope with the weight of both the elevator and the counter weight, but also flexible enough to be wound around the pulley. Examples can also be found in medical applications, such as the stents in lower extremities that require a high radial stiffness to keep the artery open, but have to be flexible enough to cope with knee bending and soft tissue deformations. In nature, structures that are either very firm or very flexibility can be found, but the combination of both is rather unique. However, the tail of seahorses and some of the closely related pipehorses is characterized by a bony armor that is mechanically hard and sufficiently tough to resist fracture from impact and crushing, yet elastic and flexible enough for controlled axial bending and prehension (Porter et al., 2013) and can thus inspire engineers to invent new applications. Potential applications that can be thought of are steerable catheters, flexible stents, earthquake resistant structures, controlled anchoring mechanisms, prehensile robots, flexible armor or protective clothing for extreme sports and stuntmen, etc. (Porter et al., 2013, Praet, 2013).

Over the past couple of years, studies were performed covering different aspects of the tail of seahorses and their close relatives (pipefishes, pipehorses and seadragons). Detailed

morphological studies showed that the musculoskeletal morphology of the seahorse tail is quite unique compared to the ancestral condition found in the (non-prehensile) pipefish tail, but also that there are alternative solutions to obtain a prehensile tail (as could be observed in pipehorses) (Hale, 1996, Neutens et al., 2014; CHAPTER 3). Morphometric studies (Bruner and Bartolino, 2008, Neutens et al., under review; CHAPTER 4) proved that there are differences in both dermal plate and vertebral morphology between and within the tail of non-prehensile and prehensile species. Bending experiments showed that seahorses not only can obtain a higher degree of curvature of the tail, but also that less force is required to bend their tail over a certain distance compared to pipefish (Neutens et al., 2014, Porter et al., 2015; CHAPTER 3 & 5). Mechanical studies indicated that both the architecture as well as the deformation mechanisms of the seahorse tail are responsible for the prehensile capacities of the tail, but also provide protection against predators (Porter et al., 2015, Porter et al., 2013). A dynamic parametric model based on the seahorse tail was created (Praet, 2013) and showed that the sequential structure of the seahorse tail can remain flexible because of the gliding joints that connect the corners of consecutive segments, but also that radial stiffness can be obtained through the support that the central vertebra provides to the dermal plates (Praet et al., 2012).

It is already known that the tail of prehensile and non-prehensile syngnathid fishes differs at least at three different levels, being the differences in skeletal morphology (as described in CHAPTER 4), the differences in muscular morphology (as described in CHAPTER 3) and the amount of segments of which the tail consists (Lourie 1999, Randall 1997). Previous studies (Hale, 1996, Porter et al., 2013, Praet et al., 2012) already stated that it are the bony plates of seahorses that play a major role in the ability to bend their tails and grasp and hold objects. However, Neutens et al. (under review; CHAPTER 4) also found, next to differences in dermal plate morphology, differences in the shape of the vertebrae between non-prehensile and prehensile tails, indicating that the morphology of these vertebrae could also influence tail prehensility. As such, the focus of this chapter will be on these differences in skeletal morphology as well as how they (individually or combined) influence tail flexibility. As it is not possible to test the implications of the individual shape characteristics in nature, it was opted to implement these in the dynamic parametric seahorse model created by Praet (2013). The first hypothesis tested is that tail flexibility (the obtained total curvature or in the energy needed to obtain this curvature) will decrease or stay equal/increase, respectively, after altering each of the five shape characteristics related to tail prehensility independently to as they occur in the pipefish or pipehorse morphotypes. The second hypothesis tested is that by combining these five characteristics (as they occur in the different morphotypes) into one model, tail prehensility

will be even more constrained in the pipefish model and less constrained in the pipehorse models (as the different characteristics influence tail prehensibility on different levels).

6.3 Material and Methods

Dynamic, parametric, rigid-body modelling is used to mimic tail grasping behavior of the different syngnathid morphotypes. The contraction of muscles (more specific the median ventral muscles) is used as input and is specified as the change in distance between the attachment points of the muscles. Displacements and rotations of the rigid bodies can be easily visualized and extracted and muscle and joint forces can be obtained after running the simulation (Praet, 2013).

6.3.1 Initial seahorse model

The initial parametric model based on the seahorse tail (*Hippocampus reidi*) was developed by Tomas Praet in the framework of an interdisciplinary project funded by the Research Foundation Flanders (FWO, grand number 3G013709) that focused on biological engineering (Praet, 2013). What follows is a short resume of this model and is based on the information found in Praet (2013, 2012), including details on skeletal element, joint and muscle modelling and how the model is created.

The model generation was performed using dedicated Python scripts in pyFormex (version 9.1), an open source software package for generating, transforming and manipulating large geometric models of 3D structures by sequence of mathematical operations. The generated input files are afterwards solved using Abaqus (version 6.11, Simulia - Dassault Systems, Vlizy-Villacoublay, France), a finite element solver that allows to easily integrate rigid (for multibody dynamic simulations - MBD) and deformable (for finite element analyses - FEA) bodies in the same model.

6.3.1.1 Skeletal elements

Detailed information on the geometry of the most proximal tail segment was determined based on high resolution μ CT-scans of the tail of an adult *Hippocampus reidi* specimen. Scans were taken at the Centre for X-ray Tomography at Ghent University (UGCT) using a tube voltage of 70 kV and a detector pitch of 127 μ m. The resulting voxel size ranged from 7 to 50 μ m, depending on the region of interest. The scans were segmented into 3D surface models using 3D Slicer (version 3.6). To avoid shrinkage of the 3D models during surface smoothing, a Humphrey's Classes algorithm (implemented in pyFormex 9.1) was chosen for smoothing. The other tail segments were thereafter generated based on the surface model

of this most proximal segment by applying appropriate geometric transformations (scaling and skewing). The amount of scaling and skewing was determined based on polynomial resp. linear approximations that best fitted measurements taken on the μ CT-data (FIGURE 6.1).

6.3.1.2 Joints and muscles

The 3D meshes of the tail segments were automatically rotated into a standardized position and the position of the joints and muscle attachment sites were automatically determined from the skeletal surface models using pyFormex. Joints and muscles were modelled using *connectors* in Abaqus. A connector is a connection between two points that can be given certain properties (*e.g.* stiffness, plasticity, damage, damping or failure). Each connector has its own axis system and the properties can be (translational or rotational) direction dependent.

Joints are modelled as *non-linear elastic connectors*. Different types of joints can be mimicked by keeping certain degrees of freedom fixed and giving others a certain stiffness.

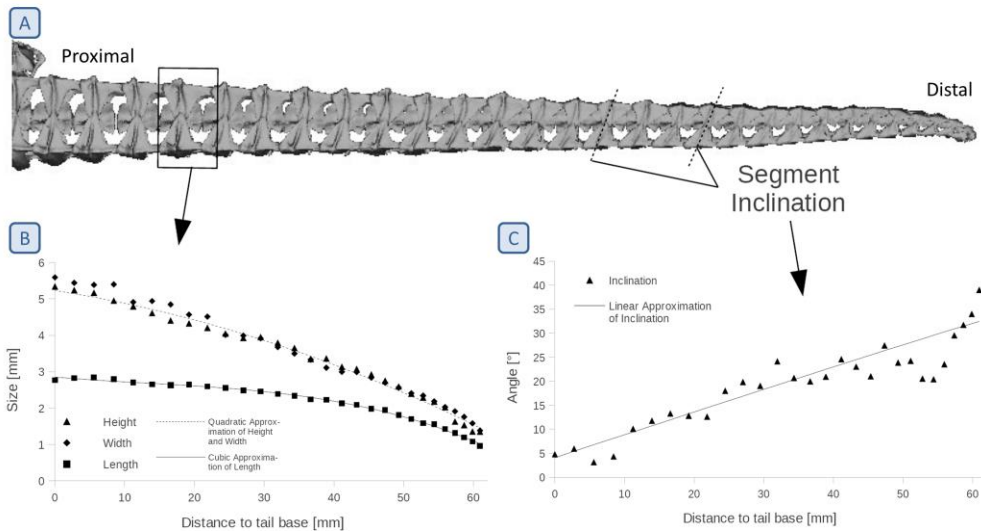


FIGURE 6.1 - Scaling and skewing of segments along the seahorse tail. (A) Overview of how segments size and inclination change from proximal to distal, (B) Segments scaling (height, width and length) in relation to the position along the tail and (C) segment skewing in relation to the position along the tail. Approximations are fitted on third-degree polynomial for the segment length, second degree polynomial for the segment height and width and a linear regression for the skewing. The Pearson product-moment correlation coefficients are 0.996 for the length, 0.988 for the width, 0.991 for the height and 0.845 for the segment skewing (adapted from Praet et al., 2012)

Four types of joints were modelled (the exact joint stiffness values can be found in TABLE 6.1 (Praet, 2013)):

- The **joints between vertebra and dermal plates** were determined by averaging of the extreme points of the processes on the vertebra with the nearest point on the appropriate dermal plate. These joints are modelled as ball-and-socket joints, meaning that all translational degrees of freedom (DOF) are limited, while the rotational DOF are kept free (FIGURE 6.2A).
- The **joints between two subsequent vertebrae** were modelled by determining the geometric center of the inner circle that is found by intersecting the vertebrae with a transverse plane that is located at 10% of the total longitudinal length of the vertebrae for both the posterior side of the vertebra proximal to the joint and the anterior side of the vertebra distal to the joint. The joint is then positioned at the average of those two points. The joints are modelled as flexible ball-and-socket joints with linear elastic parameters (FIGURE 6.2B).

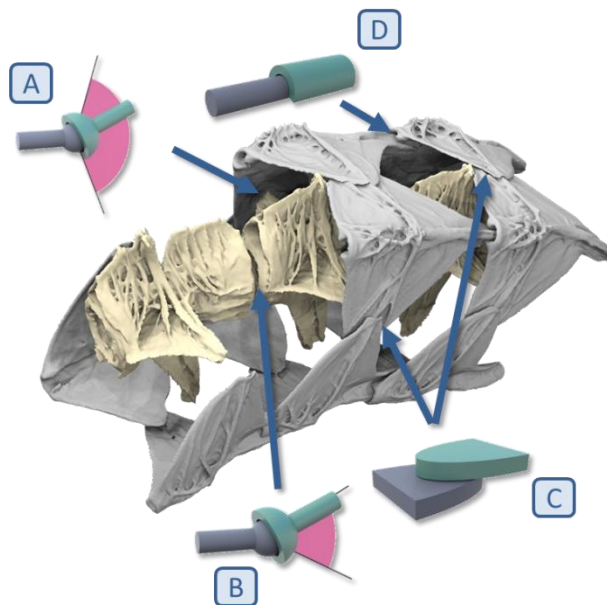


FIGURE 6.2 - Overview of the different types of joints present in the seahorse tail and how they are modelled: (A) the joints between vertebra and dermal plates modelled as ball-and-socket joints with large rotational range of motion, (B) the joints between two subsequent vertebrae modelled as ball-and-socket joints with limited rotational range of motion, (C) the joints between the plates within one segment modelled as gliding joints with minimal resistance against compression and elongation in the main gliding direction and (D) the joints between subsequent dermal plates modelled as gliding joints with a non-linear elastic response in compression along the direction of the groove of the joint and a very small linear elastic response in extension.

- The **gliding joints between the plates within one segment** are determined by averaging the extreme points on both plates that make up the joint. This also causes that the lateral joints follow the direction of the skewing. These joints are modelled as gliding joints with minimal resistance against compression and elongation in the main gliding direction. The other translational DOF are given medium elasticity, while the rotational directions have high values (FIGURE 6.2C).
- The **gliding joints between subsequent dermal plates** are determined by following the curvature of the surface of the caudal spines. The total length of the joints is not included in the model, as even at maximal bending, the caudal spine of the dorsal dermal plates are still within their respective grooves (except for some of the most distal segments). These joints are modelled as gliding joints with a non-linear elastic response in compression along the direction of the groove of the joint and a very small linear elastic response in extension. The two other translational directions were given a high linear elastic stiffness. Rotation around the distal spine has a medium stiffness, while the other two rotational directions have a high linear stiffness (FIGURE 6.2D).

	X transl	Y transl	Z transl	X rot	Y rot	Z rot
joints between vertebrae and dermal plates						
<i>at the level of the lateral spines</i>	1.00	1.00	1.00	1.00E-06	1.00E-06	1.00E-06
<i>at the level of the hemal spines</i>	0.10	0.10	0.10			
joints between two subsequent vertebrae	10.00	1.00	1.00	1.00E-06	1.00E-06	1.00E-06
joints between plates within one segment	1.00E-06	0.10	0.10	0.10	0.10	0.10
joints between subsequent dermal plates	non-linear	1.00E-06	1.00E-06	0.01	0.10	0.10

TABLE 6.1 – Assigned joint stiffnesses (in N/mm for displacement and N*mm/rad for rotation). Open cells indicate those degrees of freedom that are kept completely free (so no stiffness at all is associated with those directions) (modified from Praet (2013)). To improve stability, a stiffness of 1 μ N/mm is given in directions where joint stiffness could be assumed to be close to zero.

Muscles are modelled as *axial elements*, meaning that their behavior is only defined in the axial direction and that the muscle is free to rotate around its attachment point, but that the muscle's length is subjected to a certain behavior. For active muscle contraction, time dependent length changes of the muscle or muscle forces need to be provided. In case of passive muscle contraction, a non-linear extensibility needs to be provided for the connector that models the muscle. This extensibility is based on tensile testing of the muscle tissue, which showed that the stiffness of the epaxial muscles is much lower than that of the hypaxial ones (Praet, 2013). In order to avoid sudden peaks in forces, accelerations should be continuous throughout the simulations. Therefore a smooth-step amplitude will be used for all shortenings of the connectors that represent the muscles. For a certain muscle fiber length, this amplitude will change in time according to FIGURE 6.3.

The myosepta are attached to both the vertebrae and the dermal plates and span three consecutive segments. This is thus a severe simplification of the actual situation, as the hypaxials in seahorses span up to eight segments. Taking more segments between the connection to the vertebra and the connection to the plate would induce unrealistic situations: the beam will go outside of the tail when a certain level of bending is achieved, leaving a high angle at the attachment points to the skeleton. This would cause a direction in which the muscle pulls onto the skeleton that is too far away from the anteroposterior axis. Enabling the connectors to span more segments without affecting the pulling direction of the myomeres during bending is possible (by adding (an) intermediate point(s) in the connector, splitting the initial connector), but would also increase the complexity of the model (Praet, 2013).

The connection of the myoseptum to the vertebra is approximated by cutting the vertebra with two planes that intersect in the X-axis and are diagonal with respect to the Z-axis (FIGURE 6.4A – blue lines), calculating the four extreme points (FIGURE 6.4A – red dots) and projecting those on the cross section going through the center of mass of the vertebra (FIGURE 6.4B). The attachment site to the dermal plate was determined by cutting the plate with a plane perpendicular to the longitudinal axis (the x-axis) at 8% of the total longitudinal length of the plate (Figure 6.3C – blue line). This section was then cut again with a diagonal plane parallel to the longitudinal axis, so that only the ventral part remains for the ventral plates and the dorsal part for the dorsal plates (Figure 6.4C – green line). From this ventral or dorsal part, respectively (indicated with an X in FIGURE 6.4C), the most proximal part is now taken as the attachment point of the myomeres (FIGURE 6.4C – red dot). The different attachment points modelled are approximations of the positions of the tendons that are

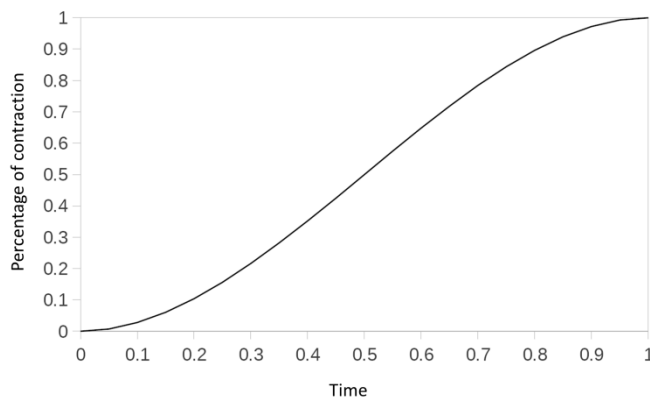


FIGURE 6.3 – Graph representing the smooth-step amplitude (mimicking muscle fiber behavior) used for muscle shortening (modified from Praet et al., 2012). A percentage of contraction of 1 indicates that the amount of contraction as specified in the parameter settings (e.g. 25%) is reached.

assumed to transmit the forces to the vertebrae and dermal plates, as it is not entirely clear where the exact sites of attachment are located.

The median ventral muscle (MVM) attachment site is determined as a point on the longitudinal axis of the hemal spine (FIGURE 6.5 – yellow line) at a position of 90% of the total length of the haemal spine (90% position based on measurements on synchrotron data) (FIGURE 6.5).

6.3.1.3 Model creation

As a tail consisting of 30 segments contains approximately 150 skeletal elements and 380 joints, the dynamic models were kept simple to reduce solving time. Each detailed surface element was replaced by a simplified rigid body, with a defined center of mass and attachment points for joints and muscles (FIGURE 6.6). The necessary parameters for

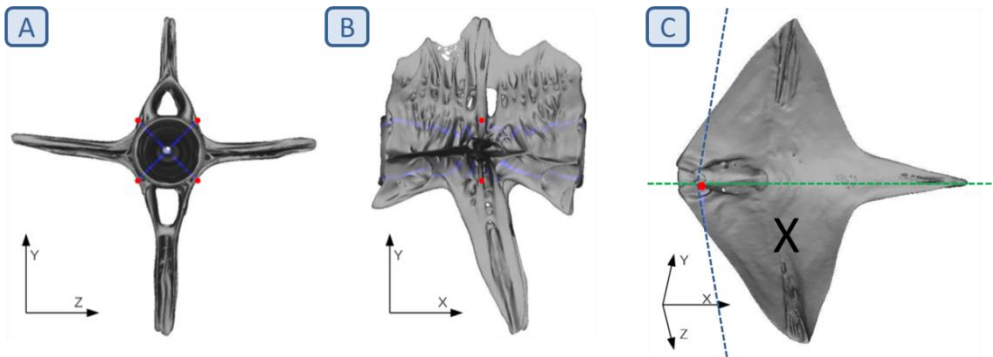


FIGURE 6.4 – Connection points of the myosepta on (A) and (B) the vertebra and (C) right ventral dermal plate (modified from Praet et al., 2012).

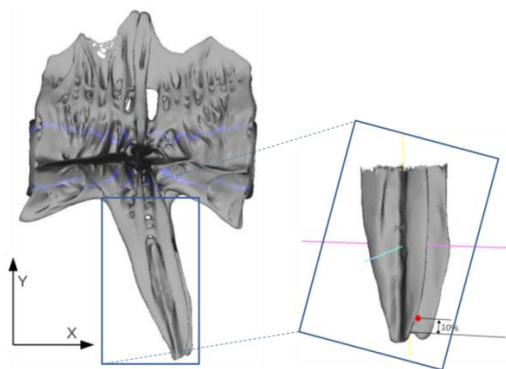


FIGURE 6.5 – Position of the attachment point of the median ventral muscle on the haemal spine (red dot) (modified from Praet, 2013).

dynamic analyses (such as mass and moment of inertia) are determined based on the 3D meshes and are inherited by the simplified geometries.

The neutral or resting position of the tail (= the position in which the tail will be when all muscles are at rest) will be taken as the initial position for the simulations. However, personal observations on anaesthetized seahorses indicate that the resting position of the seahorse tail can be very variable and that small changes of this position can be applied after manual manipulations with minimal effort. As several animals were sedated and photographed, it was opted to choose an average neutral tail position to be digitized and to be used as starting position for the multibody dynamic simulations (FIGURE 6.7).

6.3.1.4 Input parameters included in the model

Several parameters are included in the multibody dynamic model and can be found in Praet (Praet, 2013). Some of the parameters need to be provided by inputting them into a pop-up menu when starting the model generating script in pyFormex. Other, more extensive, parameters will be read in from .csv files.

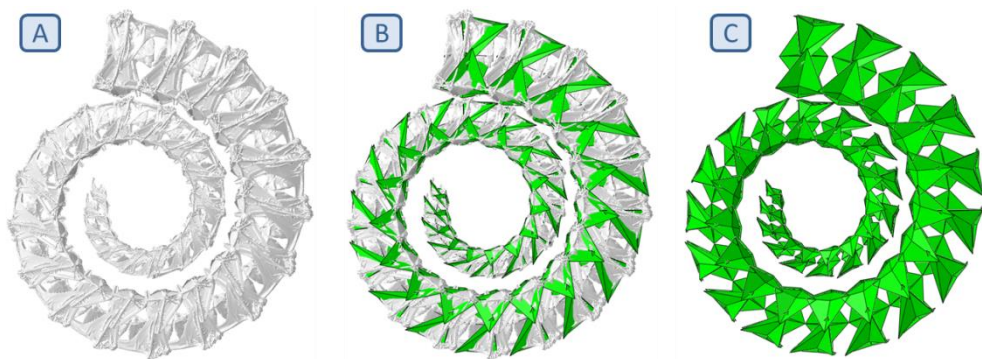


FIGURE 6.6 – Seahorse tail model containing 30 segments, shown as (A) the display bodies (based on the real seahorse geometries from μ CT-data), (B) the simplified rigid bodies mapped onto the display bodies and (C) only the simplified rigid bodies.



FIGURE 6.7 – Neutral tail position used as starting position for the multibody dynamic simulations (courtesy of Dr. Anabela Maia).

6.3.2 Adapted seahorse model

6.3.2.1 Additions

The different additions to the initial seahorse model are based on the results obtained in CHAPTER FIVE. Five shape characteristics were found that could be related to tail prehensility in seahorses and pipehorse, being the ratio of segment height vs. segment length, the inclination angle between the anterior and posterior surface of the vertebral body, the ratio of caudal spine length vs. plate length, the ratio of the medial plate edge length vs. plate length and the position of the vertebral body (relative to segment height). Initially, the goal was to implement all five shape differences encountered in this previous chapter. However, as the length of the caudal spine was not included in the initial seahorse model and it was rather difficult to implement this, it was opted to not include the difference in caudal spine length as a parameter. The edited script, with the four additions written by Tomas Praet, can be found in APPENDIX C (the parts implemented for this research are indicated in blue).

6.3.2.2 Input parameters included in the adapted seahorse model

Each addition can be implemented separately to the seahorse model by activating the module in the pop up window when running the script in pyFormex. For each addition, additional input parameters were created, which are listed below. Some of these parameters were kept constant in all models created within the framework of this thesis to make the results easily comparable (mainly the offset values).

Addition one - the inclination angle between the anterior and posterior surface of the vertebral body:

- Angle between the anterior and posterior surface of the vertebral body (if the value is positive, the inclination tends towards the ventral direction – FIGURE 6.8 blue lines).

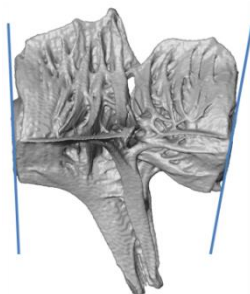


FIGURE 6.8 – Anterior and posterior surface of the vertebral body indicated on a vertebra of *Hippocampus reidi* (addition 1).

Addition two - the position of the vertebral body (relative to segment height):

- Total relative shift of the vertebral center (if the value is negative, the vertebral body shifts to a more dorsal position, e.g. a value of -0.1 shifts the vertebral body in the dorsal direction over a distance corresponding to 10% of original position of the vertebral body).
- Parameters that define the region of scaling:
 1. The distal offset corresponds to the proximal region of the haemal spine that will be scaled, e.g. a value of 0.8 causes a scaling of the proximal 80% of the spine and keeps the remaining distal 20% intact (FIGURE 6.9 - orange).
 2. The proximal offset corresponds to the proximal region of the haemal spine that won't be scaled, e.g. a value of 0.2 makes sure that the proximal 20% of the spine will not be scaled (FIGURE 6.9 - blue).

Addition three - the ratio of segment height vs. segment length (FIGURE 6.10):

- The slope and the intercept of the linear approximation of the relationship between segment height and length

Addition four - the ratio of the medial plate edge length vs. plate length (FIGURE 6.11):

- The amount of deformation of the display bodies (FIGURE 6.11 – blue area)
- The offset for the deformation area of the display bodies

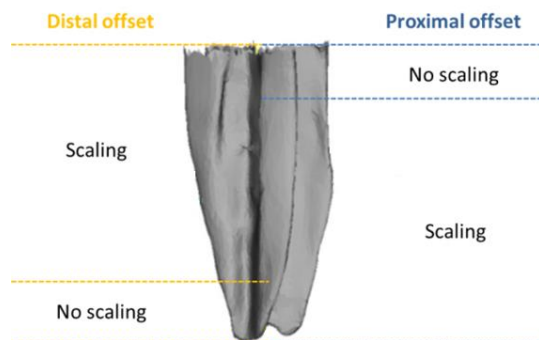


FIGURE 6.9 – Illustration of the distal and proximal offset related to addition 2 (position of the vertebral body) (modified from Praet, 2013).

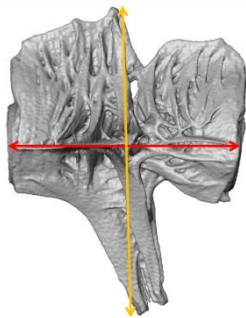


FIGURE 6.10 – Illustration of segment height (yellow arrow) and segment length (red arrow) on a vertebra of *Hippocampus reidi* (addition 3).

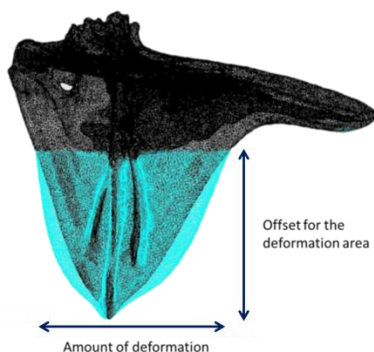


FIGURE 6.11 – Illustration of the parameters added to the model concerning addition 4 (the ratio of the medial plate edge length vs. plate length). The deformation of the plate edge is indicated in blue.

6.3.3 Simulations

Two different kinds of analyses were performed. The first analyses modelled the individual contributions of each parameter to the flexibility of the tail. This was done by running the script with each time only one of the additions included and the parameters were set in such a way that the separate models represent the condition found in seahorse, pipefish, pipehorse type I and pipehorse type II, resp., (SEE CHAPTER 3 & 4) as good as possible. This was done for all four additions. The second analyses tried to mimic the tail morphology of seahorse (initial model), pipefish, pipehorse type I and pipehorse type II, resp., by combining the four characteristics as observed in each of the morphotypes.

6.3.3.1 Parameter settings related to the initial model

All initial model parameters (as listed in 6.2.2.4) were left default, except for the model name, the number of segments (which was set to 30 in all models) and the muscle contraction settings. For the simulations performed within the framework of this thesis,

only median ventral muscle contractions were included. As the hypaxial myosepta span several vertebrae, they cannot cause fine and controlled bending between two consecutive segments and only taking the MVMs into account is thus a valid simplification to make to test the hypotheses postulated. Also, it is proven that the MVM are responsible for pure ventral bending, while the hypaxial myomeres induce both lateral and ventral bending of the tail. During a first analysis, maximal MVM strain during contraction was set to 25% of the initial muscle length. The 25% MVM shortening was chosen based on previous research (Praet et al., 2012), indicating that this is the maximal MVM shortening possible in seahorse before collision of the skeletal elements occurs. In some of the created models, a higher degree of bending could be obtained without the occurrence of collision. In these cases, the MVM contraction was set to 40% (= the maximum contraction that is biologically possible, van Leeuwen, 1992) to be able to compare maximum curvature between the different models and the corresponding required bending energy. Collision of skeletal elements was visually determined.

6.3.3.2 Parameter settings related to the adapted model

The parameter settings for the different additions are based on the values presented in CHAPTER 4 and can be found in TABLE 6.2. The offset values were kept equal in all models, to be able to easily compare the results. For the first and second addition, the values for type I and type II pipehorses are identical, and thus these two morphotypes will be discussed together for the first two model additions. Some of the values measured in CHAPTER 4 overlap between the different morphotypes (*e.g.* the angle between the anterior and posterior surface of the vertebral body in *Hippocampus zosterae* is more similar to the one of *Acentronura gracilissima* than to other seahorses). Also, for the tail of the pipehorses, which often consists of a non-prehensile proximal part and a prehensile distal part, values corresponding to the prehensile part were used as input parameters to create the different models. The models created in this 6TH CHAPTER are composed in such a way that they allow to investigate the decoupled influence of the shape differences determined in CHAPTER 4 on tail flexibility and not to exactly mimic the conditions found in nature.

6.3.3.3 Result processing using Abaqus

Two types of comparisons between the different models were made (both for the models containing the individual characteristics and those mimicking the tails of pipefish, seahorse and pipehorse). First, an MVM contraction of 25% was applied and collision of the skeletal elements was allowed. In this way, the required bending energy and the total curvature of the tail could be determined and compared between the different models. The required

Parameter	Pipefish	Seahorse	Pipehorse type I	Pipehorse type II
Addition 1 - inclination angle of the vertebral body				
Angle	0°	15°	30°	
Addition 2 - the position of the vertebral body				
Relative shift	10%	0%	-10%	
Distal offset	0.2	0.2	0.2	
Proximal offset	0.8	0.8	0.8	
Addition 3 - the ratio of segment height vs. segment length				
Slope	-0.0323	-0.0144	-0.0324	0.00007
Intercept	1.3747	1.4588	2.0299	1.0293
Addition 4 - the ratio of the medial plate edge vs. plate length				
Deformation	2.0	0.0	1.0	1.5
Offset	0.7	0.7	0.7	0.7

TABLE 6.2 – Parameter settings of the four additions used to create the models representing the different syngnathid morphotypes.

bending energy is mainly strain energy in the elastic linkages of the model, while the kinetic energy component is negligible. This required bending energy is used as a measurement of tail stiffness (the higher the required energy, the stiffer the tail) and the total curvature is used as an indication of the prehensile capacities of the tail. Second, the modelled tails were bended until collision of the skeletal elements occurs. Afterwards, the amount of contraction of the MVM and the total curvature of the tail just before collision occurs (visually determined) was calculated, as well as the required bending energy to do so. In this way, MVM shortening necessary to obtain maximal bending of the tail in the different models could be compared. It was opted to compare the bending energy and curvature between the different models, as these can provide an indication of the flexibility of the tail (the biologically relevant feature we want to study).

6.4 Results

6.4.1 Simulations of the individual shape differences

6.4.1.1 Addition one - the inclination angle between the anterior and posterior surface of the vertebral body

When comparing the total curvature of the tail in the three different models after 25% MVM contraction, it could be observed that the pipehorse model (with an inclination angle of 30°) is characterized by the highest total curvature (628°), followed by the seahorse model (inclination angle of 15° - total curvature of 566°) and the pipefish model (inclination angle of 0° - total curvature of 554°). When looking at the required bending energy to

obtain this curvature, the model with the highest total curvature (the pipehorse model) is also characterized by the highest required bending energy (16.0 mJ), while the seahorse model is characterized by the lowest required bending energy (11.6 mJ) (FIGURE 6.12). The maximum amount of MVM contraction before collision occurs is in all three models 25%. Collision of the skeletal elements when the MVM contraction is higher than 25% occurs at a different position along the tail in the different model. In the pipefish and seahorse model, collision occurs between the segments at the proximal base of the tail with those of segment 18 and 21. In the pipehorse model however, the segments of the distal tip go through those of segment 14 to 16 (FIGURE 6.12 – red line).

6.4.1.2 Addition two - the position of the vertebral body (relative to segment height)

The vertebral body in the seahorse model is positioned at 54.1% of the total segment height. A shift of resp. +10% in the pipefish model and of -10% in the pipehorse model changes the position of the vertebral body to resp. 48.5% and 59.9% of the total segment height. When comparing the total curvature of the tail after 25% MVM contraction between the three different models, it could be observed that total tail bending is lowest in





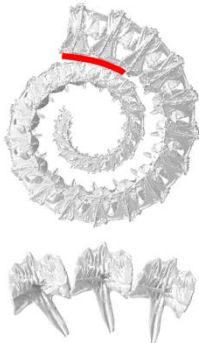
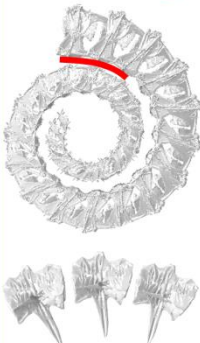
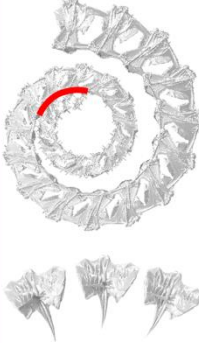
Addition 1: Inclination angle vertebrae	 0°	 +15°	 +30°
			
Required bending energy	13.7 mJ	11.6 mJ	16.0 mJ
Tail curling (relative to starting position)	554.4°	566.1°	628.3°

FIGURE 6.12– Tail curvature and required bending energy after adjusting the inclination angle between the anterior and posterior surface of the vertebral body (addition 1) in the different syngnathid morphotypes after 25% MVM contraction. Differences in vertebral morphology and how they are positioned relative to each other are illustrated by three vertebrae (segment 10-12). The red line indicates where collision between non-subsequent segments will occur first. Display bodies (and not the simple bodies) are shown in the figure.

the pipehorse model (-10% position - 467°), followed by the seahorse model (547°) and the pipefish model (+10% position - 593°). The required bending energy is the lowest in the pipehorse model (6.3 mJ), followed by the seahorse (10.5 mJ) and pipefish (17.4 mJ) model. When applying 25% MVM contraction, collision occurred in the pipefish model, but the maximal bending curvature is not yet obtained in the pipehorse model (FIGURE 6.13). Contact between plates of non-subsequent segments, and thus maximal curvature is reached at an MVM contraction of 18.0% for the pipefish model, 25% for the seahorse model and 28.7% for the pipehorse model. Now the most constrained tail bending is found in the pipefish model (488°), followed by the seahorse (547°) and pipehorse model (554°), with a corresponding required bending energy of 10.6 mJ, 10.5 mJ and 9.0 mJ, respectively (FIGURE 6.14). In all three models, collision occurs first between the segments of the most proximal part of the tail and segments 18 to 21 (FIGURE 6.14 – red line).

6.4.1.3 Addition three - the ratio of segment height vs. segment length

When comparing the total curvature of the tail after 25% MVM contraction between the four different models, it could be observed that the pipehorse type I model is characterized by the highest total curvature (594°), followed by the seahorse model (587°) and the pipefish model (578°). The lowest total curvature after 25% MVM contraction could be found in the pipehorse type II model (547°). The required bending energy is the highest in the pipefish model (18.3 mJ), followed by the type I pipehorse (15.3 mJ) and seahorse (13.2 mJ) model. The lowest bending energy was calculated for the type II pipehorse model (10.5 mJ) (FIGURE 6.15). Maximal bending (up to bone collision) was achieved at 14.4% MVM strain for the pipefish model and 19.6% for the type I pipehorse model. Collision of the skeletal elements occurs at 25% MVM strain in both seahorse and pipehorse type II. At this maximal bending, the pipefish model shows the most constrained tail bending (413°), followed by the pipehorse type I (523°) and pipehorse type II (547°) model and is highest in the seahorse model (587°). To obtain these curvatures, a bending energy of 7.8 mJ, 11.2 mJ, 10.5 mJ and 13.2 mJ, respectively, is required (FIGURE 6.16). In the pipefish and pipehorse type I model, collision first occurs between the distal tip and resp. segments 13 to 14 and segments 16 to 18. In the pipehorse II and seahorse model, collision first occurs between the base of the tail and segments 18 to 21 (FIGURE 6.16 – red line).




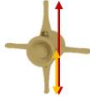
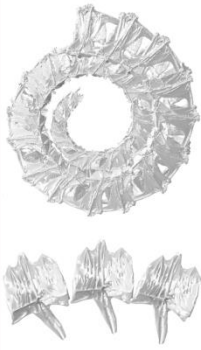


<p>Addition 2: Position vertebral body (yellow arrow/red arrow) Collision allowed</p>	 48.5%	 54.1%	 59.9%
 MVM contraction of 25%			
Required bending energy	17.4 mJ	10.5 mJ	6.3 mJ
Tail curling (relative to starting position)	593.5°	547.6°	467.1°

FIGURE 6.13 – Tail curvature and required bending energy after adjusting the relative position of the vertebral body (addition 2) in the different syngnathid morphotypes after 25% MVM contraction. Differences in vertebral morphology and how they are positioned relative to each other after MVM contraction are illustrated by three vertebrae (segment 10-12). Display bodies (and not the simple bodies) are shown in the figure.




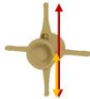
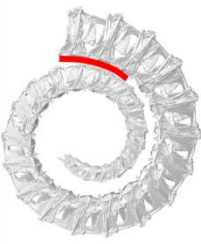


<p>Addition 2: Position vertebral body (yellow arrow/red arrow) Collision NOT allowed</p>	 48.5%	 54.1%	 59.9%
			
Amount of MVM contraction before collision occurs	18.0%	25.0%	28.7%
Required bending energy	10.6 mJ	10.5 mJ	9.0 mJ
Tail curling (relative to starting position)	488.0°	547.6°	554.0°

FIGURE 6.14 – Tail curvature, required bending energy and amount of MVM contraction after adjusting the relative position of the vertebral body (addition 2) with maximal MVM strain up to collision between dermal plates. The red line indicates where collision between non-subsequent segments will occur first. Display bodies (and not the simple bodies) are shown in the figure.

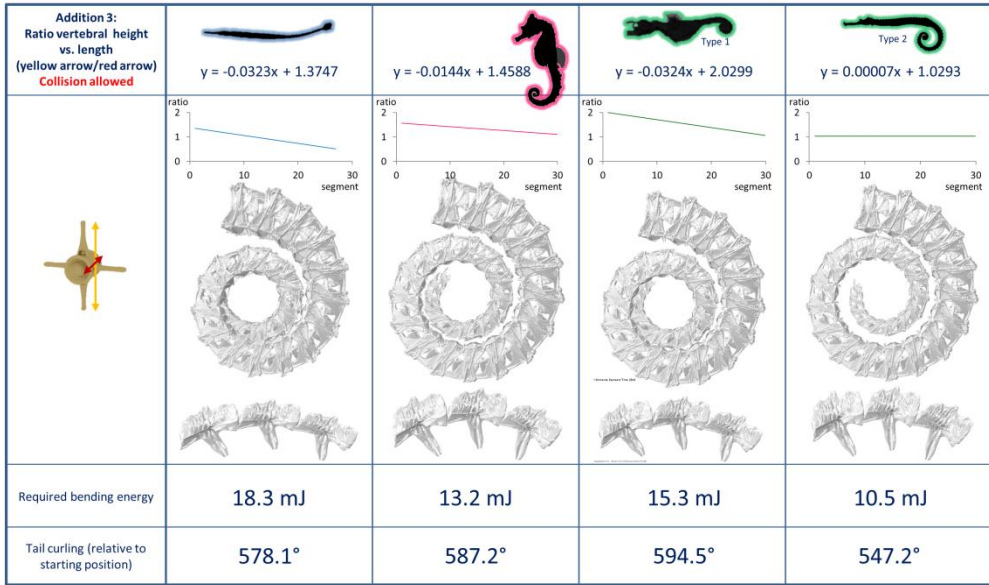


FIGURE 6.15 – Tail curvature and required bending energy after adjusting the ratio of vertebral height relative to vertebral length (addition 3) in the different syngnathid morphotypes after 25% MVM contraction. Differences in vertebral morphology and how they are positioned relative to each other after MVM contraction are illustrated by three vertebrae (segment 10-12). Display bodies (and not the simple bodies) are shown in the figure.

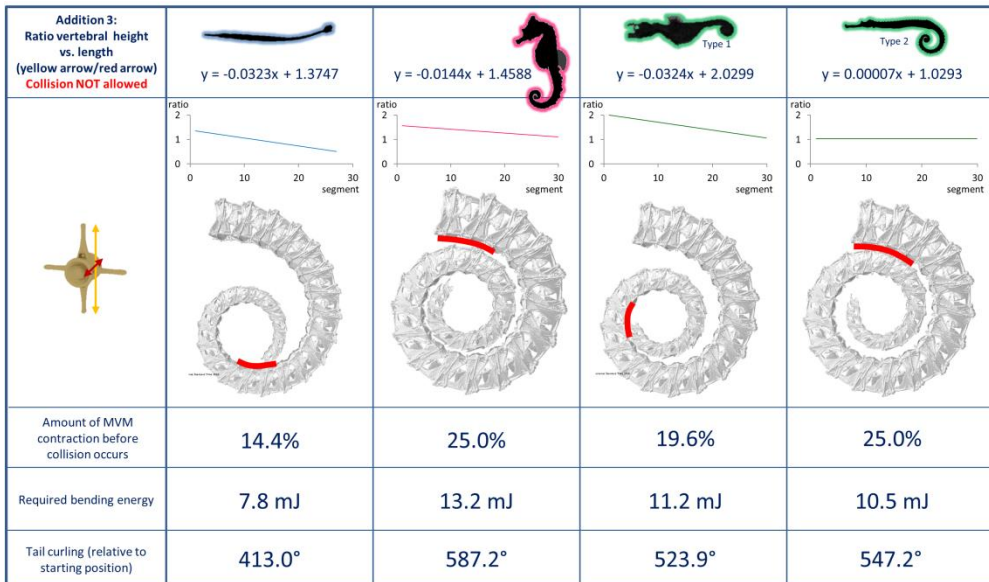


FIGURE 6.16 – Tail curvature, required bending energy and amount of MVM contraction after the ratio of vertebral height relative to vertebral length (addition 3) with maximal MVM strain up to collision between dermal plates. The red line indicates where collision between non-subsequent segments will occur first. Display bodies (and not the simple bodies) are shown in the figure.

6.4.1.4 Addition four - the ratio of the medial plate edge length vs. plate length

Simulating a tail with broader plate edges compared to the seahorse model (as observed in pipefish and both pipehorse types), did not alter bending capacities, nor the required bending energy, as in none of the models collision of the corners of the plate edges of consecutive segments occurred before the tail bends through itself (due to collision of non-consecutive segments).

6.4.2 Simulations of the combined shape differences

When comparing the total curvature of the tail after 25% MVM contraction between the four models when combining addition one, two and three, it could be observed that the pipefish model is characterized by the highest total curvature (588°), but also by the highest required bending energy (24.7 mJ). The lowest total curvature could be found in the pipehorse type II model (476°), which is also characterized by the lowest required bending energy (6.6 mJ). The seahorse and pipehorse type I models show an intermediate curvature (587° resp. 577°) and an intermediate bending energy level (13.2 mJ resp. 16.0 mJ) (FIGURE 6.17). Maximal tail bending (until collision) is most constrained in the pipefish and pipehorse type I models (416° at 12.5% MVM strain, and 426° at 14.4% MVM strain, respectively) and is most flexible in the pipehorse II model (697° at 28.7% MVM strain). An intermediate curvature is obtained in the seahorse model (587° at 25.0% MVM strain). The required bending energy increases from the pipehorse type I (6.9 mJ), the pipefish (8.3 mJ), the pipehorse type II (9.3 mJ) to the seahorse (13.2 mJ) model (FIGURE 6.18). Collision occurs first between the distal tip and segments 12 to 14 for pipefish and pipehorse type I, and segments 17 to 18 for pipehorse type II. For the seahorse this is between the proximal base and segments 18-21 (FIGURE 6.18 – red line).

6.5 Discussion

The performed simulations are all based on the initial seahorse model created by Praet (2013). For each simulation, one or more of the shape characteristics that could be related to tail prehensility (based on Neutens et al., under review) (CHAPTER 4) were added to this initial model. This means that all other skeletal characteristics of the created models still resemble those of seahorse. The different models thus look at the differences in tail flexibility and required bending energy when the seahorse tail is altered according to those traits and does not mimic the actual condition found in pipefish or pipehorse. It is possible that other characteristics (whether or not included in the model) can alter tail flexibility (e.g. differences in skeletal morphology that were not considered to be significant in the









Combination of all additions Collision allowed 25% MVM contraction	 PIPEFISH	 SEAHORSE	 PIPEHORSE Type I	 PIPEHORSE Type II
				
Required bending energy	24.7 mJ	13.2 mJ	16.0 mJ	6.6 mJ
Tail curling (relative to starting position)	588°	587.2°	577.4°	476.3°

FIGURE 6.17 – Results of adjusting the inclination angle between the anterior and posterior surface of the vertebral body, the relative position of the vertebral body as well as the ratio of vertebral height relative to vertebral length after 25% MVM contraction. Differences in vertebral morphology and how they are positioned relative to each other after MVM contraction are illustrated by three vertebrae (segment 10-12). Display bodies (and not the simple bodies) are shown in the figure.





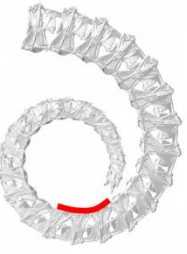
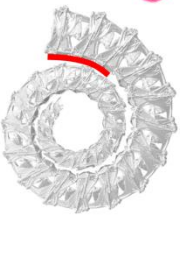


Combination of all additions Collision NOT allowed	 PIPEFISH	 SEAHORSE	 PIPEHORSE Type I	 PIPEHORSE Type II
				
Amount of MVM contraction before collision occurs	12.5%	25.0%	14.4%	28.7%
Required bending energy	8.3 mJ	13.2 mJ	6.9 mJ	15.9 mJ
Tail curling (relative to starting position)	416.8°	587.2°	426.3°	679.8°

FIGURE 6.18 – Results of adjusting the inclination angle between the anterior and posterior surface of the vertebral body, the relative position of the vertebral body as well as the ratio of vertebral height relative to vertebral length after running the model until collision occurs. The red line indicates where collision between non-subsequent segments will occur first. Display bodies (and not the simple bodies) are shown in the figure.

morphometric study (such as ornamentation), differences in skeletal morphology that were not shared by all prehensile tailed specimens or differences in muscle organization (as only the median ventral muscles are included in the different models)). These limitations may also partially explain the difference in measured, passive bending performance between the cleared and stained specimens (CHAPTER 3) and the simulations in the current chapter. Also, the modelled tails were set to comprise 30 segments, whereas in nature, prehensile tails are often composed of more than 30 segments and non-prehensile ones of fewer segments (Lourie et al., 1999, Randall et al., 1997). This can also explain why the prehensile models almost never reach the same amount of curvature as in the passive bending experiments (CHAPTER 3) and why the non-prehensile ones are more flexible.

When comparing bending performance of all models (both the ones with the individual as well as those with the combined shape differences) created after a similar 25% MVM strain with the seahorse model, two trends can be discerned (TABLE 6.3). The first trend is that tail flexibility is not remarkably altered, because a lower or higher total curvature also requires resp. less or more bending energy. This could be observed in the pipehorse type I models when the inclination angle (addition one) or the relative position of the vertebral body (addition two) are altered and in all pipehorse type II models. The second trend is a decrease in tail flexibility. This can be obtained by either (1) a lower total curvature than the

	Pipefish		Seahorse		Pipehorse type I		Pipehorse type II	
	Curvature (°)	Bending E (mJ)	Curvature (°)	Bending E (mJ)	Curvature (°)	Bending E (mJ)	Curvature (°)	Bending E (mJ)
Expansion 1	↔ 554.4	▲ 13.7	566.1	11.6	▲ 628.3	▲ 16.0	▲ 628.3	▲ 16.0
Expansion 2	↔ 593.5	▲ 17.4	547.6	10.5	▼ 467.1	▼ 6.3	▼ 467.1	▼ 6.3
Expansion 3	↔ 578.1	▲ 18.3	587.2	13.2	↔ 594.5	▲ 15.3	↔ 547.2	↔ 10.5
Combined	↔ 588.0	▲ 24.7	587.2	13.2	↔ 577.4	▲ 16.0	▼ 476.3	▼ 6.6

TABLE 6.3 – Comparison of total tail curvature (in degrees) and the required bending energy (mJ) of the pipefish and pipehorse models with the seahorse model after 25% contraction of the median ventral muscles. The symbols indicate whether the total curvature / required bending energy is in the same range as observed in the seahorse models (↔), higher (▲) or lower (▼) (range curvature seahorse model: [547.6°-587.2°], range bending energy: [10.5 mJ-13.2mJ]).

	Pipefish		Seahorse		Pipehorse type I		Pipehorse type II	
	Curvature (°)	Bending E (mJ)	Curvature (°)	Bending E (mJ)	Curvature (°)	Bending E (mJ)	Curvature (°)	Bending E (mJ)
Expansion 1	↔ 554.4	▲ 13.7	566.1	11.6	▲ 628.3	▲ 16.0	▲ 628.3	▲ 16.0
Expansion 2	▼ 488.0	↔ 10.6	547.6	10.5	↔ 554.0	▼ 9.0	↔ 554.0	▼ 9.0
Expansion 3	▼ 413.0	▼ 7.8	587.2	13.2	▼ 523.9	↔ 11.2	↔ 547.2	↔ 10.5
Combined	▼ 416.0	▼ 8.3	587.2	13.2	▼ 426.3	▼ 6.9	▲ 679.8	▼ 9.3

TABLE 6.4 – Comparison of total tail curvature (in degrees) and the required bending energy (mJ) of the pipefish and pipehorse models with the seahorse model when collision is not allowed. The symbols indicate whether the total curvature / required bending energy is in the same range as observed in the seahorse model (↔), higher (▲) or lower (▼) (range curvature seahorse model: [547.6°-587.2°], range bending energy: [10.5 mJ-13.2mJ]).

seahorse model, but requiring the same amount of bending energy or (2) by a total curvature that is approximately the same as in the seahorse, but requiring a higher amount of bending energy. This second trend occurs in the pipehorse type I model when segment dimensions (addition three) are altered and when all three shape characteristics are included at the same time and in all pipefish models.

If the models are bended until collision occurs, the same two trends as after 25% MVM contraction can be discerned, but in some models an increase in flexibility could be observed (TABLE 6.4). The first trend occurs (flexibility not significantly altered) when the inclination angle is changed in the pipehorse model and segment dimensions in the pipefish and pipehorse type II model, but also when all three shape characteristics are included at the same time in the pipefish and pipehorse type I model. The second trend (decrease in tail flexibility) was observed after altering the inclination angle (addition one) or the relative position of the vertebral body (addition two) in the pipefish model or segment dimensions in the pipehorse type I model. Here, we did also observe a third trend, showing an increase in tail flexibility. This occurs when the relative position of the vertebral body is changed to match the pipehorse morphotype or when all three shape characteristics are included at the same time in the pipehorse II model.

Considering the inclination angle between the anterior and posterior surface of the vertebral body (addition 1), Praet (2013) already suggested that it is possible that there is an energetic advantage coupled to an increase in inclination angle. The most important difference appears to be in the compression of the gliding joints between subsequent ventral plates. These joints get significantly more compressed when no inclination is included in the model. It has to be mentioned that in the study of Praet (2013), the increase in inclination angle between two consecutive segments was not only applied at the level of the vertebrae, but at the level of the complete segment. In CHAPTER 4, it was also suggested that if the inclination angle (between the anterior and posterior surface of the vertebra) increases and the relative size and shape of the intervertebral disk stays equal, there will be less deformation of the intervertebral joints during ventral tail bending. Another study however (Brainerd and Patek, 1998) stated that differences in tail flexibility can be related to amount of tail segments, rather than to differences in intersegmental angle. As the amount of segments is the same in all our models, this cannot explain the differences in flexibility. Considering the position of the vertebral body, relative to segment height (addition 2), it was already suggested that a more dorsally positioned vertebral body could be advantageous for two different reasons (CHAPTER 4). First, it creates more space for the hypaxial muscles (compared to the epaxial muscles) and because of this, it allows more

compression in the ventral compartment, allowing a higher degree of ventral bending (Praet, 2013). Second, an elongated haemal spine creates a more expanded muscle attachment site and the lever arm for ventral motion becomes more force efficient. In CHAPTER 5, it was already stated that there are two alternative hypotheses that can explain the difference in vertebral column flexibility between pipefishes and seahorses. First, if the inclination angle indeed does not influence tail flexibility, the flexibility of the vertebral column has to be mainly influenced by the position of the vertebral body. Second, the inclination angle does have an influence, but only when reaching a certain angle.

The inclination angle between the anterior and posterior surface of the vertebral body (addition one) at 25% MVM strain showed an increase in curvature in the pipehorse models, but no effect could be observed in the pipefish model (compared to the seahorse model) (TABLE 6.3). This may confirm the previously postulated hypothesis (CHAPTER FIVE) that the intersegmental angle can affect bending capacities, but only when a certain angle is reached. The energetic advantage of a higher intersegmental angle (Praet, 2013) also appears to occur at the level of the vertebrae when comparing the pipefish and seahorse model. In the pipefish model, a higher bending energy is required to bend the tail over approximately the same distance as in the seahorse model. Although a higher curvature could be reached in the pipehorse model (compared to the seahorse model), the required energy is also higher, indicating that this energetic advantage is rather limited (TABLE 6.3).

When comparing the models with the difference in position of the vertebral body (addition two) implemented after 25% MVM contraction, it could be observed that the highest curvature was obtained in the pipefish model (vertebral body positioned more ventrally compared to the seahorse model) and the lowest in the pipehorse model (vertebral body positioned more dorsally compared to the seahorse model). The longer the lever arm (haemal spine), the smaller the bending angle between two consecutive segments (FIGURE 6.19), but also the less energy required to contract the MVM with 25%. Based on the models at 25% MVM contraction, it cannot be determined if the position of the vertebral body influences tail flexibility, as a lower curvature also required less energy and vice versa. However, at maximal bending (up to collision), tail flexibility decreases in the pipefish model and increases in the pipehorse model (compared to the seahorse model) (TABLE 6.4). This thus confirms the hypothesis that tail flexibility is indeed influenced by both the inclination angle between the anterior and posterior surface of the vertebral body and the relative vertical position of the vertebral body. The hypaxial and epaxial muscles are not included in the simulations, thus the hypothesis that a more dorsally positioned vertebral

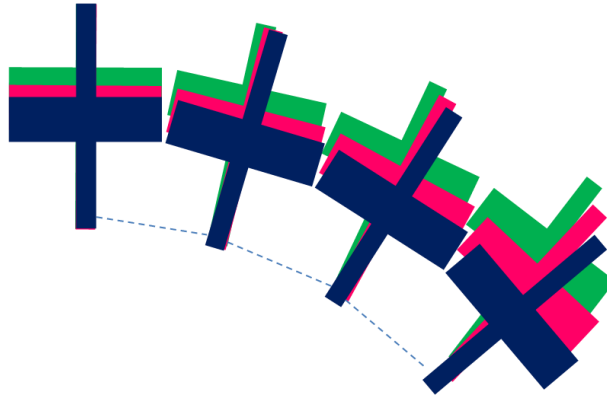


FIGURE 6.19 – Schematic overview of the influence of the position of the vertebral body (relative to vertebral height) on tail flexibility after 25% MVM contraction in the pipefish (blue), seahorse (pink) and pipehorse (green) model. The position of the MVM's is indicated by the dotted line.

body creates more space for the hypaxial muscles (compared to the epaxial muscles) and thus allowing a higher degree of ventral bending cannot be confirmed (Praet, 2013).

A difference in height/length ratio (addition 3) caused no remarkable differences in total curvature between the different models at 25% MVM contraction, but did cause differences in the required bending energy and in the position along the tail where collision of the segments occurs. If the tail models are bended until collision occurs, the pipefish model has the largest diameter of curvature (FIGURE 6.16) and will thus be less efficient for fine grasping behavior. When the height/length ratio is higher than 1, as observed in the seahorse and pipehorse type I models, the lever arm becomes longer and thus the system becomes more force efficient. Also, a smaller diameter of curvature can be obtained. However, in tails composed of such segments, more tissue compression and extension will occur at resp. the ventral and dorsal side (FIGURE 6.20A). When the height/length ratio is lower than 1, as observed at the distal end in the pipefish model, the length of the lever arm of the segments stays the same (as when the ratio is equal to 1), but the distance between the two lever arms increases, making the system less force efficient. Tails characterized by height/length ratio lower than 1 will have a larger diameter of curvature, but less compression and extension of tissue at the ventral and dorsal side will occur (FIGURE 6.20B).

Previous studies suggested that the triangular shape of the dermal plates in seahorses, compared to the rectangular shaped ones in pipefish, favors tail bending because it creates more space in between the plates of two consecutive segments. More space allows more compression of the segments at the ventral side, as collision will occur at a higher bending

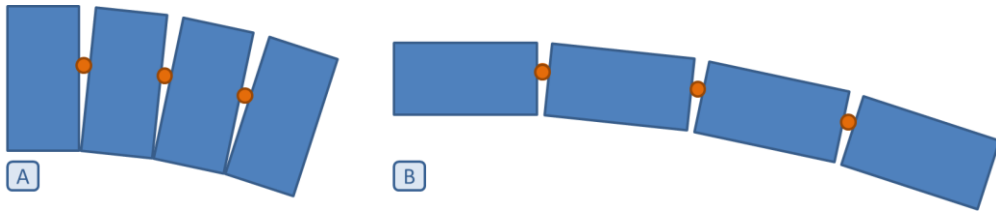


FIGURE 6.20 – Schematic overview of the influence of a difference in the segment height vs. segment length ratio when tail segments are bent over the same angle when (A) the ratio is equal to 2 (highest ratio observed in a prehensile tail) and (B) the ratio is equal to $\frac{1}{2}$ (lowest ratio observed in a non-prehensile tail), while the (relative) position of the intervertebral joint (orange dot) stays the same.

angle and soft tissue has more space for deformation (Hale, 1996, Neutens et al., under review, Porter et al., 2013, Neutens et al., 2014) (CHAPTER 3 & 4). Based on the bending experiments performed in CHAPTER 5, it could be concluded that the difference in tail stiffness between pipefish and seahorse is mainly determined by differences in dermal plate morphology and that the muscles and backbone only have a limited influence on this stiffness. However, when simulating a tail with broader plate edges (addition 4), this did not have an effect on the bending capacities or the required bending energy as in none of the models collision of the corners of the plate edges of consecutive segments occurred before the tail bends through itself (due to collision of non-consecutive segments). A possible explanation for this can be that by broadening the seahorse plate edge, it still is not similar enough to a pipefish plate to cause a significant effect on tail flexibility. The shape variation for plate edge length in CHAPTER 4 was corrected for total plate length. However, in the model, it is not possible to change the length of the caudal spine and thus a plate edge length equals to 80% of the total plate edge length could not be modelled. Also, other features, such as interlocking spines and additional intercalating plates (CHAPTER 3), occurring in the tail pipefish and possibly constraining tail flexibility are not included in the models.

The pipefish model appears to be stiffer after 25% MVM contraction when all three shape characteristics are included at the same time compared to the models where these characteristics are separately included, indicating that they influence tail flexibility at different levels (TABLE 6.3). In the pipehorse type I model, total curvature is approximately the average of the total curvature of the three models with only one shape characteristic included. However, the required bending energy is equal to the maximum bending energy observed in the three models with only one shape characteristic included, indicating that tail stiffness increases when all three shape characteristics are combined (TABLE 6.3). The pipehorse II model shows a total curvature approximately the same as the lowest curvature observed in the three models with only one shape characteristic included, but also an

equally low bending energy is required to obtain this curvature. Based on the pipehorse type II models after 25% MVM contraction, it cannot be concluded if combining the three shape characteristics influences tail flexibility (TABLE 6.3).

When the tails are bended until collision occurs and both the inclination angle, the relative position of the vertebral body and the dimensions of the segments are included, the lowest total curvature was reached in the pipefish model (TABLE 6.4). Surprisingly, the total curvature in the pipehorse type II model is only slightly higher than in the pipefish model, although the total curvature when all the additions are separately included into the model is always higher or approximately the same as in the seahorse model. It has to be mentioned that also a lower amount of bending energy is required to obtain this curvature. It thus appears that including the three shape characteristics into a single model puts geometric constraints on the bending capacity. In the pipehorse type II model the total curvature increases when combining the three shape characteristics into one model. Surprisingly this does not require a higher amount of bending energy, indicating that, when all three shape characteristics are combined, the pipehorse type II model becomes more flexible, compared to both the three pipehorse type II models with only one shape characteristic included and the seahorse model. As the inclination angle and the relative position of the vertebral body are the same in both pipehorse (type I and type II) models, it can be concluded that it are the dimensions of the segments that mainly influence tail flexibility.

CHAPTER 7: GENERAL DISCUSSION

This general discussion comprises three different parts. In the first section, an integrated discussion is given of the four results chapters (CHAPTERS 3-6). In the second section, future perspectives will be discussed. The third section deals with potentials of the syngnathid tail system to be used for bio-inspired designs.

7.1 Combining morphology, morphometrics and virtual modelling to understand the evolution of tail grasping

Although previous studies already described the (tail) morphology of certain syngnathid fishes in detail (Hale, 1996, Jungersen, 1910), the evolutionary transformations from a rigid pipefish tail to a flexible one in pipehorse and seahorse are poorly understood.

Based on ancestral state reconstructions (see CHAPTER 3, FIGURE 3.2) using different phylogenies (Hamilton et al., 2009, Teske and Beheregaray, 2009, Wilson and Orr, 2011), it can be suggested that different evolutionary strategies enabled the capacity for tail bending (both at the structural level and at the subsequent functional one), but only one of the two ancestral state reconstructions confirms that the prehensile tail evolved multiple times independently from a non-prehensile one. However, when considering the morphological data from CHAPTER 3, it seems well supported that the prehensile tail in syngnathid fishes is the result of convergent evolution. Differences between the prehensile tail of seahorse and pipehorse were found, both at the skeletal and the muscular level. It could be observed that all syngnathid fishes possessing a prehensile tail are characterized by a reduction of the plates towards the distal end of the tail, but the amount and type of plate reduction varies among the different morphotypes. Also, an intermediate plate morphology between seahorse and pipefish could be found in the pipehorses *Acentronura gracilissima* (type I) and *Haliichthys taeniophorus* (type II), with the dermal plates at their ventral side being similar to those in seahorses and the ones at their dorsal side similar to those in pipefish. In the other type II pipehorses studied, it could be observed that the proximal (rather stiff) part of the tail lacks extensive sliding joints and reflects the ancestral condition as found in pipefish. The prehensile distal part however, shows a different plate morphology from what could be observed in seahorse, type I pipehorse or pipefish. Although there is still some debate on the effect of dermal ossifications on bending capacities (Gemballa and Bartsch, 2002, Long et al., 1996), it can be argued that there is a relationship between the two in syngnathid fishes. This is based on the fact that the change in dermal plate morphology in the type II pipehorse *Syngnathoides biaculeatus* from the pipefish-like proximal plate morphology to the unique distal plate morphology starts at the same position along the tail as the steep increase in bending angle (FIGURE 3.10). Also, it could be observed that the *H.*

taeniophorus pipehorse has only restricted bending capacities in the dorsal direction, which can be related to the observed pipefish-like plate morphology at the dorsal side of the tail. This also indicates that compression of the skeletal elements constrains bending more than extension.

The modifications at the muscular level in seahorse (Hale, 1996) suggested a structural link with ventral bending capacities. However, the parallel hypaxial myoseptal organization thought to be advantageous for prehensile capacities was not observed in the studied pipehorses and is thus not a necessity for extensive tail bending. Praet (2013) already suggested that as the parallel orientated hypaxial muscles span several vertebrae (up to eight), it is unlikely that contraction of these muscles can contribute much to localized bending between two adjacent segments, but that they are a necessity to obtain a combined lateral and ventral bending (through unilateral or asymmetric bilateral contraction of the hypaxial muscles). Previous research suggested that the conical organization of axial muscles in fishes increases body stiffness during contraction (Long, 1998, Westneat et al., 1998). The parallel orientation of the myosepta thus could be needed to maintain sufficient tail flexibility during ventral bending (Praet et al., In prep.). The absence of a clear conical structure in the hypaxial muscles could also indicate that these muscles are adapted to store less elastic energy during (latero-) ventral bending (as seahorses can keep their tail curled for a prolonged period of time). During extension however, the hypaxial muscles appear to be ten times stiffer than the epaxial ones (Praet, 2013, Praet et al., 2012). This might be an explanation for the retention of the conical structure in the epaxial portion of the tail, as this is the part that will be extensively stretched during ventral bending. It is thus more likely that it is the presence of these median ventral muscles that is important for extensive ventral bending capacities. These median ventral muscles could be found in all seahorse species studied as well as in the pipehorse *S. biaculeatus*. However, they could not be reconstructed in the *H. taeniophorus* pipehorse, but it is possible that this is an artefact due to the low resolution of the scans.

Although the morphological study (CHAPTER 3) concludes that the prehensile tail in syngnathid fishes arose more than once independently (based on the phylogenetic study of Hamilton et al., 2009), it can be expected that there are shared features among prehensile species of the different lineages that are necessary to obtain an increase in bending capacity, as possessing a prehensile tail is such a derived characteristic that the morphological adaptations allowing this are possibly rather constrained.

From the morphometrics study (CHAPTER 4), five shape characteristics that might be related to increased bending capacities could be determined. At the level of the vertebrae, three

prominent shape characteristics could be observed, being the inclination angle between the anterior and posterior surface of the vertebral body (proximo-distal trend in prehensile species and inter-individual variation), the ratio of vertebral height to length (proximo-distal trend in prehensile species) and the position of the vertebral body (inter-individual variation). At the level of the dermal plates, two main axes of shape variation were found, being the relative length of the caudal spine and the relative length of the medial plated edge (dorso-ventral trend in prehensile species and inter-individual variation).

Based on the virtual, dynamic modelling of the major axes of variation of the vertebrae (as observed in the morphometric study – CHAPTER 4), it can be derived that these axes of variation indeed reflect traits that seem to improve bending capacities and are thus likely to be adaptive. It has been shown that **increasing the inclination angle between the anterior and posterior surface of the vertebral body** can alter bending capacities. Increasing this angle from 0° to 15° did not increase the amount of curvature, but resulted in a decrease in the required bending energy. When a further increase in inclination angle to 30° was imposed, an increase in curvature as well as an increase in the required bending energy could be observed. Praet (2013) already suggested that there is a relation between segment skewing and ventral bending capacities. The same study showed that an increase in inclination angle (at the level of the complete segment) is coupled to a lower bending energy usage. The models created in CHAPTER 6 showed that also by only increasing the vertebral inclination angle (instead of skewing of the complete segment) from 0° to 15° degrees the total curvature of the tail stays approximately the same, but less energy is required to obtain this curvature. However, when further increasing the inclination angle to 30°, this energetic advantage seems to be limited, as in this case a higher curvature can be reached, but also a higher amount of bending energy is required. Another possible reason why this increase in inclination angle can be advantageous for tail prehensility is that, as the angle increases and the relative size and shape of the intervertebral disk stays equal, there will be less deformation of the intervertebral joints during ventral bending. Also, this will induce a more ventrally bended resting position of the tail, and thus the same amount of muscle contraction will lead to a higher curvature. This more ventrally bended resting position, on the other hand, will further constrain dorsal bending capacities (as demonstrated by both bending experiments - CHAPTER 3 & 5).

The **ratio of vertebral height to length** mainly influences the diameter of curvature. The lower the ratio (and thus the longer segments are compared to their height), the higher the diameter of curvature. To obtain a highly precise grasping device, it is interesting to keep this ratio rather high. Not only does this high ratio influence the diameter of curvature, it

also lowers the required bending energy, as the lever arm becomes relatively larger and thus more force efficient. However, the downside of keeping this ratio rather high is that more tissue compression and extension will occur at the ventral and dorsal side of the tail, respectively. It can be expected that not only the shape of the dermal plates, but also the histological composition of the skin and the connective tissue in between the dermal plates may be adapted to cope with these large tissue deformations during (ventral) bending in seahorses. When looking at histological sections stained with a Verhoeff Elastic stain (Carson and Hladik, 2009) to determine the occurrence of elastin and collagen in the connective tissue of the tails, it can be observed that the skin of the pipefish tail is characterized by a layer of epithelial cells, covering a thin layer of collagen fibers. In seahorse however, a thick layer composed of loosely organized collagen and elastin is present just underneath the epidermis. As elastin easily stretches and recoils to its normal length and collagen is characterized by both a great tensile strength and flexibility (Liem et al., 2001), this thick layer can provide additional flexibility (elastin component) and strength (collagen component) to the seahorse skin (compared to the pipefish skin). It could also be observed that there is an additional layer composed of only collagen fibers present at the ventral side in the seahorse tail. This layer is more uniformly organized compared to the outer layer composed of both elastin and collagen. As no elastin is present in this additional layer of collagen, stretching of this part of the skin will be limited, which can be an explanation for the fact that this layer is only present at the ventral side (tissue compression during ventral bending) and not at the dorsal side (tissue extension during ventral bending). A possible explanation for the presence of this layer is to prevent overstretching during dorsal bending of the hypaxial and median ventral muscles by providing extra strength at the ventral side of the tail, as these muscles might be more sensitive to overstretching due to their parallel organization (hypaxial muscles) or their position (median ventral muscles). The elastin/collagen ratio also differs at the level of the caudal spines. As the caudal spines in seahorse have to cope with a large sliding behavior, the tip of the spine is completely embedded in elastin tissue, while the surrounding tissue in the more rigid pipefish consists largely of collagen fibers. These differences in histology also confirm the results from the bending experiments (CHAPTER 5), that both the outer skin (epidermis + underlying layer of connective tissue) and dermal plates have a remarkable influence on tail flexibility.

It could be observed that the **vertebral body is positioned more dorsally in prehensile tailed species** (compared to non-prehensile ones) and that this is related to a decrease of the amount of required bending energy to obtain approximately the same total curvature after MVM contraction. Praet (2013) already suggested that a more dorsally positioned

vertebral body allows a higher degree of ventral bending because more space is created for the hypaxial muscles (compared to the epaxials) and this will allow more compression in the ventral part of the tail. Also, a dorsal shift of the vertebral body results in a relatively longer haemal spine and creates a more expanded muscle attachment site, making the lever arm for ventral motion more force efficient.

Although no conclusions can be made on the influence of plate morphology on bending capacities by using virtual modelling, some preliminary conclusions can be made based on the bending experiments performed in CHAPTER 5. When considering the intact tail of both pipefish and seahorse, it could be observed that the tail of the pipefish specimen studied is remarkably stiffer, compared to the one of the studied seahorse specimens. After removal of the dermal plates, the overall stiffness of the tail of the pipefish specimen (corrected for size differences) was still higher than the one of the seahorse specimens, but the difference between the two morphotypes became rather small. This indicates that the shape differences between the dermal plates of both morphotypes indeed alter tail flexibility. However, it cannot be concluded how the length of the caudal spines and the length of the plate edges each contribute to tail flexibility.

From this study, it can be concluded that, although different strategies led to tail prehensility during evolution and that although the tails of convergently evolved lineages are characterized by specific tail morphologies, there are shared characteristics among them that can be linked to an increase in tail bending capacities. These characteristics occur both at the level of the vertebrae as well as at the level of the dermal plates.

7.2 Future perspectives

Some remarks and interesting future perspectives can be thought of for all four results chapters (CHAPTERS 3 to 6).

In CHAPTER 3 (Morphology), already a quite diverse amount of seahorses and pipehorses were studied. However, there are also some pipehorses (*Nerophis sp.*, *Enterulus sp.* and *Stigmatopora sp.*) that possess a wire-like tail that they can wind around structures, rather than that they show actual grasping behavior. Over the past years, several attempts were made to scan the tails of these species, but due to their very thin and long tail no good quality μ CT-scans could be obtained. As these species show a different kind of tail flexibility, it would be interesting to study their tail morphology and try to determine if they evolved yet another strategy to attain tail flexibility. As the tails of these syngnathids are very thin, it can be expected that flexibility will be mainly influenced by the decrease in size and the

dimensions of the segments. Also, as coiling combines ventral and lateral bending, adaptations at the muscular level can be expected (as it are the parallel hypaxial muscles present in seahorses that make a combined latero-ventral bending possible) and median ventral muscles are expected to be absent (as no actual ventral grasping behavior could be observed in these species).

Another interesting thing would be a detailed muscle reconstruction of more prehensile tailed species, especially of the type I pipehorses. They show an intermediate morphology between pipefish and seahorse at the skeletal level, but due to their rarity it was not possible to study their muscular morphology. It is thus still unknown if their muscle configuration also shows an intermediate pattern or resembles those of pipefish or seahorse. Also, there still is no consensus on the specific role of the different tail muscles and how they contribute to tail grasping abilities. It was already hypothesized that the median ventral muscles are responsible for sustained holding, whereas the hypaxial muscles may power fast grasping (Hale, 1996). However, the structural basis for the apparent complex motor control of which seahorses seem to be capable, is still not properly understood. Also, our research showed that the specific arrangement of the hypaxial muscles in longitudinal sheets (as observed in seahorses) is not a requirement for prehensile capacities (as this was not observed in the studied pipehorses). Also the presence of the median ventral muscle in prehensile species and the necessity of this for prehensile capacities are not yet confirmed, as these muscles could not be found in *Haliichthys taeniophorus*. However, it is not known if these muscles are indeed absent in *H. taeniophorus* or if this is an artefact due to the limited quality of the used scans. It would thus be interesting to study histological sections of pipehorses other than *Syngnathoides biaculeatus*, to confirm the presence of median ventral muscles in prehensile tailed species and to determine their necessity to obtain prehensile capacities in syngnathid fishes. It would also be interesting to use these histological sections to determine the exact attachment points of the tendons on the dermal plates and the vertebra.

Considering CHAPTER 4 (Morphometrics), it would be interesting to include more specimens of each species to take intraspecific variation into account. Unfortunately, due to the rarity of some species (all seahorse and some of the pipehorse species are on the CITES list and only a few specimens per species are present in museum collections, making it difficult to perform other analyses than (unstained) μ CT-scanning on them) and the fact that making 3D-reconstructions of all skeletal elements separately is a very time-intensive job, this was not feasible within the framework of this thesis. Also now, one randomly chosen pipefish was used as an outgroup and could only be used as a reference to compare the

characteristics found in the different prehensile morphotypes with. It would be interesting to include more non-prehensile species to determine if there is also significant shape variation among the non-prehensile species. Although the focus of this research is on the different strategies to obtain flexibility, by studying differences among the non-prehensile species, it might be possible to find characteristics that are a necessity for tail rigidity and to determine which traits are affected by natural selection and which should be retained to keep the tail completely functional.

Also, within the inter-individual part of this morphometrics study, we have been looking for traits that occur in all prehensile species and thus are a requirement for tail prehensility. However, it is possible that there are also species-specific traits that lead to an increase in tail flexibility, but that we missed because they do not occur in all prehensile species studied. It would be interesting to try to define these traits and try to mimic those species specific traits by virtual and physical modelling to determine what the influence of changing these characteristics is on bending capacities.

As ABSplus (the material used for 3D printing the experimental setup for the bending experiments - CHAPTER 5) is characterized by a stiffness that is way higher than the one of the fresh tissue tested, it can be hypothesized that the mechanical influence of the 3D printed parts will not influence the results of this study. However, until the setup is properly tested, we cannot make this assumption for sure. It can be advised to calibrate the setup properly before the tests are performed to be sure that there is no stress dissipation due to mechanical loading of the 3D-printed elements and that the force measured is only related to the bending stiffness of the tissue. To do so, it would be necessary to test three or four solid beams of different material properties (and preferably of a constant cross sectional area equal to the tails that are tested) to cover the range of stiffness's observed in the animal tissues. By comparing the results of tensile testing these three or four samples, a calibration curve can be obtained, either to prove that the 3D-printed parts can be neglected or to use to adjust the final results.

The bending experiments performed in CHAPTER 5 were mainly exploratory. It would be interesting to perform them on more specimens of different species (certainly more non-prehensile ones, as a lot of fractures occurred on the pipefish sample due to its small size). Also, no pipehorse samples were used and it would be interesting to include these. However, this will be rather difficult because of the rarity of a lot of these pipehorse species and the requirement of fresh tissue for this kind of experiments. Also, the more common pipehorse species (like *Nerophis sp.* and *Enterulus sp.*) or the commercially available ones (like *Syngnathoides biaculeatus*) are those possessing a tail of which the prehensile part is

very thin, making it difficult to remove the different layers. Also, the measuring errors on these very thin and fragile tails will be rather high.

In CHAPTER 6 (Virtual modelling), the different shape characteristics found in CHAPTER 4 were included in a dynamic, virtual model based on the tail of a seahorse (*Hippocampus reidi*) created by Tomas Praet. The different characteristics were modified, but the basic geometry used for modelling was based on a seahorse segment. In this way, the influence of changing a certain characteristic could be observed. However, it would also be interesting to start from a different basic geometry (e.g. the one of a pipefish or pipehorse) to construct the tail model. Five different characteristics were found in the morphometrics study that could possibly influence prehensile capacities. However, one of these characteristics (the length of the caudal spine) could not be included into the model (as the caudal spine was not simulated in the initial model) and another characteristic (the length of the plate edge) could only be altered on the display bodies, but not on the simplified bodies that are used for the actual calculations. It would be interesting if the length of the caudal spine was integrated into the model and if the length of the plate edge could also be altered on the simplified bodies. As such, not only the influence of a changing plate geometry on tail flexibility can be determined, but also the amount of bending energy that is required to obtain a certain curvature. Also, if the length of the caudal spine is implemented in the model, a more realistic modelling of the plate edge length can be obtained. In seahorses, the caudal spine measures approximately half the length of the complete plate. This means that by only changing the length of the plate edge, this edge will be maximum 50% of the total plate length, while in pipefish, it could be observed that the plate edge can be up to 80% of the total plate length. Without the length of the caudal spine as a parameter included in the model, the actual shape of the pipefish plates cannot be mimicked.

In the morphological study (CHAPTER 3), some small features such as interlocking spines or intercalating plates could be observed in pipefish and possibly contribute to the rigidity of the pipefish tail. For the additional interlocking spines (FIGURE 7.1), it is not known if they only function as an attachment site for the tendons of the conical myosepta or if they also influence tail prehensility. Due to their size and position, it can be hypothesized that they restrict bending by causing additional locking of the plates at the outer side of the tail curvature (thus at the dorsal plates during ventral bending and vice versa) (FIGURE 7.1). When looking at the intercalating plates in pipefish (FIGURE 3.3A), it can be observed that these plates exactly fit in between the dermal plates of consecutive plates and are connected to them by connective tissue. At first sight, this does not allow a lot of motion at

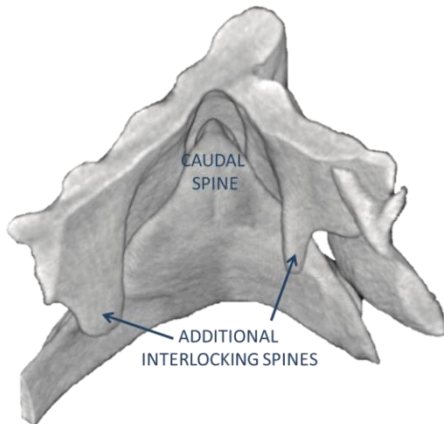


Figure 7.1 – Detail of the sliding joint between two consecutive plates in the *Corythoichthys intestinalis* pipefish, showing the caudal spine on the proximal plate and two additional interlocking spines on the distal plate (picture taken from a medial point of view).

the overlap between the intercalating and dermal plates. It would thus be interesting to model these intercalating plates and determine their influence on tail flexibility in pipefish.

During model creation, a constant median ventral muscle contraction was applied and the hypaxial and epaxial muscles were not taken into account, as the main goal was to study the influence of changing certain geometrical features on tail flexibility. Also, by doing so, the models could be easily compared. However, the differences in muscle configuration between pipefish, pipehorse and seahorse could also influence bending capacities. First, it was suggested that the function of the parallel organized hypaxial muscles is to allow a combined latero-ventral bending (Praet, 2013). It would be interesting to determine if this type of bending can also be obtained with a conical organization. Second, it was hypothesized that the parallel myoseptal organization in the hypaxial muscles of seahorses is also necessary to maintain sufficient tail flexibility. In the current models, these sheets span three segments, although in reality, they span up to eight segments (CHAPTER 3, Neutens et al., 2014). It can be expected that there will be an influence of muscle length on tail flexibility. As the muscles are now modelled over only three segments, they can be modelled as linear connectors. If they contract, no large amount of bending of the muscles themselves will occur. However, this will be the case if the muscles span more than three segments (FIGURE 7.2). Also, by spanning more segments, more points of rotation will be located between the two insertion points of the modelled muscle, but also more friction between the muscle and the surrounding tissue will occur. In pipefish and some of the pipehorse species, the tendons of the hypaxial muscles only attach to the dermal plates and not onto the vertebrae directly. The conical epaxial muscles in seahorse on the other hand connect to both the dermal plates as to the vertebrae. For the hypaxial muscles in seahorse, it is still not known if the connection of the muscles onto the skeleton is continuous along the length of the whole myoseptum or occurs by means of an attachment point at both the

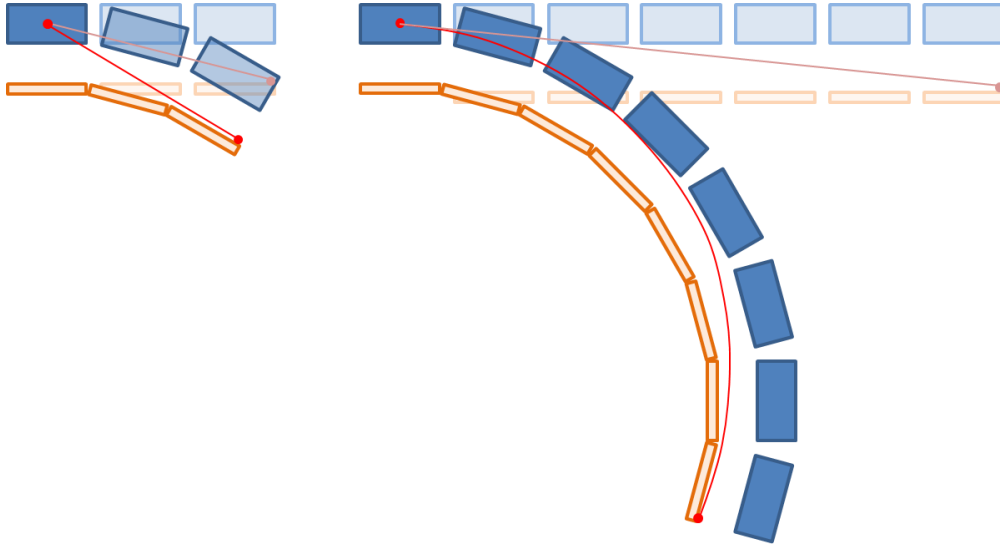


Figure 7.2 – Behavior of the hypaxial muscle during ventral bending when spanning a different amount of segments (vertebrae in blue, dermal plates in orange; light colors – stretched position, dark colors – bended position).

proximal and distal end of the myoseptum (as only one tendon could be observed). The virtual models now assume a connection of the myosepta to both the dermal plate and the vertebra. It would be interesting to model the myomeres as one muscle fiber bundle in each quadrant of the tail and insert different tendons to the plates and vertebrae in such a way that they mimic the attachment points of the tendons as observed in the different morphotypes, respectively.

7.3 Bio-mimetics and bio-inspiration

The doctoral thesis of Tomas Praet (Praet, 2013) already mentioned different potential applications inspired by the seahorse tail. In this section, two of these potential applications will be discussed and complemented with the knowledge obtained within the framework of the current thesis. The first application is based on the vertebral morphology, while the second one integrates knowledge based on plate geometry. Also one new application will be presented inspired by the geometry of both vertebrae and plates.

7.3.1 Robotics

The field of robotics (which is the branch of technology that deals with the design, construction, operation and application of robots, as well as computer systems for their control, sensory feedback and information processing) is still in its formative stage (Walker,

2013). Designers within the field of robotics are exploring a range of possibilities for robot structures, ranging from sensing and perceiving, over navigation and locomotion to grasping and manipulation (Walker, 2013). Many of today's robots are inspired by nature, and together form the field of bio-inspired or soft robotics. Certainly the specialized structures of animals provide a source of inspiration, such as the elephant trunk (Hannan and Walker, 2002), the tentacles of octopus (Calisti et al., 2011, Laschi et al., 2009), the body of snakes (Hopkins et al., 2009, Kai and Simaan, 2006, Simaan, 2005, Simaan et al., 2004, Xu and Simaan, 2006) or the tail of lizards (Sanders, 2012, Zhao et al., 2013).

The tail of syngnathid fishes is especially useful as source of inspiration in the field of continuum or backbone robotics, because of its highly flexible structure. The motivation behind continuum robots is that the shape of the backbone can be adapted to maneuver the robot within more complex environments and to conform to grasp a wider class of objects than feasible with rigid link robots. Within the field of continuum robotics, robots with segmented rigid-link backbones presenting a continuous external form have been

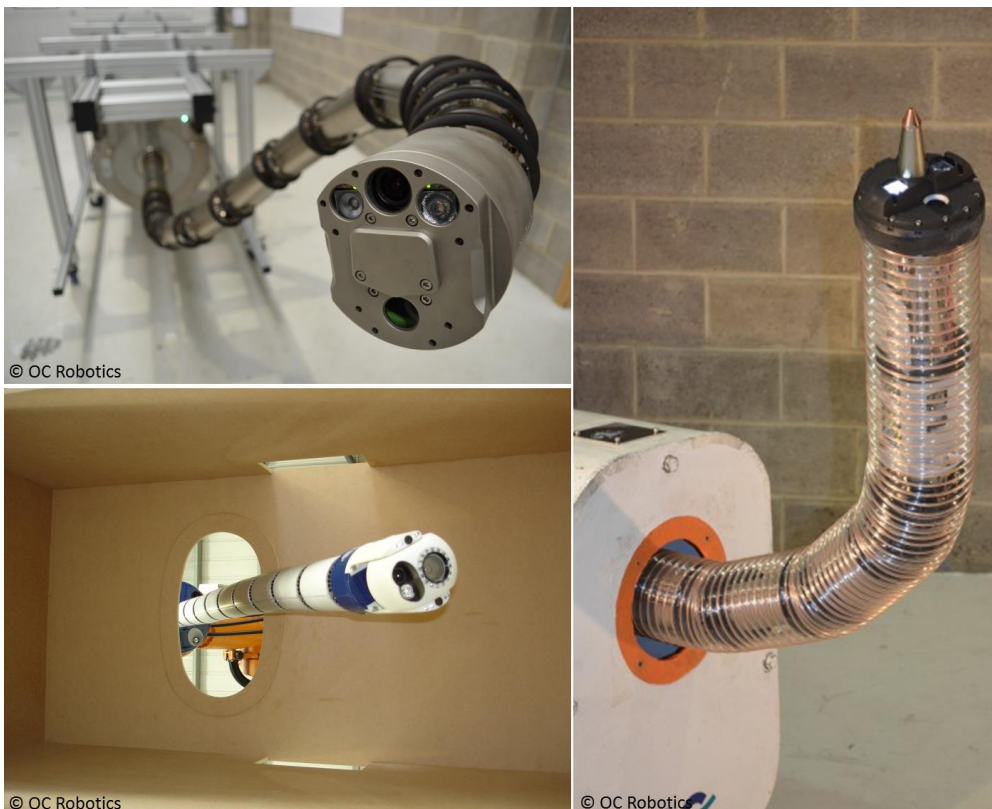


FIGURE 7.3 - Illustration of commercially available snake arm robot (developed by OC Robotics).

developed (Hannan and Walker, 2001, Aoki et al., 2004, Ohno and Hirose, 2001, Tsukagoshi et al., 2001), sometimes called continuum-style robots. Although designs like this are rather rare, some became a commercial success (e.g. the snake-arm designs – FIGURE 7.3). These robot arms are composed of serially connected modular rigid-link sections and the serially segmented tail can thus be used as inspiration for the development or innovation of such robot arms.

The disadvantage of working with a backbone consisting of non-deformable segments is that bending behavior cannot be induced by using a central cable (as is often the case in robot arms consisting of a deformable backbone – e.g. the octopus arm designed by Calisti et al. (2011)). However, an interesting simplification that could be used in designs inspired on the syngnathid tail is the principle of having one single cable away from the central axis to induce bending (e.g. at the level of the median ventral muscles – Praet, 2013). Pulling this cable would generate bending in one direction. By attaching cables on all four vertebral spines, bending in any direction can be achieved by pulling one or two of the cables. However, this bending behavior will be restricted to an overall bending of the structure and no local bending can be induced (Praet, 2013).

To induce local bending, it would be interesting to use several cables, each running through a specific part of the robotic arm and inducing bending in a limited subset of segments. Praet (Praet, 2013) suggested using the principle of a Bowden cable to cause local bending behaviors (FIGURE 7.4).

By combining this design with the knowledge obtained in the current thesis, it can be optimized depending on the needs required considering a certain bending performance. By

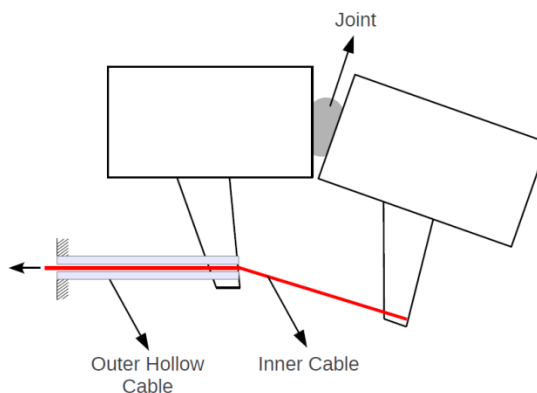


FIGURE 7.4 - Design of two segments of which the backbone for a robotic arm exists, created by Praet (2013). A Bowden cable located at the position of the median ventral muscle is used to induce bending between two consecutive segments.

changing the dorso-ventral position of the central axis, the system can be more or less force efficient, but also the amount of tissue deformation will be different (FIGURE 7.5A & 7.5B - red bar). Assuming that the central axis divides the volume enclosed by the plates, a position at 50% of segment height will create two equal volumes (Figure 7.5A). By changing the position of the vertebral axis, these ventral and dorsal compartments will become asymmetric in volume (Figure 7.5B). By integrating the axis of rotation at the level of the scarf joint of the dorsal dermal plates, one single compartment can be created (FIGURE 7.5C). The down-side of this design will be that tissues at the ventral side of the compartment will be highly deformed (FIGURE 7.5C – red bar). However, a system like this would be suited to be filled with or to transport highly deformable materials (such as fluids). As the seahorse design comprises a lot of gaps, a waterproof coverage is needed. It can be opted to locate this at the level of the skin. However, it would also be interesting to locate this cover material underneath the plates. In this way, the coverage has to undergo less deformation and will be better protected against damage. Another advantage of this is that the fluid will be in a separate compartment and will not come into contact with the plates, which will be less of an obstruction for laminar flow.

Combining plates and vertebrae in one robotic model possibly complicates the design and the manufacturing process, but on the other hand provides some interesting features, such as resistance against compression. To reduce the complexity of the model, it would be interesting to design a cast consisting of two instead of four individual plates per segment, integrate the central axis of rotation at the level of the dermal plates and reduce the amount of sliding joints to two (only at the ventral side - Figure 7.5C). A system like this is

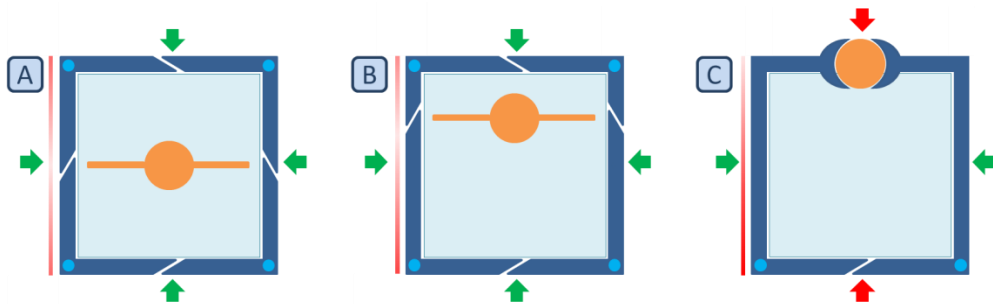


Figure 7.5 – Influence of changing the relative position of the vertebral body illustrated by intersections at the level of the vertebral joint, with the vertebral body (A) at 50% of the vertebral height, (B) at a more dorsal position and (C) integrated at the level of the scarf joint between the two dorsal plates. The green arrows indicate that the system is highly resistant to compression in the indicated direction, while the red ones indicate a low resistance. The red bars illustrate the amount of tissue deformation during ventral bending (the darker, the more deformation). (vertebral body – orange, dermal plates – dark blue, sliding joints – light blue dots).

still (partly) compression-resistant, as it will be solid in the dorso-ventral direction (Porter et al., 2015) (FIGURE 7.5C - red arrows), but still compressible in the lateral direction (FIGURE 7.5C - green arrows).

To further optimize the robotic design to specific needs, two other features can be adapted, being the inclination angle between two consecutive segments and the dimensions of the segments. By changing the inclination angle, bending behavior in a certain direction can be favored over the other bending directions. Depending on how fine or robust the required bending behavior should be, the height/length ratio of the elements can be altered, leading to a different diameter of curvature.

7.3.2 Potentials for protective clothing

Previous research on the Senegal bichir (*Polypterus senegalus*) showed that fish scales already inspired designers for the development of innovative weaponized armor fitted to the human body (Stevermer, 2014, Zolotovskiy, 2012, Duro-Royo et al., 2015) (FIGURE 7.6A). The principle behind this is based on the rhomboid scales of *P. senegalus* that interlock into structural rings through the interface of peg-and-socket joints (FIGURE 7.6B). This allows a great range of flexibility, while still providing structure and bracing under load. The main focus of their research was the human wrist, because combat moves are often directed at injuring the wrist of an opponent. The geometrical variation observed in the dermal plates of syngnathid fishes can be used to optimize designs like this and to alter them to create new designs to protect other joints of the human body. An example of this would be to replace the currently used 2D joint (Figure 7.6B) with a 3D joint (such as a ball-and-socket joint). In this way, different directions of motion can be combined, leading to a more flexible and less resistant structure.

The dermal plates of fishes can not only provide inspiration for the development of innovative weaponized armor, but also for the development of protective clothing for sports- and stuntmen. During extreme winter sports, such as skiing, snowboarding or ice skating, most fractures occur at the level of the knee, wrist or elbow (Move to Cure, 2012). To protect these flexible joints, structures that are characterized by a combination of firmness and flexibility would be very interesting. Existing designs are often very firm, but only allow a limited amount of flexibility. Examples of this are knee and elbow protection for (ice) skaters and volleyball players (FIGURE 7.7A), the protective shell in the gloves of snowboarders (embracing both sides of the wrist), the equipment of a hockey goalie (FIGURE 7.7B) or crash pants to protect the tailbone (FIGURE 7.7C).

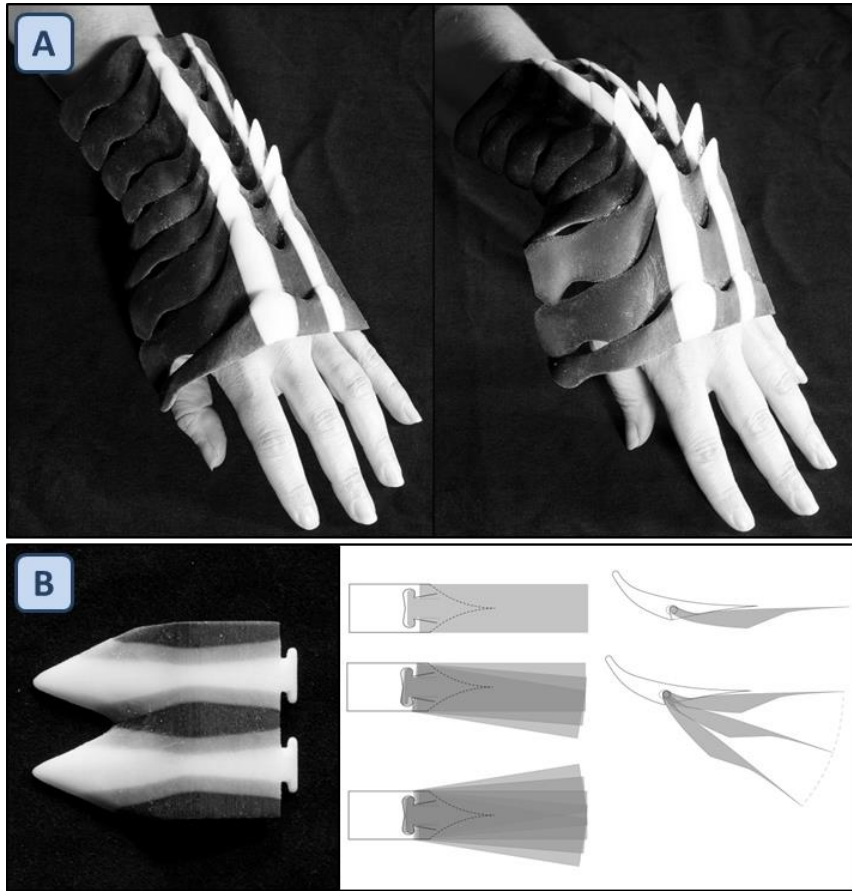


FIGURE 7.6 – Development of wrist protection based on the scales of *Polypterus senegalus*. (A) Range of motion for the wrist beyond which the scales will lock together and brace the wrist against injury and (B) abstracting and modifying the scale geometry of *P. senegalus* scale geometry to create an original joint design (adapted from Stevermer, 2014).



FIGURE 7.7 – Examples of protective clothing for sportsmen. (A) Knee protection for ice skating, (B) equipment for a hockey goalie and (C) crash pants for snowboarding.

The dermal plates found in syngnathid tails can provide a source of inspiration to invent new designs for protective clothing at the level of the joints, in which the central axis is formed by the leg or arm of a person. A good example of this is the outfit of a hockey goalie, which is cumbersome and heavy weighted to cope with the high impact of the puck. Using a design consisting of only dermal plate-inspired structures would still cause damage to the underlying bone. However, when using the leg of the goalie as a central backbone and the dermal plates as protective cast, the space in between these two structures (where the syngnathid muscles would be located) can be filled with shock-absorbing materials to prevent bruising or fracture of the leg. As the feet and shins have the highest risk of being hit by the puck and as this part of the protective clothing does not have to be highly flexible, the design of protective clothing for this region of the leg can be inspired by the heavily plated pipefish tail. However, at the level of the knee joint, a certain degree of flexibility is required and this can be obtained by using the dermal plate configuration as observed in seahorse.

Another example is the protective clothing for (ice)skaters. Existing designs often consist of a solid shell, without any articulation. This results in highly protective designs, but with limited amounts of flexibility. Although these shells are sufficient to protect the (elbow and knee) joints, intensive use, including lots of falling, can lead to heavy bruises of the skin at the level of the borders of the immobile shell. A new, modular, articulating, wraparound design inspired by the syngnathid tail, however, would not only increase the amount of flexibility, but also diminishes the amount of bruising, as no cutting borders are present. A downside of this design is that a squared structure might be too robust and impede certain motions. A solution for this might be inspired by the body of certain syngnathid fishes, which have a hexagonal cross-section instead of a squared one (as observed in the tail). It would be interesting to make physical prototypes (as in Porter et al., 2015) to test whether there are big differences in flexibility and compression force resistance between the squared architecture and the hexagonal one to see if this can provide a more elegant design. As the main goal is to provide protection against fracture or compression and not to puncture, the fact that there are gaps in between consecutive segments is not a problem.

7.3.3 Modular racing circuit for kids

According to a survey conducted by speelgoedmagazine.nl, parents think that toys for their kids need to be innovative, durable, original and educational. Using the syngnathid tail as source of inspiration to design a modular racing circuit is both innovative and original. Current racing circuits often consist of larger, fixed parts that are limited in the way they can be combined (FIGURE 7.8). The idea of a modular racing circuit (FIGURE 7.9) is based on

the same principles as the ones found in syngnathid tails, but reduced to only the ventral half of the tail and applied in an analogous, but rearranged way to form a functional toy. To do so, the two ventral dermal plates are fused (thus together forming a U-shaped structure) and a central backbone is integrated in the middle (at the point where two separate plates normally overlap – FIGURE 7.10B & 7.10C). Two modules interconnect by a ball-and-socket joint at the level of the integrated backbone and by ball-and-socket sliding joints at the top of the two ridges (FIGURE 7.10D & 7.10E). The joints were rearranged because when the central axis would be at the same places as the vertebral column in syngnathid fishes (as shown in FIGURE 7.10B), it will obstruct the passage of the car on the track. To maintain stability, positioning the central axis at the ventral side (FIGURE 7.10C) requires a position switch of the caudal spines to the dorsal side (FIGURE 7.10D), as otherwise they are positioned at the same level as the central axis. The joint at the level of the caudal spine was transformed into a sliding ball-and-socket joint instead of only a sliding joint to be able to click adjacent segments onto each other (FIGURE 7.10D & 7.10E). By using this modular system based on the seahorse tail, turns can be placed anywhere in the circuit and can be easily altered (FIGURE 7.9). Also, by placing a second module mirrored on top of another module, tunnels can be made and by using simple scaffolds, bridges and ramps can be built.

By using a modular system, the kid's creativity is tickled because he/she can design the racing circuit like he/she wants and can do this over and over again, each time designing something new. As one of the requirements for a good toy is durability, the toughness of the tail of syngnathid fishes is also an interesting feature.



FIGURE 7.8 – Illustration of a racing circuit for kids now available.

The interesting aspect for parents is that by using a modular system, the racing circuit can be stored compact in a simple box (as all parts can be separated) and that single parts can be easily replaced when broken or lost.

Not only does a modular design provide advantages for both kids and parents, it also has potential benefits for manufacturing. Using a modular system combines the benefits of standardization (as they are all similar, the parts can be produced in larger quantities, reducing production costs) with those of specialization (the same parts can be used for different combinations/designs).

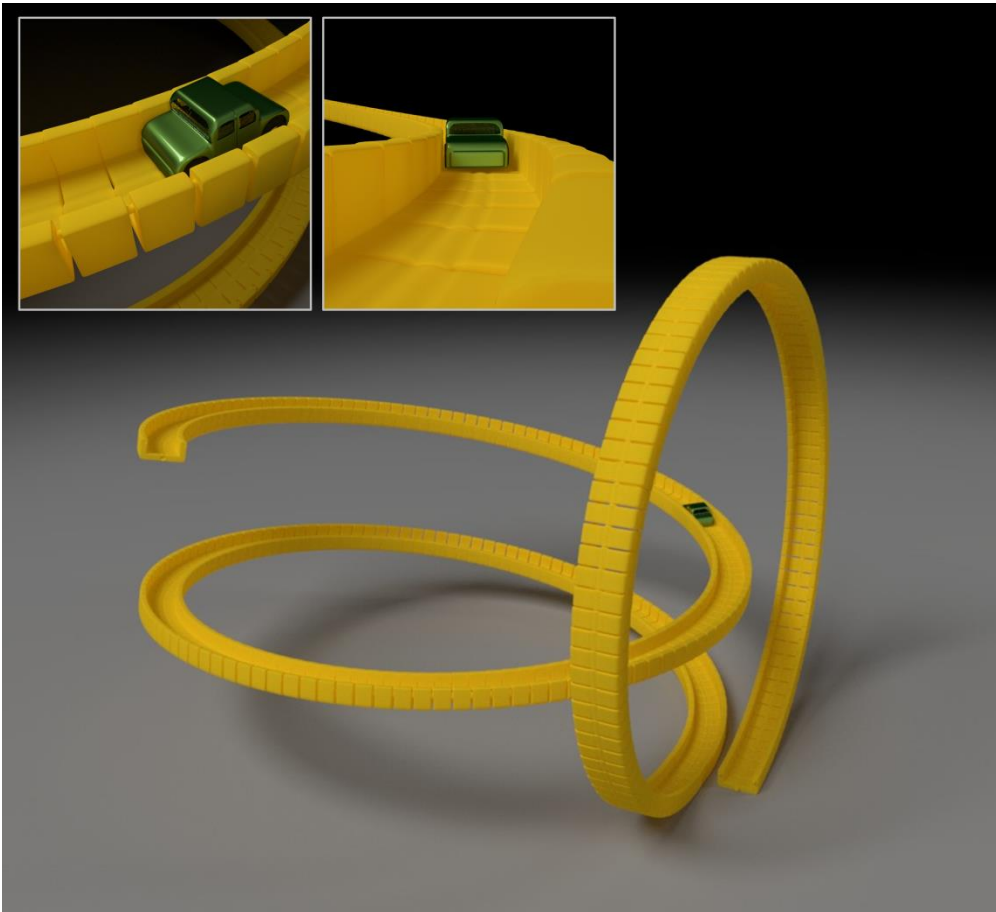


FIGURE 7.9 – Modular racing circuit based on the syngnathid tail where turns and loops can be placed anywhere in the circuit, with the insets showing how the car drives on the circuit

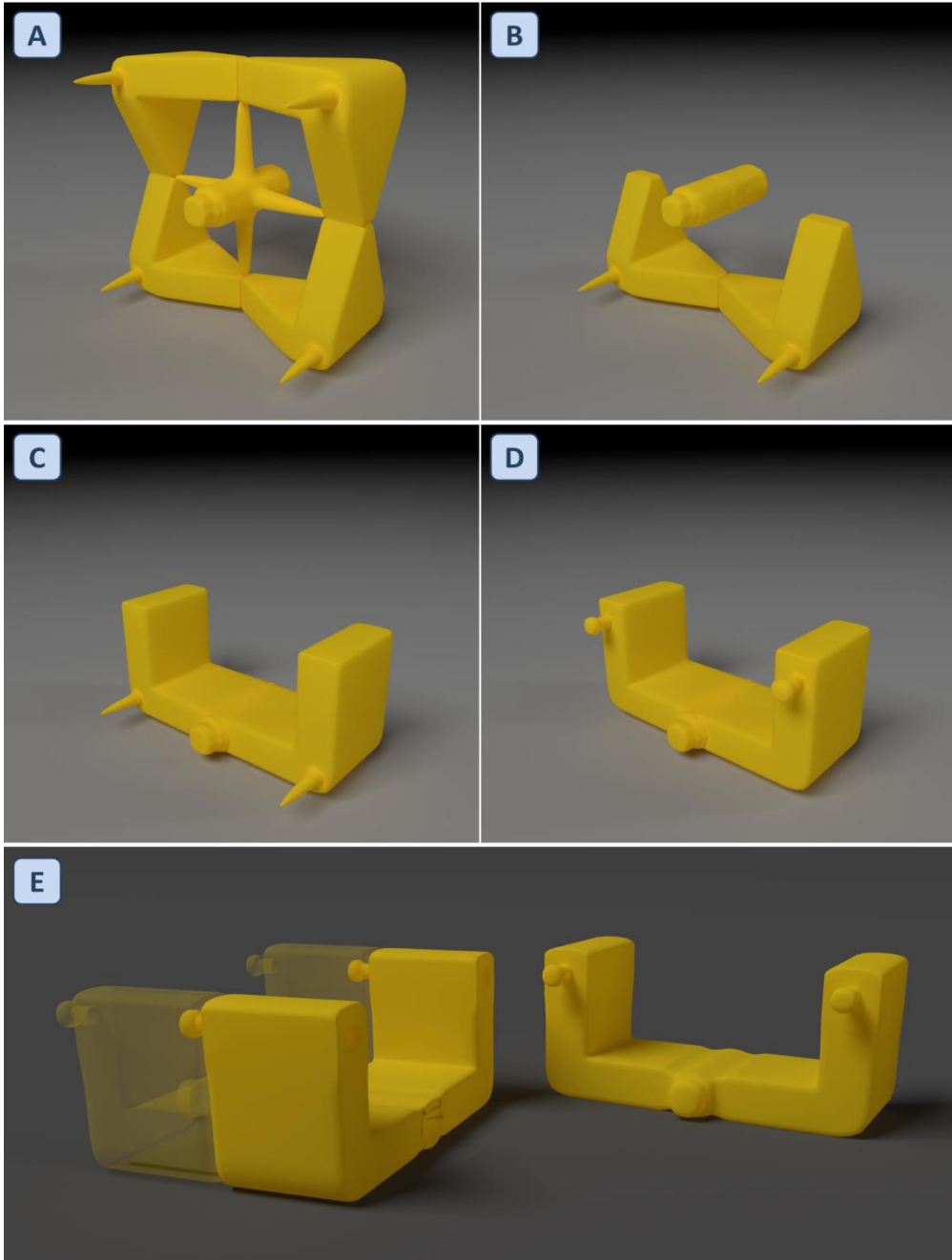


FIGURE 7.10 – Building blocks of modular racing circuit for kids. (A-D) transforming one segment of the seahorse tail into a single module of which the racing circuit consists, with (A) a simplification of a seahorse tail segment, (B) a reduction of this segment to only two plates and one central vertebra lacking spines, (C) Fusion of the two plates and integration of the central backbone into the U-shaped structure and (D) translation of the caudal spines to the dorsolateral side of the plate edge and a transformation of these sliding joints into ball-and-socket sliding joints. (E) Illustration of how the different modules interconnect with each other.

CHAPTER 8: SUMMARY

8.1 Summary

The family of the syngnathid fishes comprises five different morphotypes (seahorse, type I and type II pipehorse, pipefish and seadragon). Seahorses and pipehorses both possess a prehensile tail, a unique characteristic among teleost fishes, allowing them to grasp and hold onto substrates (such as seagrasses). Recent phylogenetic studies showed that the prehensile tail evolved independently in different lineages from a non-prehensile one (ancestral state). A first aim of this PhD research is to study the musculoskeletal morphology of the tail of the different morphotypes and to cover the evolutionary transformations necessary to obtain a prehensile tail (as observed in seahorse and both pipehorse types), starting from a rigid, non-prehensile one (as observed in pipefish and seadragon). The second focus is how we can translate the syngnathid morphology, and the evolutionary patterns associated with this, to bio-inspired designs and potential applications.

In the introduction (CHAPTER 1), a short overview of the general morphology of the fish tail is provided, as well as the phylogenetic position of the Syngnathidae and an overview of the characteristics associated with each of the five morphotypes. Also the concepts of mimicry, biomimetics and designs from nature are briefly discussed.

The material & methods section (CHAPTER 2) provides a short overview of the examined specimens, their origin and the methods they're used for. The studied species were selected based on their phylogenetic position within the Syngnathidae, so that the major clade-related morphotypes, from primitive to derived, were included. Also, a brief overview of the used techniques is provided in this second chapter.

In the 3RD CHAPTER, the patterns that characterized the convergent evolution towards tail grasping within the family of the syngnathid fishes are explored by comparing the caudal musculoskeletal organization, as well as the passive bending capacities in pipefish, pipehorse and seadragon. The overall hypothesis of this chapter is that prehensile functioning of the tail only became possible after substantial modifications of the musculoskeletal system and that the configuration in the pipehorse representatives is similar to that in seahorse and thus differing from the ancestral state as observed in pipefish representatives. To study the complex musculoskeletal morphology, histological sectioning, μ CT-scanning and phase contrast synchrotron scanning are combined with virtual 3D-reconstructions. The results suggest that the independent evolution towards tail grasping in syngnathids reflects at least two quite different strategies in which the ancestral

condition of a heavily plated and rigid system became modified into a highly flexible one. Intermediate skeletal morphologies (between the ancestral condition and seahorse) could be found in *Acentronura gracilissima* (a type I pipehorse) and in *Haliichthys taeniophorus* (a type II pipehorse), which are phylogenetically closely affiliated with seahorses. The characteristic parallel myoseptal organization (as already described in seahorse - Hale, 1996) could be shown not to be a necessity for grasping (as the ancestral conical organization is retained in the prehensile pipehorses studied), but represents an apomorphy for seahorses. One could suggest that the functionality of grasping evolved before the specialized, parallel myoseptal organization observed in seahorses. However, as the grasping system in the studied pipehorses is a totally different one, this cannot be concluded.

The 4TH CHAPTER deals with the morphological variation within and between the tails of different syngnathid fishes, by using 3D morphometric analyses based on surface meshes. Only the variation of the skeletal elements is encountered and not the differences in muscle organization. Three hypotheses were postulated: (1) prehensile species show a wider range of shape variation within one tail than non-prehensile ones, (2) differences between the dorsal and ventral plates will occur within the tail of prehensile species and (3) there will be a more constrained shape variation among prehensile species compared to non-prehensile ones. Four different analyses were performed on the tail skeleton of nine species exhibiting different levels of tail grasping capacities (four pipehorse, two seahorse, one pipefish and one seadragon species) to examine the intra-individual variation across the proximo-distal and dorso-ventral axis. In the two interspecific analyses, all vertebrae and all dermal plates were mutually compared. Five shape characteristics were found that could be related to tail prehensility in seahorses and pipehorses. At the level of the vertebrae, three prominent shape characteristics could be observed, being the inclination angle between the anterior and posterior surface of the vertebral body (proximo-distal trend in prehensile species and inter-individual variation), the ratio of vertebral height to length (proximo-distal trend in prehensile species) and the position of the vertebral body (inter-individual variation). At the level of the dermal plates, two main axes of shape variation were found, being the relative length of the caudal spine and the relative length of the medial plated edge (dorso-ventral trend in prehensile species and inter-individual variation). From this chapter, it can be concluded that prehensile tails exhibit a larger proximo-distal and dorso-ventral shape variation within the tail than non-prehensile ones. However, the hypothesis that there is a more constrained shape variation among prehensile species compared to non-prehensile ones has to be rejected.

The 5th CHAPTER covers bending experiments performed on fresh tail tissue of both seahorse and pipefish to determine if there is a difference in tail stiffness between those two morphotypes, as well as to look for regional differences within one tail. Also, it was investigated how the outer skin, dermal plates, muscles and vertebrae each contribute to the stiffness of the tail. For comparison, an experimental setup was designed by which force-displacement measurements on the passive bending response could be recorded for the different tail sections of each fish (parts of the tail composed of 5 segments, representative of the different tail regions – proximal, middle and distal). The setup was designed in such a way that the tail sections could be rotated 90° around the longitudinal axis to allow ventral, dorsal and lateral bending to be compared. The results showed that the outer skin and the dermal plates have a remarkable influence on the bending stiffness of the tails, while the muscles and vertebrae contribute to tail stiffness to a lesser extent. Also, the pipefish tail is considerably stiffer than the seahorse tail (results corrected for size-differences), which can be partly related to a difference in dermal plate morphology.

In the 6th CHAPTER, the observed shape differences within and between the tails of the different syngnathid morphotypes obtained through the morphometric analyses performed in CHAPTER 4 were implemented into a virtual, dynamic model to study if these differences can be related to tail flexibility. For each shape difference, an addition to the original model developed by Tomas Praet (Praet, 2013) was written, so that the influence of each characteristic could be studied separately, as well as the effect of combining them. Based on the virtual modelling of the major axes of variation of the vertebrae (as observed in CHAPTER 4), it can be derived that these axes indeed reflect traits that seem to improve bending capacities and are thus likely to be adaptive.

An integrated discussion of the four results chapters (CHAPTERS 3-6) is given in the general discussion (CHAPTER 7), concluding that, although different strategies led to tail prehensility during evolution and although the tails of convergently evolved lineages are characterized by specific tail morphologies, there are shared characteristics among them that can be linked to an increase in tail bending capacities. These characteristics occur both at the level of the vertebrae as at the level of the dermal plates. Next to this integrated discussion, CHAPTER 7 also discusses some interesting future perspectives and potential syngnathid-inspired designs in the field of robotics, protective clothing and children's toys.

8.2 Samenvatting

De familie van de syngnathe vissen bevat vijf verschillende morfotypes (zeepaard, type I en type II naaldpaard, zeenaald en zeedraak). Zeepaardjes en naaldpaardjes worden gekarakteriseerd door een unieke eigenschap binnen de groep van de teleoste vissen, ze hebben namelijk beide een grijpstaart die het mogelijk maakt om te grijpen naar en zich vast te houden aan substraten zoals zeegrassen. Recente fylogenetische studies toonden aan dat de grijpstaart meerdere keren onafhankelijk van elkaar ontstond vanuit een niet-grijpstaart (de ancestrale conditie). Een eerste doelstelling van dit doctoraatsonderzoek is het bestuderen van de musculoskeletale staartmorfologie en de evolutionaire transformaties die nodig waren om een functionele grijpstaart te bekomen (zoals waargenomen in zeepaardjes en naaldpaardjes), startende vanuit een rigide, niet-grijpstaart (zoals waargenomen in zeenaalden en zeedraken). De tweede doelstelling is hoe we deze syngnathe staartmorfologie, en de evolutionaire patronen die hiermee geassocieerd kunnen worden, kunnen vertalen naar biologische geïnspireerde ontwerpen en mogelijke applicaties.

In de inleiding (HOOFDSTUK 1) wordt een kort overzicht van de algemene staartmorfologie bij vissen gegeven. Ook wordt de fylogenetische positie van de Syngnathidae besproken en wordt een overzicht gegeven van de typische kenmerken van elk van de vijf morfotypes. Verder worden de concepten mimicry, biomimetica en *designs from nature* kort voorgesteld.

In Materiaal & Methodes (HOOFDSTUK 2) worden de gebruikte dieren, hun oorsprong en de methodes waarvoor ze gebruikt werden, weergegeven. De bestudeerde soorten werden geselecteerd op basis van hun fylogenetische positie binnen de familie van de Syngnathidae, zodat alle morfotypes (van fylogenetisch primitief tot geëvolueerd) in de studie opgenomen werden. Verder wordt in dit hoofdstuk een kort overzicht gegeven van de gebruikte technieken.

De patronen die de convergente evolutie naar het ontstaan van het een grijpstaart binnen de Syngnathidae karakteriseren worden beschreven in het 3^{DE} HOOFDSTUK, zowel door het vergelijken van de musculoskeletale organisatie tussen zeepaard, naaldpaard en zeenaald als door het passief opleggen van een maximale buiging van de staart. De vooropgestelde hypothese is dat het grijpvermogen van de staart enkel mogelijk is na grondige modificaties van het musculoskeletaal systeem en dat de configuratie zoals waargenomen in naaldpaardjes gelijkaardig zal aan die in zeepaardjes, en dus verschillend van de ancestrale conditie. Om de musculoskeletale organisatie te bestuderen werd gebruik gemaakt van

histologische coupes, μ CT-scans en fase contrast synchrotron scans, gecombineerd met virtuele 3D-reconstructies. De resultaten suggereren dat de onafhankelijke evolutie van de grijpstaart op minstens twee verschillende manieren kon plaatsvinden en waarbij de ancestrale conditie, bestaande uit een zeer rigide systeem, aangepast werd om zo een zeer flexibel systeem te bekomen. Intermediaire skeletale morfologieën (tussen de ancestrale conditie en zeepaard) werden aangetroffen in *Acentronura gracillissima* (een type I naaldpaardje) en *Halliichthys taeniophorus* (een type II naaldpaardje), twee soorten die fylogenetisch nauw verwant zijn met de zeepaardjes. Van de karakteristieke parallelle organisatie van de myosepta in het zeepaardje (zoals reeds eerder beschreven in Hale, 1996) kon niet aangetoond worden dat dit een vereiste is tot het bekomen van een grijpstructuur (aangezien de conische ancestrale conditie behouden werd in naaldpaardjes) waardoor dit dus een apomorfie voor zeepaardjes is. Men kan suggereren dat de functionaliteit van het grijpen eerder ontstond dan de gespecialiseerde parallelle organisatie van de myosepta zoals waargenomen in zeepaardjes. Deze stelling kan echter niet hard gemaakt worden, aangezien het grijpsysteem in de bestudeerde naaldpaardjes een totaal andere organisatie vertoont (zowel op het niveau van het skelet als van de spieren).

Het 4^{de} HOOFDSTUK behandelt de morfologische variatie binnen en tussen de staarten van verschillende syngnathie vissen, door het uitvoeren van 3D morfometrische analyses gebaseerd op oppervlakte meshes. Enkel de variatie tussen de skeletale elementen werd in kaart gebracht en niet deze tussen de verschillende spierorganisaties. Drie hypothesen werden behandeld: (1) grijpstaarten vertonen een grotere variatie binnen een staart dan niet-grijpstaarten, (2) de dorsale en ventrale dermale platen zullen verschillen binnen een staart bij prehensiele soorten en gelijkaardig zijn bij niet-prehensiele soorten en (3) de variatie tussen grijpstaarten zal beperkter zijn dan tussen niet-grijpstaarten. Vier verschillende analyses om de intra-individuele variatie te bestuderen (zowel de proximo-distale als de dorso-ventrale variatie) werden uitgevoerd op het staartskelet van negen soorten die verschillen in grijpvermogen (vier naaldpaardjes, drie zeepaardjes, één zeenaald en één zeedraak). Tijdens twee interspecifieke analyses werden alle wervels, resp. dermale platen onderling vergeleken. Vijf vormverschillen werden gevonden die mogelijks een verband hebben met het grijpvermogen van de staart in zeepaardjes en naaldpaardjes. Op het niveau van de wervels konden drie vormverschillen waargenomen worden, zijnde de inclinatie hoek tussen het voorste en achterste oppervlak van het wervelcentrum (waargenomen als proximo-distale trend in grijpstaarten en als inter-individuele trend), de ratio van wervelhoogte vs. wervellengte (waargenomen als proximo-distale trend in grijpstaarten) en de dorso-ventrale positie van het wervelcentrum (waargenomen als inter-

individuele variatie). Op het niveau van de dermale platen konden twee assen van variatie onderscheiden worden, zijnde de relatieve lengte van de caudaalstekel en de relatieve lengte van de mediale rand van de dermale platen (waargenomen als dorso-ventrale trend in grijpstaarten en als inter-individuele trend). De resultaten van dit hoofdstuk tonen aan dat grijpstaarten een grotere proximo-distale en dorso-ventrale vormvariatie vertonen binnen een staart dan niet-grijpstaarten. De hypothese dat er een beperktere vormvariatie zal zijn tussen grijpstaarten dan tussen niet-grijpstaarten kon niet bevestigd worden.

Het 5^{DE} HOOFDSTUK behandelt buigingsexperimenten uitgevoerd om te bepalen of er een verschil is in staartstijfheid tussen zeepaard en zeenaald en of dit verschilt per staartregio (proximaal, midden en distaal). Verder werd ook nagegaan hoe de verschillende lagen waaruit de staart bestaat (huid, dermale platen, spieren en wervels) bijdragen tot de stijfheid van de staart. Voor deze experimenten werd vers weefsel van beide morfotypes gebruikt. Een setup werd ontworpen, uitgetekend en geprint in 3D zodat metingen gedaan kunnen worden die de kracht meten die nodig is om een bepaalde (passieve) verplaatsing op te leggen. Deze setup is zodanig ontworpen dat de stukjes weefsel (bestaande uit 5 staartsegmenten) 90° geroteerd kunnen worden volgens hun longitudinale as teneinde dorsale, ventrale en laterale buiging te kunnen vergelijken bij elk weefselstukje. De resultaten tonen aan dat de huid en dermale platen een grote invloed hebben op de staartstijfheid, terwijl de invloed van de spieren en wervels eerder beperkt is. Eveneens kan besloten worden dat de staart van de zeenaald aanzienlijk stijver is dan die van het zeepaardje (na de resultaten te corrigeren voor grootte-verschillen) en dat dit gedeeltelijk te wijten is aan verschillen in de morfologie van de dermale platen.

De geobserveerde verschillen binnen en tussen de staarten van de verschillende syngathe morfotypes (HOOFDSTUK 4) werden in HOOFDSTUK 6 geïmplementeerd in een virtueel, dynamisch model om te bepalen of deze verschillen effectief gelinkt zijn aan grijpvermogen. Voor elk van de vormverschillen werd een uitbreiding geschreven op een bestaand model dat ontworpen werd door Tomas Praet (Praet, 2013), zodat de invloed van elk vormverschil bestudeerd kon worden. Dit gebeurde zowel voor elk vormverschil apart als voor alle vormverschillen gecombineerd in één model. Gebaseerd op de virtuele modellen van de variatie-assen van de wervels (zoals geobserveerd in HOOFDSTUK 4) kan besloten worden dat deze assen inderdaad karakteristieke voorstellen die gerelateerd kunnen worden aan een verbeterd grijpvermogen en waarvan het dus waarschijnlijk zijn dat deze adaptief zijn.

Een geïntegreerde discussie van de vier hoofdstukken die de resultaten behandelen (HOOFDSTUK 3-6) kan teruggevonden worden in HOOFDSTUK 7. Het besluit van deze discussie is dat er, alhoewel verschillende strategieën geleid hebben tot het ontstaan van een

grijpstaart gedurende de evolutie van de syngnathe vissen, bepaalde karakteristieken zijn, terug te vinden in alle grijpstaarten, die gelinkt kunnen worden aan een verbetering van het grijpvermogen. Deze karakteristieken zijn terug te vinden op zowel het niveau van de dermale platen als van de wervels. In HOOFDSTUK 7 kan ook een overzicht teruggevonden worden van enkele interessante pistes voor de toekomst en ontwerpen gebaseerd op de morfologie van syngnathen die potentieel kunnen bijdragen bij het ontwikkelen van robotica, beschermende kledij en speelgoed voor kinderen.

REFERENCES

- Abramoff MD, Magalhaes PJ, Ram SJ (2004) Image Processing with ImageJ. *Biophotonics International*, **11**, 36-42.
- Anthony R, Chevroton A (1913) Considérations sur les attitudes et la locomotion de l'Hippocampus (étude chronophotographique). *Archives de Zoologie*, **51**, 11-22.
- Aoki T, Ochiai A, Hirose S (2004) Study on slime robot development of the mobile robot prototype model using bridle bellows. *The IEEE International Conference on Robotics and Automation*, 2808-2813. New Orleans, USA.
- Ashley-Ross MA (2002) Mechanical properties of the dorsal fin muscle of seahorse (Hippocampus) and pipefish (Syngnathus). *Journal of Experimental Zoology*, **293**, 561-577.
- Azzarello MY (1990) A comparative study of the developmental osteology of Syngnathys scovelli and Hippocampus zosterae (Pisces: Syngnathidae) and its phylogenetic implications. *Evolutionary Monographs*, **12**, 90.
- Bergmann PJ, Lessard S, Russell AP (2003) Tail growth in *Chamaeleo dilepis* (Sauria : Chamaeleonidae): functional implications of segmental patterns. *Journal of Zoology*, **261**, 417-425.
- Blake RW (1976) On seahorse locomotion. *Journal of marine biology Ass. U.K.*, **56**, 939-949.
- Blake RW (1980) Undulatory median fin propulsions of two teleosts with different modes of life. *Canadian Journal of Zoology*, **58**, 2116-2119.
- Boistel R, Herrel A, Daghfous G, et al. (2010) Assisted walking in Malagasy dwarf chameleons. *Biology Letters*, **6**, 740-743.
- Brainerd EL, Patek SN (1998) Vertebral Column Morphology, C-Start Curvature, and the Evolution of Mechanical Defences in Tetraodontiform Fishes. *American Society of Ichthyologists and Herpetologists*, 14 pp.
- Bray DJ (2011) Fishes of Australia: Syngnathiformes. (<http://www.fishesofaustralia.net.au/home/order/18>).
- Breder CM (1926) The locomotion of fishes. *Zoologica*, **4**, 159-297.
- Breder CM, Edgerton HE (1942) An analysis of the locomotion of the seahorse, Hippocampus, by means of high speed cinematography. *Annals of the New York Academy of Science*, **XLIII**, 145-172.
- Browning A, Ortiz C, Boyce MC (2013) Mechanics of composite elasmoid fish scale assemblies and their bioinspired analogues. *Journal of the Mechanical Behavior of Biomedical Materials*, **19**, 75-86.
- Bruner E, Bartolino V (2008) Morphological Variation in the Seahorse Vertebral System. *International Journal of Morphology*, **26**, 247-262.
- Burdak VD (1986) Morphologie fonctionelle du tegument ecailleux des poissons. *Cybium*, **10**, 147 pp.
- Calisti M, Giorelli M, Levy G, et al. (2011) An octopus-bioinspired solution to movement and manipulation for soft robotics. *Bioinspiration & biomimetics*, **6**, 10 pp.
- Carson FL, Hladik C (2009) *Histotechnology: a self-instructional text*, ASCP Press.
- Chen P, Schirer J, Lin Y, et al. (2011) Predation versus protection: fish teeth and scales evaluated by nanoindentation. *Journal of Materials Research*, **27**, 100-112.
- Chen W-J, Bonillo C, Lecointre G (2003) Repeatability of clades as a criterion of reliability: a case study for molecular phylogeny of Acanthomorpha (Teleostei) with larger number of taxa. *Molecular Phylogenetics and Evolution*, **26**, 262-288.
- Claes P, Reijniers J, Shriver MD, et al. (2015) An investigation of matching symmetry in the human pinnae with possible implications for 3D ear recognition and sound localization. *Journal of Anatomy*, **226**, 60-72.

- Consi TR, Seifert PA, Triantafyllou MS, Edelman ER (2001) The dorsal fin engine of the seahorse (*Hippocampus sp.*). *Journal of Morphology*, **248**, 80-97.
- Dawson CE (1985) *Indo-Pacific Pipefishes*, Ocean Springs, MS: Gulf Coast Research Laboratory.
- De Mestral G (1973) Adhesive element in cloth form. (Patent n° 132513). Switzerland.
- Deane AS, Russo GA, Muchlinski MN, Organ JM (2014) Caudal vertebral body articular surface morphology correlates with functional tail use in antropoid primates. *Journal of Morphology*, **275**, 1300-1311.
- Descamps E, Sochacka A, De Kegel B, Van Loo D, Van Hoorebeke L, Adriaens D (2014) Soft tissue discrimination with contrast agents using micro-CT scanning. *Belgian Journal of Zoology*, **144**, 20-40.
- Dettai A, Lecointre G (2005) Further support for the clades obtained by multiple molecular phylogenies in the acanthomorph bush. *Comptes Rendus Biologies*, 674-689.
- Duro-Royo J, Zolotovskiy K, Mogas-Soldevila L, et al. (2015) MetaMesh: a hierarchical computational model for design and fabrication of biomimetic armored surfaces. *Computer-Aided Design*, **60**, 14-27.
- Franz-Odendaal TA, Adriaens D (2014) Comparative developmental osteology of the seahorse skeleton reveals heterochrony amongst *Hippocampus sp.* and progressive caudal fin loss. *EvoDevo*, **5**, 1-11.
- Fratzl P, Kolednik O, Fischer FD, Dean MN (2016) The mechanics of tessellations - bioinspired strategies for fracture resistance. *Chemical Society Reviews*.
- Futuyma DJ (2005) *Evolution*, Sinauer Associates, Inc., Sunderland, Massachusetts, USA.
- Gemballa S, Bartsch P (2002) Architecture of the Integument in Lower Teleostomes: Functional Morphology and Evolutionary Implications. *Journal of Morphology*, **253**, 290-309.
- Gemballa S, Ebmeyer L, Hagen K, et al. (2003) Evolutionary transformations of myoseptal tendons in gnathostomes. *Proceedings of The Royal Society B*, **270**, 1229-1235.
- Gemballa S, Konstantinidis P, Donley JM, Sepulveda C, Shadwick RE (2006) Evolution of high-performance swimming in sharks: Transformations of the musculotendinous system from subcarangiform to thunniform swimmers. *Journal of Morphology*, **267**, 477-493.
- Gemballa S, Roder K (2004) From head to tail: The myoseptal system in basal actinopterygians. *Journal of Morphology*, **259**, 155-171.
- Gemballa S, Vogel F (2002) Spatial arrangement of white muscle fibers and myoseptal tendons in fishes. *Comparative Biochemistry and Physiology Part A*, **133**, 1013-1037.
- German RZ (1982) The functional morphology of the caudal vertebrae in New World monkeys. *American Journal of Physical Anthropology*, **58**, 453-459.
- Giachetti A, Mazzi E, Piscitelli F, et al. (2014) SHREC'14 Track: Automatic location of landmarks used in manual anthropometry. In *Eurographics Workshop on 3D Object Retrieval* (eds Bustos B, Tabia H, Vandeborre JP, Veltkamp R). Strasbourg, France.
- Gomon MF (2007) A new genus and miniature species of pipehorse (Syngnathidae) from Indonesia. *International Journal of Ichthyology*, **13**, 25-30.
- Gordon AM, Huxley AF, Julian FJ (1966) The variation in isometric tension with sarcomere length in vertebrate muscle fibres. *The Journal of Physiology*, **184**, 170-192.
- Hale ME (1996) Functional morphology of ventral tail bending and prehensile abilities of the seahorse, *Hippocampus kuda*. *Journal of Morphology*, **227**, 51-65.
- Hall SJ (1999) *Basic biomechanics*, McGraw-Hill, Boston.

- Hamilton H, Saarman NP, Moore E, Short G, Simison WB (2009) A molecular phylogeny of syngnathid fishes. *8th annual Indo-Pacific fish conference*. Fremantle, Western Australia.
- Hammer O, Harper DAT, Ryan PD (2001) Past: Paleontological statistic software package for education and data analysis. *Paleontologia Electronica*, **4**, 1-9.
- Hannan MW, Walker ID (2001) Analysis and experiments with an elephant's trunk robot. *Advanced Robotics*, **15**, 847-858.
- Hannan MW, Walker ID (2002) Kinematics and the Implementation of an Elephant's Trunk Manipulator and Other Continuum Style Robots. *Journal of Robotic Systems*, **20**, 45-63.
- Harkness JM (2002) In appreciation: a lifetime of connections: Otto Herbert Schmitt, 1913-1998. *Physics in Perspective*, **4**, 456-490.
- Hebrank MR (1982) Mechanical properties of fish backbone in lateral bending and tension. *J. Biomechanics*, **15**, 85-89.
- Hebrank MR, Hebrank JH (1986) The mechanics of fish skin - lack of an external tendon role in two teleosts. *Biological Bulletin*, **171**, 236-247.
- Helfman GS, Collette BB, Facey DE, Bowen BW (2009) *The Diversity of Fishes - Biology, Evolution and Ecology*, Wiley - Blackwell.
- Herrel A, Aerts P, De Vree F (1998) Ecomorphology of the lizard feeding apparatus: a modelling approach. *Netherlands Journal of Zoology*, **48**, 1-25.
- Herrel A, Tolley KA, Measey GJ, et al. (2013) Slow but tenacious: an analysis of running and gripping performance in chameleons. *Journal of Experimental Biology*, **2013**, 1025-1030.
- Hildebrand CM (1995) *Analysis of Vertebrate Structure*, John Wiley and Sons Inc., New York.
- Hopkins JK, Spranklin BW, Gupta SK (2009) A survey of snake-inspired robot designs. *Bioinspiration & biomimetics*, **4**, 19 pp.
- Jungersen HFE (1910) *The Structure of the Aulostomidae, Syngnathidae and Solenostomidae*, Høst.
- Kai X, Simaan N (2006) Actuation compensation for flexible surgical snake-like robots with redundant remote actuation. In *IEEE International conference on robotics and automation*, pp. 1448-1454. Orlando, Florida.
- Kardong KV (1998) *Vertebrates: comparative anatomy, function, evolution*, Kane, K.T.
- Kawahara R, Miya M, Mabuchi K, et al. (2008) Interrelationships of the 11 gasterosteiform families (sticklebacks, pipefishes, and their relatives): A new perspective based on whole mitogenome sequences from 75 higher teleosts. *Molecular Phylogenetics and Evolution*, **46**, 224-236.
- Kuiter RH (2003) *Seahorses, pipefishes and their relatives*, TMC Publishing, Chorleywood, United Kingdom.
- Kuiter RH (2009) *Seahorses and their relatives*, Aquatic Photographics, Seaford, Australia.
- Laschi C, Mazzolai B, Mattoli V, Cianchetti M, Dario P (2009) Design of a biomimetic robotic octopus arm. *Bioinspiration & biomimetics*, **4**, 8 pp.
- Lees J, Märss T, Wilson MVH, Saat T, Spilev H (2011) The sculpture and morphology of postcranial dermal armor plates and associated bones in gasterosteiforms and syngnathiforms inhabiting Estonian coastal waters. *Acta Zoologica*, **93**, 422-435.
- Lepora NF, Verschure P, Prescott TJ (2013) The state of the art in biomimetics. *Bioinspiration & biomimetics*, **8**, 11 pp.
- Liem KF, Bemis WE, Walker WF, Grande L (2001) *Functional Anatomy of the Vertebrates: an Evolutionary Perspective*, Thomson Books/Cole.

- Lindsey CC (1978) Form, function and locomotory habits in fish. In *Fish physiology* (eds Hoar WS, Randall DJ), pp. 576. New York: Academia Press.
- Long JH (1998) Muscles, Elastic Energy, and the Dynamics of Body Stiffness in Swimming Eels. *American Zoology*, **38**, 771-792.
- Long JH, Adcock B, Root RG (2002) Force transmission via axial tendons in undulating fish: a dynamic analysis. *Comparative Biochemistry and Physiology Part A - Molecular and Integrative Physiology*, **133**, 911-929.
- Long JH, Hale ME, McHenry MJ, Westneat MW (1996) Functions of fish skin: flexural stiffness and steady swimming of longnose gar *Lepisosteus osseus*. *The Journal of Experimental Biology*, **199**, 2139-2151.
- Long JH, Nipper KS (1996) The importance of body stiffness in undulatory propulsion. *American Zoology*, **36**, 678-694.
- Lourie SA, Randall JE (2003) A new pygmy seahorse, *Hippocampus denise* (Teleostei: Syngnathidae), from the Indo-Pacific. *Zoological Studies*, **42**, 8 pp.
- Lourie SA, Vincent ACJ, Hall HJ (1999) *Seahorses: an identification guide to the world's species and their conservation*, Project seahorse, London, UK.
- Maia A, Adriaens D (in prep.) Tail grasping kinematics in *Hippocampus reidi*. *in prep.*
- Metscher BD (2009) MicroCT for developmental biology: a versatile tool for high-contrast 3D imaging at histological resolutions. *Developmental dynamics*, **238**, 632-640.
- Move to Cure (2012) Top 5 meest voorkomend skiblessures en hoe ze te voorkomen.). Antwerpen.
- Munro ISR (1958) Handbook of Australian Fishes, no. 24. *Australian Fisheries Newsletter*, **17**, 97-100.
- Near TJ, Dornburg A, Eytan RI, et al. (2013) Phylogeny and tempo of diversification in the superradiation of spiny-rayed fishes. *Proceedings of the National Academie of Sciences*, **110**, 12738-12743.
- Neutens C, Adriaens D, Christiaens J, et al. (2014) Grasping convergent evolution in syngnathids: a unique tale of tails. *Journal of Anatomy*, **224**, 710-723.
- Neutens C, De Dobbelaer B, Claes P, Adriaens D (under review) Prehensile and non-prehensile tails among syngnathid fishes: what's the difference? *Zoology*.
- Nowroozi BN, Brainerd EL (2012) Regional variation in the mechanical properties of the vertebral column during lateral bending in *Morone saxatilis*. *Journal of the Royal Society Interface*, 13 pp.
- Ohno H, Hirose S (2001) Design of slime robot and its gait of locomotion. In *the IEEE/RSJ International Conference on Intelligent Robots and Systems*, pp. 707-715. Maui, Hawaii, USA.
- Organ JM (2010) Structure and Function of Platyrrhine Caudal Vertebrae. *Anatomical Record-Advances in Integrative Anatomy and Evolutionary Biology*, **293**, 730-745.
- Peters HM (1951) Beiträge zur ökologischen physiologie des seepherdes (*Hippocampus brevis*). *Zeitschrift für vergleichende Physiologie*, **33**, 207-265.
- Porter MM, Adriaens D, Hatton RL, Meyers MA, McKittrick J (2015) Why the seahorse tail is square. *Science*, **349**.
- Porter MM, Novitskaya E, A.B. C-C, Meyers MA, McKittrick J (2013) Highly deformable bones: Unusual deformation mechanisms of seahorse armor. *Acta Biomaterialia*, **9**, 6763-6770.
- Praet T (2013) The biomechanical structure of the seahorse tail as a source of inspiration for industrial design. Doctoral thesis, *Faculty of engineering and architecture*. Ghent: Ghent University.

- Praet T, Adriaens D, Maia A, et al. (In prep.) Combined flexibility and stiffness of the seahorse tail: a modelling approach.
- Praet T, Adriaens D, Van Cauter S, Masschaele B, De Beule M, Verheghe B (2012) Inspiration from nature: dynamic modelling of the musculoskeletal structure of the seahorse tail. *International Journal for Numerical Methods in Biomedical Engineering*, 15 pp.
- Randall JE, Allen GR, Steene RC (1997) *Fishes of the Great Barrier Reef and Coral Sea*, University of Hawaii
- Rohlf FJ (2008) *tpsDig: Thin Plate Spline Digitise*, State University of New York at Stony Brook, New York.
- Rommens T (2010) Ruimelijke en structurele interactie van skeletelementen in een gepantserde, prehensiele structuur: staartskelet bij zeepaardjes (*Hippocampus*). Bachelor thesis, Ghent: Ghent University.
- Roos G, Leysen H, Van Wassenbergh S, et al. (2009) Linking Morphology and Motion: a Test of a Four-Bar Mechanism in Seahorses. *Physiological and Biochemical Zoology*, **82**, 7-19.
- Rudykh S, Ortiz C, Boyce MC (2015) Flexibility and protection by design: imbricated hybrid microstructures of bio-inspired armor. *Soft Matter*, **11**, 2547-2552.
- Sanders R (2012) Leaping lizards and dinosaurs inspire robot design. (<http://news.berkeley.edu/2012/01/04/leaping-lizards-show-robots-the-value-of-a-tail/>). Berkeley News.
- Schmitz RJ (1995) Ultrastructure and function of cellular components of the intercentral joint in the percoid vertebral column. *Journal of Morphology*, **226**, 1-24.
- Simaan N (2005) Snake-like units using flexible backbones and actuation redundancy for enhanced miniaturization. *2005 IEEE International Conference on Robotics and Automation*, 3012-3017.
- Simaan N, Taylor R, Flint P (2004) High dexterity snake-like robotic slaves for minimally invasive telesurgery of the upper airway. *Medical Image Computing and Computer-Assisted Intervention - Miccai 2004, Pt 2, Proceedings*, 17-24.
- Sire J-Y, Donoghue PCJ, Vickaryous MK (2009) Origin and evolution of the integumentary skeleton in non-tetrapod vertebrates. *Journal of Anatomy*, **214**, 409-440.
- Snyders J, Claes P, Vandermeulen D, Suetens P (2014) Development and comparison of non-rigid surface registration algorithms and extensions. (manual), pp. 43. Leuven: KU Leuven.
- Stevermer T (2014) Weaponized armor. (<https://tylerstevermer.wordpress.com/2014/12/23/weaponized-armor/>).
- Stiller J, Wilson NG, Rouse GW (2015) A spectacular new species of seadragon (Syngnathidae). *Royal Society Open Science*, **2**, 1-12.
- Stölting KN, Wilson AB (2007) Male pregnancy in seahorses and pipefish: beyond the mammalian model. *BioEssays*, **29**, 884-869.
- Sudo S, Tsuyuki K, Ito Y, Ikohagi T (2002) A study on the surface shape of fish scales. *JSME International Journal Series C - Mechanical System Machine Elements and Manufacturing*, **2**, 413-418.
- Taylor WR, Van Dyke GC (1985) Revised procedures for staining and clearing small fishes and other vertebrates for bone and cartilage study. *Cybium*, **9**, 107-119.
- Teske PR, Beheregaray LB (2009) Evolution of seahorses' upright posture was linked to Oligocene expansion of seagrass habitats. *Biology Letters*, **5**, 521-523.

- Teske PR, Cherry MI, Matthee CA (2004) The evolutionary history of seahorses (Syngnathidae : Hippocampus): molecular data suggest a West Pacific origin and two invasions of the Atlantic Ocean. *Molecular Phylogenetics and Evolution*, **30**, 273-286.
- Timoshenko S (1955) Chapter 5 - Deflection of beams. In *Strength of Materials, Part I*. Van Nostrand Reinhold Company.
- Tsukagoshi H, Kitagawa A, Segawa M (2001) Active hose: an artificial elephant's nose with maneuverability for rescue operations. In *the IEEE International Conference on Robotics and Automation*, pp. 2454-2459. Seoul, Korea.
- van Leeuwen J (1992) Muscle Function in Locomotion. In *Advances in Comparative and Environmental Physiology* (ed Gillis R), pp. 191-250. Berlin: Springer-Verlag.
- Van Leeuwen J (1999) A mechanical analysis of myomere shape in fish. *The Journal of Experimental Biology*, **202**, 3405-3414.
- Van Wassenbergh S, Roos G, Ferry L (2011) An adaptive explanation for the horse-like shape of seahorses. *Nature Communications*, **2**, 5 pp.
- Vernerey FJ, Barthelat F (2010) On the mechanics of fishscale structures. *International Journal of Solids and Structures*, **47**, 2268-2275.
- Vincent JFV, Bogatyreva OA, Bogatyreva NR, Bowyer A, Pahl A-K (2006) Biomimetics: its practice and theory. *Journal of the Royal Society Interface*, **3**, 471-482.
- Walker ID (2013) Continuous backbone "continuum" robot manipulators. *ISNR Robotics*, **2013**, 19 pp.
- Weber H (1926) Beiträge zur Bewegungsphysiologie der Hippocampus-Arten. *Zeitschrift für vergleichende Physiologie*, **5**, 1-36.
- Wen L, Weaver JC, Lauder GV (2014) Biomimetic shark skin: design, fabrication and hydrodynamic function. *The Journal of Experimental Biology*, **217**, 1656-1666.
- Westneat MW, Hale ME, McHenry MJ, Long JH (1998) Mechanics of the fast-start: muscle function and the role of intramuscular pressure in the escape behavior of *Amia calva* and *Polypterus palmas*. *Journal of Experimental Biology*, **201**, 3041-3055.
- Wilson AB, Orr JW (2011) The evolutionary origins of Syngnathidae: pipefishes and seahorses. *Journal of Fish Biology*, **78**, 1603-1623.
- Wilson NG, Rouse GW (2010) Convergent camouflage and the non-monophyly of 'seadragons' (Syngnathidae: Teleostei): suggestions for a revised taxonomy of syngnathids. *Zoologica Scripta*, **39**, 551-558.
- Xu K, Simaan N (2006) Actuation compensation for flexible surgical snake-like robots with redundant remote actuation. *2006 IEEE International Conference on Robotics and Automation*, 4148-4154.
- Yang W, Chen IH, Gludovatz B, Zimmerman EA, Ritchie RO, Meyers MA (2013a) Natural Flexible Dermal Armor. *Advanced Materials*, **25**, 31-48.
- Yang W, Gludovatz B, Zimmerman EA, Bale HA, Ritchie RO, Meyers MA (2013b) Structure and fracture resistance of alligator gar (*Atractosteus spatula*) armored fish scales. *Acta Biomaterialia*, **9**, 5876-5889.
- Yuille AL, Grzywacz NM (1989) A mathematical analysis of the motion coherence theory. *International Journal of Computer Vision*, **3**, 155-175.
- Zhao J, Zhao T, Xi N, Cintron FJ, Mutka MW, Xiao L (2013) Controlling Aerial Maneuvering of a Miniature Jumping Robot Using Its Tail. *IEEE/RSJ International Conference on Intelligent Robots and Systems (IROS)*. Tokyo, Japan.

- Zhu D, Ortega C, Motamedi R, Szewciw L, Vernerey FJ, Barthelat F (2011) Structure and mechanical performance of a "modern" fish scale. *Advanced Biomaterials*, **14**, B185-B194.
- Zippel KC, Glor RE, Bertram JEA (1999) On caudal prehensility and phylogenetic constraint in lizards: The influence of ancestral anatomy on function in *Corucia* and *Furcifer*. *Journal of Morphology*, **239**, 143-155.
- Zolotovskiy K (2012) BioConstructs - Methods for Bio-inspired and Bio-fabricated Designs. Master dissertation, *Department of Architecture*, pp. 74. Massachusetts Institute of Technology.

CURRICULUM

1 Publications

Neutens, C., P. Urban, M. De Beule & D. Adriaens (in prep.) - To bend or not to bend: tail stiffness in seahorses vs. pipefishes, *Acta Biomaterialia*

Neutens, C., B. De Dobbelaer, P. Claes & D. Adriaens (resubmitted) - Prehensile and non-prehensile tails among syngnathid fishes: what's the difference?, *Zoology*

Neutens, C., D. Adriaens, J. Christiaens, B. De Kegel, M. Dierick, R. Boistel & L. Van Hoorebeke (2014) - Grasping convergent evolution in syngnathids: a unique tale of tails, *Journal of Anatomy*, 224(6): 710-723.

2 Congress contributions

2.1 Active contributions

Neutens C., B. De Dobbelaer, P. Claes, T. Praet, M. Porter, M. De Beule, J. Christiaens, B. De Kegel, M. Dierick, R. Boistel & D. Adriaens (2016) - *Transforming tails into tools: syngnathid fishes used as bio-inspiration*. 11th International Congress of Vertebrate Morphology (Washington D.C., USA). (oral presentation).

Neutens C., B. De Dobbelaer, P. Claes and D. Adriaens (2015) – *Prehensile and non-prehensile tails among syngnathid fishes: what's the difference?* *Zoology* (Amsterdam, The Netherlands). (oral presentation).

Neutens C., P. Urban, M. De Beule and D. Adriaens (2015) – *To bend or not to bend: seahorses vs. pipefishes*. *Zoology* (Amsterdam, The Netherlands). (poster presentation, winner best poster award).

Neutens C., T. Praet, M. De Beule, M. Dierick & D. Adriaens (2014) – *The seahorse tail as inspiration for serially articulated systems*. WCCM XI – ECCM V – ECFD VI (Barcelona, Spain). (oral presentation).

Neutens C., D. Adriaens, J. Christiaens, B. De Kegel, M. Dierick, R. Boistel & L. Van Hoorebeke (2013) – *A unique muscular organization unraveled in seahorse tails by combining μ CT-scanning with old school histological sectioning*. Tomography for Scientific Advancement symposium (London, UK). (poster presentation).

Neutens C., D. Adriaens, J. Christiaens, B. De Kegel, M. Dierick, R. Boistel & L. Van Hoorebeke (2013) – *Functional morphology of a unique muscular organization in the prehensile tail of seahorses*. 10th International Congress of Vertebrate Morphology (Barcelona, Spain). (symposium talk).

Neutens C., D. Adriaens, J. Christiaens, D. Van Loo, B. De Kegel, R. Boistel & L. Van Hoorebeke (2013) - *Evolutionary morphology of the prehensile tail in syngnathid fishes: from pipefish to seahorse*. Annual meeting Society of Integrative and Comparative Biology (San Francisco, USA). (oral presentation).

Adriaens, D., C. Neutens, J. Christiaens, D. Van Loo, B. De Kegel, R. Boistel & L. Van Hoorebeke (2012) - *Evolutionary morphology of the caudal musculoskeletal system in syngnathid fish: from swimming to prehension ... in different ways*. XIVth International Congress of Ichthyology (Liege, Belgium). (oral presentation).

Gilissen, E. & C. Neutens (2011) - *La structure externe et la structure profonde des sillons corticaux chez l'homme et les grands singes, une approche renouvelée de l'anatomie cérébrale comparée réalisée à l'aide des nouvelles méthodes d'imagerie*. 1836^{ème} réunion scientifique de la SAP (Paris, France). (oral presentation).

2.2 Passive contributions

Neutens C., B. De Dobbelaer, P. Claes, D. Adriaens* (2015) – *3D surface-based morphometrics used to determine the intraspecific differences within the tail of syngnathid fishes*. Annual meeting of the Society of Integrative and Comparative Biology (West Palm Beach, USA). (oral presentation).

Adriaens, D., T. Praet, C. Neutens, M.M. Porter, M. De Beule, J. McKittrick & B. Verhegghe (2015) - *Computer modelling and biomimetics in order to understand the evolution of tail grasping in seahorses*. Annual Meeting of the American Association of Anatomists at the Experimental Biology 2015 conference, Boston March 28th-31st. (oral presentation).

Neutens C., D. Adriaens*, J. Christiaens, B. De Kegel, M. Dierick, R. Boistel & L. Van Hoorebeke (2013) - *Increased tail flexibility in syngnathid fishes: from pipefish to seahorse*. Interdisciplinary Approaches in Fish Skeletal Biology (Tavira, Portugal). (oral presentation).

Adriaens D., T. Praet, C. Neutens, A. Maia, M. De Beule & B. Verhegghe (2013) - *From the evolution of the seahorse tail towards bio-inspired serially articulated systems*. Workshop on Emergent Design in Biological and Bioinspired Materials: Beyond the Rule of Mixtures (Massachusetts Institute of Technology, Cambridge, USA). (oral presentation).

Adriaens, D., C. Neutens, J. Christiaens, D. Van Loo, B. De Kegel, R. Boistel & L. Van Hoorebeke (2012) - *Evolutionary morphology of the caudal musculoskeletal system in syngnathid fish: from swimming to prehension ... in different ways*. Annual meeting of the Society of Integrative and Comparative Biology (Charleston, USA). (oral presentation).

Adriaens, D., C. Neutens, J. Christiaens, D. Van Loo, B. De Kegel, R. Boistel & L. Van Hoorebeke (2011) - *Convergent evolution of a unique skeletal system in fishes: the grasping tail in syngnathids*. 2nd Workshop on Interdisciplinary Approaches in Fish Skeletal Biology (Tavira, Portugal). (oral presentation).

Gilissen, E. & C. Neutens (2011) - *Surface and deep structure of the central sulcus is the human and chimpanzee neocortex*. Annual Meeting of the American Association of Physical Anthropologists (Minneapolis, USA). (oral presentation).

2.3 As a member of the organizing committee

6th International Conference of Craniocervical Systems in Vertebrae, July 7th-10th 2015, Ghent, Belgium

3 Workshops

"High-resolution X-ray computed tomography: A guide to image acquisition, visualization and analysis", UGCT - University of Ghent, Ghent, Belgium (7-9 September 2015).

"Introduction to Abaqus", Dassault Systemes, Maarssens, the Netherlands (3-5 December 2012).

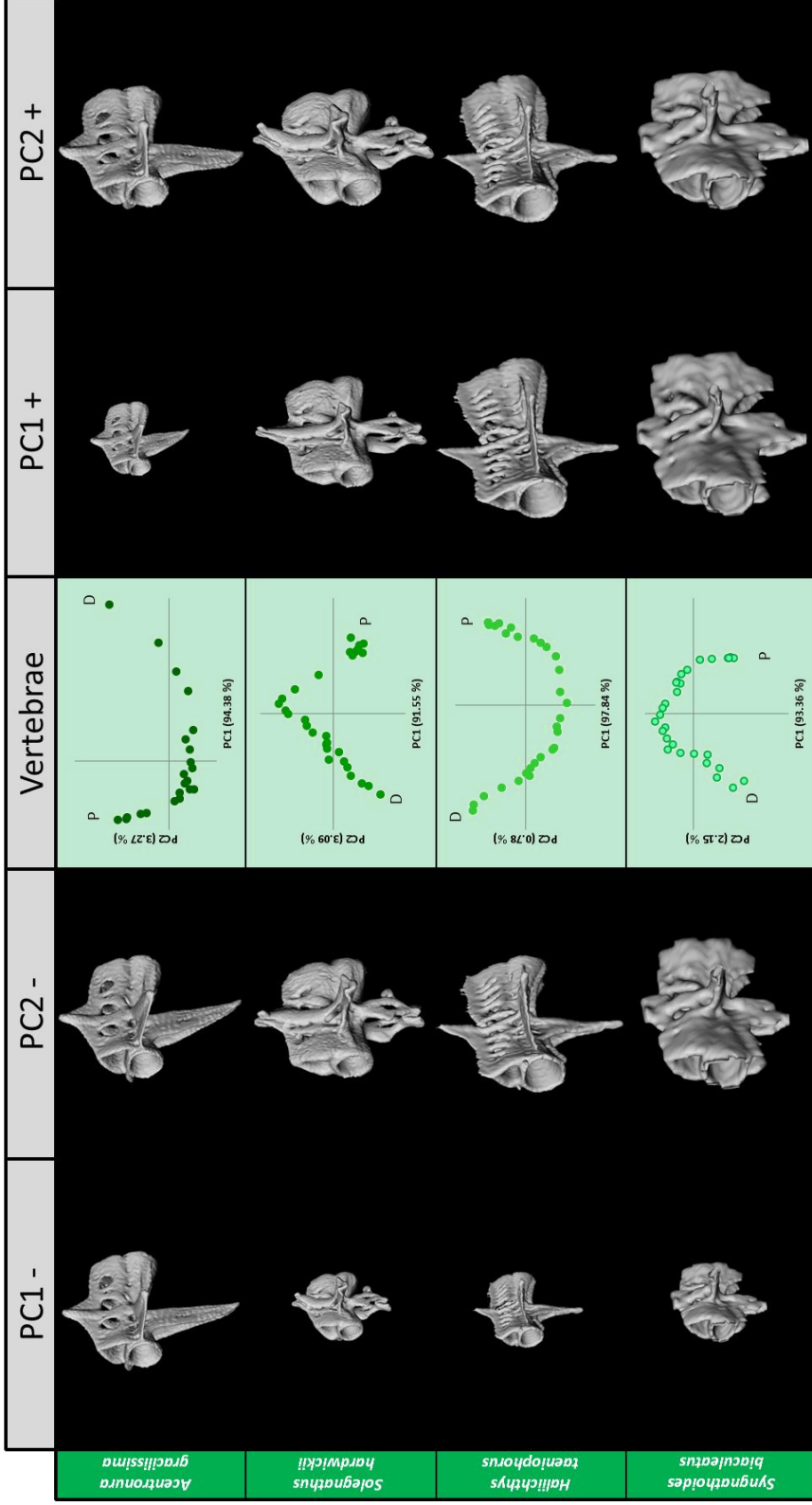
"Locomorph Summerschool on Morphology and Morphosis in Animals and Robots", University of Southern Denmark, Odense, Denmark (23-27 August 2012).

APPENDIX A

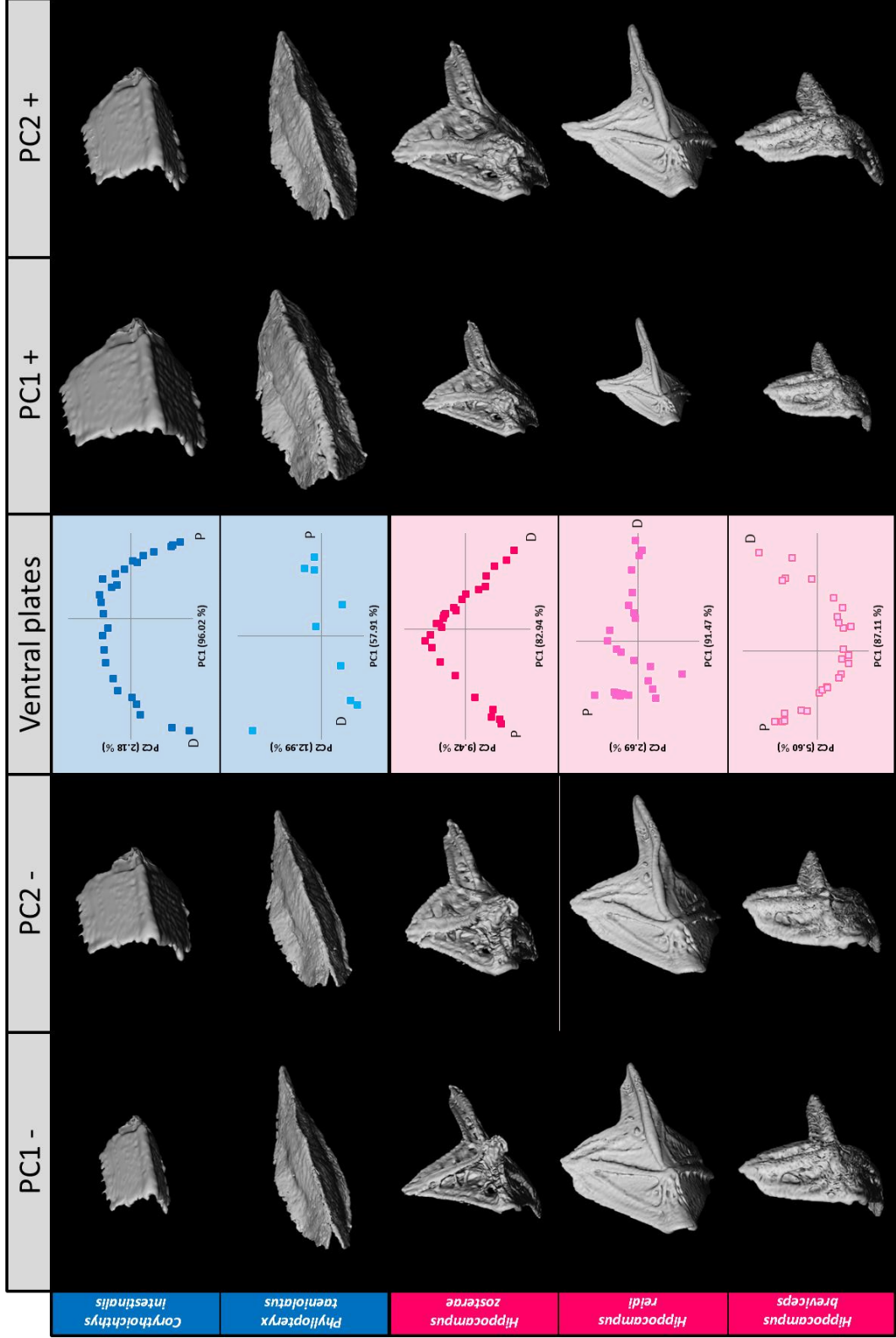
Overview of specimen specific shape changes

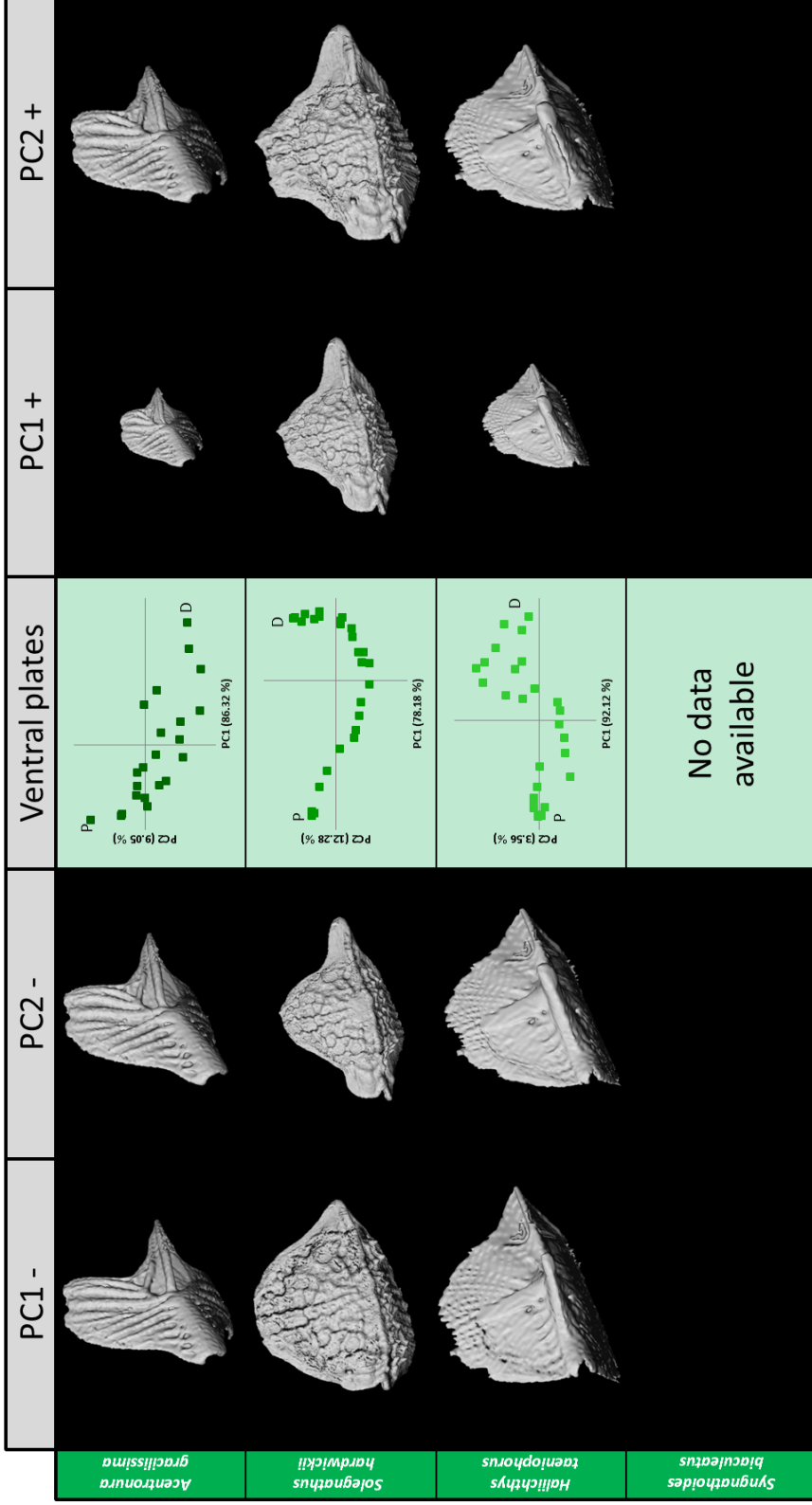
(RESULTS SECTION CHAPTER 4)

	PC1 -	PC2 -	Vertebrae	PC1 +	PC2 +
<i>Corythoichthys intestinalis</i>					
<i>Phyllipteryx taeniolatus</i>					
<i>Hippocampus zosterae</i>					
<i>Hippocampus reidi</i>					
<i>Hippocampus breviceps</i>					

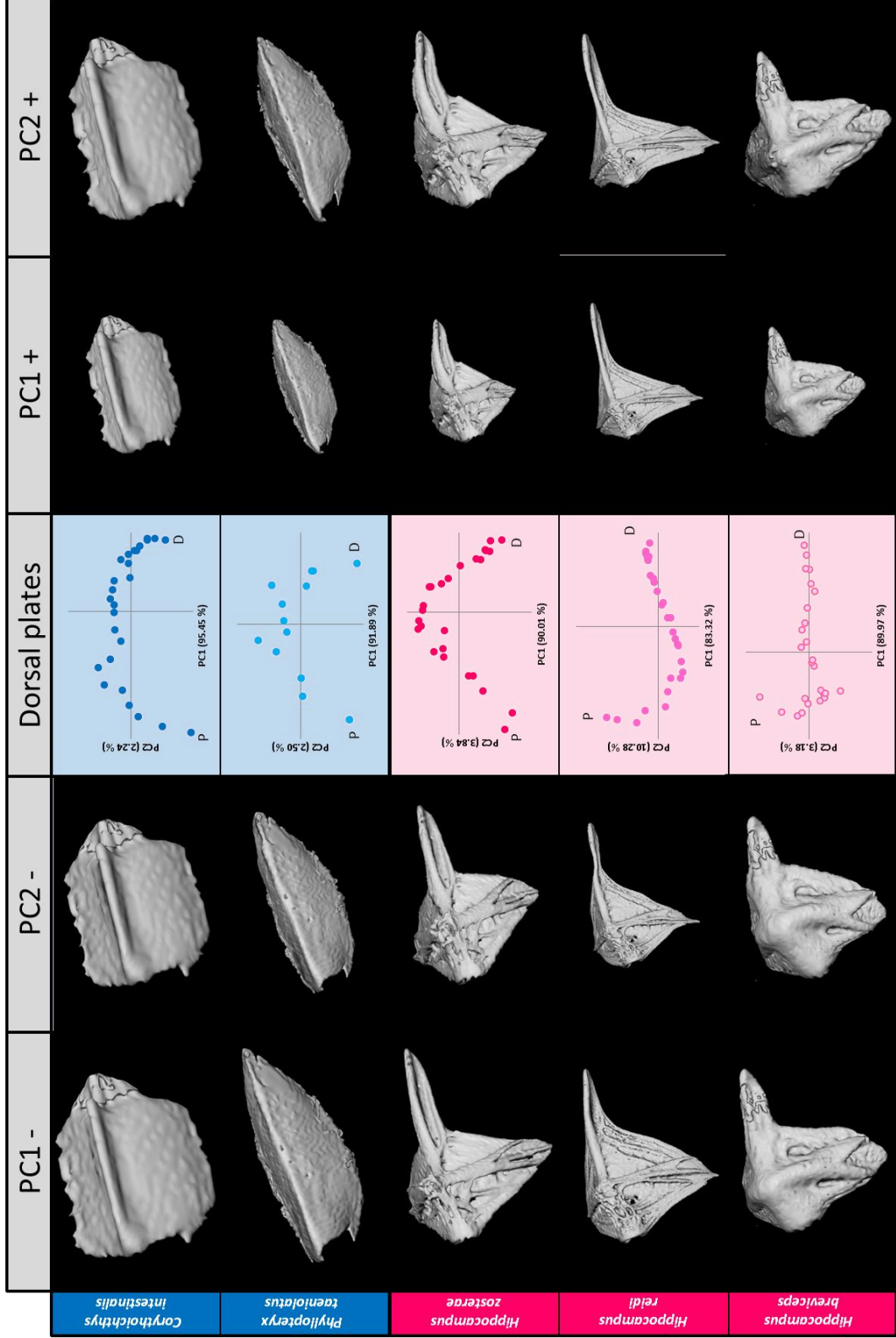


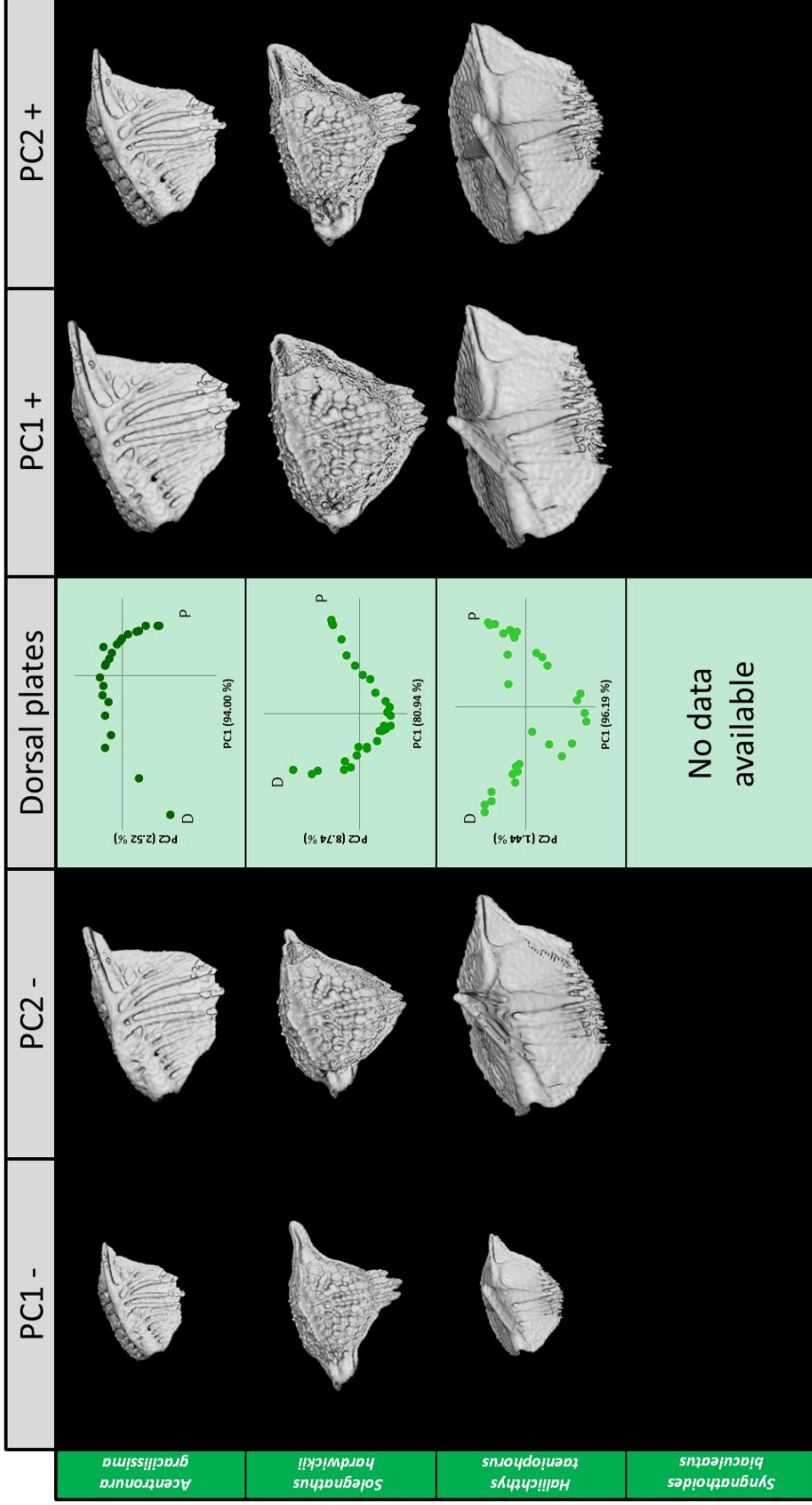
APPENDIX A.1 - First and second principal components axis of the vertebrae in pipefish and seadragon (blue), seahorses (pink) and pipehorses (green). Figures showing the shape changes along these two axes at the extremes of their distribution.





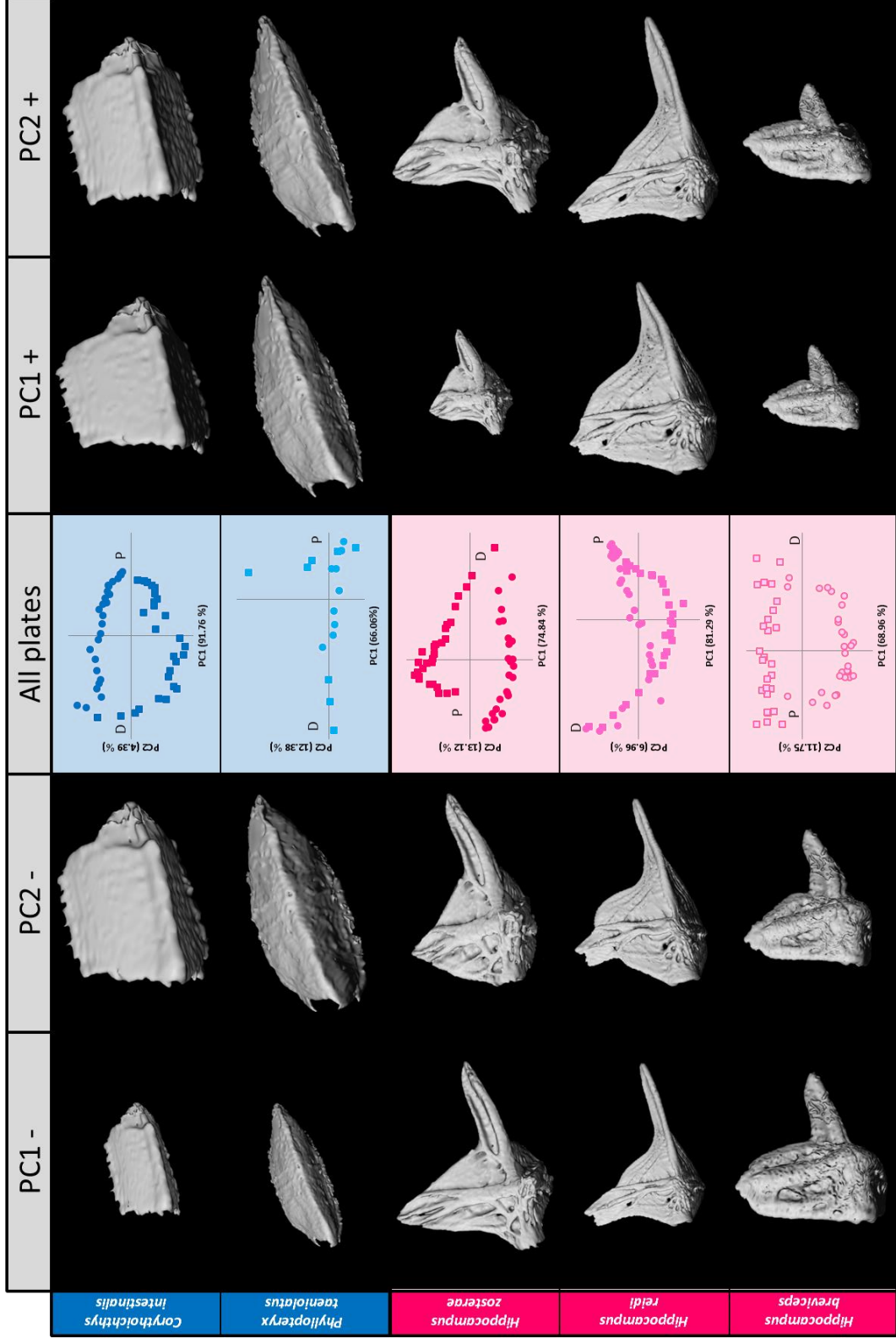
APPENDIX A.2 - First and second principal components axis of the ventral plates in pipefish and seadragon (blue), seahorses (pink) and pipehorses (green). Figures showing the shape changes along these two axes at the extremes of their distribution.

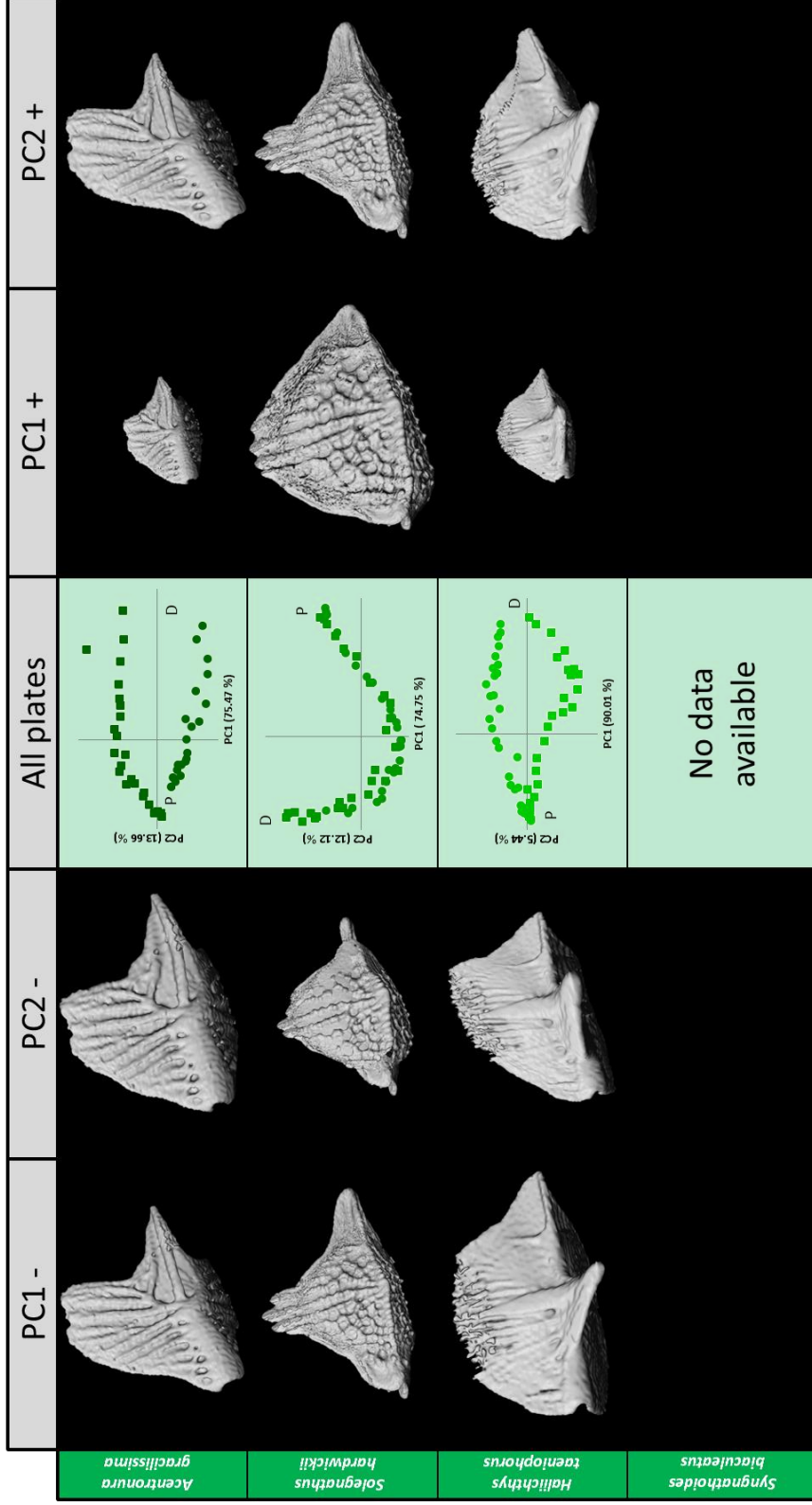




APPENDIX A.3 - First and second principal components axis of the dorsal plates in pipefish and seadragon (blue), seahorses (pink) and pipehorses (green). Figures showing the shape changes along these two axes at the extremes of their distribution.

Prognathodes
Stiphodon





APPENDIX A.4 - First and second principal components axis of all dermal plates in pipefish and seadragon (blue), seahorses (pink) and pipehorses (green). Figures showing the shape changes along these two axes at the extremes of their distribution.

APPENDIX B

Measurements shape differences

(CHAPTER 4)

	<i>Corythoichthys intestinalis</i>	<i>Phyllopteryx taeniolatus</i>	<i>Hippocampus reidi</i>	<i>Hippocampus breviceps</i>	<i>Hippocampus zosterae</i>	<i>Acentronura gracilissima</i>	<i>Solegnathus hardwickii</i>	<i>Syngnathoides biaculeatus</i>	<i>Haliichthys taeniophorus</i>		
Segment dimensions (in mm)											
	height	length	height	length	height	length	height	length	height	length	
proximal											
					3.44	2.10			4.79	7.56	
					3.80	2.01			4.69	7.35	
					4.14	1.98			4.57	6.93	
					3.96	1.95			4.46	6.38	
				5.76	3.82	3.95	1.92	1.30	0.94	1.33	0.85
				5.60	3.67	3.83	1.92	1.27	1.03	1.36	0.89
	6.60	4.84		5.48	3.72	3.68	1.89	1.24	0.96	1.33	0.85
	6.70	4.95		5.31	3.69	3.83	1.88	1.20	0.90	1.36	0.89
	6.45	5.02		5.16	3.66	3.57	1.86	1.17	0.89	1.33	0.85
	6.34	4.83		5.06	3.63	3.46	1.85	1.09	0.85	1.30	0.85
	6.09	5.03		4.89	3.57	3.52	1.83	1.03	0.83	1.30	0.85
	5.91	4.91		4.87	3.56	3.50	1.84	1.03	0.81	1.30	0.85
	5.70	4.94		4.68	3.42	3.39	1.80	1.01	0.81	1.25	0.82
	5.60	4.93		4.55	3.31	3.25	1.77	1.05	0.79	1.18	0.79
	5.28	5.03		4.35	3.26	3.11	1.75	1.05	0.79	1.10	0.79
	5.13	5.02		4.26	3.19	3.02	1.67	1.03	0.76	1.08	0.79
	4.86	4.92		3.85	3.16	2.90	1.68	1.00	0.78	1.07	0.79
	4.74	4.83		3.92	3.00	2.79	1.59	0.97	0.78	1.00	0.77
	4.45	4.79		3.78	2.87	2.71	1.56	0.94	0.76	1.00	0.77
	4.19	4.52		3.58	2.83	2.53	1.55	0.88	0.74	1.00	0.77
	3.94	4.41		3.34	2.66	2.41	1.48	0.87	0.69	1.00	0.77
	3.66	4.50		3.18	2.62	2.26	1.45	0.86	0.71	1.00	0.77
	3.44	4.49		3.13	2.51	2.07	1.39	0.80	0.70	1.00	0.77
	3.26	4.25		2.92	2.41	1.96	1.33	0.76	0.67	1.00	0.77
	3.05	4.18		2.71	2.28	1.90	1.24	0.72	0.63	1.00	0.77
	2.76	4.05		2.56	2.11	1.76	1.17	0.69	0.63	1.00	0.77
	2.55	3.85		2.35	2.00	1.65	1.12	0.64	0.61	1.00	0.77
	2.38	3.77		2.20	1.81	1.52	1.07	0.57	0.57	1.00	0.77
	2.23	3.65		2.03	1.72	1.32	1.00	0.55	0.53	1.00	0.77
	2.13	3.69		1.81	1.67	1.22	0.94	0.51	0.49	1.00	0.77
	1.97	3.54		1.51	1.41	1.07	0.85	0.44	0.45	1.00	0.77
	1.91	3.24		1.31	1.27	0.93	0.80	0.38	0.42	1.00	0.77
distal	2.00	2.85		1.10	1.12	0.86	0.72	0.33	0.39	-0.04	0.31

	<i>Corythoichthys intestinalis</i>	<i>Phyllopteryx taeniolatus</i>	<i>Hippocampus reidi</i>	<i>Hippocampus breviceps</i>	<i>Hippocampus zosterae</i>	<i>Acentronura gracilissima</i>	<i>Solegnathus hardwickii</i>	<i>Syngnathoides biaculeatus</i>	<i>Haliichthys taeniophorus</i>	
Inclination angle (in degrees) between posterior and anterior surface of the vertebral body										
	angle	SD	angle	SD	angle	SD	angle	SD	angle	SD
proximal										
			3.87	0.41	1.15	0.61			2.44	0.61
			1.21	0.73	2.89	0.38			2.14	1.05
			5.35	0.52	2.74	0.59	4.39	0.38	2.04	0.50
	3.07	0.73	0.28	0.22	0.88	0.37	8.16	1.01	3.01	0.66
	0.53	0.46	5.51	0.39	4.71	0.62	1.59	0.31	4.58	0.77
	0.38	0.25	4.70	0.47	7.30	0.60	2.93	0.36	2.87	0.37
	0.49	0.33	6.55	0.33	6.64	0.73	1.92	0.58	4.92	0.58
	0.46	0.30	6.54	0.42	6.71	0.82	1.23	0.35	4.92	0.58
	0.48	0.36	8.55	0.33	6.62	0.88	2.01	0.45	4.08	0.66
	0.67	0.54	8.85	0.30	8.67	0.43	5.83	0.40	7.68	0.83
	0.38	0.23	8.20	0.47	7.82	0.55	2.65	0.32	8.09	0.64
	0.30	0.33	10.25	0.47	7.83	0.66	11.11	0.40	10.81	1.11
	0.33	0.29	7.44	0.34	11.24	0.63	13.06	0.25	10.70	0.54
	0.71	0.52	15.08	0.48	10.85	0.89	10.59	0.79	11.52	1.03
	0.61	0.49	6.59	0.36	13.14	0.75	14.79	0.63	15.11	0.96
	3.99	1.05	12.77	0.14	11.96	1.25	17.08	0.73	16.30	0.45
	1.71	1.13	11.90	0.49	11.52	0.72	16.28	1.10	16.23	0.72
	0.43	0.21	10.13	0.43	15.31	1.78	16.27	0.92	15.96	0.83
	0.41	0.23	13.17	0.36	13.43	1.08	17.02	0.78	16.69	0.72
	3.10	0.66	11.76	0.35	11.86	0.64	18.08	0.76	17.85	0.43
	0.92	0.47	12.22	0.50	16.45	0.79	18.69	0.36	17.35	0.81
	1.26	0.68	9.82	0.59	14.32	0.77	19.13	0.53	20.52	0.36
	0.40	0.31	15.34	0.39	14.08	0.50	14.64	0.55	16.61	0.75
	1.68	1.35	14.19	0.79	12.28	0.46	18.76	0.79	18.03	0.80
	3.10	1.36	10.58	1.01	13.26	0.50	19.21	0.78	21.05	0.67
	3.06	1.91	10.20	0.73	12.31	0.75	24.62	0.82	18.48	0.34
	1.78	1.26	8.09	1.42	9.17	0.95	20.77	0.55	20.67	1.11
	6.67	2.47	12.04	1.29	18.32	1.39	23.06	0.43	22.49	0.62
	0.90	0.44	4.53	1.57	13.23	1.08	24.05	1.35	27.96	1.72
distal	1.09	0.89	10.25	1.55	15.24	0.78	24.85	1.48	32.77	1.15

	<i>Corythaichthys intestinalis</i>		<i>Phyllopteryx taeniolatus</i>		<i>Hippocampus reidi</i>		<i>Hippocampus breviceps</i>		<i>Hippocampus zosterae</i>		<i>Acetronura gracilissima</i>		<i>Solegnathus hardwickii</i>		<i>Syngnathoides biaculeatus</i>		<i>Haliichthys taeniorphus</i>		
Plate length (in mm)																			
	dorsal	ventral	dorsal	ventral	dorsal	ventral	dorsal	ventral	dorsal	ventral	dorsal	ventral	dorsal	ventral	dorsal	ventral	dorsal	ventral	
proximal							2.55	2.83										9.04	9.36
							2.80	2.62										9.08	9.08
					4.89	4.93	2.94	2.71					21.42	22.12				9.20	9.09
					5.26	4.79	2.60	2.65					20.47	20.80				9.10	9.08
		5.82	6.06			5.17	4.66	2.83	2.52	1.29	1.29			19.87	19.73			8.69	8.76
		6.03	6.17			5.52	4.94	3.09	2.61	1.28	1.32			18.18	17.92			8.80	8.55
		5.94	6.00			4.93	4.71	2.52	2.58	1.37	1.35			17.22	16.76			8.83	8.53
		6.02	5.98			5.03	4.59	2.80	2.35	1.25	1.35			16.02	14.81			8.54	8.31
		5.97	6.08			4.97	4.23	2.57	2.47	1.18	1.28			14.61	12.96			8.41	7.98
		5.94	5.98			5.17	4.46	2.88	2.36	1.18	1.22	1.25	1.14	13.63	12.11			8.00	7.72
		5.94	6.04			4.52	4.08	2.50	2.41	1.06	1.13	1.23	1.10	12.95	10.96			7.94	7.48
		5.93	6.03			4.41	4.05	2.61	2.31	1.12	1.10	1.22	1.08	11.75	9.77			7.63	7.14
		5.97	5.87			4.13	4.14	2.74	2.26	1.07	0.99	1.16	1.04	11.22	8.59			7.34	6.62
		5.91	5.87			4.27	3.84	2.37	2.14	1.12	0.98	1.20	1.02	10.83	7.85			6.87	6.09
		5.75	5.90			3.82	3.47	2.62	2.08	1.09	0.97	1.23	0.98	10.69	7.15			6.53	5.40
		5.55	5.71			3.84	3.36	2.27	2.02	1.05	0.91	1.13	0.95	10.44	6.72			6.30	5.16
		5.63	5.60			3.60	3.52	2.20	2.04	1.05	0.89	1.14	0.90	10.25	6.03			5.96	4.86
		5.52	5.60			3.90	3.31	2.21	1.86	1.05	0.86	1.10	0.91	10.18	5.88			5.56	4.58
		5.40	5.47			3.41	3.11	2.04	1.77	0.99	0.87	1.10	0.90	10.16	5.69			5.33	4.40
		5.34	5.44			3.28	3.09	2.04	1.76	0.93	0.83	1.07	0.83	10.08	6.55			4.89	4.04
		5.12	5.08			3.20	2.97	1.88	1.66	0.89	0.78	1.02	0.86	10.09	6.13			4.86	3.79
		5.06	5.09			3.27	2.74	1.80	1.59	0.90	0.77	0.98	0.84	9.80	5.56			4.60	3.65
	4.90	4.90	10.09	9.77	2.80	2.58	1.64	1.57	0.91	0.77	0.95	0.80	9.50	4.74			4.33	3.84	
	4.83	4.72	9.32	9.83	2.64	2.49	1.61	1.47	0.90	0.78	0.98	0.78	9.21	3.89			4.20	3.79	
	4.67	4.71	9.05	9.47	2.62	2.36	1.50	1.40	0.82	0.74	0.93	0.78	8.84	3.44			3.97	3.30	
	4.65	4.44	8.50	9.37	2.42	2.07	1.44	1.29	0.81	0.70	0.86	0.77	8.43	3.91			3.77	3.14	
	4.40	4.25	8.50	9.14	2.20	2.03	1.41	1.25	0.73	0.67	0.83	0.73	7.98	3.64			3.58	3.08	
	4.04	4.06	9.05	8.28	2.00	1.74	1.28	1.23	0.68	0.64	0.82	0.68	7.76	3.32			3.39	3.00	
	3.98	4.06	7.57	7.84	1.70	1.55	1.17	1.14	0.65	0.58	0.75	0.67	7.33	3.23			3.10	2.47	
	3.73	3.64	7.15	7.15	1.53	1.45	0.91	1.05	0.58	0.54	0.68	0.61	6.65	2.80			2.85	2.40	
	3.42	3.44	6.76	6.75	1.28	1.26	0.94	0.91	0.54	0.49	0.62	0.54	6.24	1.36			2.68	2.11	
distal	2.25	2.68	6.52	5.84	1.08	1.02	0.00	0.88	0.50	0.47	0.46	0.48	6.73	1.04			2.33	1.68	

	<i>Corythaichthys intestinalis</i>		<i>Phyllopteryx taeniolatus</i>		<i>Hippocampus reidi</i>		<i>Hippocampus breviceps</i>		<i>Hippocampus zosterae</i>		<i>Acetronura gracilissima</i>		<i>Solegnathus hardwickii</i>		<i>Syngnathoides biaculeatus</i>		<i>Haliichthys taeniorphus</i>		
Caudal spine length (in mm)																			
	dorsal	ventral	dorsal	ventral	dorsal	ventral	dorsal	ventral	dorsal	ventral	dorsal	ventral	dorsal	ventral	dorsal	ventral	dorsal	ventral	
proximal					2.37	2.35	1.21	1.34										2.23	2.67
					2.54	2.55	1.20	1.52					5.06	5.62				2.23	2.58
					2.41	2.37	1.14	1.31	0.59	0.63			4.74	4.83				2.21	2.53
		1.43	1.61			2.19	2.37	1.14	1.35	0.61	0.66			4.70	4.84			2.25	2.43
		1.49	1.63			2.05	2.25	1.06	1.28	0.62	0.67			4.61	4.58			2.05	2.39
		1.33	1.68			1.97	2.32	1.04	1.23	0.66	0.63			4.23	4.36			2.02	2.39
		1.26	1.59			1.99	1.89	0.99	1.14	0.60	0.64			4.15	3.84			1.85	2.27
		1.20	1.53			1.78	1.97	0.96	1.10	0.58	0.60	0.46	0.54	4.07	3.83			1.85	2.28
		1.16	1.59			1.68	1.94	0.96	1.14	0.54	0.59	0.46	0.54	3.91	3.71			1.90	2.08
		1.22	1.54			1.65	2.06	0.95	1.07	0.53	0.53	0.47	0.54	3.90	3.12			1.77	2.14
		1.14	1.37			1.56	2.04	0.92	1.07	0.49	0.49	0.46	0.53	3.58	2.74			1.84	2.08
		1.13	1.45			1.41	1.78	0.87	1.03	0.48	0.53	0.48	0.52	3.71	1.30			1.68	2.03
		1.04	1.39			1.35	1.54	0.90	0.98	0.42	0.48	0.46	0.51	3.77	0.00			1.82	1.92
		0.89	1.11			1.26	1.60	0.87	0.97	0.43	0.45	0.43	0.50	3.56	0.00			1.69	1.92
		0.93	1.21			1.14	1.56	0.80	0.94	0.45	0.44	0.45	0.48	3.26	0.00			1.67	1.83
		0.93	1.25			1.22	1.65	0.77	0.89	0.40	0.43	0.44	0.46	3.49	0.00			1.56	1.88
		0.98	1.13			0.97	1.57	0.76	0.84	0.40	0.42	0.43	0.44	3.46	0.00			1.52	1.85
		0.87	1.06			0.90	1.44	0.69	0.82	0.35	0.43	0.40	0.43	3.59	0.00			1.51	1.87
		0.90	1.18			1.02	1.43	0.63	0.75	0.32	0.39	0.37	0.41	3.37	0.00			1.44	2.01
		0.78	0.98			1.02	1.36	0.57	0.76	0.32	0.44	0.35	0.41	3.37	0.00			1.33	1.89
		0.76	1.01			0.91	1.30	0.53	0.72	0.32	0.37	0.33	0.40	3.20	0.00			1.33	1.82
		0.67	0.85	2.17	2.35	0.83	1.20	0.49	0.70	0.32	0.42	0.35	0.38	3.15	0.00			1.31	1.68
		0.66	0.85	1.97	2.06	0.83	1.05	0.47	0.63	0.28	0.37	0.30	0.37	3.06	0.00			1.28	1.80
		0.65	0.71	1.64	1.93	0.83	1.05	0.47	0.63	0.28	0.37	0.30	0.37	3.00	0.00			1.23	1.72
		0.75	0.71	1.82	1.79	0.72	1.07	0.37	0.53	0.29	0.36	0.29	0.35	2.80	0.00			1.18	1.50
		0.59	0.69	1.45	1.42	0.63	0.95	0.39	0.51	0.22	0.33	0.28	0.33	2.71	0.00			1.01	1.48
		0.60	0.66	1.36	1.57	0.57	0.77	0.40	0.45	0.22	0.33	0.28	0.33	2.87	0.00			0.98	1.40
		0.48	0.69	1.26	1.52	0.63	0.73	0.38	0.45	0.19	0.32	0.25	0.31	2.57	0.00			0.96	1.25
		0.55	0.55	1.22	1.39	0.52	0.66	0.33	0.45	0.17	0.28	0.23	0.26	2.59	0.00			0.74	0.96
		0.28	0.45	1.32	1.30	0.45	0.61	0.22	0.39	0.18	0.22	0.21	0.25	2.01	0.00			0.71	0.91
	distal	0.00	0.42	1.12	1.19	0.40	0.49	0.13	0.33	0.19	0.23	0.11	0.22	1.96	0.00			0.67	0.71

Vertebra	<i>Corythaichthys intestinalis</i>	<i>Phyllopteryx taeniolatus</i>	<i>Hippocampus reidi</i>	<i>Hippocampus breviceps</i>	<i>Hippocampus zosterae</i>	<i>Acenronura gracilissima</i>	<i>Solegnathus hardwickii</i>	<i>Syngnathoides biaculeatus</i>	<i>Haliichthys taeniophorus</i>		
Medial plate edge length (in mm)											
	dorsal ventral	dorsal ventral	dorsal ventral	dorsal ventral	dorsal ventral	dorsal ventral	dorsal ventral	dorsal ventral	dorsal ventral		
proximal				0.87 0.54 0.94 0.81					6.29 7.14 6.10 6.85		
			0.92 4.93 1.02 4.79	0.97 1.01 0.92 1.05			11.90 11.18 11.21 9.38		6.05 6.86 5.90 6.85		
	4.37 4.18 4.48 4.11 4.42 4.39 4.49 4.27 4.63 4.35 4.58 4.38 4.44 4.33 4.32 4.26 4.49 4.28 4.58 4.30 4.33 4.16 4.64 4.19 4.33 4.01 4.27 4.20 4.22 4.22 4.14 4.12 3.91 3.77 4.08 4.03 3.91 3.56 4.08 3.46 3.86 3.46 3.73 3.36 3.26 3.40 3.05 3.22 3.08 3.34 2.94 3.04 2.53 2.71			0.99 4.66 1.10 4.94 1.13 4.71 1.07 4.59 1.03 4.23 1.07 4.46 1.09 4.08 0.98 4.05 0.87 4.14 0.98 3.84 0.94 3.47 0.98 3.36 0.95 3.52 0.92 3.31 0.91 3.11 0.81 3.09 0.89 2.97 0.77 2.74 0.72 2.58 0.64 2.49 0.63 2.36 0.60 2.07 0.52 2.03 0.47 1.74 0.35 1.55 0.39 1.45 0.37 1.26			0.22 0.26 0.29 0.24 0.32 0.25 0.26 0.26 0.28 0.20 0.28 0.21 0.22 0.20 0.26 0.17 0.25 0.16 0.23 0.17 0.24 0.17 0.25 0.15 0.67 0.24 0.66 0.22 0.70 0.18 0.68 0.17 0.61 0.15 0.60 0.15 0.59 0.13 0.60 0.10 0.57 0.14 0.59 0.09 0.58 0.07 0.53 0.09 0.48 0.10 0.50 0.09 0.16 0.09 0.39 0.09		0.72 0.42 7.73 7.34 7.22 6.41 6.96 4.38 6.86 3.56 6.08 3.82 6.41 3.59 6.05 2.91 5.81 2.96 5.83 1.87 5.79 2.08 5.49 1.88 5.47 1.84 5.26 1.59 4.63 1.62 5.04 1.45 4.41 1.44 4.54 1.42 3.80 1.20 4.27 1.31 3.99 1.18 3.98 0.85		5.49 5.90 5.32 5.54 4.99 5.47 4.95 4.99 5.02 4.61 4.69 4.15 4.07 3.57 4.05 3.02 3.86 2.93 3.63 2.50 3.46 2.33 3.04 2.15 2.74 1.90 2.75 1.66 2.72 1.38 2.48 1.39 2.35 1.30 2.33 1.46 2.10 1.25 2.32 1.11 2.15 1.12 1.97 0.94 2.03 0.87 1.78 0.66
distal	1.91 2.19	4.27 3.27	0.25 1.02	0.27 0.20	0.06 0.08	0.39 0.06	3.55 0.37		1.45 0.59		

APPENDIX C

Adjusted PyFormex script

(CHAPTER 6)


```

#!/usr/bin/pyformex --gui
##
## Created by Tomas Praet for the seahorse project
## Intended pyFormex version 0.9.1
## Extended version of the script: 20151230
##

"""Script seahorse

.. Description

Seahorse kinematic modelling
-----

This script allows you to create an Abaqus input file that simulates the
kinematics of the seahorse tail under different conditions.

At the very least you need to start from a .pgf file that contains 1 full
seahorse tail skeleton segment (consisting of 5 separate skeletal elements).

The 5 skeletal elements are:

- A central vertebra (ve)
- A left-ventral dermal plate (lv)
- A right-ventral dermal plate (rv)
- A left-dorsal dermal plate (ld)
- A right-dorsal dermal plate (rd)

Starting from these surface models, a simple model with the same kinematic
properties will be created (i.e. point masses and inertias will be inherited
by the simple model).

Optional files:

- a pgf file containing the display bodies
- a pgf file containing the deformable bodies

The connections are, in this specific order:

1) Dorsal joint (ld-rd)
2) Ventral joint (lv-rv)
3) Left lateral joint (lv-ld)
4) Right lateral joint (rv-rd)
5) Longitudinal lv joint (lv-lv+1)
6) Longitudinal rv joint (rv-rv+1)
7) Longitudinal ld joint (ld-ld+1)
8) Longitudinal rd joint (rd-rd+1)
9) Longitudinal ve joint (ve-ve+1)
10) Left lateral socket joint (ve-ld)
11) Right lateral socket joint (ve-rd)
12) Median ventral muscle (ve-ve+1)
13) Left hypaxial myomere muscle (lv+dist-ve)
14) Right hypaxial myomere muscle (rv+dist-ve)
15) Left epaxial myomere muscle (ld+dist-ve)
16) Right epaxial myomere muscle (rd+dist-ve)
17) Temporary ventral joint (ve-lv)

"""

from gui.draw import *
from plugins.trisurface import *
from mesh import *
from plugins.formex_menu import *
import script
import odict
import connectivity

```

```

from plugins.fe abq import *
import arraytools
import timer
#from definitions import *      # My personal definitions
from gui.colorscale import *

# Standard Parameter Values
*****

# Expansion 1
veInclExpansion = False      #
Model expansions of year 2016
thetaExp1 = 10.

# Expansion 2
veScalingExpansion = False
elementScaling = 0.1
elementScalingLower = 0.2    # Central offset
elementScalingUpper = 0.8    # Distal offset

# Expansion 3
heightRatio = False
exp3a1 = -0.0357
exp3a0 = 1.464
referenceSegmentNumber = 3

# Expansion 5
plateShapeExpansion = True
plateDeformation = 1.
plateDefOffset = 0.5

#-----
n = 8
movement = -1.
distal = 2
dispBody = True
fixProx = True
damping = False
deform = False
deformList = [3, 4]
skewing = True
pre = True
numberOfFrames = 20

#-----
myDir = '/home/tomas/pyformex/myscripts/Seahorse'      # Main
dirteactory of the seahorse project
fn = myDir + '/input/referenceSegment.pgf'             # Reference
segment, containing surface of ve, rv, lv, rd, ld
fndispbody = myDir + '/input/displayBodies.pgf'       # Display
versions of the reference segment (used only in visualisation)
fndeformable = myDir + '/input/deformableSegment.pgf' # Volume
version of the reference segment, used when one (or more) segments need to
deform
fncontraction = myDir + '/input/naturalContraction.csv' # File
containing the MVM contraction as percentage of initial length
fnnonlinearsliding = myDir + '/input/nonLinearSliding.csv' # Non-linear
elastic behavior of the sliding joints
fnpassive = myDir + '/input/passiveMuscleResponse.csv' # Non-linear
elastic behavior of passive (dorsal) muscles
neutralPosition = myDir + '/input/preContraction.csv' # Initial
contraction applied to bring the tail in the rest position
fnforcehmm = myDir + '/input/hmmPartofmaxforce.csv'    # Force
applied to the HMM muscles (as opposed to the displacement driven
simulations)

```



```

fnforcemvm = myDir + '/input/mvmPartofmaxforce.csv' # Force
applied to the HMM muscles (as opposed to the displacement driven
simulations)
#fnmyom = myDir + '/input/myomere.off' # Real
geometry of the myomere muscle, not used!

props = [0,3,1,4,2]
names = ['ve','lv','rv','ld','rd']
d = 8.437
cor = 0.94
cutOffDerm = 0.23 # Percentage of axial length of the dermal plate where the
sliding joint is
slidDist = 1./15.

#-----
input = True
fnexp = myDir + '/output'
inputName = 'modelName'
density = 1.800e-9 # Only needed for deformable bone segments
end = False
contrInput = True

#-----
slidLow, slidHigh, slidMed = 0.00001, 1., 1.
sockLow, sockHigh = 0.00001, 100.
vetraltempsock = 1.
dampSliding = [0.01,0.01,0.01,0.01,0.01,0.01]
dampSocket = [0.01,0.01,0.01,0.01,0.01,0.01]
passive = 0.03 #Elasticity of the passive muscles

#----- Muscles
naturalContr = True
mvm, hmm, emm = True, True, True
mvmAct, hmmLeft, hmmRight, emmAct = False, True, True, False
myomLeftContr = -1.
myomRightContr = -1.
hmma, hmmb, hmhc = 38.77, -7.027, -0.0008876 # Passive stiffness parameters
per mm2 in exp(a*x+b)+c
emma, emmb, emmc = 32.70, -8.833, -0.0001459
hmmrelarea = 0.1699
emmrelarea = 0.0923
forcesMVM = False # TEMP
mvmFromFile = True
forcesHMM = False # TEMP
hmmFromFile = True

#-----
stepTime = 0.5
stepIncrement = 1.e-5

#-----
viewDisp = False
viewSimp = False
viewSimpleExp = False
viewDispExp = False

#Direction of the sliding joints
up = arraytools.normalize(asarray([-0.62634951,0.,0.42389572])-asarray([-
0.63005251,0.,-0.15473217]))
down = arraytools.normalize(asarray([-0.93915737,0.,-0.05773956])-asarray([-
0.99404377,0.,-0.55462927]))
left = arraytools.normalize(asarray([-0.69299185,-0.13044357,0.])-asarray([-
0.74889135,-0.56058884,0.]))
right = arraytools.normalize(asarray([-0.89820284,-0.05185318,0.])-asarray([-
0.93810195,-0.4103508,0.]))

```

```

# Connection declaration: connections contains the point numbers that make up
the connection, while partListCoefficients contains the part numbers
partListCoefficients = asarray([[3, 4], [1, 2], [1, 3], [2, 4], [1, 1], [2,
2], [3, 3], [4, 4], [0, 0], [0, 3], [0, 4], [0, 0], [0, 1], [0,2], [0, 3],
[0, 4], [0, 1]])
connections = asarray([[3,3],[3,3],[2,2],[2,2],[4,5], [4,5], [4,5],
[4,5],[3,2],[4,6],[5, 6], [7,6],[12, 6],[11, 6],[10, 7],[9, 7],[6,3]])
axisList = asarray(['Dorsal', 'Ventral', 'LateralLeft', 'LateralRight',
'VentralLeft', 'VentralRight', 'DorsalLeft', 'DorsalRight', 'SocketVe',
'Socket2', 'Socket2','Muscle', 'HypaxialLeft', 'HypaxialRight',
'EpaxialLeft', 'EpaxialRight', 'Xaxis'])
partListCoefficients = partListCoefficients.ravel() # These don't need to be
ranked

#Other
Deg = pi/180.

# Definitions
*****
def localDensity(l, L = 61.902):
    """Mass density of the tail. l is the distance from the tail tip, L the
total length of the tail."""
    return (0.101 * l / L + 1.009)/1e9

def localStrain(l, L = 61.902):
    """Local strain of normal myomere muscles at a distance l from the tail
base. L the total length of the tail."""
    return (7.554 * l / L + 1.197) / 100.

def localFraction(l, L = 61.902):
    """Local bone volume fraction"""
    return 0.115 * l / L + 0.10105

def poly(x, c0, c1, c2=0, c3=0, c4=0, c5=0, c6=0):
    """Returns the result of a polynomial in x, currently limited to 6
degrees"""
    return c0+c1*x+c2*x**2+c3*x**3+c4*x**4+c5*x**5+c6*x**6

def rotateInPlace(self,angle=[0.,0.,0.], inert=False, centre=None):
    """Rotate a part around its centre"""
    if centre != None:
        if isinstance(centre, int):
            centre = self.coords[centre]
        elif inert:
            centre = TriSurface(self).inertia()[0]
        else:
            centre = average(self.bbox(), axis=0)
    Deg = pi/180.
    return
self.copy().rot(angle[0]/Deg,0,around=centre).rot(angle[1]/Deg,1,around=centr
e).rot(angle[2]/Deg,2,around=centre)

def readCsv(self, sep=',', heather=0):
    """Read csv data list from a file. Heather determines the number of lines
to skip."""
    fil = file(self, 'r')
    data = asarray([map(float,line.strip('\n').strip(' ').split(sep)) for
line in fil.readlines()[heather:]])
    fil.close()
    return data

def scaleAtDist(distance=0):
    """What is the scaling factor for a segment at distance from first
segment?
The scaling for segment 3 is 0"""
    return (distance-8.437)/(-13.5185)+5.30595

```

```

def scaleAtDistance(x=0,x0=8.4369061558):
    """Scaling factor for respectively the length, height and width in
    function of the distance.
    This is the non-linear version! (Polynomial of degree 2 and 3)"""
    a = poly(x,2.85104644,-0.016058217,0.000405324,-0.0000104337)
    a0 = poly(x0,2.85104644,-0.016058217,0.000405324,-0.0000104337)
    b = poly(x,5.233357882,-0.030061115,-0.000524151,0.)
    b0 = poly(x0,5.233357882,-0.030061115,-0.000524151,0.)
    return [a/a0,b/b0,b/b0]

def skewAtDistance(x=0,x0=8.4369061558):
    """Skewing of the segments at distance x"""
    sk = poly(x,-0.65822345,1.580320511,-0.047910219,0.000533391)
    sk0 = poly(x0,-0.65822345,1.580320511,-0.047910219,0.000533391)
    return sk-sk0

def neutralAngleAtDistance(d=0.):
    """Measured angle at a certain tail distance"""
    return poly(d, 88.7245361, -0.01925855)

def expansion3Ratio(n = 1, a1 = 0.75, a0 = 0.391):
    """Returns the vertebral height over length ratio at segment n"""
    return poly(float(n),a0,a1)

def middlePoint(self,pos,tol,dr=False):
    """Find the rotation point of the vertebra"""
    box = self.bbox()
    if pos:
        F = self.clip(self.centroids()[:,0]-box[1,0]+tol)
    else:
        F = self.clip(box[0,0]+tol-self.centroids()[:,0])
    edg = where(F.nEdgeConnected() <= 1)[0]
    edge = connectivity.connectedLineElems(F.edges[edg])
    inner = argsort([i.shape[0] for i in edge])[-2]
    innerEdge = edge[inner]
    X = F.coords[unique(innerEdge)]
    if dr:
        for i in edge:
            draw(F.coords[i],color=green,linewidth=3)
            draw(X,color=magenta,marksize=10)
    return Coords(average(X,axis=0))

def hemalAngle(self,inAngle=-20.,Xcor=0.1,Xperc=0.20,Yperc=0.30,dr=False):
    """Determine the angle over which the hemal process is rotated, starting
    from an initial angle"""
    F = self.copy().rot(inAngle,2)
    F = F.trl(-F.inertia()[0])
    box = F.bbox()
    temp = F.toFormex().clip(Xperc*(box[1,0]-box[0,0])-
    abs(F.centroids()[:,0]+Xcor))
    hemal = temp.clip((box[0,1]+Yperc*(box[1,1]-box[0,1]))-
    temp.centroids()[:,1])
    Chemal,Themal=inertia.inertia(hemal.coords)
    Iprin,Iaxes = inertia.principal(Themal,sort=True,right_handed=True)
    if dr:
        #draw(temp,color=green,linewidth=2.0)
        draw(hemal,color=red,linewidth=3.0)
        siz = hemal.dsize()
        H = unitAxes().scale(1.1*siz).affine(Iaxes.transpose(),Chemal)
        A = 0.1*siz * Iaxes.transpose()
        G = Formex([[Chemal,Chemal+Ax] for Ax in A],3)
        draw([G,H])
        draw(hemal)
    Zangle = arctan(Iaxes[1][2]/Iaxes[0][2])*180./pi
    Zangle = sign(Zangle)*(90.-abs(Zangle))

```

```

    angle = inAngle+Zangle
    message('The hemal angle is %s degrees' % angle)
    return angle

def skew(self, angle, box):
    """Skew the segment to account for changing element shape and position
    throughout the tail"""
    centr = 0.5*(box[0,1]+box[1,1])
    Deg = pi/180.
    for i in self.coords:
        i[0] += tan(angle*Deg)*(i[1]-centr)

def mess(self, time):
    """Returns a message that includes the time that has gone by after
    self"""
    message("Timer : %s seconds after %s" %(time.seconds(), self))
    return

def doVertebralScaling(self, height, scalingFactor, b0, b1, h1, h2):
    """Expansion 1 definition"""
    for i in self.coords:
        if i[1]>0:
            scale = scalingFactor / b1
            if i[1]>b1*h1 and i[1]<b1*h2:
                i[1] = (i[1]-b1*h1) * (1.+scale) + b1*h1
            elif i[1]>b1*h2:
                i[1] = b1*h1 + (b1*h2-b1*h1) * (1.+scale) + i[1] - b1*h2

        else:
            scale = scalingFactor * (-1.) / b0
            if i[1]<b0*h1 and i[1]>b0*h2:
                i[1] = (i[1]-b0*h1) * (1.-scale) + b0*h1
            elif i[1]<b0*h2:
                i[1] = b0*h1 + (b0*h2-b0*h1) * (1.-scale) + i[1] - b0*h2
    return self

def plateTriangulation(self, a, offset):
    """Expansion 5 definition"""
    b = self.bbox()
    h = b[1,2]-b[0,2]
    m = [0., b[1,1], b[1,2]]
    for i in self.coords:
        d = distance([0., i[1], i[2]], m)
        if d/h > offset:
            factor = 1.+ (d/h-0.5) * a
            i[0] *= factor
    return self

def readContraction(self, n=30, sep=','):
    """Reads the contraction list from a file"""
    return readCsv(self, sep=sep, header=1)[:n].ravel()[n:]

def readStiffness(self, sep=';'):
    """Reads the stiffness list from a file"""
    return readCsv(self, sep=sep)

def readPrecontract(self, sep=';', header=1):
    """Read the element position after precontraction"""
    d = {}
    fil = file(self, 'r')
    for line in fil.readlines()[header:]:
        data = line.strip('\n').strip(' ').split(sep)
        name = (data[0][:-9]).lower()
        d[name] = map(float, data[1:])
    #data = asarray([line.strip('\n').strip(' ').split(sep) for line in
    fil.readlines()[header:]])

```

```

    return d

def cut(self, dir=1, posside=True, tol=0.1, sel=False):
    """Returns a the part of self in a certain direction"""
    b = self.bbox()
    cent = self.centroids()
    if posside:
        treshold = b[1, dir] - tol * (b[1, dir] - b[0, dir])
        a = 1.
    else:
        treshold = b[0, dir] + tol * (b[1, dir] - b[0, dir])
        a = -1.
    if sel:
        return where(a * cent[:, dir] > a * treshold)
    else:
        return TriSurface(self.select(where(a * cent[:, dir] > a *
treshold)))

def getLandmark(self, dir=0, posside=True, neighbour=8, dr=False, target=1.,
tol=0.1, legend=False):
    """Find the position of a landmark"""
    F = cut(self, dir, posside, 1.5*tol)
    val = nan_to_num(F.curvature(neighbours=neighbour) [2])
    if dr:
        CS =
ColorScale('RAINBOW',val.min(),val.max(),0.5*(val.min()+val.max()),1.)
        cval = array(map(CS.color,ravel(val)))
        cval = cval.reshape(append(val.shape,cval.shape[-1]))
        col = cval[F.elems]
        draw(F, color=col)
    if legend:
        CL = ColorLegend(CS,100)
        CLA = decors.ColorLegend(CL,10,10,30,200,dec=2)
        pf.canvas.addDecoration(CLA)
    val[unique(F.elems[cut(F, dir, posside, tol, sel=True)])] += 5.
    return F.coords[argsort(abs(val-target-5.)) [0]]

def cutMiddle(self, dir=0, tol=0.1):
    """Returns the middle part of self"""
    b = self.bbox()
    cent = self.centroids()
    treshold = tol * (b[1, dir]-b[0, dir])
    return TriSurface(self.select(where(abs(cent[:, dir]-b.mean(0) [dir]) <
treshold)))

def distance(P, Q):
    """Returns the distance between P and Q.
    P can be a point (vector) or an array of points (list of vectors), in
    which case an array with all the distances is returned."""
    P, Q = asarray(P), asarray(Q)
    if len(P.shape)==1:
        return length(P - Q)
    else:
        return length(asarray([i-Q for i in P]))
#*****
*

# Writing Definitions
#*****

def
connector(fil,number,instance1,node1,instance2,node2,elset,behavior='Sliding'
,axis='Axis_Xaxis',constr='Cartesian, Cardan'):
    if behavior is None:
        fil.write("*Element, type=CONN3D2\n\
%s, %s.%s, %s.%s\n\

```

```

*Connector Section, elset=%s\n\
%s\n\"%s\", \n" % (number, instance1, node1, instance2, node2, elset, constr, axis))
    else:
        fil.write("**Element, type=CONN3D2\n\
%s, %s.%s, %s.%s\n\
*Connector Section, elset=%s, behavior=%s\n\
%s\n\"%s\", \n" %
(number, instance1, node1, instance2, node2, elset, behavior, constr, axis))

def orientation(fil, name, x1, y1, z1, x2, y2, z2):
    fil.write("**Orientation, name=\"%s\" \n%s, %s, %s, %s, %s\n , 0.\n" %
(name, x1, y1, z1, x2, y2, z2))

def wire(fil, number, instance1, node1, instance2=None, node2='', name='Wire-'):
    fil.write("**Nset, nset=%s%s, instance=%s\n%s, \n" %
(name, number, instance1, node1))
    if instance2 is not None:
        fil.write("**Nset, nset=%s%s, instance=%s\n%s, \n" %
(name, number, instance2, node2))
    fil.write("**Elset, elset=%s%s\n%s, \n" % (name, number, number))

def behavior(fil, name, components):
    fil.write("**Connector Behavior, name="+name+"\n")
    #fil.write("**Connector Behavior, name="+name+", extrapolation=LINEAR\n")
    fil.write("\
*Connector Elasticity, component=1\n %s, \n\
*Connector Elasticity, component=2\n %s, \n\
*Connector Elasticity, component=3\n %s, \n\
*Connector Elasticity, component=4\n %s, \n\
*Connector Elasticity, component=5\n %s, \n\
*Connector Elasticity, component=6\n %s, \n" % tuple(components))

def complexBehavior(fil, name, components, usedComponents = [1, 2, 3, 4, 5,
6], extraPolation = False, nonLinearComponent = 0, nonLinearList = []):
    if extraPolation:
        name += ', extrapolation=LINEAR'
    fil.write("**Connector Behavior, name="+name+"\n")
    for comp in usedComponents:
        if comp == nonLinearComponent:
            try:
                lin = asarray(nonLinearList).reshape(-1, 2)
            except:
                message('The list of nonlinear stiffness values is
incorrect.')
        fil.write("**Connector Elasticity, nonlinear, component=%s\n" %
comp)
        for i in lin[::-1]:
            fil.write("%s, %s\n" % (-i[0], -i[1]))
            fil.write("0., 0.\n" )
            fil.write("0.00001, 0.9\n" )
        else:
            fil.write("**Connector Elasticity, component=%s\n %s, \n" % (comp,
components[comp-1]))

def passiveBehavior(fil, name, area, parameters, length=1., component = 0,
prestretch=0.05, extraPolation = False, max=0.50, step=0.01):
    """Write the passive response of a muscle with area, length, and
parameters [a,b,c] to file fil"""
    if extraPolation:
        name += ', extrapolation=LINEAR'
    fil.write("**Connector Behavior, name="+name+"\n")
    fil.write("**Connector Elasticity, nonlinear, component=%s\n" %
(component+1))
    a, b, c = parameters[0], parameters[1], parameters[2]
    fil.write("-0.00001, -%s\n" % (0.9*length))
    fil.write("%s, %s\n" % (0., 0.))

```

```

        zero = exp(a*prestretch+b)+c          #Recalculate the curve with the
prestretching
        for i in arange(step, max, step):
            fil.write("%s, %s\n" % ((exp(a*(i+prestretch)+b)+c-zero)/area,
i*length))

def damp(fil, components):
    fil.write("\
*Connector Damping, component=1\n %s, \n\
*Connector Damping, component=2\n %s, \n\
*Connector Damping, component=3\n %s, \n\
*Connector Damping, component=4\n %s, \n\
*Connector Damping, component=5\n %s, \n\
*Connector Damping, component=6\n %s, \n" % tuple(components))

#*****
*

# Menu interaction definitions
*****

def changeFn():
    changeDirectory('fn', fn, filter='pgf')

def changeFnDispBody():
    changeDirectory('fndispbody', fndispbody, filter='pgf')

def changeFnDeformable():
    changeDirectory('fndeformable', fndeformable, filter='pgf')

def changeFnContraction():
    changeDirectory('fncontraction', fncontraction, filter='csv')

def changeFnPreContraction():
    changeDirectory('fnprecontraction', fnprecontraction, filter='csv')

def changeFnNonLinearSliding():
    changeDirectory('fnnonlinearsliding', fnnonlinearsliding, filter='csv')

def changeFnPassive():
    changeDirectory('fnpassive', fnpassive, filter='csv')

def changeForcemvm():
    changeDirectory('fnforcemvm', fnforcemvm, filter='csv')

def changeForcehmm():
    changeDirectory('fnforcehmm', fnforcehmm, filter='csv')

def changeFnExp():
    changeDirectory('fnexp', fnexp, dir=True)

def changeNeutralPosition():
    changeDirectory('neutralPosition', neutralPosition, filter='csv')

def changeDirectory(self, old, filter='*', dir=False):
    if filter != '*':
        filter = '*' + filter
    fn = widgets.FileSelection(old, filter, dir=dir).getFilename()
    if fn:
        res.updateData({self:fn})

#*****
*

def run():
    global n, fnexp, deformList, viewSimp, res, precontraction

```

```

# Parameters dialog
*****
res = widgets.InputDialog(
    caption='Seahorse project',
    items=[
        _T('Expansion', [
            _I('veInclExpansion',veInclExpansion,text='Vertebral
inclination expansion (1)'),
            _G('Expansion 1', [
                _I('thetaExp1',thetaExp1,text='Angle of the vertebra of
the first expansion'),
            ]),
            _I('veScalingExpansion',veScalingExpansion,text='Vertebral
centre scaling expansion (2)'),
            _G('Expansion 2', [
                _I('elementScaling',elementScaling,text='Total relative
shift of the center (negative is dorsal)'),
                _I('elementScalingLower',elementScalingLower,text='Proximal offset'),
                _I('elementScalingUpper',elementScalingUpper,text='Distal
offset'),
            ]),
            _I('heightRatio',heightRatio,text='Vertebral height/length
ratio expansion (3)'),
            _G('Expansion 3', [
                _I('exp3a1',exp3a1,text='a1'),
                _I('exp3a0',exp3a0,text='a0'),
            ]),
            _I('plateShapeExpansion',plateShapeExpansion,text='Plate
triangular shape expansion (5)'),
            _G('Expansion 5', [
                _I('plateDeformation',plateDeformation,text='Amount of
deformation'),
                _I('plateDefOffset',plateDefOffset,text='Offset for the
deformation area'),
            ]),
        ]),
        _T('Simulation', [
            _G('General', [
                _I('input',input,text='Create input file'),
                _I('inputName',inputName,text='Input filename'),
                _I('n',n,text='Number of segments'),
            ]),
            _G('Simulation features', [
                _I('skewing',skewing,text='Skew the segments'),
                _I('end',end,text='Add a fixed tail tip segment'),
                _I('fixProx',fixProx,text='Fix the first vertebra'),
                _I('dispBody',dispBody,text='Display body'),
                _I('stepTime',stepTime,text='Total time'),
                _I('stepIncrement',stepIncrement,text='Time increment'),
                _I('numberOfFrames',numberOfFrames,text='Number of output
frames'),
                _I('pre',pre,text='Include precontraction'),
            ]),
            _G('Deformable bodies', [
                _I('deform',deform,text='Include deformable bodies'),
                _I('deformList',deformList,text='List of deformable
segments'),
            ]),
            _G('Extra', [
                _I('tempV',True,text='Temporary ventral joint'),
            ]),
        ]),
        _T('Muscles', [
            _I('mvm',mvm,text='Median Ventral Muscles'),
            _G('Median Ventral Muscles', [

```



```

        _I('mvmAct', mvmAct, text='Active MVM contraction'),
        _I('forcesMVM', forcesMVM, text='Use forces for the
MVM'),
        _I('mvmFromFile', mvmFromFile, text='Get the forces from
a file'),
        _I('movement', movement, text='MVM contraction'),
        _I('contrInput', contrInput, text='Use file for
contractions'),
    ]),
    _I('distal', distal, text='Myomere muscle segment span'),
    _I('hmm', hmm, text='Hypaxial Myomere Muscles'),
    _G('Hypaxial Myomere Muscles', [
        _I('naturalContr', naturalContr, text='Use natural
myomere contraction'),
        _I('forcesHMM', forcesHMM, text='Use forces for the
HMM'),
        _I('mvmFromFile', mvmFromFile, text='Get the forces from
a file'),
        _I('hmmLeft', hmmLeft, text='Active Left HMM
contraction'),
        _I('hmmRight', hmmRight, text='Active Right HMM
contraction'),
        _I('myomLeftContr', myomLeftContr, text='Left HMM
contraction'),
        _I('myomRightContr', myomRightContr, text='Right HMM
contraction'),
        _I('hmmrelarea', hmmrelarea, text='Relative area of the
hmm muscle'),
        _I('hmma', hmma, text='Parameter a in passive response'),
        _I('hmmb', hmmb, text='Parameter b in passive response'),
        _I('hmmc', hmhc, text='Parameter c in passive response'),
    ]),
    _I('emm', emm, text='Epaxial Myomere Muscles'),
    _G('Epaxial Myomere Muscles', [
        _I('emmAct', emmAct, text='Active EMM contraction'),
        _I('emmrelarea', emmrelarea, text='Relative area of the
emm muscle'),
        _I('emma', emma, text='Parameter a in passive response'),
        _I('emmb', emmb, text='Parameter b in passive response'),
        _I('emmc', emmc, text='Parameter c in passive response'),
    ]),
    ]),
    _T('Elasticity', [
        _G('Elasticity values', [
            _I('slidLow', slidLow, text='Sliding elasticity main
direction'),
            _I('slidHigh', slidHigh, text='Sliding elasticity other
directions'),
            _I('sockLow', sockLow, text='Socket rotational
elasticity'),
            _I('sockHigh', sockHigh, text='Socket translational
elasticity'),
            _I('passive', passive, text='Elasticity of passive
muscles'),
        ]),
    ]),
    _T('Script', [
        _G('Internal script options', [
            _I('d', d, text='Initial distance between segments'),
            _I('cor', cor, text='Percentage of size in X direction'),
            _I('cutOffDerm', cutOffDerm, text='Percentage of sliding
joint'),
            _I('names', names, 'Names of the segments'),
            _I('props', props, text='Segment properties'),
        ]),
    ]),
    ]),

```

```

        _T('Files',[
            _G('General file options',[
                _I('fn',fn,text='Segments file',
buttons=[('Edit',changeFn)]),
                _I('fn dispbody',fn dispbody,text='Display body file',
buttons=[('Edit',changeFnDispBody)]),
                _I('fnexp',fnexp,text='Abaqus input file directory',
buttons=[('Edit',changeFnExp)]),
                _I('fn deformable',fn deformable, text='Deformable body
file', buttons=[('Edit',changeFnDeformable)]),
                _I('fn contraction',fn contraction, text='Contraction list
file', buttons=[('Edit',changeFnContraction)]),
                _I('fn nonlinear sliding',fn nonlinear sliding,
text='Nonlinear sliding file', buttons=[('Edit',changeFnNonLinearSliding)]),
                _I('fn passive',fn passive, text='Passive muscle
elasticity file', buttons=[('Edit',changeFnPassive)]),
                _I('neutralPosition',neutralPosition, text='Neutral
position and rotation', buttons=[('Edit',changeNeutralPosition)]),
                _I('fn forcemvm',fn forcemvm, text='File for ventral
forces', buttons=[('Edit',changeForcemvm)]),
                _I('fn forcehmm',fn forcehmm, text='File for myomere
forces', buttons=[('Edit',changeForcehmm)]),
            ]),
        ]),
        _T('View',[
            _G('Mesh exporting options',[
elements'),
                _I('viewSimp',viewSimp,text='Export the simple skeletal
elements'),
                _I('viewDisp',viewDisp,text='Export the display skeletal
segments'),
                _I('viewSimpleExp',viewSimpleExp,text='Export the simple
segments'),
                _I('viewDispExp',viewDispExp,text='Export the display
segments'),
            ]),
        ]),
        _T('Old', [
            _G('Some old feature that are rarely changed', [
                _I('damping',damping,text='Connector damping'),
            ]),
        ]),
    ],
    enablers=[
        ('input', True, 'inputName'),
        ('deform', True, 'deformList'),
        ('mvm', True, 'Median Ventral Muscles'),
        ('hmm', True, 'Hypaxial Myomere Muscles'),
        ('emm', True, 'Epaxial Myomere Muscles'),
        ('hmmLeft', True, 'myomLeftContr'),
        ('hmmRight', True, 'myomRightContr'),
    ],
    actions=[
        ('Cancel',close),
        ('Accept',accept),
    ])

    res.show()

def close():
    res.close()

def accept():
    global n, res, viewSimp, deformList, mvmAct, hmmLeft, hmmRight

    res.acceptData()
    globals().update(res.results)

```

```

res.close()

elastSliding =
asarray([slidLow,slidMed,slidMed,slidHigh,slidHigh,slidHigh])
#elastSocketVe =
asarray([10.*sockHigh,sockHigh,sockHigh,sockLow,sockLow,sockLow])
elastSocketVe =
asarray([10.*sockHigh,sockHigh,sockHigh,10000.*sockLow,10000.*sockLow,10000.*
sockLow]) # TEMP FIX
elastSocket2 =
asarray([sockHigh,sockHigh,sockHigh,sockLow,sockLow,sockLow])

if hmm:
    viewSimp = True
if end:
    n -= 1
if not deform:
    deformList = []
exportfile = fnexp+'/'+inputName+'.inp'
position = empty(n)

if forcesMVM:
    mvmAct = False
if forcesHMM:
    hmmLeft, hmmRight = False, False

#*****
*

# Main
*****

clear()

tim = timer.Timer()
P = odict.Odict({})
pntCol = [0.2,0.,0.2]

#Load the parts of the segment
mess('script start', tim)
pf.GUI.drawable.readFromFile(fn)
namesTemp = pf.GUI.drawable.names
message('File contains these geometries : %s' % namesTemp)

if deform:
    pf.GUI.drawable.readFromFile(fn deformable)
    namesTemp = pf.GUI.drawable.names
    message('Volume file contains these geometries : %s' % namesTemp)
    ext = namesTemp[0][2:]
#String that was added to the deformable parts

ve,lv,rv,ld,rd =
named('ve'),named('lv'),named('rv'),named('ld'),named('rd')
ve.prop = props[0]*ones(ve.nelems(),dtype=int)
lv.prop = props[1]*ones(lv.nelems(),dtype=int)
rv.prop = props[2]*ones(rv.nelems(),dtype=int)
ld.prop = props[3]*ones(ld.nelems(),dtype=int)
rd.prop = props[4]*ones(rd.nelems(),dtype=int)

if deform:
    veDef,lvDef,rvDef,ldDef,rdDef =
named('ve'+ext),named('lv'+ext),named('rv'+ext),named('ld'+ext),named('rd'+ex
t)

# Start of Expansion 5

```

```

if plateShapeExpansion:
    ldDef = plateTriangulation(ldDef,plateDeformation,plateDefOffset)
    rdDef = plateTriangulation(rdDef,plateDeformation,plateDefOffset)
    lvDef = plateTriangulation(lvDef,plateDeformation,plateDefOffset)
    rvDef = plateTriangulation(rvDef,plateDeformation,plateDefOffset)
# End of expansion 5
quad = veDef.elems.shape[1] == 10
if quad:
    message('The deformable bodies have quadratic elements')
else:
    message('The deformable bodies have linear elements')
veDef.prop = props[0]*ones(veDef.nelems(),dtype=int)
lvDef.prop = props[1]*ones(lvDef.nelems(),dtype=int)
rvDef.prop = props[2]*ones(rvDef.nelems(),dtype=int)
ldDef.prop = props[3]*ones(ldDef.nelems(),dtype=int)
rdDef.prop = props[4]*ones(rdDef.nelems(),dtype=int)

mess('loading the parts', tim)

#draw([ve,lv,rv,ld,rd])
#draw([veDef,lvDef,rvDef,ldDef,rdDef])

#Calculate the connection points

#*****
#VE//////////
#*****
if veScalingExpansion:
    bb = ve.bbox()
    bb0, bb1 = bb[0,1], bb[1,1]
    templ = bb1
    veHeight = bb1-bb0
    scaleTot = elementScaling / (elementScalingUpper-elementScalingLower)
* veHeight
    ve =
doVertebralScaling(ve,veHeight,scaleTot,bb0,bb1,elementScalingLower,elementScalingUpper)
    c = ve.coords
    P['veM'] = TriSurface(ve).inertia()[0]
    veProx = middlePoint(TriSurface(ve),pos=False,tol=0.3,dr=False)
    veCaud = middlePoint(TriSurface(ve),pos=True,tol=0.2,dr=False)
    dx = (ve.bbox()[1,0]-ve.bbox()[0,0])*cor
    X0 = average([veProx,veCaud-[dx,0.,0.],axis=0)
    P['veProx'],P['veCaud'] = Coords(X0),Coords(X0+[dx,0.,0.])
    P['veLatL'] = getLandmark(ve, dir=2, posside=True)
    P['veLatR'] = getLandmark(ve, dir=2, posside=False)
    P['veNeurSp'] = getLandmark(ve, dir=1, posside=True)
    # Ventral muscle attachment points on the hemal process
    angle = hemalAngle(TriSurface(ve),inAngle=-
20.,Xcor=0.1,Xperc=0.20,Yperc=0.30,dr=False)
    spine = ve.copy().rot(angle,2)
    tol = 0.05
    H = spine.toFormex().clip(tol/2-abs(spine.centroids()[0,2]))
    I = H.clip(tol-abs(H.centroids()[0,1]-
(spine.bbox()[0,1]+0.10*(spine.bbox()[1,1]-spine.bbox()[0,1]))))
    #draw(I,color=green,linewidth=2.0)
    #draw(H,color=red,linewidth=1.0)
    Icoor = I.coords.reshape(-1,3)
    YY = argsort(Icoor[:,0])
    Y1,Y2 = Icoor[YY[0]],Icoor[YY[-1]]
    Y1,Y2 = argsort([distance(Y1,i) for i in
spine.coords])[0],argsort([distance(Y2,i) for i in spine.coords])[0]
    P['veMedProx'],P['veMedCaud'] = c[Y1],c[Y2]
    diag1 = TriSurface(ve).cutWithPlane(P['veM']-[tol/5., tol/5., tol/5.],
[0., 1., 1.], '+').cutWithPlane(P['veM']+[tol/5., tol/5., tol/5.], [0., 1.,
1.], '-')

```

```

diag2 = TriSurface(ve).cutWithPlane(P['veM']-[tol/5., -tol/5., tol/5.],
[0., -1., 1.], '+').cutWithPlane(P['veM']+[tol/5., -tol/5., tol/5.], [0., -
1., 1.], '-')
b1, b2 = diag1.bbox(), diag2.bbox()
#draw(diag1+diag2, color=blue)
P['veEmmL'] = Coords([P['veM'][0], max(b1[1, 1], b2[1, 1]), min([-b1[1,
2], b2[0, 2]])])
P['veEmmR'] = Coords([P['veM'][0], max(b1[1, 1], b2[1, 1]), max([b1[1,
2], b2[0, 2]])])
P['veHmmL'] = Coords([P['veM'][0], min(b1[0, 1], b2[0, 1]), min([b1[0,
2], -b2[1, 2]])])
P['veHmmR'] = Coords([P['veM'][0], min(b1[0, 1], b2[0, 1]), max([-b1[0,
2], b2[1, 2]])])

draw([P['veM'],P['veProx'],P['veCaud'],P['veLatL'],P['veLatR'],P['veMedProx']
,P['veMedCaud'],P['veNeurSp'], P['veEmmL'], P['veEmmR'], P['veHmmL'],
P['veHmmR']],color=pntCol,marksize=10)
draw(ve)
mess('ve connections and drawing', tim)

#####
#LD//////////
#####
if veScalingExpansion:
    ld =
doVertebralScaling(ld,veHeight,scaleTot,bb0,bb1,elementScalingLower,elementSc
alingUpper)
    # Start of Expansion 5
if plateShapeExpansion:
    ld = plateTriangulation(ld,plateDeformation,plateDefOffset)
# End of expansion 5
c = ld.coords
b = ld.bbox()
a = (b[1,0]-b[0,0])*slidDist
P['ldM'] = TriSurface(ld).inertia()[0]
P['ldMed'] = getLandmark(ld, dir=2, posside=False)
P['ldLat'] = getLandmark(ld, dir=1, posside=False)
cutX = b[1,0] - cutOffDerm * (b[1,0]-b[0,0])
H = ld.copy().toFormex().clip(tol/2-abs(ld.centroids()[:,0]-
cutX)).toMesh()
#draw(H,color=green,bbox='last')
cc = H.coords
P['ldCaud'] = cc[argsort(cc[:,1]+cc[:,2])[-1]]
I = ld.copy().toFormex().clip(0.05/2-abs(ld.centroids()[:,0]-cutX-
a)).toMesh()
J = ld.copy().toFormex().clip(0.05/2-abs(ld.centroids()[:,0]-
cutX+a)).toMesh()
ccl,cc2 = I.coords,J.coords
p1,p2 = ccl[argsort(ccl[:,1]+ccl[:,2])[-
1]],cc2[argsort(cc2[:,1]+cc2[:,2])[-1]]
vld = arraytools.normalize(p1-p2)
cutX = cutX-dx
sc = 5.30595/scaleAtDist(d-dx)
draw(P['ldCaud'].translate(0,-
dx).scale(1/sc),color=magenta,marksize=10,bbox='last')
H = ld.copy().toFormex().clip(tol/2-abs(ld.centroids()[:,0]-
cutX)).toMesh()
#draw(H,color=green,bbox='last')
cc = H.coords
P['ldProx'] = cc[argsort((cc[:,1]*sc-P['ldCaud'][1])**2+(cc[:,2]*sc-
P['ldCaud'][2])**2)[0]]
normal = arraytools.normalize(cross(P['ldLat']-P['ldProx'],P['ldCaud']-
P['ldProx']))
point = P['veLatL']
try:

```

```

        t =
Formex.intersectionWithPlane(Formex([[point,point+normal]]),P['ldCaud'],normal
1)[0]
    except:
        t = Formex.intersectionWithPlane(Formex([[point-
normal,point+normal]]),P['ldCaud'],normal)[0]
        P['ldSocket'] = Coords(asarray(t).reshape(3))
        b = ld.bbox()
        a = b[0, 0] + 0.08 *(b[1, 0]-b[0, 0])
        tola = 0.02
        cut = TriSurface(ld).cutWithPlane([a+tola, 0., 0.], [1., 0., 0.], '-
').cutWithPlane([a-tola, 0., 0.], [1., 0., 0.], '+')
        bcut = cut.bbox()
        cut2 = cut.cutWithPlane(average(bcut, axis=0), [0., -1., 1.], '-')
        #draw(cut2, color=blue)
        P['ldEmm'] = cut2.coords[argsort(cut2.coords[:, 1])[0]]

draw([P['ldM'],P['ldLat'],P['ldMed'],P['ldCaud'],P['ldProx'],P['ldSocket'],
P['ldEmm']],color=pntCol,marksiz=10)
    draw(ld)
    mess('ld connections and drawing', tim)

    #*****
    #RD//////////
    #*****
    if veScalingExpansion:
        rd =
doVertebralScaling(rd,veHeight,scaleTot,bb0,bb1,elementScalingLower,elementSc
alingUpper)
        # Start of Expansion 5
        if plateShapeExpansion:
            rd = plateTriangulation(rd,plateDeformation,plateDefOffset)
        # End of expansion 5
        c = rd.coords
        b = rd.bbox()
        a = (b[1,0]-b[0,0])*slidDist
        P['rdM'] = TriSurface(rd).inertia()[0]
        P['rdMed'] = getLandmark(rd, dir=2, posside=True)
        P['rdLat'] = getLandmark(rd, dir=1, posside=False)
        cutX = b[1,0] - cutOffDerm * (b[1,0]-b[0,0])
        H = rd.copy().toFormex().clip(tol/2-abs(rd.centroids()[:,0]-
cutX)).toMesh()
        #draw(H,color=green,bbox='last')
        cc = H.coords
        P['rdCaud'] = cc[argsort(cc[:,1]-cc[:,2])[-1]]
        I = rd.copy().toFormex().clip(0.05/2-abs(rd.centroids()[:,0]-cutX-
a)).toMesh()
        J = rd.copy().toFormex().clip(0.05/2-abs(rd.centroids()[:,0]-
cutX+a)).toMesh()
        cc1,cc2 = I.coords,J.coords
        p1,p2 = cc1[argsort(cc1[:,1]-cc1[:,2])[-1]],cc2[argsort(cc2[:,1]-
cc2[:,2])[-1]]
        vrd = arraytools.normalize(p1-p2)
        cutX = cutX-dx
        sc = 5.30595/scaleAtDist(d-dx)
        H = rd.copy().toFormex().clip(tol/2-abs(rd.centroids()[:,0]-
cutX)).toMesh()
        #draw(H,color=green,bbox='last')
        cc = H.coords
        draw(P['rdCaud'].translate(0,-
dx).scale(1/sc),color=magenta,marksiz=10,bbox='last')
        P['rdProx'] = cc[argsort((cc[:,1]*sc-P['rdCaud'][1])**2+(cc[:,2]*sc-
P['rdCaud'][2])**2)[0]]
        normal = arraytools.normalize(cross(P['rdCaud']-P['rdProx'],P['rdLat']-
P['rdProx']))
        point = P['veLatR']

```

```

try:
    t =
Formex.intersectionWithPlane(Formex([[point,point+normal]]),P['rdCaud'],normal)
l)[0]
except:
    t = Formex.intersectionWithPlane(Formex([[point-
normal,point+normal]]),P['rdCaud'],normal)[0]
    P['rdSocket'] = Coords(asarray(t).reshape(3))
    b = rd.bbox()
    a = b[0, 0] + 0.08 *(b[1, 0]-b[0, 0])
    tola = 0.02
    cut = TriSurface(rd).cutWithPlane([a+tol, 0., 0.], [1., 0., 0.], '-')
    cutWithPlane([a-tola, 0., 0.], [1., 0., 0.], '+')
    bcut = cut.bbox()
    cut2 = cut.cutWithPlane(average(bcut, axis=0), [0., -1., -1.], '-')
    #draw(cut2, color=blue)
    draw(rd)
    P['rdEmm'] = cut2.coords[argsort(cut2.coords[:, 1])[0]]

draw([P['rdM'],P['rdLat'],P['rdMed'],P['rdCaud'],P['rdProx'],P['rdSocket'],
P['rdEmm']],color=pntCol,marksize=10)
draw(rd)
mess('rd connections and drawing', tim)

#####
#LV//////////
#####
if veScalingExpansion:
    lv =
doVertebralScaling(lv,veHeight,scaleTot,bb0,bb1,elementScalingLower,elementSc
alingUpper)
# Start of Expansion 5
if plateShapeExpansion:
    lv = plateTriangulation(lv,plateDeformation,plateDefOffset)
# End of expansion 5
c = lv.coords
b = lv.bbox()
a = (b[1,0]-b[0,0])*slidDist
P['lvM'] = TriSurface(lv).inertia()[0]
P['lvMed'] = getLandmark(lv, dir=2, posside=False)
P['lvLat'] = getLandmark(lv, dir=1, posside=True)
cutX = b[1,0] - cutOffDerm * (b[1,0]-b[0,0])
H = lv.copy().toFormex().clip(tol/2-abs(lv.centroids()[:,0]-
cutX)).toMesh()
#draw(H,color=green,bbox='last')
cc = H.coords
P['lvCaud'] = cc[argsort(-cc[:,1]+cc[:,2])[-1]]
I = lv.copy().toFormex().clip(tol/2-abs(lv.centroids()[:,0]-cutX-
a)).toMesh()
J = lv.copy().toFormex().clip(tol/2-abs(lv.centroids()[:,0]-
cutX+a)).toMesh()
cc1,cc2 = I.coords,J.coords
p1,p2 = cc1[argsort(-cc1[:,1]+cc1[:,2])[-1]],cc2[argsort(-
cc2[:,1]+cc2[:,2])[-1]]
vlv = arraytools.normalize(p1-p2)
cutX = cutX-dx
sc = 5.30595/scaleAtDist(d-dx)
H = lv.copy().toFormex().clip(tol/2-abs(lv.centroids()[:,0]-
cutX)).toMesh()
#draw(H,color=green,bbox='last')
cc = H.coords
draw(P['lvCaud'].translate(0,-
dx).scale(1/sc),color=magenta,marksize=10,bbox='last')
P['lvProx'] = cc[argsort((cc[:,1]*sc-P['lvCaud'][1])**2+(cc[:,2]*sc-
P['lvCaud'][2])**2)[0]]
b = lv.bbox()

```

```

a = b[0, 0] + 0.08 * (b[1, 0] - b[0, 0])
tola = 0.02
cut = TriSurface(lv).cutWithPlane([a+tola, 0., 0.], [1., 0., 0.], '-')
).cutWithPlane([a-tola, 0., 0.], [1., 0., 0.], '+')
bcut = cut.bbox()
cut2 = cut.cutWithPlane(average(bcut, axis=0), [0., 1., 1.], '-')
#draw(cut2, color=blue)
P['lvHmm'] = cut2.coords[argsort(cut2.coords[:, 1])[-1]]
draw([P['lvM'], P['lvLat'], P['lvMed'], P['lvCaud'], P['lvProx']],
P['lvHmm']], color=pntCol, marksize=10)
draw(lv)
mess('lv connections and drawing', tim)

#*****
#RV//////////
#*****
if veScalingExpansion:
    rv =
doVertebralScaling(rv, veHeight, scaleTot, bb0, bb1, elementScalingLower, elementSc
alingUpper)
# Start of Expansion 5
if plateShapeExpansion:
    rv = plateTriangulation(rv, plateDeformation, plateDefOffset)
# End of expansion 5
c = rv.coords
b = rv.bbox()
a = (b[1,0]-b[0,0])*slidDist
P['rvM'] = TriSurface(rv).inertia()[0]
P['rvMed'] = getLandmark(rv, dir=2, posside=True)
P['rvLat'] = getLandmark(rv, dir=1, posside=True)
cutX = b[1,0] - cutOffDerm * (b[1,0]-b[0,0])
H = rv.copy().toFormex().clip(tol/2-abs(rv.centroids()[:,0]-
cutX)).toMesh()
#draw(H, color=green, bbox='last')
cc = H.coords
P['rvCaud'] = cc[argsort(cc[:,1]+cc[:,2])[0]]
I = rv.copy().toFormex().clip(0.05/2-abs(rv.centroids()[:,0]-cutX-
a)).toMesh()
J = rv.copy().toFormex().clip(0.05/2-abs(rv.centroids()[:,0]-
cutX+a)).toMesh()
cc1, cc2 = I.coords, J.coords
p1, p2 =
cc1[argsort(cc1[:,1]+cc1[:,2])[0]], cc2[argsort(cc2[:,1]+cc2[:,2])[0]]
vrv = arraytools.normalize(p1-p2)
cutX = cutX-dx
sc = 5.30595/scaleAtDist(d-dx)*1.01
H = rv.copy().toFormex().clip(tol/2-abs(rv.centroids()[:,0]-
cutX)).toMesh()
#draw(H, color=green, bbox='last')
cc = H.coords
draw(P['rvCaud'].translate(0,-
dx).scale(1/sc), color=magenta, marksize=10, bbox='last')
P['rvProx'] = cc[argsort((cc[:,1]*sc-P['rvCaud'][1])**2+(cc[:,2]*sc-
P['rvCaud'][2])**2)[0]]
b = rv.bbox()
a = b[0, 0] + 0.08 * (b[1, 0] - b[0, 0])
tola = 0.02
cut = TriSurface(rv).cutWithPlane([a+tola, 0., 0.], [1., 0., 0.], '-')
).cutWithPlane([a-tola, 0., 0.], [1., 0., 0.], '+')
bcut = cut.bbox()
cut2 = cut.cutWithPlane(average(bcut, axis=0), [0., 1., -1.], '-')
#draw(cut2, color=blue)
P['rvHmm'] = cut2.coords[argsort(cut2.coords[:, 1])[-1]]
draw([P['rvM'], P['rvLat'], P['rvMed'], P['rvCaud'], P['rvProx']],
P['rvHmm']], color=pntCol, marksize=10)
draw(rv)

```



```

mess('rv connections and drawing', tim)

#Create the simple models
veSimple =
Mesh([P['veM'],P['veProx'],P['veCaud'],P['veLatL'],P['veLatR'],P['veMedProx']]
,P['veMedCaud'],P['veNeurSp'], P['veEmmL'], P['veEmmR'], P['veHmmL'],
P['veHmmR']],

[[0,1,5],[0,5,6],[0,6,2],[0,2,7],[0,7,1],[0,1,3],[0,3,2],[0,2,4],[0,4,1], [0,
9, 3], [0, 7, 9], [0, 4, 8], [0, 8, 7], [0, 3, 11], [5, 0, 11], [0, 10, 4],
[0, 5, 10]],ve.prop[0])
lvSimple = Mesh([P['lvM'],P['lvLat'],P['lvMed'],P['lvCaud'],P['lvProx']],
P['lvHmm']], [[0,1,4],[0,4,2],[0,2,3],[0,3,1], [0, 4, 5]],lv.prop[0])
rvSimple = Mesh([P['rvM'],P['rvLat'],P['rvMed'],P['rvCaud'],P['rvProx']],
P['rvHmm']], [[0,2,4],[0,4,1],[0,1,3],[0,3,2], [0, 4, 5]],rv.prop[0])
ldSimple =
Mesh(Coords([P['ldM'],P['ldLat'],P['ldMed'],P['ldCaud'],P['ldProx'],P['ldSock
et'], P['ldEmm']]),[[0,3,2],[0,2,4],[0,4,5],[5,4,1],[0,5,3],[5,1,3], [0, 4,
6]],ld.prop[0])
rdSimple =
Mesh([P['rdM'],P['rdLat'],P['rdMed'],P['rdCaud'],P['rdProx'],P['rdSocket']],
P['rdEmm']], [[0,2,3],[0,5,4],[0,3,5],[3,1,5],[1,4,5],[0,4,2], [0, 4,
6]],rd.prop[0])

export({'veSimple':veSimple,'lvSimple':lvSimple,'rvSimple':rvSimple,'ldSimple
':ldSimple,'rdSimple':rdSimple})
mess('Simple model creation and export', tim)
clear()

#Calculate the corresponding points on the deformable bodies
if deform:
vePoints = findClosest(veDef, [P['veProx']-[0., 0.4, 0.],P['veCaud']-
[0., 0.4,
0.],P['veLatL'],P['veLatR'],P['veMedProx'],P['veMedCaud'],P['veNeurSp'],
P['veEmmL'], P['veEmmR'], P['veHmmL'], P['veHmmR']])
lvPoints = findClosest(lvDef,
[P['lvLat'],P['lvMed'],P['lvCaud'],P['lvProx'], P['lvHmm']])
rvPoints = findClosest(rvDef,
[P['rvLat'],P['rvMed'],P['rvCaud'],P['rvProx'], P['rvHmm']])
ldPoints = findClosest(ldDef,
[P['ldLat'],P['ldMed'],P['ldCaud'],P['ldProx'],P['ldSocket'], P['ldEmm']])
rdPoints = findClosest(rdDef,
[P['rdLat'],P['rdMed'],P['rdCaud'],P['rdProx'],P['rdSocket'], P['rdEmm']])
export({'vePoints':vePoints, 'lvPoints':lvPoints,
'rvPoints':rvPoints, 'ldPoints':ldPoints, 'rdPoints':rdPoints})
mess('deformable connection points', tim)

#draw(veDef.coords[vePoints], color=red, marksize=7)
#draw([veDef, lvDef, rvDef, ldDef, rdDef])
#draw(lvDef.coords[lvPoints], color=red, marksize=7)
#draw(rvDef.coords[rvPoints], color=red, marksize=7)
#draw(ldDef.coords[ldPoints], color=red, marksize=7)
#draw(rdDef.coords[rdPoints], color=red, marksize=7)
#draw([Mesh(veSimple.coords,veSimple.getEdges(),veSimple.prop[0]),
# Mesh(rvSimple.coords,rvSimple.getEdges(),rvSimple.prop[0]),
# Mesh(lvSimple.coords,lvSimple.getEdges(),lvSimple.prop[0]),
# Mesh(rdSimple.coords,rdSimple.getEdges(),rdSimple.prop[0]),
#
Mesh(ldSimple.coords,ldSimple.getEdges(),ldSimple.prop[0])],linewidth=3,flat=
True)

#Calculate the consecutive segments
clear()

```

```

if input:
    fil = file(exportfile,'w')
    fil.write(fmtHeading('** On %s, from script %s by Tomas Praet' %
(datetime.now(), pf.scriptName)))
    fil.write("*** Number of segments = %s\n" % n)
    fil.write("***\n** PARTS \n**\n")
    axesLeft, axesRight = [], []
    axesVe = empty((n, 2, 3))
    axesLV, axesRV, axesLD, axesRD = empty((n, 2, 3)), empty((n, 2,
3)), empty((n, 2, 3)), empty((n, 2, 3))
    axesEpaxialLeft, axesEpaxialRight = empty((n, 2, 3)), empty((n, 2,
3))
    axesHypaxialLeft, axesHypaxialRight = empty((n, 2, 3)), empty((n,
2, 3))
    contractionMvm = empty((n, 2, 3))
    contractionHmmLeft = empty((n, 2, 3))
    contractionHmmRight = empty((n, 2, 3))
    contractionEmmLeft = empty((n, 2, 3))
    contractionEmmRight = empty((n, 2, 3))
    precontraction = []

if dispBody:
    pf.GUI.drawable.readFromFile(fndispbody)
    namesTemp = pf.GUI.drawable.names
    message('File contains these geometries : %s' % namesTemp)
    selection.set(namesTemp)
    offset = ve.bbox()[0, 0]
    ve,lv,rv,ld,rd = named('ve').trl([offset, 0.,
0.]),named('lv').trl([offset, 0., 0.]),named('rv').trl([offset, 0.,
0.]),named('ld').trl([offset, 0., 0.]),named('rd').trl([offset, 0., 0.])
    ve.prop = props[0]*ones(ve.nelems(),dtype=int)
    lv.prop = props[1]*ones(lv.nelems(),dtype=int)
    rv.prop = props[2]*ones(rv.nelems(),dtype=int)
    ld.prop = props[3]*ones(ld.nelems(),dtype=int)
    rd.prop = props[4]*ones(rd.nelems(),dtype=int)
    # START OF EXPANSION NUMBER 1
    if veInclExpansion:
        veProx =
middlePoint(TriSurface(ve),pos=False,tol=0.3,dr=False)
        veCaud =
middlePoint(TriSurface(ve),pos=True,tol=0.2,dr=False)
        yCutOff = 0.5*(veProx[1]+veCaud[1])
        xCutOff = 0.5*(veProx[0]+veCaud[0])
        m = ve.bbox()[1,0]
        for i in ve.coords:
            i[0] += tand(thetaExp1)*(i[1]-yCutOff)*(i[0]-xCutOff)/m
    # END OF EXPANSION NUMBER 1
    # Start of Expansion 5
    if plateShapeExpansion:
        ld = plateTriangulation(ld,plateDeformation,plateDefOffset)
        rd = plateTriangulation(rd,plateDeformation,plateDefOffset)
        lv = plateTriangulation(lv,plateDeformation,plateDefOffset)
        rv = plateTriangulation(rv,plateDeformation,plateDefOffset)
    # End of expansion 5
    mess('display body loading', tim)

if pre:
    precontract = readPrecontract(neutralPosition) # Library containing
the translations and rotations after precontraction; currently only 30
segments!

x = 0
a, aa = 1, 1
for i in range(n):
    if (i+1) in deformList:

```

```

        ve2Def =
Mesh(veDef.coords.copy().scale(scaleAtDistance(x)).trl(0,x), veDef.elems,
veDef.prop)
        lv2Def =
Mesh(lvDef.coords.copy().scale(scaleAtDistance(x)).trl(0,x), lvDef.elems,
lvDef.prop)
        rv2Def =
Mesh(rvDef.coords.copy().scale(scaleAtDistance(x)).trl(0,x), rvDef.elems,
rvDef.prop)
        ld2Def =
Mesh(ldDef.coords.copy().scale(scaleAtDistance(x)).trl(0,x), ldDef.elems,
ldDef.prop)
        rd2Def =
Mesh(rdDef.coords.copy().scale(scaleAtDistance(x)).trl(0,x), rdDef.elems,
rdDef.prop)
        mess('deform coordinate scaling', tim)
        if skewing:
            angle = skewAtDistance(x)
            if angle<0:
                angle = 0.
            b = bbox([lv2Def,ld2Def,rv2Def,rd2Def,ve2Def])
            skew(ve2Def,angle,b)
            skew(lv2Def,angle,b)
            skew(rv2Def,angle,b)
            skew(ld2Def,angle,b)
            skew(rd2Def,angle,b)
        mess('deform coordinate skewing', tim)
        draw([ve2Def,lv2Def,rv2Def,ld2Def,rd2Def])
        mess('deform drawing', tim)
        message('The height of segment number %s is: %s' %(i+1,b[1,1]-
b[0,1]))
        b = ve2Def.bbox()
        dx = b[1,0]-b[0,0]
        message('The length of segment number %s is: %s' %(i+1,dx))
        if skewing:
            x += (dx*cor)-
0.25*tan(skewAtDistance(x)*Deg)*(tmp.bbox()[1,1]-tmp.bbox()[0,1])
        else:
            x += (dx*cor)
        if viewDisp:
            export({'veDef':ve2Def, 'lvDef':lv2Def, 'rvDef':rv2Def,
'ldDef':ld2Def, 'rdDef':rd2Def})
        if input:
            for nam,part in
zip(names,[ve2Def,lv2Def,rv2Def,ld2Def,rd2Def]):
                c = part.nelems()
                name = nam+'Def'+str(i+1)
                coor = part.coords
                fil.write("*Part, name="+name+"\n")
                writeNodes(fil,coor)
                if quad:
                    writeElems(fil,part.elems[:, [0, 1, 2, 3, 4, 7, 5, 6,
9, 8]],'C3D10M') # The quadratic elements are number differently in Abaqus!
                else:
                    writeElems(fil,part.elems, 'C3D4')
                fil.write("*Nset, nset=NALL, generate\n 1, %s, 1\n" %
len(coor))
                for massPoint in named(nam+'Points'):
                    fil.write("*Nset, nset=massPoint%s, internal\n %s,\n"
%(a, massPoint+1))
                    a += 1
                fil.write("*** Section: BoneSection"+nam+"\n*Solid
Section, elset=EALL, material=acellularBone\n,\n")
                for massPoint in named(nam+'Points'):
                    c += 1

```

```

        fil.write("*Element, type=MASS,
elset=massPoint%s_InertiaPoint\n %s, %s\n*Mass,
elset=massPoint%s_InertiaPoint\n 1e-12,\n" % (aa, c, massPoint+1, aa))
        c += 1
        fil.write("*Element, type=ROTARYI,
elset=massPoint%s_InertiaPoint_ROT\n %s,%s\n" % (aa, c, massPoint+1))
        fil.write("*Rotary Inertia,
elset=massPoint%s_InertiaPoint_ROT\n1e-12, 1e-12, 1e-12, 0., 0., 0.\n" %
(aa))

        aa += 1
        fil.write("*End Part\n**\n")
        message('Part %s written' % name)
        if nam[0] == 'l':
            axesLeft = append(axesLeft, [named(nam+'Points')[0]])
        elif nam[0] == 'r':
            axesRight =
append(axesRight, [named(nam+'Points')[0]])
            contractionMvm[i] = asarray([ve2Def.coords[vePoints[3]],
ve2Def.coords[vePoints[4]])]
            contractionHmLeft[i] = asarray([ve2Def.coords[vePoints[10]],
lv2Def.coords[lvPoints[4]])]
            contractionHmRight[i] = asarray([ve2Def.coords[vePoints[9]],
rv2Def.coords[rvPoints[4]])]
            contractionEmLeft[i] = asarray([ve2Def.coords[vePoints[8]],
ld2Def.coords[ldPoints[5]])]
            contractionEmRight[i] = asarray([ve2Def.coords[vePoints[7]],
rd2Def.coords[rdPoints[5]])]
            mess('deform input writing', tim)
        else:
            ve2 = ve.copy().scale(scaleAtDistance(x)).trl(0,x)

            # Start of Expansion number 3
            if heightRatio:
                referenceRatio = expansion3Ratio(referenceSegmentNumber,
exp3a1, exp3a0)
                newRatio = expansion3Ratio(i+1, exp3a1, exp3a0)
                ve2 = ve2.scale([1., newRatio/referenceRatio, 1.])
            # End of expansion number 3

            lv2 = lv.copy().scale(scaleAtDistance(x)).trl(0,x)
            rv2 = rv.copy().scale(scaleAtDistance(x)).trl(0,x)
            ld2 = ld.copy().scale(scaleAtDistance(x)).trl(0,x)
            rd2 = rd.copy().scale(scaleAtDistance(x)).trl(0,x)
            ve2Simple = veSimple.copy().scale(scaleAtDistance(x)).trl(0,x)

            # Start of Expansion number 3
            if heightRatio:
                newRatio = expansion3Ratio(i+1, exp3a1, exp3a0)
                ve2Simple = ve2Simple.scale([1., newRatio/referenceRatio,
1.])
            # End of expansion number 3

            lv2Simple = lvSimple.copy().scale(scaleAtDistance(x)).trl(0,x)
            rv2Simple = rvSimple.copy().scale(scaleAtDistance(x)).trl(0,x)
            ld2Simple = ldSimple.copy().scale(scaleAtDistance(x)).trl(0,x)
            rd2Simple = rdSimple.copy().scale(scaleAtDistance(x)).trl(0,x)
            position[i] = ve2Simple.coords[0][0] + abs(veSimple.bbox()[0, 0])
# The model does not start at x = 0, so need to shift the position
            #draw([ve2,lv2,rv2,ld2,rd2])
            if skewing:
                tmp =
(ve2Simple.toFormex()+rv2Simple.toFormex()+lv2Simple.toFormex()+rd2Simple.toF
ormex()+ld2Simple.toFormex()).toMesh()
                angle = skewAtDistance(x)
                if angle<0:
                    angle = 0.

```

```

        skew(ve2Simple,angle,tmp.bbox())
        skew(lv2Simple,angle,tmp.bbox())
        skew(rv2Simple,angle,tmp.bbox())
        skew(ld2Simple,angle,tmp.bbox())
        skew(rd2Simple,angle,tmp.bbox())
        tmp2 =
(ve2.toFormex()+rv2.toFormex()+lv2.toFormex()+rd2.toFormex()+ld2.toFormex()).
toMesh()

        skew(ve2,angle,tmp2.bbox())
        skew(lv2,angle,tmp2.bbox())
        skew(rv2,angle,tmp2.bbox())
        skew(ld2,angle,tmp2.bbox())
        skew(rd2,angle,tmp2.bbox())
    mess('simple coordinate scaling and skewing', tim)
    b = ve2.bbox() # Needs to be in front of the rotation!!!
    if pre:
        if viewDispExp or viewDisp or dispBody:
            ve2 = rotateInPlace(ve2.trl(ve2Simple.center() -
ve2.center()), precontract['vesimple'+str(i+1)][3:],
centre=ve2Simple.coords[0]).trl(precontract['vesimple'+str(i+1)][3:])
            lv2 = rotateInPlace(lv2.trl(lv2Simple.center() -
lv2.center()), precontract['lvsimple'+str(i+1)][3:],
centre=lv2Simple.coords[0]).trl(precontract['lvsimple'+str(i+1)][3:])
            rv2 = rotateInPlace(rv2.trl(rv2Simple.center() -
rv2.center()), precontract['rvsimple'+str(i+1)][3:],
centre=rv2Simple.coords[0]).trl(precontract['rvsimple'+str(i+1)][3:])
            ld2 = rotateInPlace(ld2.trl(ld2Simple.center() -
ld2.center()), precontract['ldsime'+str(i+1)][3:],
centre=ld2Simple.coords[0]).trl(precontract['ldsime'+str(i+1)][3:])
            rd2 = rotateInPlace(rd2.trl(rd2Simple.center() -
rd2.center()), precontract['rdsimple'+str(i+1)][3:],
centre=rd2Simple.coords[0]).trl(precontract['rdsimple'+str(i+1)][3:])
            ve2Simple = rotateInPlace(ve2Simple,
precontract['vesimple'+str(i+1)][3:],
centre=0).trl(precontract['vesimple'+str(i+1)][3:])
            lv2Simple = rotateInPlace(lv2Simple,
precontract['lvsimple'+str(i+1)][3:],
centre=0).trl(precontract['lvsimple'+str(i+1)][3:])
            rv2Simple = rotateInPlace(rv2Simple,
precontract['rvsimple'+str(i+1)][3:],
centre=0).trl(precontract['rvsimple'+str(i+1)][3:])
            ld2Simple = rotateInPlace(ld2Simple,
precontract['ldsime'+str(i+1)][3:],
centre=0).trl(precontract['ldsime'+str(i+1)][3:])
            rd2Simple = rotateInPlace(rd2Simple,
precontract['rdsimple'+str(i+1)][3:],
centre=0).trl(precontract['rdsimple'+str(i+1)][3:])
            draw([ve2Simple,lv2Simple,rv2Simple,ld2Simple,rd2Simple])
            mess('simple drawing', tim)
            if viewDisp:

export({'ld'+str(i+1)+'Disp':ld2,'lv'+str(i+1)+'Disp':lv2,'rd'+str(i+1)+'Disp
':rd2,
        'rv'+str(i+1)+'Disp':rv2,'ve'+str(i+1)+'Disp':ve2})
        if viewSimp:

export({'ldSimple'+str(i+1):ld2Simple,'lvSimple'+str(i+1):lv2Simple,'rdSimple
'+str(i+1):rd2Simple,
        'rvSimple'+str(i+1):rv2Simple,'veSimple'+str(i+1):ve2Simple})
        if viewSimpleExp:

export({'SegmentSimple'+str(i+1):(ve2Simple.toFormex()+rv2Simple.toFormex()
+lv2Simple.toFormex()+rd2Simple.toFormex()+ld2Simple.toFormex()).toMesh()})
        if viewDispExp:

```

```

export({'SegmentDisplay'+str(i+1):(ve2.toFormex()+rv2.toFormex()
+lv2.toFormex()+rd2.toFormex()+ld2.toFormex()).toMesh())
    height = bbox([lv2,ld2,rv2,rd2,ve2])
    message('The height of segment number %s is: %s'
%(i+1,height[1,1]-height[0,1]))
    dx = b[1,0]-b[0,0]
    message('The length of segment number %s is: %s' %(i+1,dx))
    if skewing:
        x += (dx*cor)-
0.25*tan(skewAtDistance(x)*Deg)*(tmp.bbox()[1,1]-tmp.bbox()[0,1])
    else:
        x += (dx*cor)
    #Calculate the neutral contraction for this segment
    hem1, hem2 = ve2Simple.coords[5], ve2Simple.coords[6]
    spineThickness = abs(hem1[0]-hem2[0])
    message('Spinethickness: %s' % spineThickness)
    neutralAngle = neutralAngleAtDistance(x)
    message('NeutralAngle: %s' % neutralAngle)
    l1 = dx-spineThickness # Muscle length before precontraction
    hemalH = ve2Simple.coords[1][1] - 0.5*(hem1[1]+hem2[1])
    l2 = dx * (1. - 2. * hemalH / (dx * tand(neutralAngle))) -
spineThickness
    neutralContr = l1 - l2
    message('NeutralContraction: %s' % neutralContr)
    precontraction.append(neutralContr)

# Write parts
if input:
    for nam,part,Part in
zip(names,[ve2Simple,lv2Simple,rv2Simple,ld2Simple,rd2Simple],[ve2,lv2,rv2,ld
2,rd2]):
        name = nam+'Simple'+str(i+1)
        #Part = TriSurface(named(nam))
        Part = TriSurface(Part)
        inertTotal = Part.inertia()
        centr = inertTotal[0]
        inert =
inertTotal[3]*localDensity(centr[0])/localFraction(centr[0])
        ncoor,nelem,coor =
part.ncoords(),part.nelems(),part.coords
        fil.write("*Part, name="+name+"\n")
        writeNodes(fil,coor)
        fil.write("%d, %14.6e, %14.6e, %14.6e\n" %
(ncoor+1,coor[0,0],coor[0,1],coor[0,2]))
        writeElems(fil,part.elems,'R3D3')
        fil.write("*Nset, nset=NALL, generate\n 1, %s, 1\n" %
ncoor)
        fil.write("*Nset, nset=%s-RefPt\n %s,\n" %
(name,ncoor+1))
        fil.write("*Element, type=MASS,
elset=%s_Inertia_MASS\n%d, %d\n" % (name,nelem+1,ncoor+1))
        fil.write("*Mass, elset=%s_Inertia_MASS\n%s,\n" %
(name,localDensity(centr[0])*Part.volume()/localFraction(centr[0])))
        fil.write("*Element, type=ROTARYI,
elset=%s_Inertia_ROTI\n%d, %d\n" % (name,nelem+2,ncoor+1))
        fil.write("*ROTARYI, elset=%s_Inertia_ROTI\n%s, %s, %s,
0., 0., 0.\n" % (name,inert[0],inert[1],inert[2]))
        fil.write("*End Part\n**\n")
        message('Part %s written' % name)
        if dispBody:
            name = nam+'Display'+str(i+1)
            ncoor,nelem,coor =
part.ncoords(),part.nelems(),part.coords
            fil.write("*Part, name="+name+"\n")
            writeNodes(fil,Part.coords)

```

```

        writeElems(fil,Part.elems,'S3')
        fil.write("**End Part\n**\n")
        message('Part %s written' % name)
    if nam[0] == 'l':
        axesLeft = append(axesLeft,[coor[0]])
    elif nam[0] == 'r':
        axesRight = append(axesRight,[coor[0]])
    if nam[:2] == 'lv':
        axesHypaxialLeft[i] =
[named('veSimple'+str(i+1)).coords[11], coor[5]]
        axesLV[i] = [coor[4], coor[3]]
    elif nam[:2] == 'ld':
        axesEpaxialLeft[i] =
[named('veSimple'+str(i+1)).coords[9], coor[6]]
        axesLD[i] = [coor[4], coor[3]]
    elif nam[:2] == 'rv':
        axesHypaxialRight[i] =
[named('veSimple'+str(i+1)).coords[10], coor[5]]
        axesRV[i] = [coor[4], coor[3]]
    elif nam[:2] == 'rd':
        axesEpaxialRight[i] =
[named('veSimple'+str(i+1)).coords[8], coor[6]]
        axesRD[i] = [coor[4], coor[3]]
    elif nam[:2] == 've':
        axesVe[i] = [coor[1], coor[2]]
        contractionMvm[i] = asarray([ve2Simple.coords[5],
ve2Simple.coords[6]])
        contractionHmmLeft[i] = asarray([ve2Simple.coords[11],
lv2Simple.coords[5]])
        contractionHmmRight[i] = asarray([ve2Simple.coords[10],
rv2Simple.coords[5]])
        contractionEmmLeft[i] = asarray([ve2Simple.coords[9],
ld2Simple.coords[6]])
        contractionEmmRight[i] = asarray([ve2Simple.coords[8],
rd2Simple.coords[6]])
        mess('simple exporting', tim)

    if end:
        l,d1 = 1.5*dx,0.4
        coor =
Coords([veSimple.coords[1],lvSimple.coords[4],rvSimple.coords[4],ldSimple.coo
rds[4],
rdSimple.coords[4],veSimple.coords[1]+[1,0.,0.],0.5*(lvSimple.coords[4]+ldSim
ple.coords[4])+[1*d1,0.,0.],
0.5*(rvSimple.coords[4]+rdSimple.coords[4])+[1*d1,0.,0.],0.5*(rdSimple.coords
[4]+ldSimple.coords[4])+[1*d1,0.,0.],
0.5*(rvSimple.coords[4]+lvSimple.coords[4])+[1*d1,0.,0.])).scale(scaleAtDista
nce(x)).trl(0,x)
        elems =
[[0,5,6],[0,5,7],[0,5,8],[0,5,9],[3,5,6],[1,5,6],[1,5,9],[2,5,9],[2,7,5],[5,7
,4],[4,8,5],[3,5,8]]
        tip = Mesh(coor,elems)
        if skewing:
            skew(tip,skewAtDistance(x),tip.bbox())
        #draw(coor,color=green,marksize=8)
        draw(tip)
        #drawNumbers(tip.coords)

    if not input:
        return

    if end:
        Part = TriSurface(ve2)

```

```

inertTotal = Part.inertia()
ncoor,nelem,coor = tip.ncoords(),tip.nelems(),tip.coords
centr = inertTotal[0]
inert = inertTotal[3]*localDensity(centr[0])/localFraction(centr[0])
fil.write("**Part, name=tip\n")
writeNodes(fil,tip.coords)
fil.write("%d, %14.6e, %14.6e, %14.6e\n" %
(ncoor+1,coor[0,0],coor[0,1],coor[0,2]))
writeElems(fil,tip.elems,'R3D3')
fil.write("**Nset, nset=NALL, generate\n 1, %s, 1\n" % ncoor)
fil.write("**Nset, nset=tip-RefPt\n %s,\n" % (ncoor+1))
fil.write("**Element, type=MASS, elset=tip_Inertia_MASS\n%d, %d\n" %
(nelem+1,ncoor+1))
fil.write("**Mass, elset=tip_Inertia_MASS\n%s,\n" %
(5*localDensity(centr[0])*Part.volume()/localFraction(centr[0])))
fil.write("**Element, type=ROTARYI, elset=tip_Inertia_ROTI\n%d, %d\n"
% (nelem+2,ncoor+1))
fil.write("**ROTARYI, elset=tip_Inertia_ROTI\n%s, %s, %s, 0., 0.,
0.\n" % (5*inert[0],5*inert[1],5*inert[2]))
fil.write("**End Part\n**\n")
message('Part tip written')

mess('tip creating and exporting', tim)

if contrInput:
    try:
        tmp = readContraction(fncontraction, n-1)
    except:
        tmp = readContraction(fncontraction, n-1, sep=';') # In case
the seperation symbol is not ','
    if not pre:
        contractionMvm =[distance(contractionMvm[i][1],
contractionMvm[i+1][0])*movement*tmp[i] for i in range(n-1)]
    else:
        if naturalContr:
            #contractionMvm =[distance(contractionMvm[i][1],
contractionMvm[i+1][0])*movement*localStrain(position[i])*2. for i in
range(n-1)] # For compliance with natural hmm contraction!
            contractionMvm =[distance(contractionMvm[i][1],
contractionMvm[i+1][0])*movement*localStrain(position[i])*1.1 for i in
range(n-1)] # For compliance with natural hmm contraction!
        else:
            contractionMvm =[distance(contractionMvm[i][1],
contractionMvm[i+1][0])*movement*tmp[i] for i in range(n-1)]
        else:
            contractionMvm =[distance(contractionMvm[i][1],
contractionMvm[i+1][0])*movement for i in range(n-1)]
            lengthHmmLeft = [distance(contractionHmmLeft[i, 0],
contractionHmmLeft[i+distal, 1]) for i in range(n-distal)] # Length needed
for passive response
            lengthHmmRight = [distance(contractionHmmRight[i, 0],
contractionHmmRight[i+distal, 1]) for i in range(n-distal)]
            segmentsdirections = [arraytools.normalize(asarray([axesVe[i, 1] -
axesVe[i, 0]])) for i in range(n)] # Longitudinal axis of each segment
            muscledirectionsleft =
asarray([arraytools.normalize(contractionHmmLeft[i+distal, 1]-
contractionHmmLeft[i, 0]) for i in range(n-distal)]) # Longitudinal axis of
the muscles
            muscledirectionsright =
asarray([arraytools.normalize(contractionHmmRight[i+distal, 1]-
contractionHmmRight[i, 0]) for i in range(n-distal)])
            if hmmLeft:
                factor =
asarray([cos(vectorPairAngle(segmentsdirections[i+distal/2],muscledirectionsl
eft[i])) for i in range(n-distal))).ravel() # This factors in that the
strain is not in the direction of the muscle

```



```

        if naturalContr:
            #contractionHmmLeft = [distance(contractionHmmLeft[i, 0],
            contractionHmmLeft[i+distal,
            1])*localStrain(position[i+distal/2])*myomLeftContr/factor[i] for i in
            range(n-distal)]
            contractionHmmLeft = [distance(contractionHmmLeft[i, 0],
            contractionHmmLeft[i+distal,
            1])*localStrain(position[i+distal/2])*myomLeftContr for i in range(n-distal)]
        else:
            contractionHmmLeft = [distance(contractionHmmLeft[i, 0],
            contractionHmmLeft[i+distal, 1])*myomLeftContr/factor[i] for i in range(n-
            distal)]
        if hmmRight:
            factor =
            asarray([cos(vectorPairAngle(segmentsdirections[i+distal/2],muscleDirectionsR
            ight[i])) for i in range(n-distal)]).ravel()
            if naturalContr:
                #contractionHmmRight = [distance(contractionHmmRight[i, 0],
                contractionHmmRight[i+distal,
                1])*localStrain(position[i+distal/2])*myomRightContr/factor[i] for i in
                range(n-distal)]
                contractionHmmRight = [distance(contractionHmmRight[i, 0],
                contractionHmmRight[i+distal,
                1])*localStrain(position[i+distal/2])*myomRightContr for i in range(n-
                distal)]
            else:
                contractionHmmRight = [distance(contractionHmmRight[i, 0],
                contractionHmmRight[i+distal, 1])*myomRightContr/factor[i] for i in range(n-
                distal)]

        if hmm:
            hmmL =
            asarray([arraytools.normalize(named('veSimple'+str(i+1)).coords[connections[1
            2,0]-1]-named('lvSimple'+str(i+1+distal)).coords[connections[12,1]-1]) for i
            in range(n-distal)])
            hmmR =
            asarray([arraytools.normalize(named('veSimple'+str(i+1)).coords[connections[1
            3,0]-1]-named('rvSimple'+str(i+1+distal)).coords[connections[13,1]-1]) for i
            in range(n-distal)])
            if emm:
                emmL =
                asarray([arraytools.normalize(named('veSimple'+str(i+1)).coords[connections[1
                4,0]-1]-named('ldSimple'+str(i+1+distal)).coords[connections[14,1]-1]) for i
                in range(n-distal)])
                emmR =
                asarray([arraytools.normalize(named('veSimple'+str(i+1)).coords[connections[1
                5,0]-1]-named('rdSimple'+str(i+1+distal)).coords[connections[15,1]-1]) for i
                in range(n-distal)])
                lengthEmmLeft = [distance(contractionEmmLeft[i, 0],
                contractionEmmLeft[i+distal, 1]) for i in range(n-distal)]
                lengthEmmRight = [distance(contractionEmmRight[i, 0],
                contractionEmmRight[i+distal, 1]) for i in range(n-distal)]

        # Forces
        if forcesMVM:
            if mvmFromfile:
                forceMVM = -readCsv(fnforcemvm, heather=1).ravel()
            else:
                forceMVM = ones((n-1))*-0.04

        if forcesHMM:
            if hmmFromfile:
                forceHMM = -readCsv(fnforcehmm, sep=';',
            heather=1).ravel().reshape(-1, 2)
            else:
                forceHMM = ones((n-2, 2))*-0.04

```

```

    parts = asarray([[j+'Simple'+str(i) for j in names] for i in range(1,
n+1)])
    for i in deformList:
        parts[i-1] = [j+'Def'+str(i) for j in names]
    instances = asarray([ i + '_Instance' for i in parts.ravel()]).reshape(-
1, 5)
    if dispBody:
        displayParts = delete(asarray([[j+'Display'+str(i) for j in names]
for i in range(1, n+1)]), asarray(deformList) - 1, 0)
        connectList = resize(connections.ravel(), (n, 2*len(connections)))
        for i in deformList:
            j = connectList[i-1]-2          # -1 because Abaqus counts from 1,
and another -1 because the deformable bodies have no extra centre mass
            connectList[i-1] = asarray([ldPoints[j[0]], rdPoints[j[1]],
lvPoints[j[2]], rvPoints[j[3]], lvPoints[j[4]], ldPoints[j[5]],
rvPoints[j[6]], rdPoints[j[7]],
lvPoints[j[8]], lvPoints[j[9]], rvPoints[j[10]], rvPoints[j[11]],
ldPoints[j[12]], ldPoints[j[13]], rdPoints[j[14]], rdPoints[j[15]],
vePoints[j[16]], vePoints[j[17]], vePoints[j[18]],
ldPoints[j[19]], vePoints[j[20]], rdPoints[j[21]], vePoints[j[22]],
vePoints[j[23]],
lvPoints[j[24]], vePoints[j[25]], rvPoints[j[26]],
vePoints[j[27]], ldPoints[j[28]], vePoints[j[29]], rdPoints[j[30]],
vePoints[j[31]], vePoints[j[32]], lvPoints[j[33]]]) + 1
            partList = asarray([i[partListCoefficients] for i in parts])
            instanceList = asarray([i+'_Instance' for i in
partList.ravel()]).reshape(n, -1)

        axesLeft, axesRight = asarray(axesLeft).reshape(-1, 2, 3),
asarray(axesRight).reshape(-1, 2, 3)

    # Write Assembly
    fil.write("***\n** ASSEMBLY \n**\n")
    fil.write("**Assembly, name=Assembly\n**\n")
    for part, instance in zip(parts.ravel(), instances.ravel()):
        fil.write("**Instance, name=%s, part=%s \n" % (instance, part))
        fil.write("**End Instance\n")

    if dispBody:
        for part in displayParts.ravel():
            fil.write("**Instance, name=%s, part=%s \n" % (part+"_Instance",
part))
            fil.write("**End Instance\n")
    if end:
        fil.write("**Instance, name=tip_Instance, part=tip \n")
        fil.write("**End Instance\n")

    # Write Rigid Bodies
    a = 1
    for part in parts.ravel():
        if part[-4:-1] != 'Def':
            fil.write("*** Constraint: RigidBody-%s\n" % a)
            fil.write("**Rigid Body, ref node="+part+"_Instance."+part+"-
RefPt, elset="+part+"_Instance.Eall, tie nset="+part+"_Instance.Nall\n")
            a += 1
    if end:
        fil.write("*** Constraint: RigidBody-%s\n" % a)
        fil.write("**Rigid Body, ref node=tip_Instance.tip-RefPt,
elset=tip_Instance.Eall, tie nset=tip_Instance.Nall\n")
        a += 1

    if dispBody:
        for part in displayParts.ravel():

```



```

if i > n-distal or not hmm:
    check = False
else:
    inst2 = instanceList[i-1+distal, 2*t+1]
    node2 = connectList[i-1+distal, 2*t+1]
    constraint = 'Axial, '
    ax += str(i)
    if p[1][0] == '1':
        contractionListHmmLeft =
append(contractionListHmmLeft, [a])
        if hmmLeft:
            behav = None
            myomLeft += str(a)+', '
            if i%12==0:
                myomLeft += '\n'
        else:
            behav = 'PassiveHmm'+str(i)
    else:
        contractionListHmmRight =
append(contractionListHmmRight, [a])
        if hmmRight:
            behav = None
            myomRight += str(a)+', '
            if i%12==0:
                myomRight += '\n'
        else:
            behav = 'PassiveHmm'+str(i)
elif ax[:7] == 'Epaxial': #The epaxial myomere connection wire
    if not emm or i > n- distal:
        check=False
    else:
        inst2 = instanceList[i-1+distal, 2*t+1]
        node2 = connectList[i-1+distal, 2*t+1]
        constraint = 'Axial, '
        ax += str(i)
        if not emmAct:
            behav = 'PassiveEmm'+str(i)
        else:
            if p[1][0] == '1':
                behav = None
                epmyomleft += str(a)+', '
                if i%12==0:
                    epmyomleft += '\n'
                contractionListEmmLeft =
append(contractionListEmmLeft, [a])
            else:
                behav = None
                epmyomright += str(a)+', '
                if i%12==0:
                    epmyomright += '\n'
                contractionListEmmRight =
append(contractionListEmmRight, [a])
        else:
            inst2 = p[1]

    if check:
        ax = 'Axis_' + ax
        connector(fil, a, inst1, j[0], inst2, node2, 'Wire-'+str(a),
        constr=constraint, behavior=behav, axis=ax)
        a += 1

#Boundary limitations for the first segment
connector(fil,a,instanceList[0][4],5,instanceList[0][5],5,'Wire-
'+str(a),axis='Axis_Socket2')
a += 1

```

```

connector(fil,a,instanceList[0][6],5,instanceList[0][7], 5,'Wire-
'+str(a),axis='Axis_Socket2')
a += 1

#Boundary limitations for the final element
if end:
connector(fil,a,instanceList[-1][8],connectList[-
1][8],'tip_Instance',2,'Wire-'+str(a),axis='Axis_VentralLeft')
a += 1
connector(fil,a,instanceList[-1][10],connectList[-
1][10],'tip_Instance',3,'Wire-'+str(a),axis='Axis_VentralRight')
a += 1
connector(fil,a,instanceList[-1][12],connectList[-
1][12],'tip_Instance',4,'Wire-'+str(a),axis='Axis_DorsalLeft')
a += 1
connector(fil,a,instanceList[-1][14],connectList[-
1][14],'tip_Instance',5,'Wire-'+str(a),axis='Axis_DorsalRight')
a += 1
connector(fil,a,instanceList[-1][16],connectList[-
1][16],'tip_Instance',1,'Wire-
'+str(a),behavior='SocketVe',axis='Axis_SocketVe'+str(n))
a += 1
else:
connector(fil,a,instanceList[-1][4],4,instanceList[-1][5],4,'Wire-
'+str(a),axis='Axis_Socket2')
a += 1
connector(fil,a,instanceList[-1][6],4,instanceList[-1][7], 4,'Wire-
'+str(a),axis='Axis_Socket2')
a += 1

#Write boundary Conditions sets
if fixProx:
b = 1
else:
b = int((n+1)/2)
fil.write("*Nset, nset=fixation, instance=veSimple%s_Instance\n%s,\n" %
(b,veSimple.ncoords()+1))
fil.write("*Elset, elset=medianVentrols\n")
fil.write(medianVentrol+"\n")
if hmm and hmmLeft:
fil.write("*Elset, elset=myomeresLeft\n")
fil.write(myomLeft+"\n")
if hmm and hmmRight:
fil.write("*Elset, elset=myomeresRight\n")
fil.write(myomRight+"\n")

#Write axes
orientation(fil,'Axis_Dorsal',up[0],up[1],up[2],-up[2],up[1],up[0])
orientation(fil,'Axis_Ventral',down[0],down[1],down[2],-
down[2],down[1],down[0])
orientation(fil,'Axis_LateralLeft',left[0],left[1],left[2],-
left[1],left[0],left[2])
orientation(fil,'Axis_LateralRight',right[0],right[1],right[2],-
right[1],right[0],right[2])
#orientation(fil,'Axis_SocketVe', 1., 0., 0., 0., 1., 0.)
orientation(fil,'Axis_Socket2', 1., 0., 0., 0., 1., 0.)
orientation(fil,'Axis_Xaxis', 1., 0., 0., 0., 1., 0.)
#orientation(fil,'Axis_Muscle', 1., 0., 0., 0., 1., 0.)
orientation(fil,'Axis_DorsalLeft',vld[0],vld[1],vld[2],-
vld[2],vld[1],vld[0]) #Needs to be part dependent
orientation(fil,'Axis_DorsalRight',vrd[0],vrd[1],vrd[2],-
vrd[2],vrd[1],vrd[0])
orientation(fil,'Axis_VentralLeft',vlv[0],vlv[1],vlv[2],-
vlv[2],vlv[1],vlv[0])

```

```

orientation(fil,'Axis_VentralRight',vrv[0],vrv[1],vrv[2],-
vrv[2],vrv[1],vrv[0])

for i in range(n): #Seperate axes for each of the lateral joints
(skewing on these axes)
    axL, axR = axesLeft[i,0]-axesLeft[i,1], axesRight[i,0]-axesRight[i,1]
    orientation(fil,'Axis_LateralLeft'+str(i+1),axL[0],axL[1],axL[2],-
axL[1],axL[0],0.)
    orientation(fil,'Axis_LateralRight'+str(i+1),axR[0],axR[1],axR[2],-
axR[1],axR[0],0.)

for i in range(n-1): # Axes for the longitudinal joints
    v1 = arraytools.normalize(average(asarray([axesVe[i, 1] - axesVe[i,
0], axesVe[i+1, 1] - axesVe[i+1, 0]]), axis=0))
    orientation(fil,'Axis_SocketVe'+str(i+1),v1[0],v1[1],v1[2],-
v1[1],v1[0],0.)
    orientation(fil,'Axis_Muscle'+str(i+1),v1[0],v1[1],v1[2],-
v1[1],v1[0],0.)
    v1 = arraytools.normalize(average(asarray([axesLV[i, 1] - axesLV[i,
0], axesLV[i+1, 1] - axesLV[i+1, 0]]), axis=0))
    orientation(fil,'Axis_VentralLeft'+str(i+1),v1[0],v1[1],v1[2],-
v1[1],v1[0],0.)
    v1 = arraytools.normalize(average(asarray([axesRV[i, 1] - axesRV[i,
0], axesRV[i+1, 1] - axesRV[i+1, 0]]), axis=0))
    orientation(fil,'Axis_VentralRight'+str(i+1),v1[0],v1[1],v1[2],-
v1[1],v1[0],0.)
    v1 = arraytools.normalize(average(asarray([axesLD[i, 1] - axesLD[i,
0], axesLD[i+1, 1] - axesLD[i+1, 0]]), axis=0))
    orientation(fil,'Axis_DorsalLeft'+str(i+1),v1[0],v1[1],v1[2],-
v1[1],v1[0],0.)
    v1 = arraytools.normalize(average(asarray([axesRD[i, 1] - axesRD[i,
0], axesRD[i+1, 1] - axesRD[i+1, 0]]), axis=0))
    orientation(fil,'Axis_DorsalRight'+str(i+1),v1[0],v1[1],v1[2],-
v1[1],v1[0],0.)

for i in range(n-distal):
    axEL, axER = arraytools.normalize(asarray(axesEpaxialLeft[i+distal,
1]-axesEpaxialLeft[i, 0])),
arraytools.normalize(asarray(axesEpaxialRight[i+distal, 1]-
axesEpaxialRight[i, 0]))
    orientation(fil,'Axis_EpaxialLeft'+str(i+1),axEL[0],axEL[1],axEL[2],-
axEL[1],axEL[0],0.)

orientation(fil,'Axis_EpaxialRight'+str(i+1),axER[0],axER[1],axER[2],-
axER[1],axER[0],0.)

if hmm:
    for i in range(n-distal):
        axHL, axHR =
arraytools.normalize(asarray(axesHypaxialLeft[i+distal, 1]-
axesHypaxialLeft[i, 0])),
arraytools.normalize(asarray(axesHypaxialRight[i+distal, 1]-
axesHypaxialRight[i, 0]))

orientation(fil,'Axis_HypaxialLeft'+str(i+1),axHL[0],axHL[1],axHL[2],-
axHL[1],axHL[0],0.)

orientation(fil,'Axis_HypaxialRight'+str(i+1),axHR[0],axHR[1],axHR[2],-
axHR[1],axHR[0],0.)

#Write wires
a=1

for i in range(1, n+1):
    for p, j,ax,t in zip(instanceList[i-1].reshape(-1, 2), connectList[i-
1].reshape(-1, 2), axisList, range(len(axisList))):

```

```

        check = True
        if ax == 'Muscle' and i==n:
            check = False
        inst1 = p[0]
        node2 = j[1]
        if ax == 'Xaxis' and not tempV:
            check = False
        if p[0][:2] == p[1][:2]:
            if i > n-1:
                check = False
            else:
                inst2 = instanceList[i][2*t+1]
                node2 = connectList[i][2*t+1]
        elif ax[:8] == 'Hypaxial':
            #The myomere connection
wire
            if i > n-distal or not hmm:
                check = False
            else:
                inst2 = instanceList[i-1+distal, 2*t+1]
                node2 = connectList[i-1+distal, 2*t+1]
        elif ax[:7] == 'Epaxial':
            #The epaxial myomere
connection wire
            if i > n-distal or not emm:
                check = False
            else:
                inst2 = instanceList[i-1+distal, 2*t+1]
                node2 = connectList[i-1+distal, 2*t+1]
        else:
            inst2 = p[1]
        if check:
            wire(fil,a,inst1,j[0],inst2,node2)
            a += 1

#Boundary limitations for the first segment
wire(fil,a,instanceList[0][4],5,instanceList[0][5],5)
a+=1
wire(fil,a,instanceList[0][6],5,instanceList[0][7],5)
a+=1

if end:
    wire(fil,a,instanceList[-1][8],connectList[-1][8],"tip_Instance",2)
    a+=1
    wire(fil,a,instanceList[-1][10],connectList[-1][10],"tip_Instance",3)
    a+=1
    wire(fil,a,instanceList[-1][12],connectList[-1][12],"tip_Instance",4)
    a+=1
    wire(fil,a,instanceList[-1][14],connectList[-1][14],"tip_Instance",5)
    a+=1
    wire(fil,a,instanceList[-1][16],connectList[-1][16],"tip_Instance",1)

else:
    wire(fil,a,instanceList[-1][4],4,instanceList[-1][5],4)
    a+=1
    wire(fil,a,instanceList[-1][6],4,instanceList[-1][7],4)
    a+=1

fil.write("**End Assembly\n")

# Write Connector behaviors
behavior(fil,'Sliding',elastSliding)
if damping:
    damp(fil,dampSliding)
behavior(fil, 'StiffSliding', 100.*elastSliding)
if damping:

```

```

    damp(fil,dampSliding)

    fil.write("*Connector Behavior, name=PassiveLinear\n\
    *Connector Elasticity, component=1\n %s,\n" % passive)

    pasList = readStiffness(fnpassive)
    complexBehavior(fil, 'Passive', [0], usedComponents = [1], extraPolation
= True, nonLinearComponent = 1, nonLinearList = pasList)

    # Passive muscle response
    for i in range(n-distal):
        localArea = (scaleAtDistance(position[i+distal/2])[1])**2
        passiveBehavior(fil, 'PassiveHmm'+str(i+1), localArea * hmmrelarea,
[hmma, hmmb, hmmbc], lengthHmmLeft[i])
        passiveBehavior(fil, 'PassiveEmm'+str(i+1), localArea * emmrelarea,
[emma, emmb, emmbc], lengthEmmLeft[i])

    stifList = readStiffness(fnnonlinearssliding)
    complexBehavior(fil, 'NonLinearSliding', [0,
slidHigh,slidHigh,slidMed,slidHigh,slidHigh], usedComponents = [1, 2, 3, 4,
5, 6], extraPolation = True, nonLinearComponent = 1, nonLinearList =
stifList/10.)
    if damping:
        damp(fil,dampSliding)
        complexBehavior(fil, 'StiffNonLinearSliding', [0,
100*slidHigh,100*slidHigh,100*slidHigh,100*slidHigh,100*slidHigh],
usedComponents = [1, 2, 3, 4, 5, 6], extraPolation = True, nonLinearComponent
= 1, nonLinearList = stifList)
        if damping:
            damp(fil,dampSliding)

    behavior(fil,'HighElasticity',[1000,1000,1000,1000,1000,1000]) #Used to
temporary cancel out a joint

    #fil.write("*Connector Behavior, name=VentralTemp\n\
    *Connector Elasticity, component=2\n %s,\n" % (100.))

    complexBehavior(fil, 'VentralTemp', [vetraltempsock, vetraltempsock,
vetraltempsock], usedComponents = [1, 2, 3], nonLinearComponent = 8)

    behavior(fil,'SocketVe',elastSocketVe)
    #complexBehavior(fil, 'SocketVe', elastSocketVe, usedComponents = [4, 5,
6]) # TEMPORARY
    behavior(fil,'Socket2',elastSocket2)
    if damping:
        damp(fil,dampSocket)
    behavior(fil, 'StiffSocket', 100*elastSocketVe)
    if damping:
        damp(fil,dampSocket)

    fil.write("*Amplitude, name=SmoothAmplitude, definition=SMOOTH
STEP\n0.,0.,%s,1.\n" % stepTime)

    #The material properties (only if deformable parts are present)
    if deform:
        fil.write("***\n** MATERIALS\n**\n")
        fil.write("**Material, name=acellularBone\n\
        *Density\n %s, \n\
        *Elastic\n 6.48, 0.3\n" % (density))

    #The boundary conditions
    fil.write("***\n** BOUNDARY CONDITIONS\n**\n")
    if mvm and mvmAct:
        for i in range(n-1):
            fil.write("*** Name: MedianVentralContr%s Type: Connector
displacement\n\

```



```

*Connector Motion\n%s, 1\n" %(i+1, contractionList[i]))
    if hmm and hmmLeft:
        for i in range(n-1-distal):
            fil.write("*** Name: HmmLeft%s Type: Connector displacement\n\
*Connector Motion\n%s, 1\n" %(i+1, contractionListHmmLeft[i]))
            if hmm and hmmRight:
                for i in range(n-1-distal):
                    fil.write("*** Name: HmmRight%s Type: Connector displacement\n\
*Connector Motion\n%s, 1\n" %(i+1, contractionListHmmRight[i]))
                    fil.write("*** Name: Fix Type: Symmetry/Antisymmetry/Encastre\n\
*Boundary\nfixation, ENCASTRE\n")

    # Write the STEPS

# Contraction step
    fil.write("*** -----
----\n\
** \n\
** STEP: Contraction\n**\n\
*Step, name=Contraction\n")
    if deform:
        fil.write("**Dynamic, Explicit\n, %s\n" % (stepTime))
    else:
        fil.write("**Dynamic, Explicit, direct user control\n%s, %s\n" %
(stepIncrement, stepTime))
        # Contractions
        fil.write("**Bulk Viscosity\n0.06, 1.2\n\
**\n** BOUNDARY CONDITIONS\n**\n")
        if mvm and mvmAct:
            for i in range(n-1):
                fil.write("*** Name: DisplMvm%s Type: Connector displacement\n\
*Connector Motion, amplitude=SMOOTHAMPLITUDE\n\
%s, 1, %s\n" % (i+1, contractionList[i], contractionMvm[i]))
            if hmm and hmmLeft:
                for i in range(n-distal):
                    fil.write("*** Name: DisplHmmLeft%s Type: Connector
displacement\n\
*Connector Motion, amplitude=SMOOTHAMPLITUDE\n\
%s, 1, %s\n" % (i+1, contractionListHmmLeft[i], contractionHmmLeft[i]))
            if hmm and hmmRight:
                for i in range(n-distal):
                    fil.write("*** Name: DisplHmmRight%s Type: Connector
displacement\n\
*Connector Motion, amplitude=SMOOTHAMPLITUDE\n\
%s, 1, %s\n" % (i+1, contractionListHmmRight[i], contractionHmmRight[i]))
        # Forces
        if mvm and forcesMVM:
            for i in range(n-1):
                fil.write("*** Name: forceMVM%s Type: Connector force\n\
*Connector Load, amplitude=SMOOTHAMPLITUDE\n\
Wire-%s, 1, %s\n" % (i+1, contractionList[i], forceMVM[i]))

            if hmm and forcesHMM:
                for i in range(n-2):
                    fil.write("*** Name: forceHMMLeft%s Type: Connector force\n\
*Connector Load, amplitude=SMOOTHAMPLITUDE\n\
Wire-%s, 1, %s\n" % (i+1, contractionListHmmLeft[i], forceHMM[i, 0]))
                for i in range(n-2):
                    fil.write("*** Name: forceHMMRight%s Type: Connector force\n\
*Connector Load, amplitude=SMOOTHAMPLITUDE\n\
Wire-%s, 1, %s\n" % (i+1, contractionListHmmRight[i], forceHMM[i, 1]))

        # Output
        fil.write("*** OUTPUT REQUESTS\n\
*Restart, write, number interval=1, time marks=NO\n\

```

```
** FIELD OUTPUT: F-Output-3\n\  
*Output, field, variable=PRESELECT, NUMBER INTERVAL=%s\n" % numberOfFrames)  
  
    # Assembly level element definitions are not yet supported in Abaqus/CAE.  
  
    fil.write("*** HISTORY OUTPUT: H-Output-3\n")  
    fil.write("*Output, history, variable=PRESELECT, time interval=%s\n" %  
(stepTime/float(numberOfFrames))) # Number interval can not be used with  
History  
    fil.write("**End Step\n")  
  
    fil.close()  
    zoomAll()  
    mess('end of writing', tim)  
    message("Input file written: %s" % exportfile)  
    message("_____")  
  
if __name__ == 'draw':  
    run()  
# End
```